Aus dem Institut für Klinische Pharmakologie und Toxikologie
der Medizinischen Fakultät Charité – Universitätsmedizin Berlin

DISSERTATION

Investigating the role of PGE_2/15-keto-PGE_2/EP2/EP4 axis in kidney biology and disease

Untersuchung der Rolle der PGE_2/15-keto-PGE_2/EP2/EP4-Achse in der Nierenbiologie und bei Nierenerkrankungen

zur Erlangung des akademischen Grades
Doctor of Philosophy (PhD)

vorgelegt der Medizinischen Fakultät
Charité – Universitätsmedizin Berlin

von

Aikaterini Kourpa

Datum der Promotion: 30.06.2024

Table of contents

List of tables

List of figures

List of abbreviations

GH	Glomerular hyperfiltration
PGE_2	Prostaglandin E_2
PGF_{2a}	Prostaglandin F_{2a}
PGD_2	Prostaglandin D_2
GFB	Glomerular filtration barrier
EM	Electron microscopy
COX	Cyclooxygenase
$dmPGE_2$	16,16-dimethyl prostaglandin E_2
MWF	Munich Wistar Frömter rat
SHR	Spontaneously hypertensive rat
qPCR	Quantitative real-time PCR
MRI	Magnetic resonance imaging
DEGs	Differentially expressed genes
hpf	Hours post fertilization
SBP	Systolic blood pressure
CrCl	Creatinine clearance
RNA-seq	RNA sequencing
gc-EGFP	Vitamin D binding protein tagged with enhanced green fluorescent protein
ESRD	End stage renal disease
PGs	Prostaglandins
CKD	Chronic kidney disease
FFSS	Fluid flow shear stress

FSGS	Focal segmental glomerulosclerosis
GBM	Glomerular basement membrane
AA	Arachidonic acid
cAMP	Cyclic adenosine monophosphate
PPAR-γ	Peroxisome proliferator-activated receptor gamma
DAPI	4′,6-Diamidin-2-phenylindol
h	Hour(s)
min	Minute(s)
SD	Standard deviation
nt	Nucleotides
µL	Microliter
µm	Micrometer
µM	Micromolar

Abstract

Albuminuria represents a hallmark of both early kidney injury and chronic kidney disease (CKD). The importance of albuminuria as a prognosis marker is demonstrated by recent observations showing the high correlation of albuminuria with the probability of developing end-stage renal disease (ESRD).

Prostaglandins are lipid mediators demonstrating a crucial signaling role in various processes. PGE_2 is known to be the most abundant prostaglandin across tissues and has been found to be implicated in the regulation of renal homeostasis through its EP (EP1-4) receptors signaling, as well as affecting the incidence and progression of various kidney diseases. In addition, PGE_2 is implicated in proteinuria by affecting glomerular filtration barrier (GFB) permeability and its elevated levels are linked to increased fluid flow shear stress (FFSS) in podocytes. Despite the extensively studied role of PGE_2 on kidney physiology, the metabolic products occurring from its catabolism are considered biologically inactive. Recent *in vitro* data reported the ability of 15-keto-PGE_2 to activate EP receptors, however, the potential physiological roles of 15-keto-PGE_2 need to be investigated. Moreover, the role of PGE_2/15-keto-PGE_2/EP2/EP4 axis in kidney biology and glomerular morphology, as well as the potential renoprotective effect of combined pharmacological blockade of EP2 and EP4 receptors need to be further investigated.

In this study, I demonstrated that exogenous stimulation of zebrafish embryos with PGE_2 resulted in an albuminuria-like phenotype, mimicking the suggested PGE_2 effects on GFB dysfunction. Importantly, combined pharmacological blockade of EP2 and EP4 receptors significantly reduced the albuminuria phenotype in both zebrafish and the Munich Wistar Frömter (MWF) rat, a model of glomerular hyperfiltration (GH) and albuminuria. Using lipidomic analysis, it was shown that both PGE_2 and 15-keto-PGE_2 were present at considerable levels in zebrafish embryos and the latter could bind and stabilize EP2 and EP4 receptors on the plasma membrane in a yeast model. High-resolution image analysis revealed that the exogenous treatment with either PGE_2 or 15-keto-PGE_2 perturbed glomerular vascularization during zebrafish development. Specifically, I showed that elevated levels of PGE_2 or 15-keto-PGE_2 caused intercalation defects between podocytes and endothelial cells of glomerular capillaries, significantly affecting the podocyte surface area. Importantly, these defects were significantly reversed by combined blockade of EP2 and EP4 receptors.

Altogether, these findings support two key conclusions: a) a confirmed role of PGE_2 in the development of albuminuria in GH, while demonstrating a renoprotective potential of combined pharmacological blockade of EP2 and EP4 receptors, and b) 15-keto-PGE_2 has a biologically active role and may potentially modulate the EP receptor signaling *in vivo*, thus playing a role in kidney biology.

Zusammenfassung

Albuminurie ist ein Merkmal der frühen Nierenschädigung als auch der chronischen Nierenerkrankung (CKD). Die Bedeutung von Albuminurie als Prognosemarker wurde durch jüngsten Studien belegt, in denen gezeigt wurde, dass Albuminurie mit der Wahrscheinlichkeit der Entwicklung einer Nierenerkrankung im Endstadium (ESRD) korreliert.

PGE_2, dass in allen Geweben am häufigsten vorkommende Prostaglandin, wirkt über seine EP(EP1-4) -Rezeptoren, beeinflusst das Auftreten und Fortschreiten verschiedener Nierenerkrankungen, erhöht die Durchlässigkeit der glomerulären Filtrationsbarriere (GFB) und kann so zu Proteinurie führen. Eine Hochregulierung von PGE_2 in Podozyten ist mit einem erhöhten Scherstress des Flüssigkeitsstroms (FFSS) verbunden, wie er bei glomerulärer Hyperfiltration (GH) beobachtet wird. Trotz umfassender Studien zur Rolle von PGE_2 für die Nierenphysiologie werden die PGE_2 Metabolite weitgehend als biologisch inaktiv angesehen. Obwohl neue In-vitro Daten auf eine Aktivierung der EP-Rezeptoren durch 15-keto-PGE_2 hindeuten, blieb bislang ungeklärt, ob 15-keto-PGE_2 auch eine physiologische Rolle spielt. Zudem muss untersucht werden, welche Funktion die PGE_2/15-keto-PGE_2/EP2/EP4-Achse in der Nierenbiologie und der glomerulären Morphologie hat und ob eine duale pharmakologischen Blockade von EP2-/EP4-Rezeptoren eine potenzielle renoprotektive Wirkung hat.

In dieser Arbeit habe ich gezeigt, dass die exogene Stimulation von Zebrafisch-Embryonen mit PGE_2 einen Albuminurie-ähnlichen Phänotyp hervorruft, welcher die erwarteten Effekte von PGE_2 auf die GFB-Dysfunktion nachahmt. Eine kombinierte pharmakologische Blockade von EP2-/EP4-Rezeptoren reduzierte signifikant den Albuminurie-Phänotyp sowohl in Zebrafischen als auch in der Munich Wistar Frömter Ratte, einem Modell für GH und Albuminurie. Lipidomanalysen haben gezeigt, dass sowohl PGE_2 als auch 15-keto-PGE_2 in Zebrafischembryonen in beträchtlichen Mengen vorhanden sind. 15-keto-PGE_2 konnte EP2-/EP4-Rezeptoren in der Plasmamembran eines Hefemodells binden und stabilisieren. Die exogene Behandlung mit PGE_2 oder 15-keto-PGE_2 störte die glomeruläre Vaskularisierung während der Entwicklung des Zebrafisches. Vor allem erhöhte Konzentrationen von PGE_2 oder 15-keto-PGE_2 verursachten Defekte bei der Interkalation zwischen Podozyten und Endothelzellen der glomerulären Kapillaren, was die Oberfläche der glomerulären Filtrationsbarriere

erheblich beeinträchtigte. Diese Defekte konnten durch die kombinierte Blockade von EP2-/EP4-Rezeptoren aufgehoben werden.

Insgesamt stützen diese Ergebnisse zwei wichtige Schlussfolgerungen: a) die Rolle von PGE_2 bei der Entwicklung von Albuminurie bei GH wurde bestätigt und zusätzlich wurde gezeigt, dass die duale pharmakologische Blockade von EP2-/EP4-Rezeptoren einen renoprotektiven Effekt hat, und b) 15-keto-PGE_2 hat eine biologisch aktive Rolle und kann möglicherweise die EP-Rezeptor-Signalübertragung in vivo modulieren und somit eine Rolle in der Nierenbiologie spielen.

Synopsis

Part of the present dissertation has been previously published in the following research publications:

1. Kourpa, Aikaterini; Kaiser-Graf, Debora; Sporbert, Anje; Philippe, Aurélie; Catar, Rusan; Rothe, Michael; Mangelsen, Eva; Schulz, Angela; Bolbrinker, Juliane; Kreutz, Reinhold; Panáková, Daniela**. **15-keto-Prostaglandin E_2 exhibits bioactive role by modulating glomerular cytoarchitecture through EP2/EP4 receptors**. *Life Sciences* 2022;310:121114. doi: 10.1016/j.lfs.2022.121114.

2. Kourpa, Aikaterini*; Schulz, Angela*; Mangelsen, Eva; Kaiser-Graf, Debora; Koppers, Nils; Stoll, Monika; Rothe, Michael; Bader, Michael; Purfürst, Bettina; Kunz, Severine; Gladytz, Thomas; Niendorf, Thoralf; Bachmann, Sebastian; Mutig, Kerim; Bolbrinker, Juliane; Panáková, Daniela; Kreutz, Reinhold**. **Studies in Zebrafish and Rat Models Support Dual Blockade of EP2 and EP4 (Prostaglandin E_2 Receptors Type 2 and 4) for Renoprotection in Glomerular Hyperfiltration and Albuminuria.** *Hypertension.* 2023;80:771-782. doi:10.1161/HYPERTENSIONAHA.122.20392

3. Mangelsen, Eva.; Rothe, Michael.; Schulz, Angela.; Kourpa, Aikaterini.; Panáková, Daniela.; Kreutz, Reinhold.; Bolbrinker, Juliane**. **Concerted EP2 and EP4 Receptor Signaling Stimulates Autocrine Prostaglandin E2 Activation in Human Podocytes**. *Cells* 2020;9:1256. doi: 10.3390/cells9051256

(*Authors contributed equally, ** correspondence)

1. Introduction

1.1 Vertebrate kidney

1.1.1 The human kidney

The human kidney comprises the main blood filtration organ of the body, reabsorbing water, nutrients, and ions, concentrating the urine, removing waste products and excess fluid from the body, therefore maintaining a homeostatic balance, and achieving blood pressure control[1–3]. Human kidney consists of around a million of nephrons, which constitute the main structural and functional unit of the organ[1,3,4]. Each nephron contains 5 essential and distinct segments: the glomerulus (responsible for the blood filtration), the proximal and distal tubules, the loop of Henle and the collecting duct[1–3]. The glomerulus, the part of nephron responsible of the blood filtration, is composed of a small blood vessels network (capillaries) and contains specialized cells that form the principal filtration apparatus, called glomerular filtration barrier (GFB)[5]. The GFB is comprised by a layer of fenestrated endothelial cells, the glomerular basement membrane (GBM) and highly differentiated and specialized epithelial cells, the podocytes[6,7]. The latter are connected through crucial adherence junctions called slit diaphragms, that allow podocytes and therefore the GFB, to regulate selective filtration of blood into an ultrafiltrate[8]. This specialized filter allows the passage and excretion of molecules of molecular weight of up to 70 kDa, while it prohibits the elimination of larger molecules, mainly proteins like albumin[9]. In kidney disease conditions, where the GFB has suffered vital damage, the albumin is eliminated from the vasculature, leading to the pathological state of albuminuria, that can be initially diagnosed by the detection of albumin traces in the urine[9,10].

Among other vertebrates, the human kidney shares a very similar segmentation pattern with zebrafish despite important distinct differences associated with the diverse living environment i.e., terrestrial versus aquatic, that can affect the development and/or function of different organs, including the kidney[11]. The high similarity between human and zebrafish kidney constitutes the latter as a great model for studying kidney morphology and development and investigating a plethora of kidney related pathological conditions[12–15].

1.1.2 The zebrafish kidney

During the recent decades, the various experimental tools using zebrafish (*Danio rerio*) as an animal model have significantly improved, allowing to expand and perform many vertebrate developmental and disease studies. This model possesses various strengths and advantages among which are: high genetic similarity to humans (around 70%), *ex utero* fertilization and development of embryos, numerous offspring on weekly bases with robust growth rate and ease of experimental manipulation, and nearly transparent embryo's body that allows monitoring of internal organs and structures[16–18]. The above characteristics constitute an excellent tool for achieving high-throughput drug screenings, testing several chemical compounds, and performing detailed phenotypic analysis[18–20]. Due to the close functional analogy between human and zebrafish organs, the latter has been widely used to gain better insights into different disease conditions, such as cancer[21], diabetes[22,23], cardiovascular[24,25] and brain[26] defects as well as various kidney pathological states[27–29].

The zebrafish embryonic kidney, called pronephros, comprises the primary kidney structure of the organism and displays high similarity to mammalian metanephros[30]. Apart from blood filtration, the pronephros is responsible for water and ions excretion and osmoregulation maintenance[31]. The pronephros consists of only two nephrons derived from the lateral plate mesoderm, comparably to the intermediate mesoderm of mammals[11,13]. The two nephrons consist of two glomeruli that are fused together at the embryo midline around 48 hours post fertilization (hpf), abutting the dorsal aorta, the main blood vessel of the embryo for the circulation of oxygenated blood[11,13]. The nephron segmentation in zebrafish resembles that of higher vertebrates including human; the zebrafish pronephros does not contain specialized regions like the loop of Henle or the thick ascending limb, however, it contains proximal and distal tubules, divided into convoluted and straight as well as early and late parts, respectively[11,30]. The corpuscles of Stannius, responsible for the maintenance of calcium balance, is located between the distal tubules' segments[32]. The last segment of the nephron is the pronephric duct which is comparable to the collecting duct in humans, while the tubular epithelium lining from the glomerulus to the duct is fusing to the cloaca, a common exit portal for waste products from the gut and pronephros[13,30]. At 72 hpf, the GFB of the zebrafish pronephros is complete and functional, containing podocytes with extended interdigitating foot processes, a fenestrated endothelium and a GBM, covering the glomerular capillaries, thus demonstrating strong structural and functional similarity to the metanephric GFB of higher vertebrates[30].

All the above in combination with the simplicity of the zebrafish pronephros and the fact that more than 80% of human disease-associated genes have orthologues in the zebrafish genome[33], render embryonic pronephros as a great model for renal research, allowing the further investigation of complicated kidney diseases, such as glomerulopathies, polycystic kidney disease, and FSGS.

1.2 Prostaglandins

1.2.1 Prostaglandin E_2

Arachidonic acid (AA), a polyunsaturated omega-6 fatty acid, is the precursor for the synthesis of prostaglandins (PGs), a group of important bioactive lipid mediators[34]. AA is converted to PGs, including prostaglandin E_2 (PGE_2), F_{2a} (PGF_{2a}) and D_2 (PGD_2) by the cyclooxygenases 1 and 2 (COX1, COX2) and specialized enzymes for each of the PGs types, the prostaglandin synthases[34,35]. PGs have been discovered in practically all tissues of both humans and other vertebrates and a plethora of studies have emphasized their critical function in a variety of physiological and pathological conditions, including tissue inflammation, cancer, homeostatic balance regulation and maintenance, hematopoiesis, and renal physiology[36–43]. The most prevalent prostaglandin among them is PGE_2, which has been widely studied in recent years, for its function in various organs, including the kidney[35,43,44]. It has been extensively highlighted that PGE_2 is involved in both normal renal physiology as well as pathogenic pathways underlying the onset and development of chronic kidney disease (CKD)[35,44].

There are two steps involved in the inactivation of PGE_2. The first and rate-limiting step is catalyzed by 15-prostaglandin dehydrogenase (15-PGDH), resulting in the synthesis of 15-keto-PGE_2[45] , while prostaglandin reductase (PTGR or Δ^{13}-PG-Reductase) is the responsible enzyme producing 13,14-dihydro-15-keto-PGE_2 during the second and last step of PGE_2 degradation[45,46]. Both metabolites, 15-keto-PGE_2 and 13,14-dihydro-15-keto-PGE_2, were previously thought to have no biologically active role[45,47]. However, recent *in vitro* investigations have indicated that 15-keto-PGE_2 may operate as a partial agonist of PGE_2 receptors and replace PGE_2 in the signaling processes by activating the generation of cAMP[48,49]. Furthermore, recent studies in different models reported that 15-keto-PGE_2 can activate peroxisome proliferator-activated receptor gamma (PPAR-γ), an important receptor implicated in diabetic nephropathies[50–52]. Importantly, there is still debate over the physiological significance of PGE_2 metabolites, and more

specifically 15-keto-PGE_2. What role does it play in kidney biology and its ability to activate PGE_2 EP receptors *in vivo* demands further investigation.

1.2.2 Prostaglandin E_2 receptors

PGE_2 functions by binding to the EP1, EP2, EP3, and EP4 G-protein-coupled prostaglandin receptors[53,54]. Their expression and function in human and mammals have been previously reported in various studies. In zebrafish, EP1 receptor has been detected mainly in the gill, muscle, brain, but also in the kidney[55,56]. In contrast, EP3 has been reported to be hardly expressed in the zebrafish kidney, while it appeared to be essential for lymphatic vessel development during embryogenesis[38,55]. The expression of both EP2 and EP4 receptors in the zebrafish nephron has been highlighted in previous studies, demonstrating the expression of these receptors in the zebrafish kidney among other tissues[37,57,58] as well as supporting their crucial role in hematopoiesis[37]. It has been shown that both receptors demonstrate an important role in the regulation of pronephric tubules segmentation in the framework of PGE_2 metabolism[57].

A recent study published in the framework of the present thesis demonstrated the expression of EP1, EP2 and EP4 in a human immortalized podocyte cell line *in vitro*, while EP3 receptor expression was not confirmed[59]. Moreover, the functional role of EP2 and EP4 receptors was supported by using pharmacological blockade of both receptors, revealing that autocrine PGE_2 activation in human podocytes depends on concerted EP2 and EP4 signaling[59]. These receptors may therefore serve as key targets for the development of therapeutic approaches against a variety of renal conditions associated with PGE_2 signaling.

1.3 Thesis Research questions

My thesis focuses on the role of PGE_2 pathway in the kidney physiology and development and targets *in vivo* the PGE_2 catabolic pathway in zebrafish embryos. Despite the fact that the renal pathological effects of PGE_2 have been extensively studied[35,43,44], it is yet to be investigated its potential implications in normal glomerular morphology and cytoarchitecture. Namely, it is yet to be determined whether PGE_2 affects the podocytes-endothelial cells physiological interactions important for the establishment of the functional GFB and the overall renal activity. Furthermore, as

already mentioned above, the metabolic products of PGE_2, 15-keto-PGE_2 and 13,14-dihydro-15-keto-PGE_2, have been considered biologically inactive until recently[45,47–49], and their role in kidney pathophysiology needs to be further elucidated.

The research aims of the present thesis are summarized as follows:

1. Study the renal implications of PGE_2 and 15-keto-PGE_2 by establishing a zebrafish disease model that mimics the pathological albuminuria state in glomerular hyperfiltration.
2. Analyze and evaluate the effects of exogenous PGE_2 and 15-keto-PGE_2 stimulation in glomerular cytoarchitecture and ultrastructure.
3. Further study the bioactive role of 15-keto-PGE_2 and its ability to bind EP2 and EP4 receptors.
4. Investigate the potential renoprotective effect of the separate and/or combined pharmacological blockade of EP2 and EP4 receptors *in vivo* and analyze their ability to reverse the adverse effects of PGE_2 and 15-keto-PGE_2 stimulation, thus serving as potential therapeutic targets for PGE_2 pathway-associated kidney diseases.

2. Methods

2.1 Materials

2.1.1 Equipment and software

Table 1. List of equipment used.

Equipment	Manufacturer
Hybridization Oven, HB-1000 Hybridizer	UVP
M165 Fluorescent Microscopy	Leica
Zeiss LSM980 Airyscan	Zeiss
Zeiss LSM700	Zeiss
MD G33 Brightfield Microscopy	Leica
Cryostat microtome	Leica
Steamer	WMH
Ultracut E ultramicrotome	Leica
FEI Morgagni Electron Microscope with Morada CCD Camera	EMSIS GmbH
Agilent 6495 Triplequad mass Spectrometer	Agilent Technologies
MR system	Bruker Biospec 94/20, Bruker Biospin, Ettlingen, Germany
NextSeq 2000 system	Illumina
TapeStation RNA and DNA ScreenTape	Agilent Technologies

Table 2. List of software used.

Software	Vendor/URL
ImageJ	https://imagej.nih.gov/ij/
Adobe Illustrator 2021 26.2	Adobe Systems, Inc. (San Jose, US)
Adobe Photoshop 2021 22.4.3	Adobe Systems, Inc. (San Jose, US)

GraphPad Prism 9 for Mac OS X, Version 9.0	GraphPad Software, Inc. (La Jolla, US)
Microsoft® Excel for Mac	Microsoft
ZEN Blue	Zeiss
Huygens Professional 22.04	Scientific Volume Imaging (SVI)
Imaris version 9.9	Bitplane AG, Zurich, Switzerland
String database	https://string-db.org/
MARS data analysis software	BMG Labtech

2.1.2 Chemicals and reagents

Table 3. List of the chemicals and the reagents used in the experiments.

Chemical/Reagent	Source	Cat#
Methyl Blue	Sigma-Aldrich	319112
Tricaine	PharmaQ	
ProLong™ Gold Antifade Mountant with 4',6-diamidino-2-phenylindole (DAPI)	Invitrogen	P36935
Paraformaldehyde 16%	ThermoFisher Scientific	28908
Tissue-Tek O.C.T Compound	Sakura	12351753
TSA Plus Fluorescein	PerkinElmer	NEL741001KT
TSA Plus Cyanine 3	PerkinElmer	NEL744001KT
TSA Plus Cyanine 5	PerkinElmer	NEL745001KT
4′,6-Diamidin-2-phenylindol (DAPI)	Sigma-Aldrich	D9542
Antigen Unmasking Solution	Vector Laboratories, Inc.	H-3300
Dimethylsulfoxide (DMSO)	Sigma-Aldrich	276855
16,16-dimethyl-PGE_2 ($dmPGE_2$)	Cayman	Cay14750-1
15-keto-PGE_2	Cayman	Cay14720-1
EP2 receptor antagonist	Sigma-Aldrich	PF04418948

EP4 receptor antagonist	Sigma-Aldrich	ONO-AE3-208
Indomethacin	Sigma-Aldrich	I0200000
BSA AlexaFluor555	ThermoFisher Scientific	A34786
Methyl cellulose	Sigma-Aldrich	1424506
TopVision low melting point agarose	ThermoFisher Scientific	R0801
Uranyl acetate	SERVA	77870

2.1.3 Critical commercial assays

Table 4. List of commercially available kits.

Kits	Source	Cat#
RNAscope Multiplex Fluorescent v2 Kit	Advanced Cell Diagnostics	323110
CloneAmp HiFi PCR Premix	TaKaRa Bio Inc.	639298
5X InFusion® HD Enzyme Premix	TaKaRa Bio Inc.	102518
rCutSmart™ Buffer	New England Biolabs	B6004
NanoGlo® Extracellular Detection System	Promega Corporation	N2420
First Strand cDNA Synthesis Kit	ThermoFisher Scientific	K1612
NEBNext Ultra II Directional RNA Library Prep Kit for Illumina	New England Biolabs	E7530

2.1.4 Buffers and solutions

Table 5. List of buffers used.

Name	Composition
E3 Embryo Medium	5 mM NaCl, 0.17 mM KCl, 0.33 mM $CaCl_2$, 0.33 mM $MgSO_4$; pH 7.4
PBST	1× PBS, 0.1% Triton X-100
Midiprep Tris buffer	Macherey-Nagel

2.1.5 RNAscope probes

Table 6. List of the probes used for the RNAscope.

Probe	Source	Cat#
Dr-*ptger2a*; Accession No: NM_200635.1 Target Region (bp): 2-926	Advanced Cell Diagnostics	859901-C2
Dr-*ptger4b;* Accession No: NM_001128367.1 Target Region (bp): 550-1488	Advanced Cell Diagnostics	859911-C3

2.1.6 Zebrafish (*Danio rerio*) lines

Table 7. Transgenic zebrafish lines.

Zebrafish Line	Source	ZFIN-ID
Tg(wt1b:eGFP) ^{li1}	Reference 60	ZDB-ALT-071127-1
Tg(fabp10a:eGFP) ^{mi1000}	Zhou & Hildebrandt (2012)[61]	ZDB-ALT-121003-1

2.1.7 Yeast model

Table 8. Yeast strain used.

Strain	Genotype	Source
MMY28 strain *(S. cerevisiae)*	*W303-1A fus1::FUS1-HIS3 FUS1-lacZ::LEU2 far1Δ::ura3Δ gpa1Δ::ADE2Δ sst2Δ::ura3Δ MMY9 ste2Δ::G418*^{R} *TRP1::Gpa1/*$G_{\alpha s(5}$	GlaxoSmithKline[62]

2.1.8 Plasmids

Table 9. List of plasmids used for the yeast experiments.

Vector	Source
pBiT3.1-N [CMV/HiBiT/Blast]	Promega Corporation
p42GPD yeast	GlaxoSmithKline[62]

2.1.9 Primers

Table 10. List of cloning primers used for the yeast constructs.

Construct	Forward primer (5'-3')	Reverse primer (5'-3')
hEP2-HiBiT	CGAGCGGTGGGAATTCGATGGGCAATGCCTCCAATGAC	AAGCTTGACCTCTAGATCAAAGGTCAGCCTGTTTACTGGC
hEP4-HiBiT	CGAGCGGTGGGAATTCCATGTCCACTCCCGGGGTC	AAGCTTGACCTCTAGATTATATACATTTTTCTGATAAGTTCAGTGTTTCACT
hEP2-HiBiT-p426GDP	TAGAACTAGTGGATCCATGGTGAGCGGCTGGCGG	GCTTGATATCGAATTCTCAAAGGTCAGCCTGTTTACTGGC
hEP4-HiBiT-p426GDP	TAGAACTAGTGGATCCATGGTGAGCGGCTGGCGG	GCTTGATATCGAATTCTTATATACATTTTTCTGATAAGTTC

Table 11. List of primers for the quantitative real-time PCR analysis in the MWF rat. (Adapted from reference 63).

Gene	Ensembl no.	Sense Primer	Antisense Primer	Amplicon	Exon
Adamts4	ENSRNOT0000000471	AACTCCCTGTTCCCCAGACT	CCTGCTGCCGTACAAGGATA	230	8 + 9
Apcs	ENSRNOT0000001209	GCTGCTGCTTTGGATGTCTG	CTGCAGCGGTTTTTCTAGCC	145	1 + 2
Car15	ENSRNOT0000000031	ATCTGACGTCCACCTTTGCG	ATCTGTGAGTGGTCTGGGGT	221	7 + 8
Cks2	ENSRNOT0000007615	TCAGACAAGTACTTCGACGAGC	TCTTTTGGAAGAGGCCGTCTA	203	1
Col3a1	ENSRNOT0000000495	TGTTAACGGACAAATAGAGAGTCTT	CATCTTGCAGCCTTGGTTAGG	142	48 + 49
Cry1	ENSRNOT0000000912	TGAGGACCTTGATGCCAATCT	ACGATGACTTCCACACCAGC	201	2 + 3
Dlgap3	ENSRNOT0000001921	CCTCCTGCAGCTCTCCATTG	CGCGAGGGCTTCTTTGGTAT	135	11 + 12
Ifi27l2b	ENSRNOT0000003201	GCCAAGATGATGTCTGCTGC	CGAGGGTTAAACTGGTGGAGA	235	3 + 4
Havcr1	ENSRNOT0000000957	ATTGTTGCCGAGTGGAGAT	TGTGGTTGTGGGTCTTGTAGT	125	3 + 4
Lcn2	ENSRNOT0000001877	GGCCGACACTGACTACGACC	GCCCCTTGGTTCTTCCGTAC	106	4 + 5
Manf	ENSRNOT0000001910	ATGATGCCGCCACCAAGATC	CCCCCAATCGTCCAGGATTT	200	3 +4
Map3k7	ENSRNOT0000000765	ACTCCATCCCAATGGCGTATC	GGTCCTTTTCATCCTGGTCCA	201	15-17
Npas2	ENSRNOT0000005957	TCCAAGTCCTGACTCCCACC	GTGGAGAGAAGGAGCGAGTC	201	20 + 21
Nphs1	ENSRNOT0000004521	CTGAAGACCATGGAGCTCGG	ATCCCAGGATGGTAATGGCG	120	8 +9
Nphs2	ENSRNOT0000009486	TGAATGTGGACGAGGTTCGA	AGAGGACAAGAAGCCACTCG	129	1 + 2
Nr1d1	ENSRNOT0000001253	GTGCGGGAGGTGGTAGAATT	CGCTGAAGTCAAACATGGCA	235	6 + 7
Pdpn	ENSRNOT0000002031	GACATGGTGAACCCAGGTCT	AATGGGAGGCTGTGTTGGTA	108	2 + 3
Sdr9c7	ENSRNOT0000000591	AGCTGGTTGATAGGGGCATG	TCCAGCATTGTTCACCAGGG	200	3 + 4
Sfn	ENSRNOT0000004395	TGTCTGTCCATCCTCGGAGT	TCTCTTCAGACCCCTCCTCG	250	2
Tac3	ENSRNOT0000000567	TTGAAGAGAACACCCCCAGC	TGGGGGTAGAGGCTGTTCAT	209	6 + 7
Tmem86a	ENSRNOT0000001868	CATGGTGTCTCCGGTCACTG	AGAAGACGAGTCCCGCAAAG	233	1 + 2

2.2 Methods

The following methods are included and described in the publication listed in the reference list as references **63** and **64**, that comprise part of my thesis. The LC/ESI-MS/MS methodology used to characterize the PGE_2 pathway in whole zebrafish embryo and in the rat glomerular tissue was established in the study cited in reference **59**.
For both zebrafish and rat models, the 'Principles of Laboratory Animal Care' (NIH publication no. 86–23, revised 1985) and the current version of German Law on the Protection of Animals and EU directive 2010/63/EU on the protection of animals were followed.

2.2.1 Zebrafish husbandry

Zebrafish (*Danio rerio*) were bred, raised, and maintained following the FELASA guidelines[65], the guidelines of the Max-Delbrück Center for Molecular Medicine in the Helmholtz association and the local authority for animal protection (Landesamt für Gesundheit und Soziales, Berlin, Germany). The zebrafish transgenic lines used in the present thesis were *Tg(wt1b:EGFP)^{li1}* [60] *and Tg(fabp10a:gc-EGFP)^{mi1000}* [61]. Embryos were kept in E3 embryo medium at 28.5 °C, under standard laboratory conditions in all the experiments.

2.2.2 Rat breeding

Munich Wistar Frömter (MWF) male rats with an inherited nephron deficiency were used as a model of GH and albuminuria[66,67]. The rats were attained from our MWF/Rkb (RRID: RGD_724569, laboratory code Rkb, http://dels.nas.edu/ilar/) colony at the Charité-Universitätsmedizin Berlin, Germany and experiments were performed following the guidelines of the Charité-Universitätsmedizin Berlin and the local authority for animal protection (Landesamt für Gesundheit und Soziales, Berlin, Germany). The grouping of the rats was based on regular 12 h diurnal cycles with automated light switching (lights on from 8:00 am to 8:00 pm) and climate-controlled conditions at 22 °C. The rats were fed a normal diet containing 0.2% NaCl and had free access to food and water. Urinary albumin excretion in 24-h, creatinine clearance, and systolic blood pressure by the tail-cuff method in awake rats, was determined as reported[66]. At the end of the study (at 12 weeks of age), animals were anesthetized by intraperitoneal (i.p). injection with ketamine-xylazine (60 mg Ketamin and 12 mg Xylazin per kg body

weight). Blood was obtained retrobulbar and lithium heparinate plasma was used for creatinine level measurements. Kidneys were obtained, decapsulated, and sieved using a 125 µm steel sieve. Glomeruli were kept on the sieve, rinsed off with PBS, centrifuged, snap-frozen, and stored at −80 °C for lipidomic analysis. For transcriptomic analysis, the dissected cortex of the left kidney was immediately snap-frozen and stored at -80 °C. For glomerular morphology analysis, the right kidneys (*n*=6-8/group) were fixed in 2.5% glutaraldehyde solution and were preserved in 330 mosmol sucrose/1x PBS + 0.02% NaN3.

2.2.3 HiBiT-tagged hEP2/hEP4 receptor constructs.

To generate hEP2-/ hEP4-HiBiT constructs with a HiBiT-taq, the full-length human Prostaglandin E Receptor 2 (hEP2) and 4 (hEP4) cDNAs were cloned into the pBiT3.1-N [CMV/HiBiT/Blast] vector including a short linker attached to the N-terminal receptor sequences. This was done by first preparing the cDNA from conditionally immortalized human podocytes[68], and designing primers that spanned either the start codon (forward-primers) or stop codon (reverse-primers) of the hEP2/ hEP4 receptor sequences. Full-length hEP2 and hEP4 cDNA sequences were amplified using CloneAmp HiFi PCR Premix and the designed cloning primers. Primer sequences are listed in 2.1.9. Restriction digestion of the pBiT3.1-N [CMV/HiBiT/Blast] vector was performed using CutSmart™ Buffer and *EcoR*I and *Xba*I restriction enzymes (New England Biolabs). The PCR products were integrated into the vector using the 5X In-Fusion® HD Enzyme Premix and the resulting plasmid was transformed into One Shot™ TOP10 chemically competent *E.coli* (Thermo Fisher Scientific). Sanger sequencing (LGC genomics) was used for the confirmation of the plasmid sequences.

Apart from the pBiT3.1-N vector, the hEP2-/hEP4-HiBiT constructs were also cloned into the p426GPD yeast plasmid[62] using cloning primers of Table 10. The forward primer was designed with a 5’ flanked complementary to the yeast plasmid, spanning a *BamH*I restriction site and the HiBiT-tag start codon. The reverse primer was designed with a 5’overhang spanning a restriction site close to the stop codon of the hEP2/ hEP4 sequence as well as the respective stop codon. Purified pBiT3.1-N [CMV/HiBiT/Blast] vector with integrated hEP2/ hEP4 sequences was used as a template for PCR amplification. Ligation, transformation, and sequencing performed as described above.

2.2.4 Yeast culture and transformation.

Prior to transformation, yeasts stored on glycerol beads at -80°C were thawed and plated on YPD plates for 2 days at 30°C before liquid pre-cultures were incubated in YPD medium shaking overnight at 30°C. Transformed yeasts grew on WHAUL plates supplemented with histidine (WHAUL-His) for three days. Three clones were picked and transferred on new WHAUL-His plates and incubated overnight at 30°C. On the next day, clones were pre-cultured in WHAUL-His medium overnight shaking at 30°C in flat 96-well plates (TPP).

The p426GPD plasmids carrying either hEP2-HiBiT or hEP4-HiBiT construct were transformed into *S.cerevisiae* (MMY28 yeast model) using lithium acetate (LiAc)/ single-stranded DNA (ssDNA)/ polyethylene glycol (PEG) method[62].

Brief description of the method:

100mL of yeast extract peptone dextrose (YPD) medium was inoculated with 1.5mL yeast pre-culture and incubated for 2 hours shaking at 30°. Yeast cultures were centrifuged and washed, and the pellets were suspended in 1mL LiAcTE. For transformation, 5µL of ssDNA (10mg/mL, Sigma-Aldrich), 1µg plasmids and for mock-transformed controls the corresponding volume of Midiprep Tris buffer solution (Macherey-Nagel), 50µL yeast solution and 300µL LiAc PEG TE were mixed and incubated at room temperature for 10 min and then subjected to heat shock at 42°C for 20 min. The yeast solutions were then plated on WHAUL-His plates.

2.2.5 Expression of the receptors on the yeast membrane.

The expression of hEP2 and hEP4 receptors on the yeast membrane was studied using the NanoGlo® Extracellular Detection System. This system focuses on detecting the expression of HiBiT-tagged protein/receptor. Incubation with the NanoGlo® Extracellular reagent results in a luminometry signal that reflects the number of receptors on the plasma membrane. If the ligand of interest can bind the HiBiT-tagged receptor, a modification in the receptor's expression is triggered, causing a change in the luminometry signal. The yeast pre-cultures were diluted 1:5 in WHAUL- medium and 5 µL of yeast dilution were incubated with 100µL WHAUL- medium supplemented with BU Salts for 20h. Following 20h incubation, yeasts were stimulated for 20 min with 100nM PGE_2, 1µM 15-keto-PGE_2 or plain medium for untreated control. Nine transformed colonies and one mock-transformed colony that served as a negative control, were tested at a time. Then, yeasts were treated with the Nano-Glo®

Extracellular Detection System according to the manufacturer's instructions. Briefly, yeast solutions after stimulation were transferred to white 96-well plates (Corning Inc.). Thereby, one stimulated yeast solution was split into 2 wells after mixing. Equal volume of the reagent (consisting of NanoGlo® Extracellular Detection Buffer, NanoGlo® HiBiT Extracellular Substrate diluted 1:50 and LgBiT Protein diluted 1:100) was added to the yeast solutions. After shaking for 5 minutes, luminescence was measured using a FLUOstar Omega microplate reader (BMG Labtech) and analyzed with Optima and MARS software (BMG Labtech). Colonies with luminescence values lower than the medium control and the negative yeast control were considered unsuccessful transformations and excluded from analysis.

2.2.6 Lipidomic analysis of whole zebrafish embryo and MWF rat glomerular tissue.

The lipidomic analysis was performed by liquid chromatography electrospray ionization tandem mass spectrometry (LC/ESI-MS/MS) following the protocol reported recently[59]. The zebrafish embryos at two different developmental stages, 48 hpf and 120 hpf, as well as, isolated glomeruli of young MWF at the onset of albuminuria (8 weeks of age) and of albuminuria resistant spontaneously hypertensive rats (SHR) were frozen using liquid nitrogen and analyzed using an Agilent 1290 HPLC system with binary pump, multisampler and column thermostat with a Zorbax Eclipse plus C-18, 2.1 × 150 mm, 1.8 µm column using a solvent system of aqueous acetic acid (0.05%) and acetonitrile. A gradient starting with 5% organic phase was used, which was increased within 0.5 min to 32%, 16 min to 36.5%, 20 min to 38%, 28 min to 98% and held there for 5 min, was used for the elution. The flow rate was set at 0.3 mL/min and the injection volume was 20 µL. The HPLC was coupled with an Agilent 6495 Triplequad mass spectrometer with electrospray ionization source. Source parameters: Drying gas: 115 °C/16 L/min, Sheath gas: 390 °C/12 L/min, Capillary voltage: 4300 V, Nozzle voltage: 1950 V, and Nebulizer pressure: 35 psi.

2.2.7 Pharmacological approach used for the analysis of glomerular morphology and GFB integrity.

For the phenotypic evaluation of the zebrafish embryonic kidney and the functional assessment of GFB integrity, the transgenic lines *Tg[wt1b:EGFP]*[60] and *Tg[fabp10a:gc-EGFP]*[61] were used, respectively. The glomerular morphology was evaluated using

Tg[wt1b:EGFP] zebrafish embryos that allow the observation of podocytes and parietal epithelial cells of the glomerulus, as well as part of the proximal pronephric tubules[60]. For the evaluation of GFB integrity, *Tg[fabp10a:gc-EGFP]* larvae were used. This strain expresses the fluorescent albumin surrogate (*gc-EGFP*), consisting of a vitamin D binding protein fused to enhanced green fluorescent protein in the liver from which it is released into the blood stream and circulates in the blood[61] under normal conditions, allowing its observation in the trunk vasculature. Upon GFB damage, *gc-EGFP* will leak through the glomerular filtration barrier, which results in a decrease of the fluorescence in the trunk vasculature of the embryos, mimicking thereby an albuminuria-like phenotype.

The drugs were applied to the zebrafish embryos between 6 hpf and 48 hpf for the early treatment and between72 hpf and 96 hpf for the late treatment. For the drug treatments, the E3 media was completely drawn off the embryos and the desirable solution of DMSO vehicle control, dmPGE$_2$ (a long-active derivative of PGE$_2$) or 15-keto-PGE$_2$, PF-04418948, ONO-AE3-208 and Indomethacin in E3 water was applied on zebrafish embryos. For the PGE$_2$ and 15-keto-PGE$_2$ stimulation, 125 µM and 500 µM concentrations were used, respectively. For the separate and combined blockade of EP2 and EP4 receptors, 20 µM EP2 and 20 µM EP4 receptors antagonists in E3 water with either 125 µM dmPGE$_2$ or 500 µM 15-keto-PGE$_2$ were used. For blocking the COX activity, 30 µM Indomethacin with 125 µM dmPGE$_2$ was used. Controls were treated only with DMSO (% adjusted to the solvent ratio in drug solution) in E3 water. The embryos were placed in a 28.5°C incubator until phenotypic analysis. At the end of the late treatments, embryos were categorized based on the fluorescence signal as “GFP +” (visible gc-EGFP fluorescence signal in the trunk vasculature) or “albuminuria-like phenotype” (partial or complete loss of *gc-EGFP* fluorescence signal in the trunk vasculature).

For the *in vivo* imaging, 48 hpf and 96 hpf zebrafish larvae were anesthetized with 0.1% tricaine in E3 solution and embedded in methyl cellulose. Fluorescent images were acquired using Leica M165 stereomicroscope with a Leica DFC450 camera attached.

2.2.8 Subcellular analysis and 3D reconstruction of the glomerulus.

For the confocal microscopy imaging, the pronephros of fixed *Tg[wt1b:eGFP]* zebrafish embryos at 48 hpf or 96 hpf were used. Prior to the fixation, the anesthetized

embryos (in 0.02% tricaine (w/v)) were injected in the sinus venosus or the descending cardinal vein with 20 mg/ml BSA Alexa Fluor555 conjugate diluted in in 150 mM NaCl. The injected embryos were fixed after 20 min in 4% PFA and 0.1% Triton-X 100 in PBS buffer for 2 h at RT or overnight at 4°C. Nuclei were stained using DAPI overnight at 4°C. After removal of the yolk and mounting in 0,8% low-melting point agarose, the kidneys of whole-mount fixed embryos at 48 hpf or 96 hpf were imaged using a Confocal Zeiss LSM 980 Airyscan microscope with a LD C-Apochromat 40 x NA1.1 water objective and Zen Blue v.3.2 software. Confocal z-stacks of all channels were acquired sequentially with identical parameters and similar 3D orientation for all samples. Images were analyzed using ImageJ software.

The 3D confocal images were first deconvolved using Huygens Professional 22.04 software. The 2D segmentation, an important step for the creation of the 3D glomerular surface, was performed using Imaris software (version 9.9). A 3D surface covering the total glomerular volume was created by tracing the surface outline of EGFP-positive cells for every second section of the z-stack manually, while as a next step the surface creation was achieved using the automated segmentation feature. As regards the EGFP-signal, the fluorescence derived by EGFP-positive cells inside the glomeruli was included, while the green-fluorescent signal coming from the early part of proximal tubules was excluded.

2.2.9 Cryosectioning and immunofluorescence *in situ* hybridization (RNAscope)

For the preparation of the samples for the cryo-tissue cutting, 48 hpf *Tg[wt1b:EGFP]* embryos were fixed in 4% PFA in PBS overnight at 4 °C, washed with PBS for 3 x 10 min and treated overnight with 30% sucrose in PBS. The embryos were then positioned vertically and frozen in Tissue-Tek O.C.T Compound (Sakura) on dry ice. Using a cryostat I cut tissue slices of 7 µm. Slides containing the tissue slices were stored at -80 °C until further processing.

Fluorescent *in situ* hybridization (RNAscope) was used to visualize single mRNA molecules expressed in individual cells in the zebrafish embryonic kidney. The assay was performed according to the manufacturer's instructions for fixed frozen tissues. The 7 µm cryo-sections were dried for 30 min at room temperature and then washed with PBS for 5 min. Next, the slides were incubated at 99°C for 15min with an antigen retrieval solution (ACD) using a steamer. The *Dr-ptger2a* and *Dr-ptger4b* probes were

used, while for the signal development TSA plus fluorophores fluorescein, Cyanine3 and Cyanine5 were applied in a dilution ratio 1:1000. The slides were mounted with ProLong Gold antifade reagent with DAPI. For the imaging, the Zeiss LSM700 confocal microscopy was used and image analysis was performed with the ImageJ/Fiji and Photoshop software.

2.2.10 Electron microscopy analysis in zebrafish and rat kidney

The ultrastructural analysis of the glomeruli was performed in 96 hpf zebrafish embryos with a modified method as recently reported[66]. The embryos were embedded in Poly/Bed^{R} 812 (Polysciences, Eppelheim, Germany) and cut with Ultracut E ultramicrotome. Ultrathin sections (70nm) were drawn on a copper grid and counterstained with lead citrate 3% stabilized solution (ULTROSTAIN 2, Leica) for 30 min and uranyl acetate for 5 min in the Leica EM AC20 contrasting device. Images were acquired with a FEI Morgagni electron microscope and a Morada CCD camera.

The quantification of podocyte foot process width and number of slit diaphragms per µm of the GBM in both zebrafish embryos and MWF rats was performed as previously described[69]. ImageJ/Fiji software was used for the measurement of the length of the GBM and the counting of the number of slit diaphragms overlying the GBM. The mean of foot process width (W_{FP}) was calculated as the total GBM length (ΣGBM) measured in one glomerulus divided by the total number of slits (ΣSlits) counted and multiplied by π/4, that serves as a correction factor for the random orientation of the foot processes sectioning, following the formula:

$$W_{FP} = \frac{\pi}{4} \cdot \frac{\Sigma GBM length}{\Sigma Slits}$$

2.2.11 Reverse transcription and qPCR

Quantitative real-time PCR (qPCR) was used to assess targeted mRNA expression analysis of selected candidates that were associated with GFB function and kidney injury in the setting of GH and albuminuria[66]. First-strand cDNA synthesis was carried out on 2 µg of total RNA using the First Strand cDNA Synthesis Kit following the manufacturer's protocol. Isolated glomeruli of rat strains were analyzed at week 4 and week 8[66]. qPCR of each gene was performed in a 7000 Real-Time PCR System (Applied Biosystems) with version 1.2.3 software or a 7500 Fast Real-Time PCR

System with version 2.0.6 software (Applied Biosystems) using the comparative quantification cycle method as reported (Fast SYBR® Green Master Mix or Power SYBR® Green PCR Master Mix; Applied Biosystems)[66].

2.2.12 Bulk RNA-seq analysis

Unbiased transcriptome analysis by RNA-seq analysis was performed in (*n*=5/group) for all groups of MWF rats obtained at the end of study period following a modified recently reported protocol66. The mRNA expression was further validated using qPCR and network analysis of protein-protein interactions was done using STRING software. The cDNA library was prepared using NEBNext Poly(A) mRNA magnetic isolation and sequencing was done on NextSeq 2000 system. Quality control of the RNA and library was done using TapeStation RNA and DNA ScreenTape.. Initial quality control of the demultiplexed raw data was performed using FastQC version 0.11.9. Trimmomatic version 0.39 was used for quality trimmed of raw reads utilizing a sliding window of 4 nt with a minimal average quality of 15. Adapter sequences and low-quality ends (minimal quality: 3) were removed. Reads below a minimal read length of 15 nt after trimming were dropped. The resulting reads were aligned to the Ensembl Rnor_6.0 reference genome using HISAT270. The aligned reads were sorted using samtools version 1.9 and gene counts were determined using HTSeq version 0.12.4 and the Ensembl annotation version 104.6. DESeq2 R package version 1.32.0 was used for differential expression analysis. Genes with absolute fold change value <1 were excluded. Genes were considered significantly differentially expressed if the adjusted P-value was <0.05. PCA plots and heatmaps were created using pcaExplorer and gplots R packages.

2.2.13 Magnetic resonance imaging (MRI) analysis of MWF rat kidney

For MRI analyses, animals (*n*=14-15 per group, each) were anaesthetized with 6 ml/kg body weight i.p. Urethan 20% in H_2O. MRI data were acquired on a 9.4 Tesla small animal MR system using a linear radiofrequency volume resonator and a 4-channel surface coil array tailored for rats. T_2 maps were acquired using a multi-slice multi-echo spin echo (MSME) protocol (TR = 500 ms, flip angle α=90, first echo time and interecho time TE_1 = ΔTE= 6.4 ms, 13 echoes). A multi-gradient echo (MGE) protocol was used to acquire T_2* maps (TR = 50 ms, flip angle α=16, first echo time and interecho time TE_1 = ΔTE= 2.1 ms, 10 echoes, 4 averages). MR data acquisition used an in-plane spatial

resolution of 230 x 450 µm², a 1.4 mm slice thickness and respiration gating for motion compensation.

2.2.14 Statistics

Statistical analysis was performed using GraphPad Prism version 6.07 or 9 or SPSS Statistics 28.0.0.0.2. The following statistical tests were used for normally distributed data: Wilcoxon test, two-tailed unpaired t test with Welch's correction, one-way ANOVA with Tukey's multiple comparisons post-test or Bonferroni's post hoc analysis, and two-way ANOVA with Tukey's multiple comparisons post-test.

For not normally distributed data, the tests used were: Kruskal-Wallis test with Dunn's post-hoc analysis and Mann-Whitney test. Data were tested for normal distribution using Shapiro-Wilk test, while the identification of outliers was performed by Grubbs' outliers test ($\alpha = 0.05$).

In all graphs error bars are presented as means ±SD and $P < 0.05$ were considered statistically significant. Specific details of the statistical analyses performed are given in Figure legends.

3. Results

3.1 PGE_2 pathway is conserved in zebrafish.

Prostaglandins (PGs) are synthesized from AA with participation of COX and respective PGs synthase enzymes (Fig 1A). In this study, the physiological significance of PGE_2 and its metabolite 15-keto-PGE_2 in living organisms was explored by using the zebrafish model. To determine the prostaglandin levels and analyze the total prostaglandin metabolic pathway in the zebrafish embryos, I used a LC/ESI-MS/MS-based method at two time points: 48 and 120 hpf, prior to and after the GFB formation, respectively. The use of the zebrafish model was beneficial, as it allowed for examination of the effects of small molecules and metabolites in the organism. It is worth mentioning here that, the zebrafish embryo's nourishment relies on its yolk content during early stages[71], making the lipidomic study of the whole embryo reliable and accurate[72] as it was not impacted by exogenous factors like food intake.

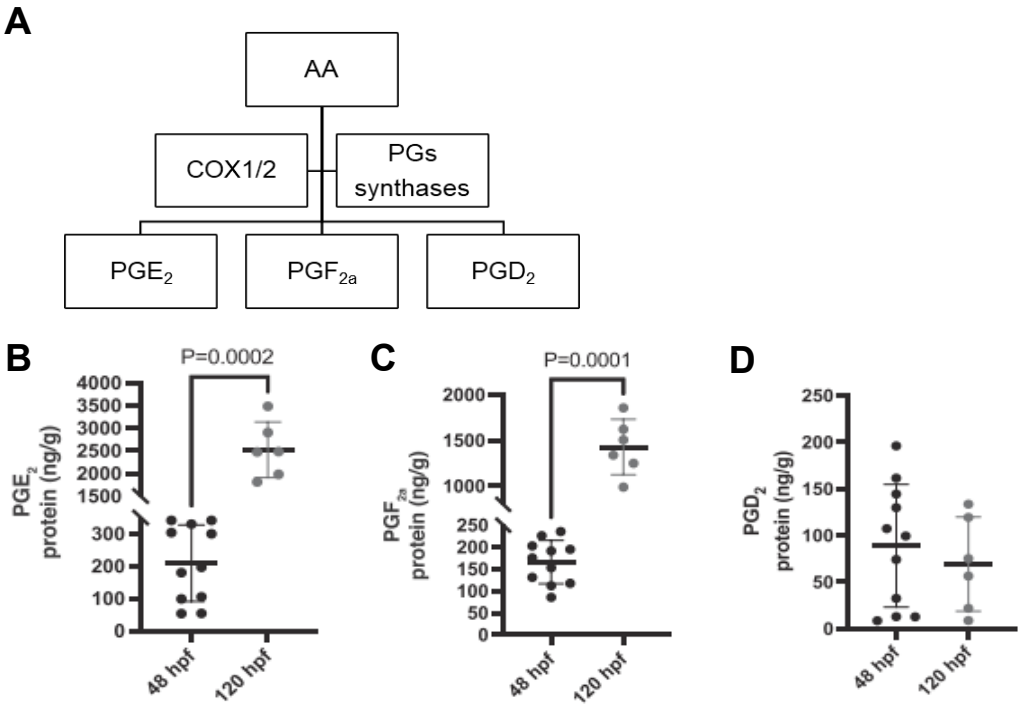

Figure 1. Lipidomic analysis of the main PGs. (A) Synthesis of the three main PGs, PGE_2, PGF_{2a} and PGD_2 from AA with the participation of cyclooxygenases and specific prostaglandin synthases. Lipidomic levels of (B) PGE_2 (P=0.0002), (C) PGF_{2a} (P=0.0001) and (D) PGD_2 at 48 hpf (N=11, n=275) and 120 hpf (N=6, n=150). Less points in some graphs indicate missing values due to non-detectable levels; n represents biologically independent samples over N independent experiments. For the statistics: two-tailed unpaired t-test with Welch's correction was performed; Values plotted as mean ±SD and P<0.05 considered significant. One outlier was identified and removed among the lipidomic PGE_2 values at 48 hpf together with the respective values for the two metabolites in Figure 2A and B. Adapted from reference 64.

All main prostaglandins, namely PGE_2, PGF_{2a} and PGD_2 as well as their catabolic products were detected in the wild-type zebrafish whole embryo extracts (Fig. 1B-D, 2). PGE_2 appeared to be the most abundant prostaglandin in both 48 and 120 hpf (Fig. 1C). PGE_2 and PGF_{2a} mean levels at 120 hpf (2522.13 ng/g and 1427.59 ng/g, respectively) were approximately one order of magnitude higher than at 48 hpf (209.36 ng/g and 165.98 ng/g, respectively) (Fig. 1C, D), while PGD_2 levels remained constant (Fig. 1E). 15-keto-PGE_2 metabolite was present, but at roughly 10-fold lower levels than PGE_2, with mean levels of 16.82 ng/g and 77.37 ng/g at 48 hpf and 120 hpf, respectively (Fig. 2A). At 48 hpf, 15-keto-PGE_2 levels were higher than 15-keto-PGF_{2a} levels, but both metabolites were present at similar levels at 120 hpf (Fig. 2A, C). The downstream metabolites of 15-keto-PG, 13,14-dihydro-15-keto-PG, exhibited a similar pattern. (Fig. 2B, D, E).

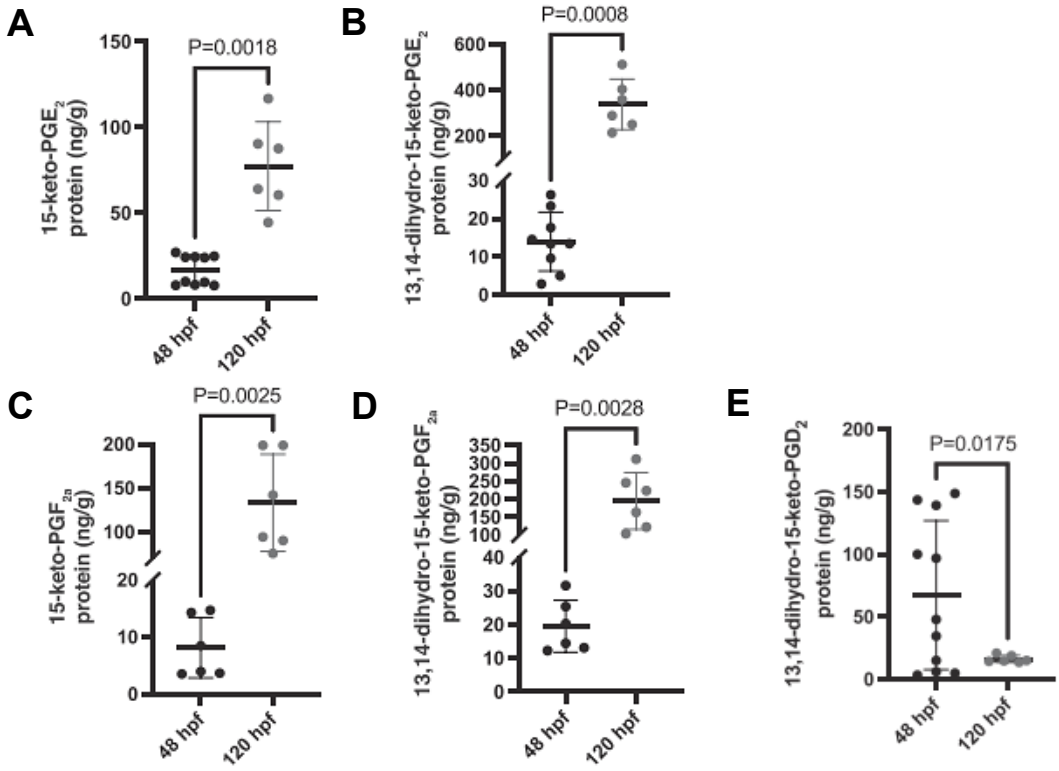

Figure 2. Lipidomic analysis of the main PGs' metabolites. (A) 15-keto-PGE_2 (P=0.0018), (B) 13,14-dihydro-15-keto-PGE_2 (P=0.0008), 15-keto-PGF_{2a} (P=0.0025), 13,14-dihydro-15-keto-PGF_{2a} (P=0.0028) and (E) 13,14-dihydro-15-keto-PGD_2 (P=0.0175) at 48 hpf (N=11, n=275) and 120 hpf (N=6, n=150). Less points in some graphs indicate missing values due to non-detectable levels; n represents biologically independent samples over N independent experiments. For the statistics: two-tailed unpaired t-test with Welch's correction was performed; Values plotted as mean ±SD and P<0.05 considered significant. Adapted from reference 64.

To confirm whether the PGE_2 pathway is metabolically conserved between zebrafish and higher vertebrates including humans, I performed pharmacological inhibition of COX enzymatic activity using indomethacin, a well-characterized non-selective COX inhibitor[73]. Indeed, COX inhibition that normally leads to reduction in PGE_2 production, profoundly reduced the PGE_2 levels (7.2±1.6 ng/g, 87.8% suppression) in zebrafish embryos at 48 hpf (Fig. 3), indicating the conserved prostaglandin metabolism in zebrafish. Thus, the quantitative analysis demonstrated here, showed that like in other animal models and humans[74–77], PGE_2 is the predominant prostaglandin in zebrafish embryos and its metabolite, 15-keto-PGE_2, is also comparatively abundant, highlighting its potential function in organismal physiology.

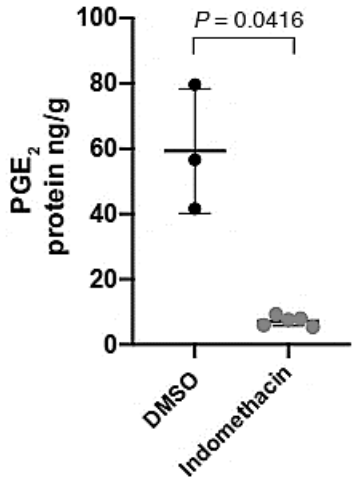

Figure 3. PGE_2 metabolism is conserved in zebrafish. Lipidomic analysis graph demonstrating significantly lower levels of PGE_2 (*P*=0.0416) after COX inhibition with 30μM Indomethacin (*N*=5, *n*=125); DMSO used as vehicle control (*N*=3, *n*=75). Two-tailed unpaired t-test with Welch's correction; Values plotted as mean ±SD and *P*<0.05 considered significant. Adapted from reference 63.

3.2 EP2 and EP4 receptors are expressed in the zebrafish pronephros.

To investigate and confirm the expression of EP2 and EP4 receptors prior to the pharmacological treatments, I performed fluorescent *in situ* hybridization (RNAscope assay, see Methods section for details) to visualize single mRNA molecules expressed in individual cells at 48 hpf in the zebrafish *Tg[wt1b:EGFP]* embryos labeling the glomeruli and the primary part of the pronephric tubules. Both EP2 (*ptger2a*) and EP4 (*ptger4b*) receptors are expressed in the glomerulus and tubules of the zebrafish pronephros (Fig.4). Markedly, the semi-quantitative analysis revealed a higher abundance of both receptors in the tubules (Fig.5).

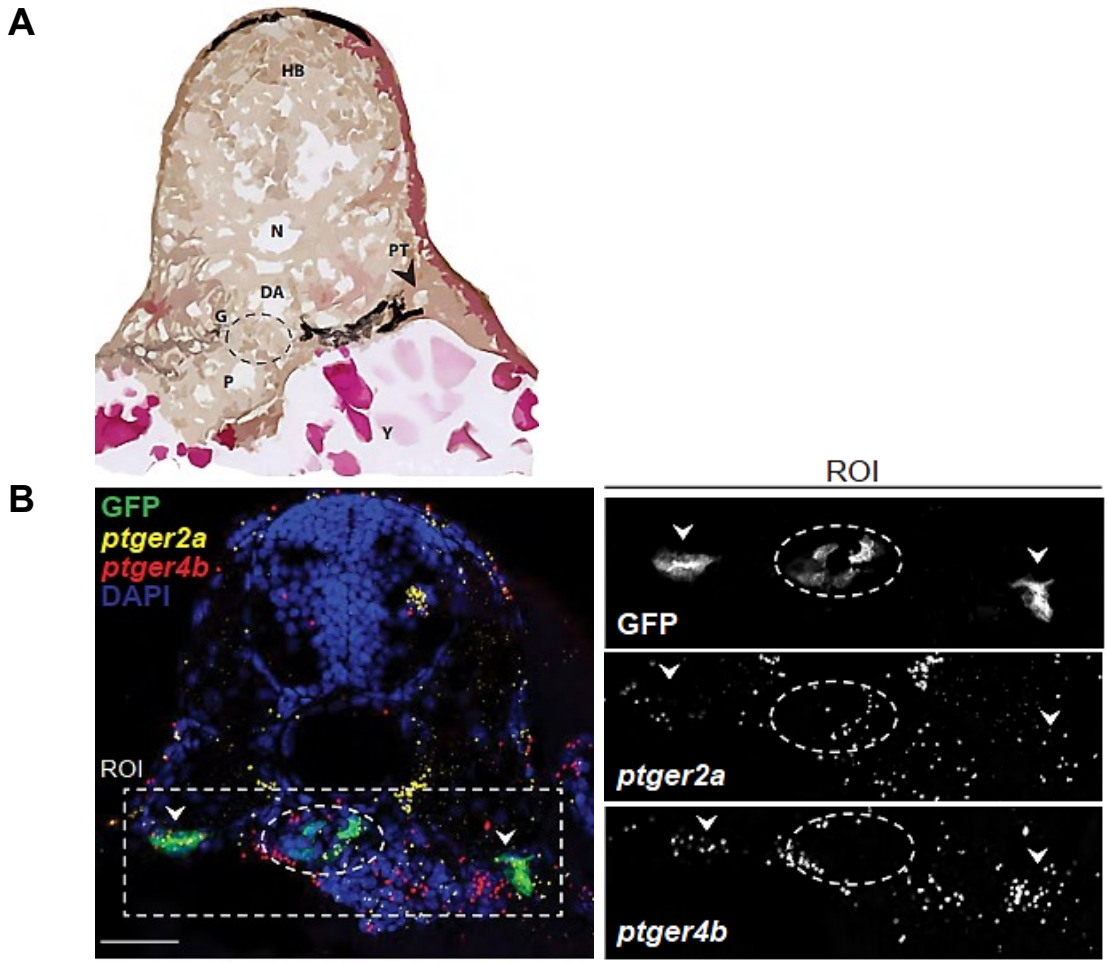

Figure 4. Fluorescent *in situ* hybridization of zebrafish embryo at 48 hpf. (A) Histological section of 48 hpf zebrafish embryo processed with "cutout" filter, demonstrates primary organs including glomerulus and kidney tubules; HB, hindbrain; N, notochord; DA, dorsal aorta; G, glomerulus, PT, pronephric tubules; P, pancreatic islet; Y, yolk. (B) RNAscope of EP2 (ptger2a) (yellow) and EP4 (ptger4b) (red) receptors in the zebrafish embryonic kidney at 48 hpf sectioned from the zebrafish transgenic line *Tg[wt1b:EGFP];* DAPI used for nuclei staining. Scale bar = 34 µm; dashed rectangle indicates the region of interest (ROI); dashed circles show the glomerulus and arrowheads indicate the pronephric tubules. Adapted from reference 63.

3.3 Both PGE_2 and 15-keto-PGE_2 bind EP2 and EP4 receptors *in vitro.*

[The experiments in the yeast were conducted in collaboration with the PhD student Debora Kaiser-Graf (AG Kreutz, SFB-1365)].

The activation of both EP2 and EP4 receptors by PGE_2 is widely investigated in numerous studies[53,57,59,78–80], however only recently its metabolite, 15-keto-PGE_2, (Fig. 6A) was shown to be able to bind both receptors *in vitro*[48,49]. The Nano-Glo® HiBiT extracellular detection system (see Methods for details) was used, to better understand the interaction between 15-keto-PGE_2 and the EP receptors. The assay was applied in the MMY28 yeast strain[62], in which the single GPCR was replaced upon transformation to express individually HiBiT-tagged human EP2 (hEP2) and EP4 (hEP4) receptors

(Fig. 6B). This allowed the quantification of the relative membrane expression of hEP2 and hEP4 receptors, before and after prostaglandin ligand stimulation (Fig. 6B). The transformed yeast cells were incubated with either 100nM PGE_2 or 1µM 15-keto-PGE_2 for 20min (Fig. 6B). The receptor count on the membrane was significantly increased, for both receptors, after the stimulation with both PGE_2 and 15-keto-PGE_2 as compared to the non-stimulated (absence of ligand) control condition (Fig. 6C, D).

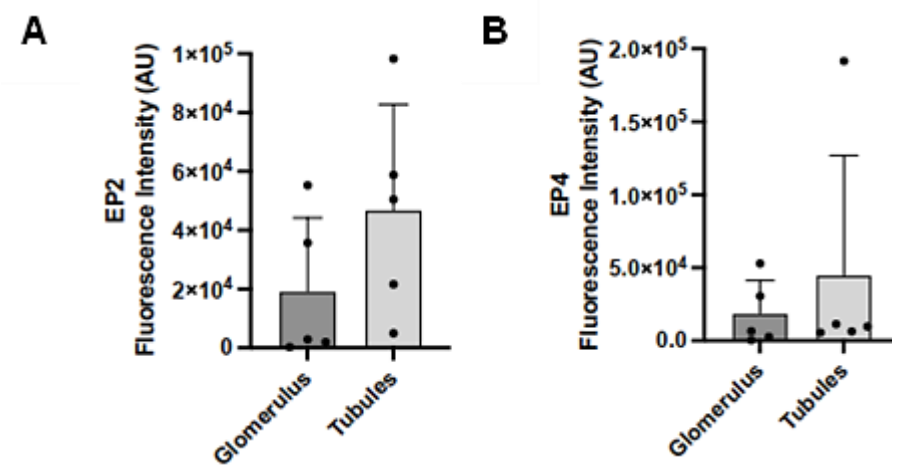

Figure 5. Semi-quantitative analysis of the fluorescence intensity. Analysis of (A) EP2 and (B) EP4 transcripts expressed in the GFP positive cells in the kidney area of *Tg[wt1b:EGFP]* embryos used for the histological sections on which the RNAscope analysis was performed (*N*=3, *n*=5); Two-tailed unpaired t test with Welch's correction; values are plotted as mean ± SD. Adapted from reference 63.

Our *in vitro* experiments indicated that apart from the well-established role of PGE_2[53,57,59,78–80], 15-keto-PGE_2 is also able to bind both EP2 and EP4 receptors and stabilize them on the plasma membrane, in agreement with recently published data[49].

3.4 Exogenous exposure to 15-keto-PGE_2 affects the early kidney development.

PGE_2 has been extensively reported to regulate the kidney development in zebrafish[57,81–83]. However, the potential biological effects of its metabolite, 15-keto-PGE_2, remain unresolved. Here, I opted for investigating the potential role of 15-keto-PGE_2 in zebrafish kidney biology. The pharmacological approach used for this purpose is similar to drug screenings that have previously demonstrated prostaglandin effects in the kidney morphogenesis[57].

I used the transgenic line *Tg[wt1b:EGFP]* to perform phenotypic assessment of the embryo development as well as kidney formation using brightfield and fluorescence microscopy (Fig. 7). Prior to the formation of GFB, namely from 6 hpf to 48 hpf, the embryos were exposed to the DMSO vehicle and 15-keto-PGE_2 (500 µM) (Fig. 7B). After early treatment with 15-keto-PGE_2, no profound phenotypic defects were detected

in the embryos at 48 hpf, with the exception of mild fluid accumulation (edema) observed in the yolk area, characteristic of kidney dysfunction (Fig. 7B, C). Overall, the morphology of the embryonic kidney was significantly affected and associated with the impaired glomerular development and defects in the pronephric tubular angle (Fig. 7B).

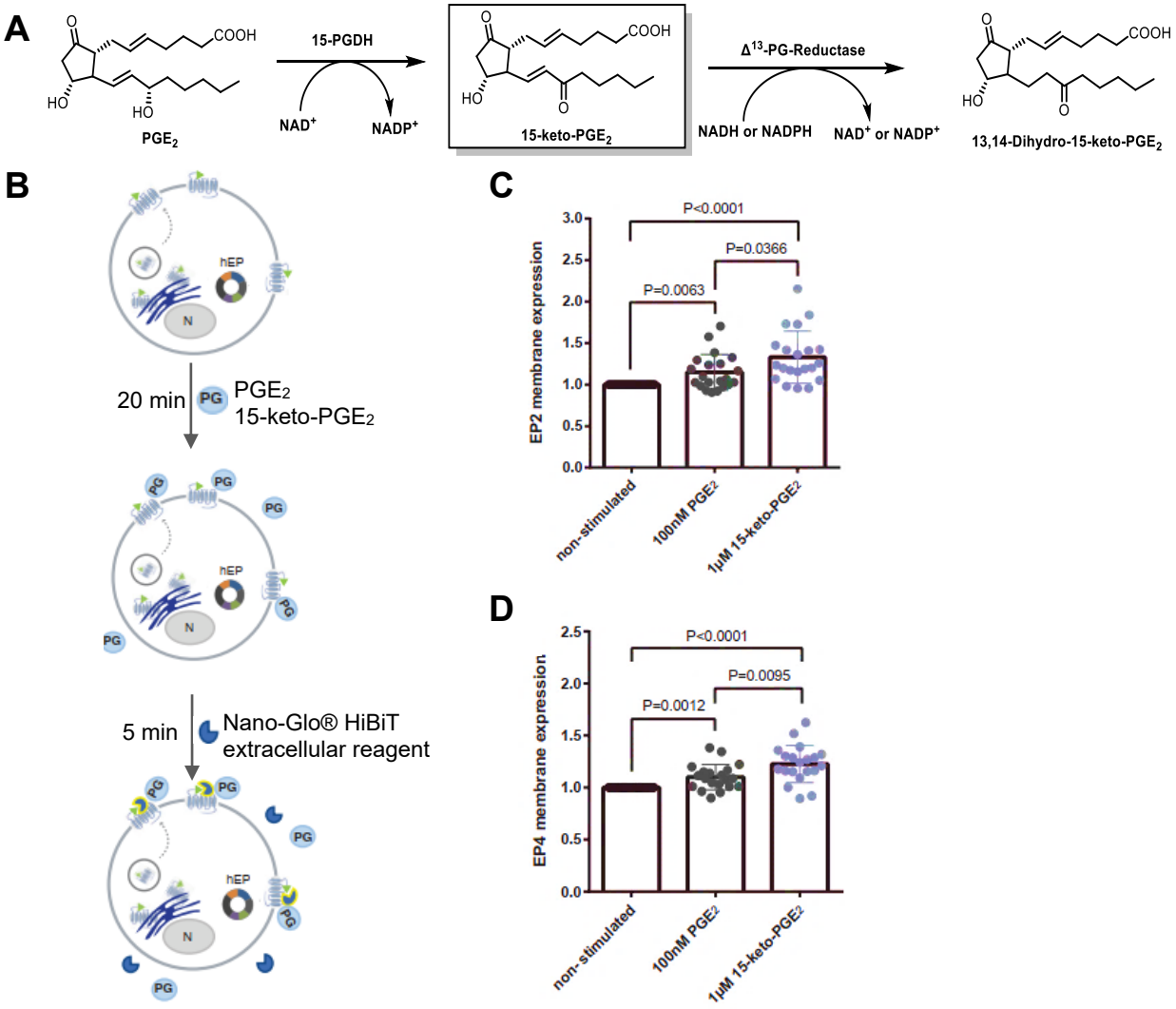

Figure 6. PGE_2 metabolic product, 15-keto-PGE_2 binds EP2 and EP4 receptors *in vitro*. (A) Inactivation pathway of PGE_2, highlighting the 15-keto-PGE_2 metabolite. (B) Schematic of Nano-Glo® HiBiT Extracellular Detection system assay for the measurement of the receptors membrane expression. First, either PGE_2, 15-keto-PGE_2, or an equal volume of medium (non-stimulated control), was used for the 20 min stimulation of the HiBiT-tagged hEP2 or hEP4 receptors on the yeast membrane to allow ligand binding. As a second step, the number of receptors on the membrane was quantified by the Nano-Glo® HiBiT extracellular reagent (containing Buffer, substrate, and LgBiT protein), resulting in generated luminescence by structural complementation of LgBiT proteins with extracellular displayed HiBiT-tags; N represents cell nucleus. Quantification graphs of the cell membrane expression of (C) HiBiT-tagged hEP2 and (D) HiBiT-tagged hEP4 receptors, after 20 min stimulation with PGE_2 (dark grey) and 15-keto-PGE_2 (light grey). Statistics were performed with the Wilcoxon test and Mann-Whitney tests. For EP2: non-stimulated vs PGE_2 P=0.0063; non-stimulated vs 15-keto-PGE_2 P<0.0001; PGE_2 vs 15-keto-PGE_2 P=0.0366. For EP4: non-stimulated vs PGE_2 P=0.0012; non-stimulated vs 15-keto-PGE_2 P<0.0001; PGE_2 vs 15-keto-PGE_2 P=0.0095. Values are plotted as mean ± SD; $P < 0.05$ is considered significant; one outlier was identified among EP2-transfected and two outliers among EP4-transfected yeasts (for all yeast experiments conducted on the same day). Adapted from reference 64.

3.5 PGE_2, but not 15-keto-PGE_2 causes albuminuria-like phenotype *in vivo.*

After confirming that the PGE_2 pathway is conserved in zebrafish and its catabolism yields considerably high levels of 15-keto-PGE_2, which is able to bind and stabilize both EP2 and EP4 receptors *in vitro*, I proceeded with the exogenous pharmacological treatments to test its potential physiological role *in vivo*. In order to investigate and characterize how PGE_2 and its metabolite affect GFB integrity at functional level, I used a zebrafish transgenic line *Tg[fabp10a:gc-EGFP]* that allows the evaluation of GFB defects by monitoring the excretion of gc-EGFP, thus mimicking the albuminuria-like phenotype in the developing zebrafish embryos[61]. The vitamin D protein tagged with green fluorescent protein (gc-EGFP) is normally present in the vasculature of healthy embryos, but upon GFB damage leaks through the glomeruli resulting in an albuminuria-like phenotype.

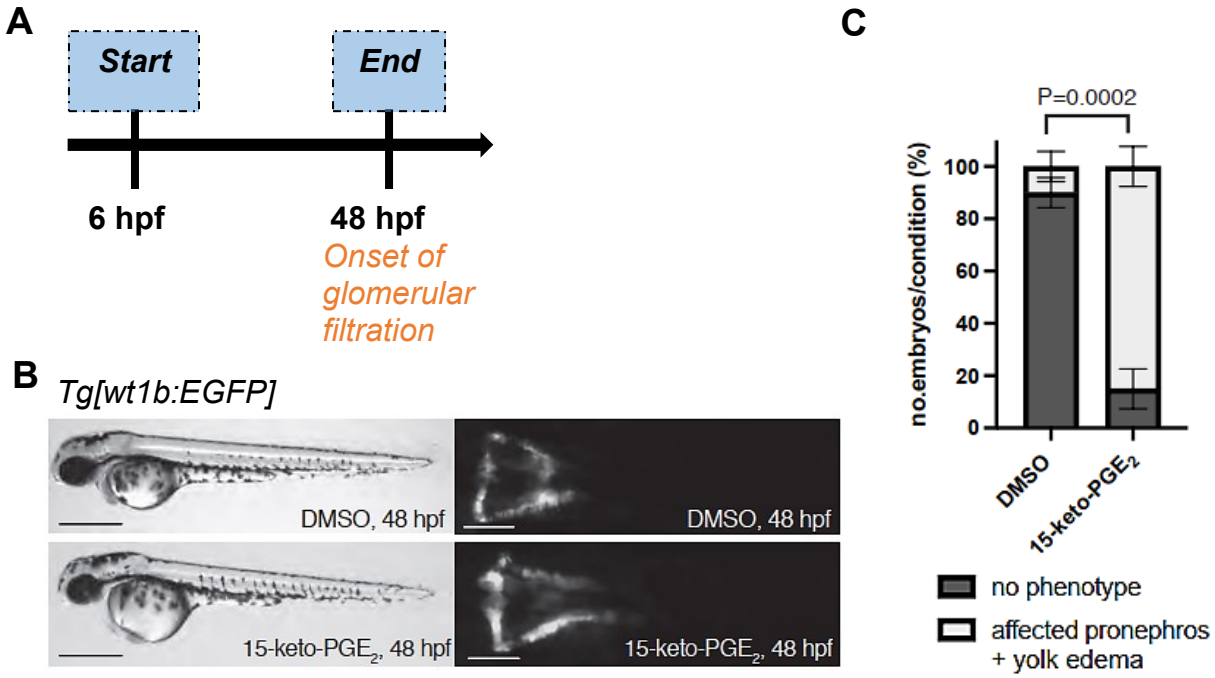

Figure 7. Early treatment with 15-keto-PGE_2 affects zebrafish embryonic kidney at 48 hpf. (A) Pharmacological early exposure to 15-keto-PGE_2, starting from 6 hpf until 48 hpf. (B) Brightfield and fluorescence microscopy images of *Tg[wt1b:EGFP]* embryos at 48 hpf, after exposure to DMSO 0.88 % (upper panel) and 15-keto-PGE_2 500 µM (lower panel). Scale bar: 500 µm for brightfield images and 200 µm for fluorescent images. (C) Phenotypic analysis (N = 3, n = 30 for each condition) of 48 hpf zebrafish embryos, grouped in two categories: “no phenotype” (pronephros morphology remains unaffected after DMSO treatment) or “affected pronephros + yolk edema” (affected pronephros after exposure to 15-keto-PGE_2); Percentage values are plotted as mean ± SD; n represents biologically independent samples over N independent experiments; Ordinary two-way ANOVA with Tukey's multiple comparison test (P = 0.0002); $P < 0.05$ considered significant. Adapted from reference 64.

The embryos were exposed to either a long-acting derivative of PGE_2, $dmPGE_2$ (125µM), or 15-keto-PGE_2 (500µM) from 72 hpf to 96 hpf, i.e., after the complete formation of the functional GFB (Fig. 8A). Zebrafish embryos appeared normal after stimulation with PGE_2 and exhibited only lack of swim bladder formation (Figure 8B) when inspected with brightfield microscopy. However, a marked reduction of EGFP fluorescence in the trunk vasculature of *Tg[fabp10a:gc-EGFP]* embryos exposed to PGE_2 was observed when compared to the control conditions, thus mimicking an albuminuria-like phenotype and indicating the leakage of the gc-EGFP protein and a functional permeability defect of the GFB (Fig. 8B, 9A). Exogenous exposure to 15-keto-PGE_2 resulted in the defects of the body axis in the embryos at 96 hpf, the absence of the swim bladder formation, and the expansion of the liver (Fig. 8C). Interestingly, in contrast to PGE_2 treatment, no significant GFB permeability defects (albuminuria-like phenotype) were observed as the GFP signal was comparable between the control and 15-keto-PGE_2-treated embryos (Fig. 9B).

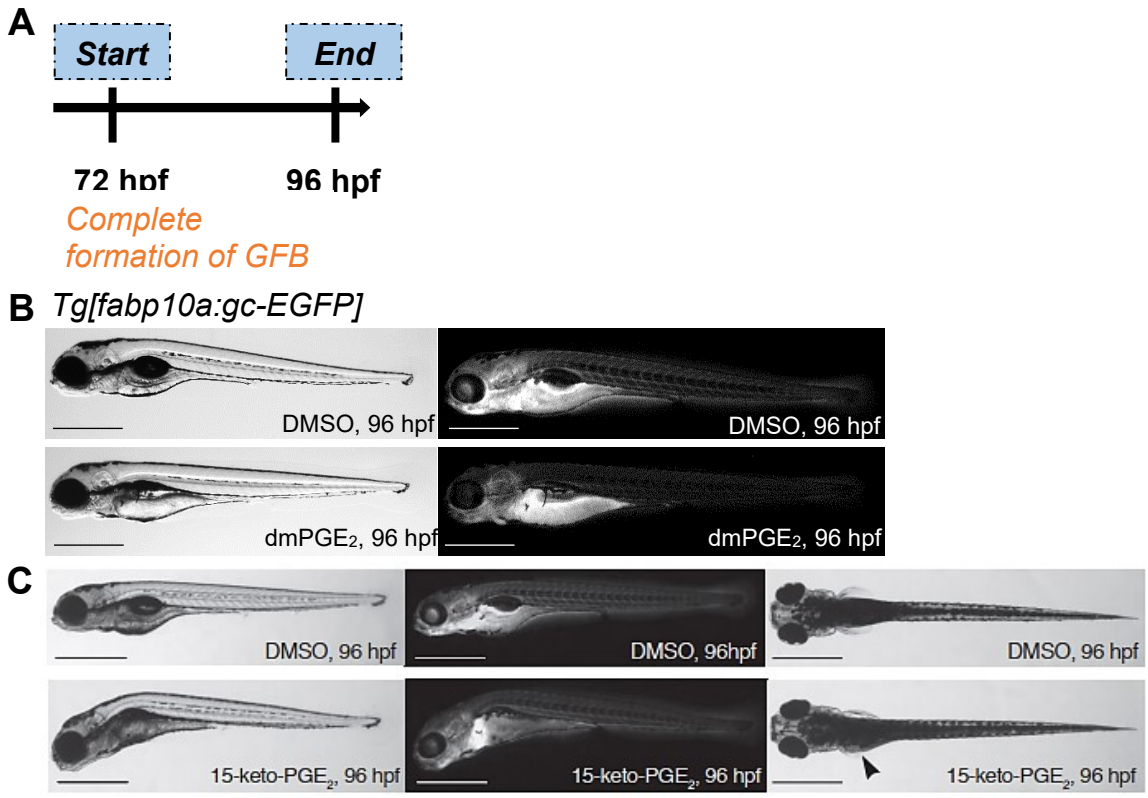

Figure 8. Late pharmacological exposure to $dmPGE_2$ and 15-keto-PGE_2. (A) Late treatment experimental design, starting from 72 hpf until 96 hpf. (B) Brightfield and fluorescence microscopy images of *Tg[fabp10a:gc-EGFP]* embryos at 96 hpf, after exposure to DMSO vehicle 0.32 % (upper panel) and $dmPGE_2$ 125 µM (lower panel). *N*=6, *n*=120 for each condition; Scale bar: 1 mm. (C) Brightfield and fluorescence microscopy images of *Tg[fabp10a:gc-EGFP]* embryos at 96 hpf, after exposure to DMSO vehicle 0.88 % (upper panel) and 15-keto-PGE_2 500µM (lower panel). *N*=3, *n*=60 for each condition; arrowhead indicates liver expansion; Scale bar: 1mm. *n* represents biologically independent samples over *N*-independent experiments. Adapted from reference 64.

3.6 EP2 and EP4 antagonists rescue the albuminuria phenotype in both zebrafish and rat models.

Based on recent *in vitro* data highlighting the importance of PGE_2/EP2/EP4 signaling in human podocytes injury and glomerular hyperfiltration (GH)[59], I aimed to study the effects of the same pathway *in vivo*. Since I demonstrated that exogenous PGE_2 exposure resulted in albuminuria-like phenotype *in vivo* (see section 3.5), indicating the implication of this pathway in the albuminuria development, I was prompted to investigate the potential renoprotective role of separate or combined pharmacological blockade of EP2 and EP4 receptors, which concerted signaling has been previously reported to play a crucial role in podocytes injury[59]. It has been shown that MWF rat, an established animal model of albuminuria/proteinuria and hypertension, demonstrates elevated levels of glomerular PGE_2 in young MWF at the onset of albuminuria (8 weeks of age) as compared to albuminuria resistant spontaneously hypertensive rats (SHR)[59] (Fig. 10).

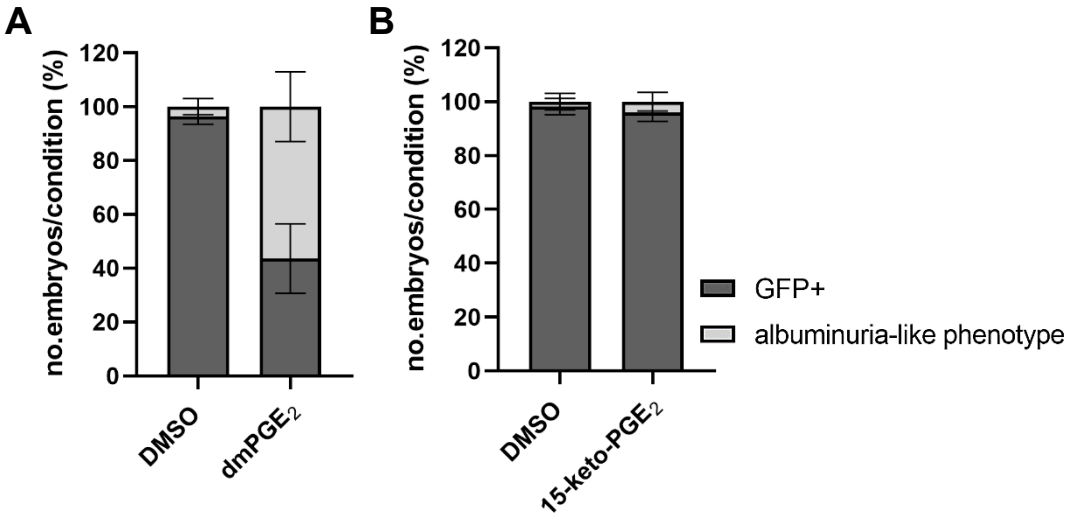

Figure 9. Exposure to PGE_2, but not 15-keto-PGE_2 causes albuminuria-like phenotype. (A) Quantitative analysis of *Tg[fabp10a:gc-EGFP]* zebrafish embryos' phenotype at 96 hpf after exposure to either $dmPGE_2$ (A) or 15-keto-PGE_2 (B). Significant fluorescence reduction was observed after treatment with $dmPGE_2$, while no profound fluorescence signal change was detected after exogenous exposure to the metabolite. Statistics performed with ordinary two-way ANOVA with Tukey's multiple comparison test (P <0.0001 for graph A and P = 0.8438 for graph B). In both graphs, embryos are categorized as "GFP +" (fluorescence signal (gc-EGFP) observed in the trunk vasculature) or "albuminuria-like phenotype" (partial or complete loss of gc-EGFP fluorescence signal in the trunk vasculature); Percentage values are plotted as mean ± SD; P < 0.05 considered significant. Adapted from references 63 and 64.

Here, I followed similar pharmacological approach, as described in section 3.5, for separate and combined blockade of EP2 and EP4 receptors *in vivo* using the PF-04418948 and ONO-AE3-208 antagonists, respectively. Apart from the *Tg[fabp10a:gc-*

EGFP] zebrafish embryos, treated from 72 hpf to 96 hpf, MWF rats (experiments performed by Dr. rer. medic. Angela Schulz, AG Kreutz, SFB-1365) were also exposed to the same EP receptors antagonists, starting the treatment at the onset of albuminuria at 4 weeks and continue until 12 weeks. The time-course analysis of the albuminuria phenotype in urine samples collected in metabolic cages for 24h[66] was performed at 4, 8 and 12 weeks of age.

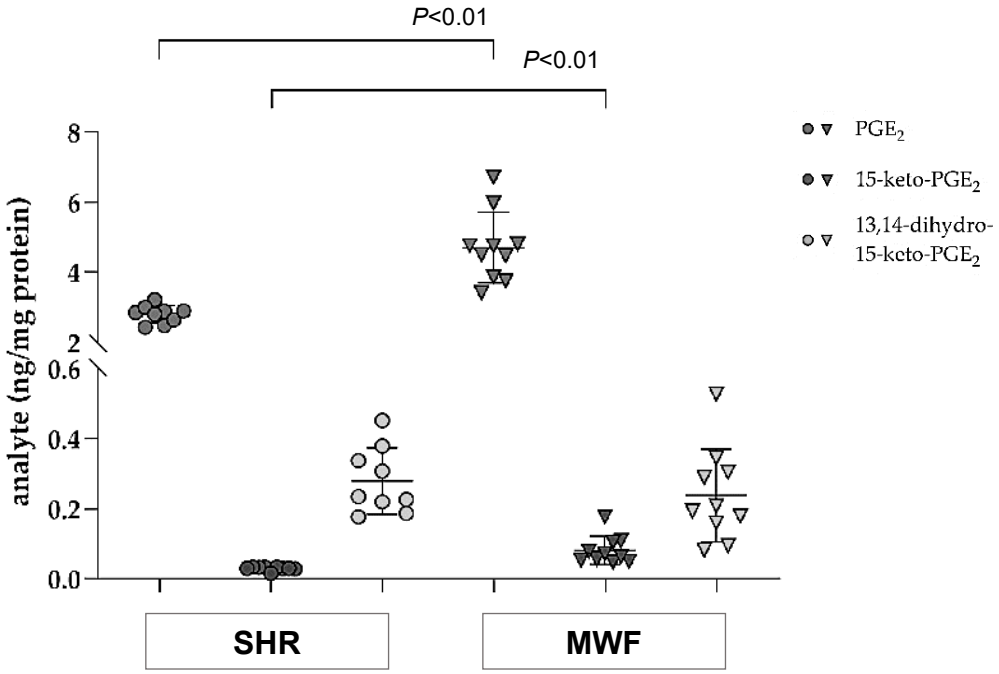

Figure 10. Lipidomic analysis on MWF rat glomeruli. Measured levels of PGE_2 (grey), 15-keto-PGE_2 (dark grey), and 13,14-dihydro-15-keto-PGE_2 (light grey) in the glomeruli of MWF (triangles) and SHR (circles) rats at 8 weeks of age. Elevated levels of glomerular PGE_2 and 15-keto-PGE_2 in MWF compared to SHR, while for 13,14-dihydro-15-keto-PGE_2 no significant changes in the glomerular levels were detected between the strains. Each data point represents a single animal; values plotted as mean ± SD per rat strain consisting of n=9–10 animals each; Two-tailed Student's t-test; P< 0.01; $P < 0.05$ considered significant. Adapted from reference 59.

In zebrafish, the albuminuria-like phenotype caused by exogenous PGE_2 exposure was significantly reversed by either separate or combined blockade of EP2 and EP4 receptors, as well as by indomethacin treatment (Fig. 11A, B). In MWF rat, albuminuria was not significantly reduced by the separate EP2 or EP4 blockade. However, combined EP2 and EP4 blockade resulted in a profound and significant suppression of albuminuria compared to the control and single EP4 receptors blockade at 8 weeks, while at 12 weeks there was a significant difference compared to all groups (Fig. 11C). Importantly, the dual blockade induced no changes in either systolic blood pressure (Fig. 12A) or creatinine clearance (Fig. 12B).

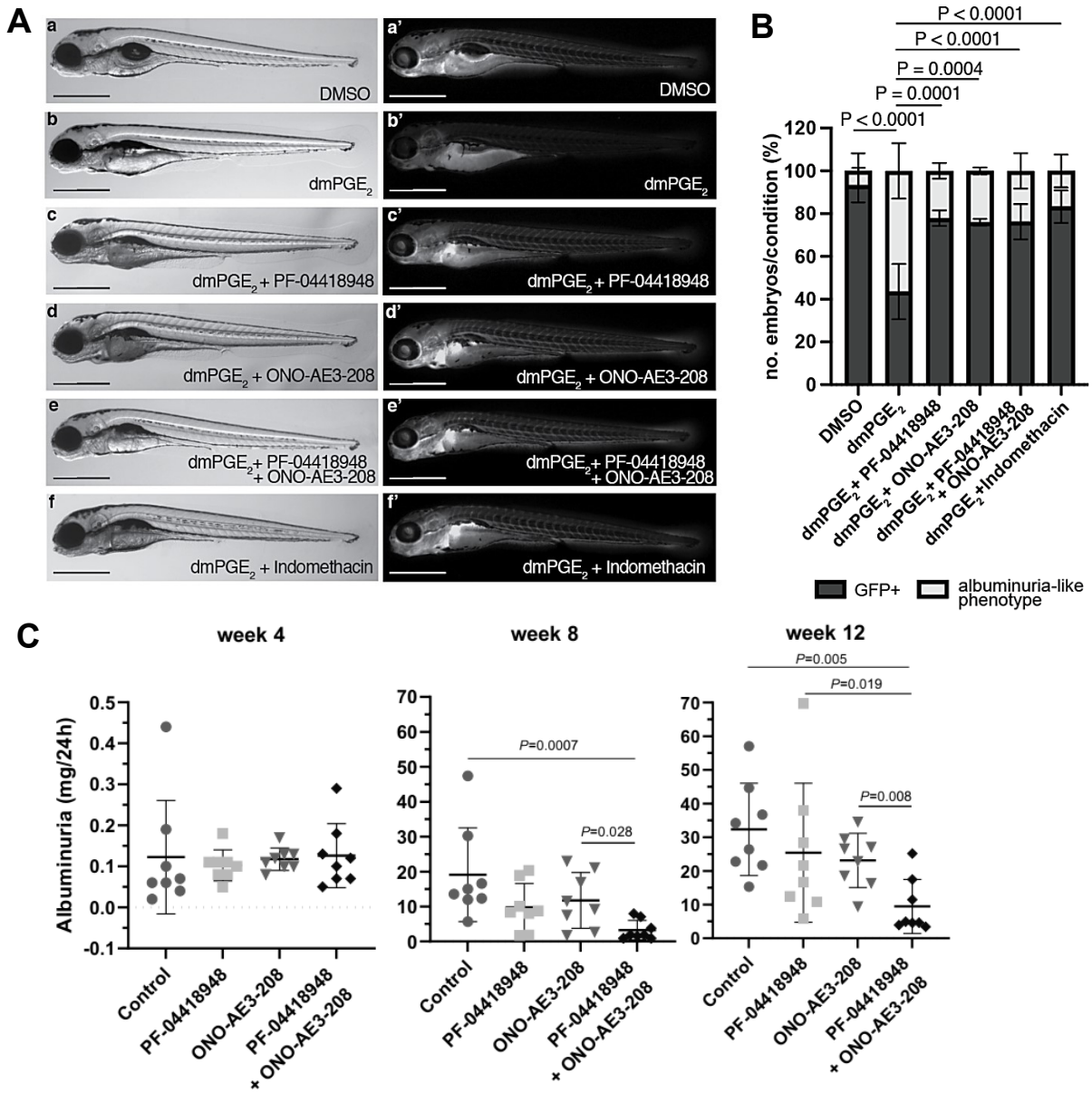

Figure 11. Combined pharmacological blockade of EP2 and EP4 receptors rescues albuminuria in both zebrafish and MWF rat.

(A) Brightfield and fluorescence microscopy images of *Tg[fabp10a:gc-EGFP]* embryos at 96 hpf, following pharmacological treatments: (a, a') DMSO (vehicle) 0,32 %, (b, b') dmPGE$_2$ 125 µM, (c, c') dmPGE$_2$ 125 µM + PF-04418948 20 µM, (d, d') dmPGE$_2$ 125 µM + ONO-AE3-208 20 µM, (e, e') dmPGE$_2$ 125 µM + PF-04418948 20 µM + ONO-AE3-208 20 µM, (f, f') dmPGE$_2$ 125 µM + indomethacin 30 µM; *N*=6, *n*=120 for each of the conditions except treatments c and d (*N*=3, *n*=60); Scale bar = 1mm. (B) Quantitative analysis of the phenotype observed in drug-treated *Tg[fabp10a:gc-EGFP]* embryos at 96 hpf. Embryos are categorized as "GFP +" (green fluorescence signal visible in the trunk vasculature) or "albuminuria-like phenotype" (partial or complete loss of gc-EGFP fluorescence signal in the trunk vasculature). Percentage data are plotted as mean ± SD; *n* represents biologically independent samples over *N* independent experiments; Ordinary two-way ANOVA with Tukey's multiple comparison test. (C) Time-course analysis of urinary albumin excretion in male MWF rats during the onset of albuminuria between week 4 and 12. Rats per group *n*=7-8 for each condition; Two-way ANOVA with Bonferroni's post hoc analysis, used for the statistical analysis, showed a significant correlation between treatment groups and the different time-points (*P*=0.002) regarding albuminuria levels. Albuminuria was significantly increased over time, with the dual blockade group demonstrating a significant difference compared to all other groups (*P*<0.01, respectively). Adapted from reference 63.

Overall, the *in vivo* pharmacological experiments performed in both animal models, reveal the importance of PGE_2/EP2/EP4 signaling in GH and albuminuria and highlight the renoprotective role of combined EP receptors blockade as potential therapeutic targets.

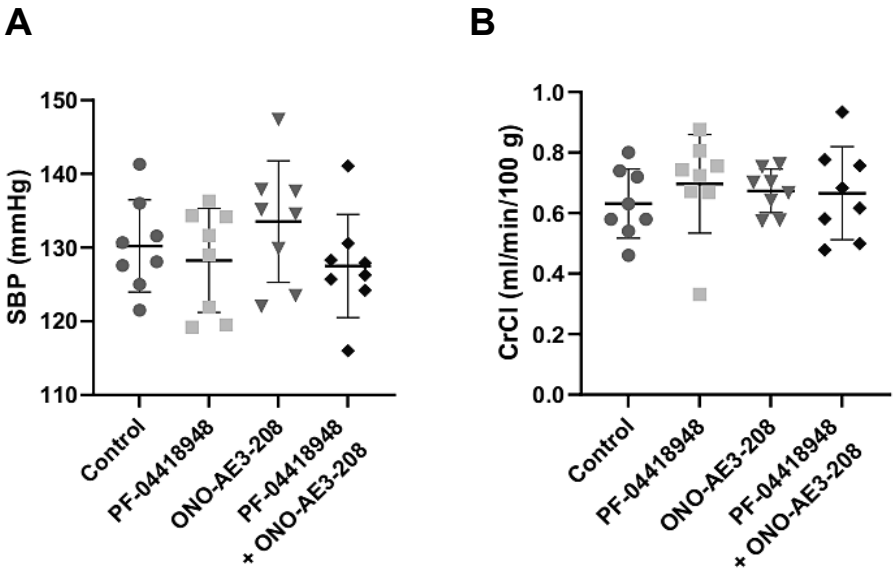

Figure 12. Time-course analysis of systolic blood pressure and creatinine clearance. (A) systolic blood pressure (SBP) and (B) creatinine clearance (CrCl) in male MWF rats at 12 weeks of age. Rats per group *n*=7-8 for each condition; One-way ANOVA with Bonferroni's post hoc analysis. Adapted from reference 63.

3.7 Glomerulus development and vascularization in the zebrafish pronephros.

I aimed to understand the changes in glomerular structure resulting from different pharmacological treatments (dmPGE_2, 15-keto-PGE_2, and EP receptor antagonists) using 3D high-resolution confocal microscopy imaging to resolve the cytoarchitecture of the glomerulus at a subcellular level. Previous visualization of glomerular morphology changes during kidney development in zebrafish has been limited[84–89]. In the present thesis, I used the *Tg[wt1b:EGFP]* zebrafish line to study the critical stages of glomerulus formation. The analysis followed five developmental stages (30, 48, 52, 72, 120 hpf) and in addition bovine serum albumin (BSA) marked with AlexaFluor555 was used to label the glomerular vasculature (endothelial cells-formed capillaries) as previously reported[90].

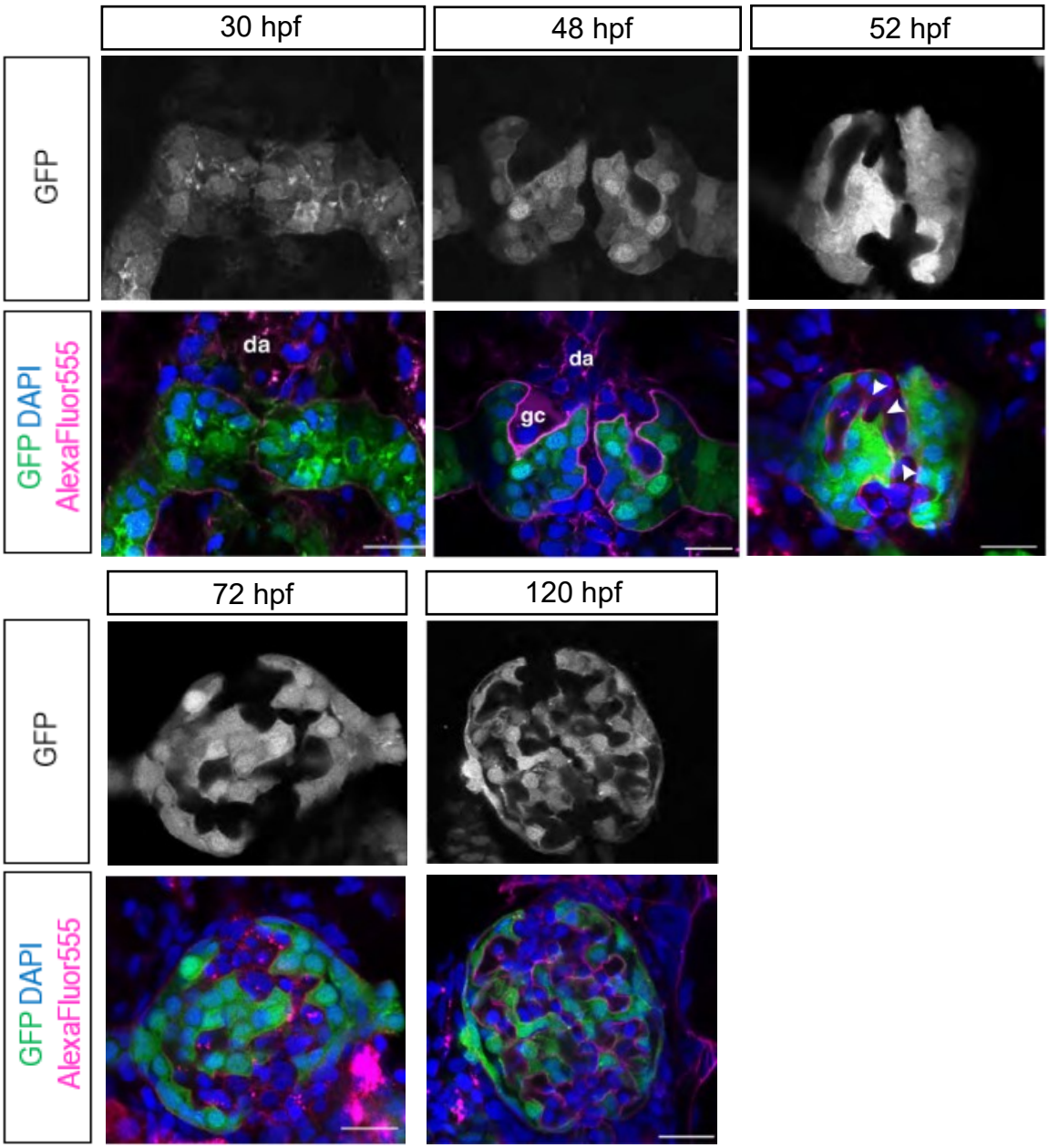

Figure 13. Morphological visualization of zebrafish embryonic glomerulus. Representative 3D high-resolution confocal microscopy images (single confocal section) of the *Tg[wt1b:EGFP]* zebrafish glomeruli at five different developmental stages (30 hpf, 48 hpf, 52 hpf, 72 hpf and 120 hpf). The glomerular podocytes and parietal epithelial cells presented in grayscale (top panels) and in green (in merge, lower panels), while the glomerular endothelial cells-capillaries are shown in magenta (BSA-AlexaFluor555, in merge), and cells nuclei in blue (DAPI, in merge). Podocyte protrusions (arrowheads) start surrounding the glomerular capillaries are observed at 52 hpf. Dorsal aorta (da) and characteristic glomerular cleft (gc) are observed at the early developmental stages of the glomerulus. Scale bar = 10 μm. Adapted from reference 64.

At 30 hpf, in nephron primordia stage (the most immature stage of the nephrons), the glomeruli appear as a non-vascularized group of cells directly abutting the dorsal aorta

at the embryo midline (Fig.13, 30 hpf). During the next developmental steps, at 48 hpf, endothelial cells slowly begin to invade and occupy the area between the nephron primordia, thus driving the invagination of the podocytes and establishing the characteristic glomerular cleft (Fig.13, 48 hpf). In the following developmental stage, at 52 hpf, the intricate intercalation of podocytes spreads around the steadily expanding glomerular capillaries (Fig.13, 52 hpf), resulting at 72 hpf in the formation of podocytes finger-like projections intertwining with forming capillaries, similar to the interlaced fingers of clasped hands (Fig.13, 72 hpf). At this stage the formation of GFB is complete in zebrafish[11,84,91]. The complicated intercalation between endothelial cells and podocytes persists until 120 hpf (Fig.13, 120 hpf). In the end, the glomeruli and functioning filtration system are fully matured as a result of the increasing infoldings of the GBM caused by cell-cell contacts between endothelial cells and podocytes.

3.8 Kidney defects after exogenous PGE_2 stimulation - glomerular cytoarchitecture and ultrastructure analysis.

It has been shown that increased fluid flow shear stress in glomeruli results in elevated levels of PGE_2 that causes podocyte damage and potential albuminuria[59].

As described in section 3.5, I established a zebrafish disease model that mimics the pathological albuminuria state by exposing zebrafish embryos to $dmPGE_2$ after the complete formation of GFB, namely from 72 hpf to 96 hpf (Fig. 8B, 11A). I performed a detailed analysis of the glomerular cytoarchitecture using *Tg[wt1b:EGFP]* transgenic line in combination with angiography using BSA conjugated with AlexaFluor555 to mark the endothelial cells of glomerular capillaries.

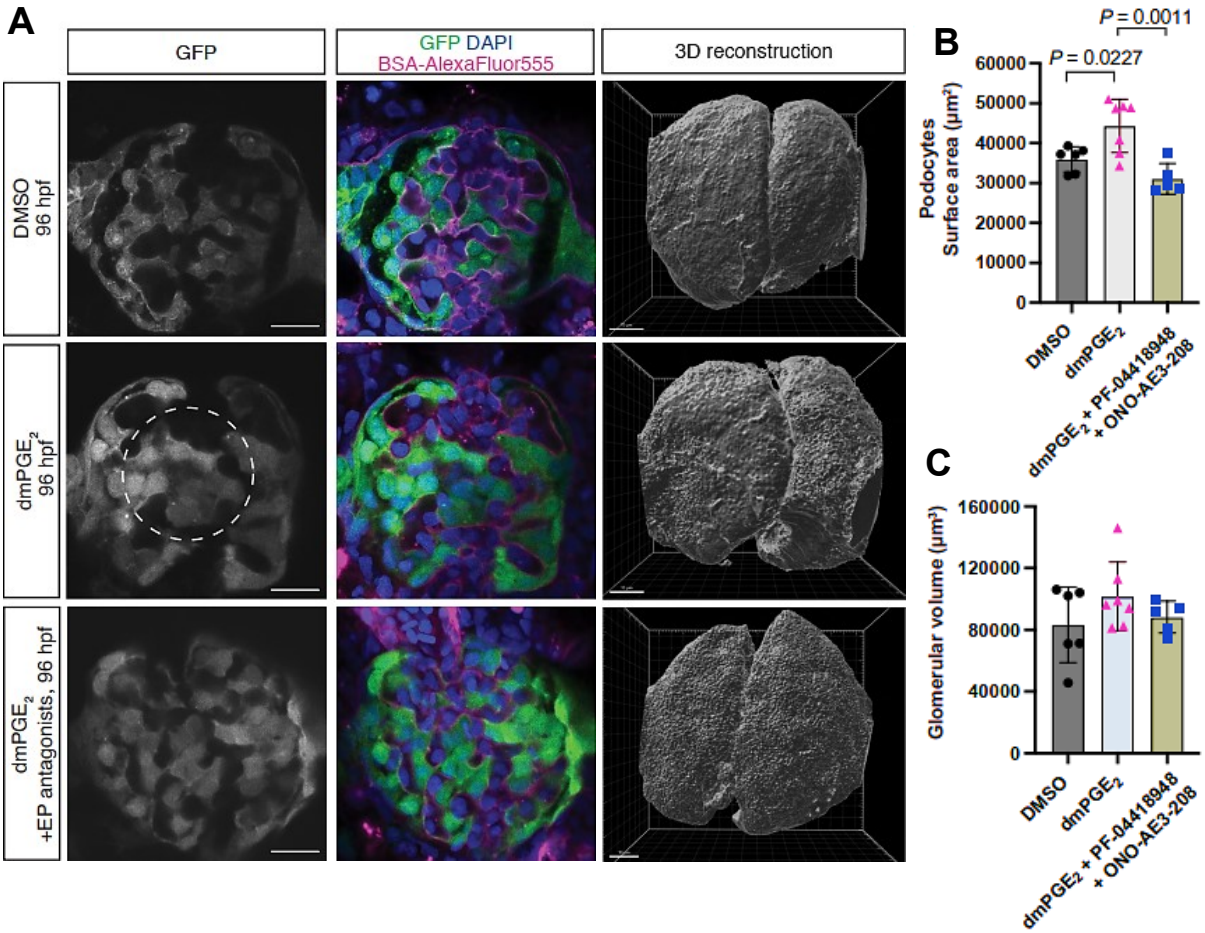

Figure 14. Exogenous PGE_2 treatment affects glomerular cytoarchitecture and the podocyte surface area. (A) High-resolution confocal microscopy analysis of the glomerulus at 96 hpf after DMSO vehicle 0.96% (top) (N = 3, n = 6) $dmPGE_2$ 125 µM (middle) (N = 3, n = 7), and $dmPGE_2$ 125 µM + PF-04418948 20 µM + ONO-AE3-208 20 µM (bottom) (N = 3, n =5); Representative 2D grayscale and pseudo-colored images (left and middle panels, respectively) and 3D glomerular reconstruction (right panels) of *Tg[wt1b:EGFP]* zebrafish glomeruli at 96 hpf; Scale bar = 10 µm; dashed circle indicates the podocyte intercalation defects. (B,C) Quantitative graphs of podocytes surface area and the glomerular volume of the glomeruli analyzed for the different pharmacological treatment groups; Ordinary one-way ANOVA with Tukey's multiple comparison test was performed for both graphs; in graph B: DMSO vs $dmPGE_2$ (P = 0.0227), $dmPGE_2$ vs dmPGE2 + PF-04418948+ ONO-AE3-208 (P = 0.0011) and DMSO vs $dmPGE_2$ + PF-04418948 + ONO-AE3-208 (P = 0.2748). No significant changes were observed in glomerular volume. Values are plotted as mean ± SD; $P < 0.05$ is considered significant. In all confocal microscopy images, the glomerular podocytes and parietal epithelial cells are shown either in greyscale or in green (EGFP); endothelial cells of glomeruli capillaries are marked in magenta (BSA-AlexaFluor555) and cells nuclei in blue (DAPI). One sample from DMSO and two samples from the combined EP2 and EP4 blockade were excluded from the analysis as the imaging resolution did not provide distinct glomerular GFP positive boundaries for proper surface outline of the glomeruli. Adapted from reference 63.

The exogenous stimulation with PGE_2 had a profound impact on the maturation of the glomeruli in zebrafish embryos at 96 hpf (Fig. 14). High-resolution confocal imaging allowed me to observe the cellular defects arising after the PGE_2 exposure, by revealing impaired podocyte intercalation around the glomerular capillaries (Fig. 14A, middle panels). Importantly, apart from the profound reduction of the albuminuria-like

phenotype described above, the glomerular morphology was also restored after combined pharmacological blockade of EP2 and EP4 receptors (Fig. 14A, bottom panels). I used 3D reconstruction and surface rendering to quantify the defects in the GFP-labeled glomeruli using segmentation techniques. Additionally, I measured glomerular volume and podocyte surface area in three different conditions: DMSO-treated, dmPGE2-treated and dmPGE$_2$+EP2/EP4 blockade (Fig. 14B, C). This analysis revealed a significant increase of podocyte surface area in response to dmPGE$_2$ exposure (Fig. 14B), which might consequently affect GFB function. Importantly, both podocyte intercalation and surface area defects were restored after combined blockade of EP2 and EP4 receptors (Fig. 14A, B), supporting the importance of the PGE$_2$/EP2/EP4 signaling axis for GFB integrity.

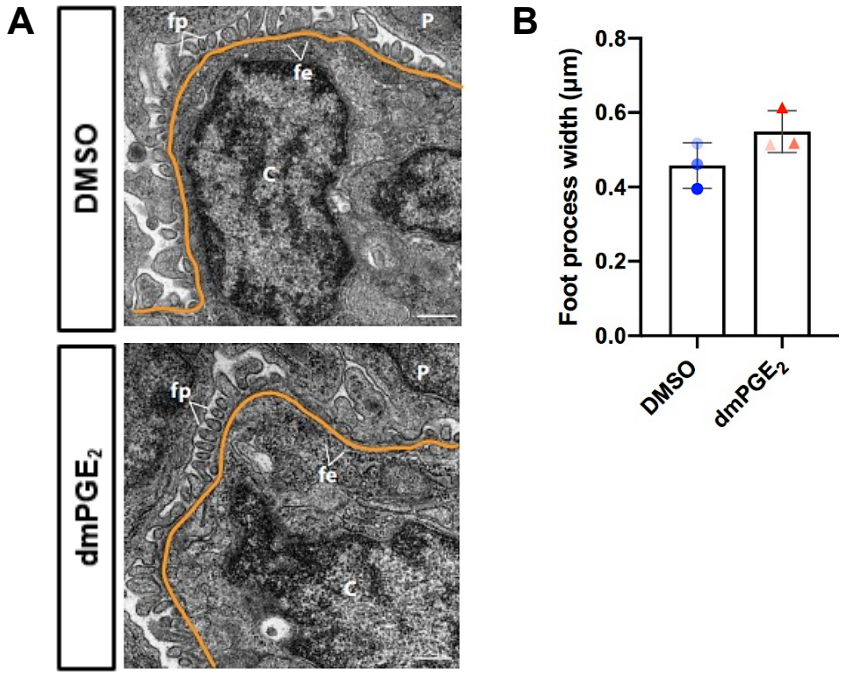

Figure 15. Ultrastructural analysis of 96 hpf zebrafish glomeruli after exposure to PGE$_2$. Pharmacological treatment with (A) DMSO vehicle 0.32% (top) and dmPGE$_2$ 125 µM (bottom); Scale bar=1µm; fe, fenestrated endothelium; fp, foot processes; C, capillaries; P, podocyte cell body. GBM is indicated with the colored line. (B) Quantitative analysis of foot process width (n = 3 for each condition) indicative of potential foot process effacement; Two-tailed unpaired t test with Welch's correction (P = 0.1303). Values are plotted as mean ± SD; P<0.05 is considered significant. Adapted from reference 63.

Ultrastructural analysis of the glomeruli was performed in both zebrafish embryos at 96 hpf and MWF rats at 12 weeks of age, using EM.

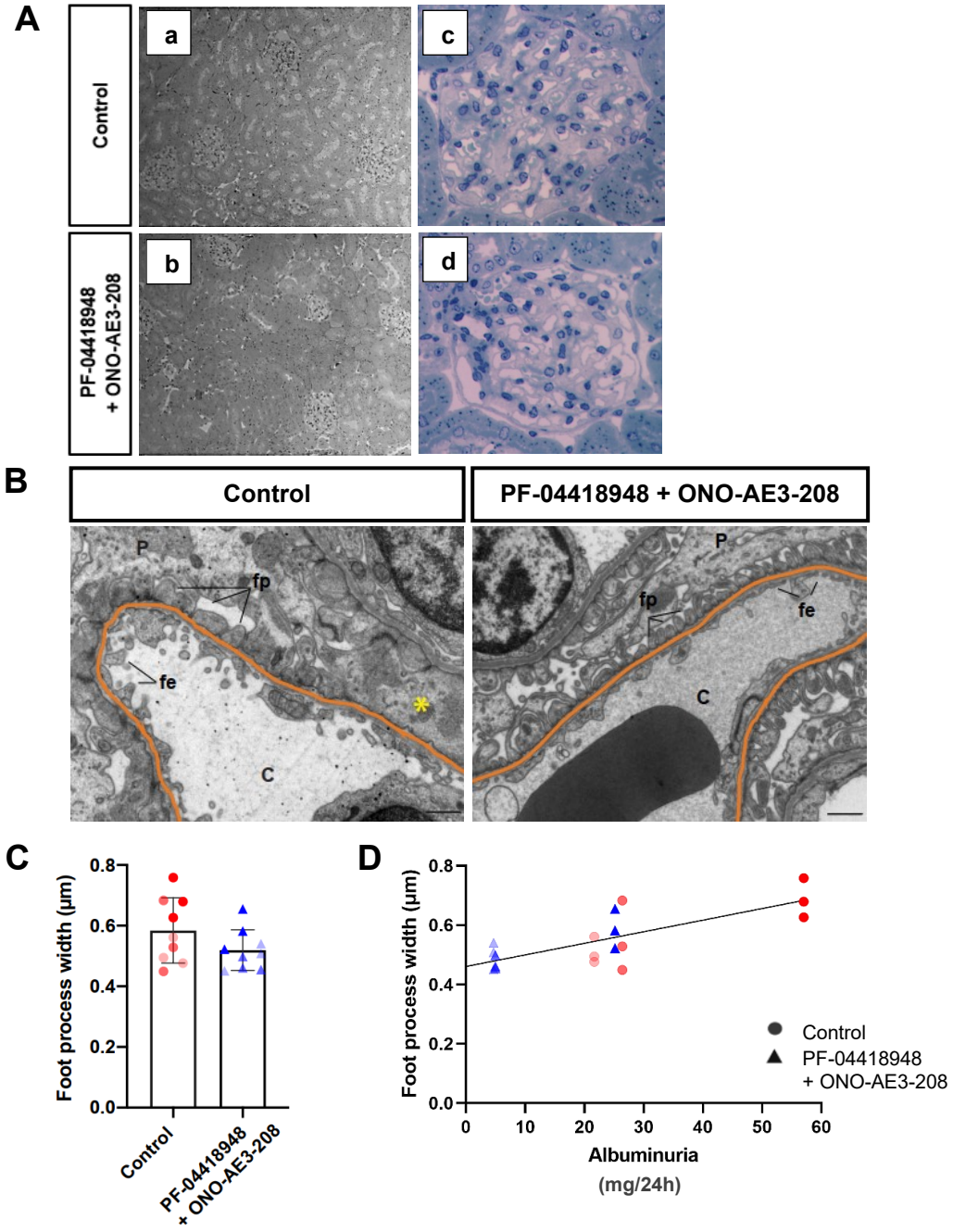

Figure 16. Ultrastructural analysis of MWF rat glomeruli after combined pharmacological blockade of EP2 and EP4 receptors. (A) Representative brightfield images of semi-thin renal sections from MWF control (top, panels a, c) and MWF+PF-04418948+ONO-AE3-208 (bottom, panels b, d) rats, show no obvious differences in glomerular morphology between the groups; original magnification x10 (panels a, b) and x200 (panels c, d). (B) Representative EM images of MWF control (left) and dual EP receptors blockade (right); Scale bar = 1 µm; fe, fenestrated endothelium; fp, foot processes; C, capillaries; P, podocyte cell body. GBM is indicated with the colored line; asterisk (*) indicates foot process effacement. (C) Quantitative analysis of foot process width (n = 9 glomeruli per group, obtained from 3 animals for each condition). The glomeruli derived from one animal are labeled with different shades of red for the control and blue for the antagonists-treated group. Two-tailed unpaired t test with Welch's correction (P = 0.149); Values are plotted as mean ± SD; P<0.05 is considered significant. (D) Spearman correlation plots show a significant correlation between albuminuria levels (mg/24h) and foot process width; correlation (r=0.599, P=0.0086); color code is the same as in graph C. Adapted from reference 63.

The qualitative analysis did not reveal any statistically significant alterations or defects in the GFB and glomerular capillaries in neither of the animal models (Fig. 15, 16B-D). Furthermore, the examination of kidney structure through light microscopy showed no alterations in response to EP2 and EP4 blockage in young MWF rats (Fig. 16A).

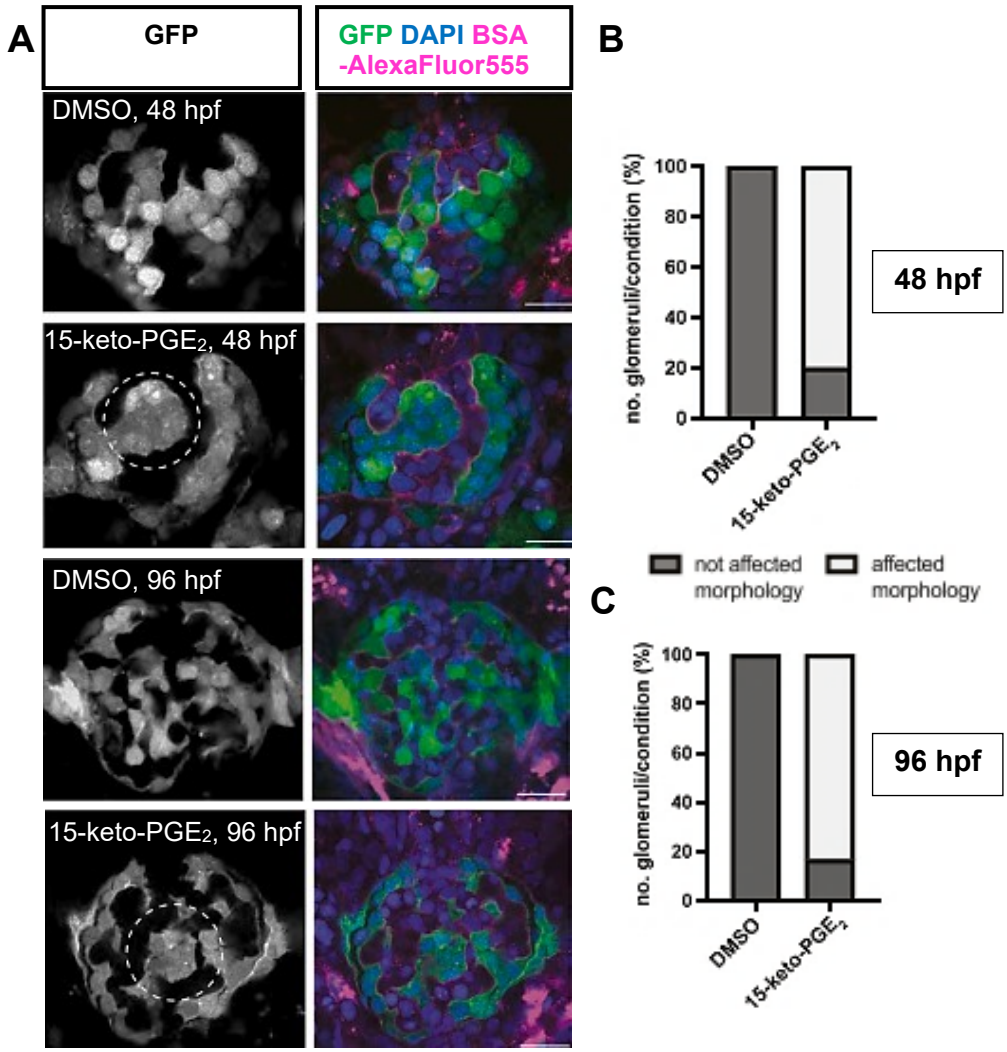

Figure 17. Glomerular morphological analysis after exposure to 15-keto-PGE_2. (A) Representative high-resolution confocal images of DMSO 0.88%- and 15-keto-PGE_2 500µM- treated *Tg[wt1b:EGFP]* embryos at 48 hpf (top two panels) and at 96 hpf (bottom two panels). For 48 hpf: *N*=2, *n*=5 for both conditions; For 96 hpf: *N*=3, *n*=7 for DMSO and *N*=3, *n*=6 for 15-keto-PGE_2; dotted-line circle indicates podocyte intercalation defects. (B, C) Quantification graphs showing the percentage of imaged glomeruli with affected morphology at 48 hpf and 96 hpf, respectively, after exposure to DMSO (no glomerular defect) and 15-keto-PGE_2 (4 out of 5 imaged glomeruli showed affected morphology at 48 hpf and 5 out of 6 imaged glomeruli were affected at 96 hpf). In all images, the glomerular podocytes and parietal epithelial cells are shown either in greyscale or in green (EGFP), endothelial cells of glomeruli capillaries are marked in magenta (BSA-AlexaFluor555) and cells nuclei in blue (DAPI); Scale bar=10 µm. Adapted from reference 64.

The quantitative analysis showed that the foot process width in the dmPGE$_2$-treated embryos was found to be numerical increased as compared to the DMSO condition, but no profound foot process effacement was observed in the EM images (Fig. 15). The same applied for the MWF rat, for which I performed a quantitative analysis by comparing the MWF control vs MWF/EP2+EP4-treated groups. The analysis showed a numerically lower mean value of the width of podocytes foot processes in response to combined EP2/EP4 blockade as compared to untreated MWF control, in three randomly selected animals from each of the two groups (Fig. 16C). Notably, a significant positive correlation between albuminuria and foot process width (r = 0.599, P = 0.0086) was detected indicating that treatment-induced albuminuria decrease has a beneficial effect on podocyte damage (Fig. 16D). Altogether, although the ultrastructural analysis did not reveal profound foot process changes, e.g., effacement, the subcellular analysis performed in zebrafish glomeruli supports that the albuminuria-like phenotype reported here, might arise as a result of the changes in the cellular interactions between podocytes and endothelial cells in response to elevated PGE$_2$.

3.9 Kidney morphological defects after exogenous 15-keto-PGE$_2$ stimulation.

Following the same approach as for the dmPGE$_2$ treatment, I proceeded with the analysis of the glomerular cytoarchitecture after early (from 6 hpf to 48 hpf) and late (from 72 hpf to 96 hpf) treatment with the PGE$_2$ metabolite, 15-keto-PGE$_2$. Early exposure to the drug resulted in overall pronephric defects (see section 3.4), while the late treatment did not induce the albuminuria development (see section 3.5).

High-resolution confocal imaging used for detailed subcellular analysis, revealed impaired podocyte intercalation around the forming glomerular capillaries after 15-keto-PGE$_2$ exposure in both 48 hpf and 96 hpf (Fig. 17). Notably, the glomerular morphology was restored after combined pharmacological blockade of EP2 and EP4 receptors at 96 hpf (Fig. 18A). For the quantification of the glomerular defects, I performed, as in dmPGE$_2$ condition, a 3D reconstruction and surface rendering of the glomeruli labeled with GFP.

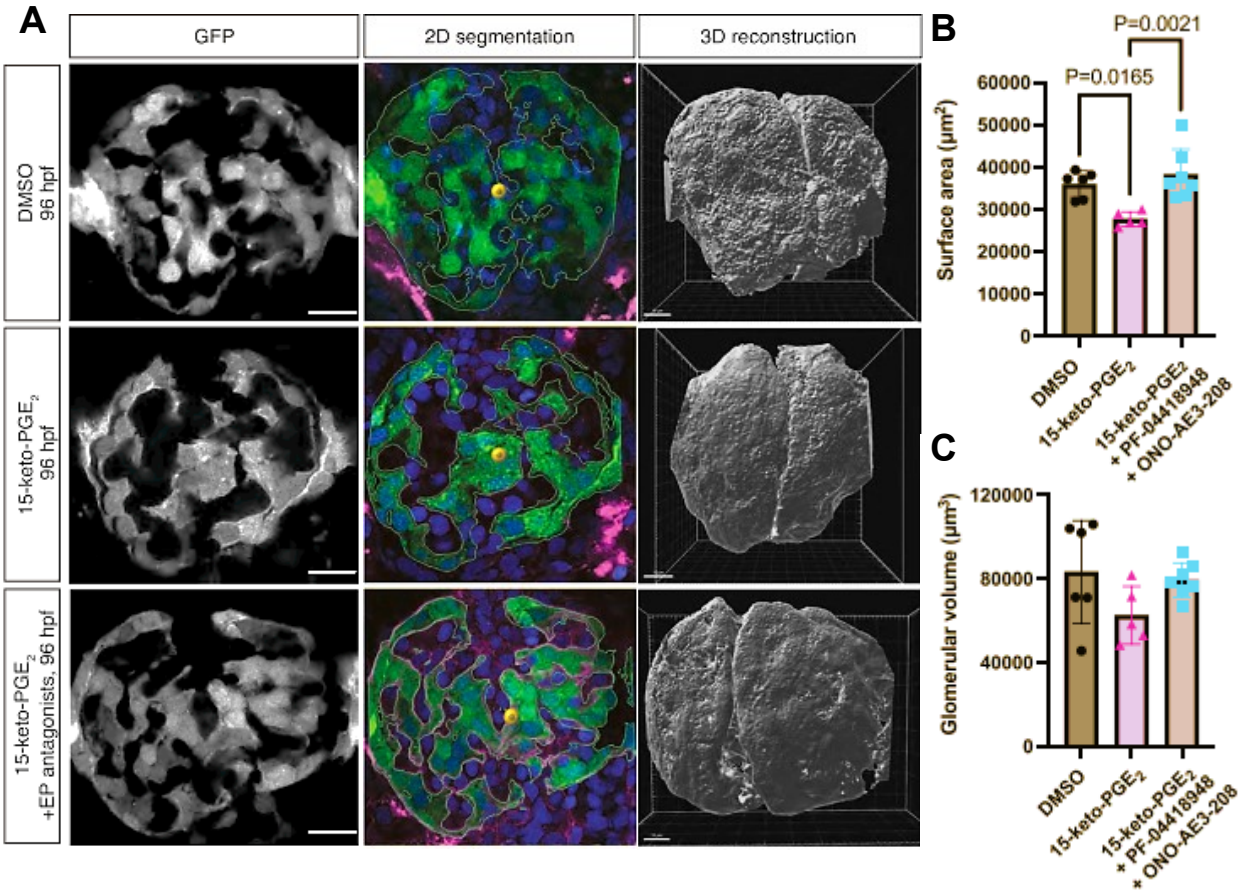

Figure 18. Exogenous 15-keto-PGE$_2$ treatment affects glomerular cytoarchitecture and the podocyte surface area. (A) High-resolution confocal microscopy analysis of the glomerulus at 96 hpf after DMSO vehicle 0.96% (top) (*N*=3, *n*=6) 15-keto-PGE$_2$ 500 µM (middle) (*N*=3, *n*=5), and 15-keto-PGE$_2$ 500 µM + PF-04418948 20 µM + ONO-AE3-208 20 µM (bottom) (*N*=2, *n*=7); Representative 2D grayscale and pseudo-colored images (left and middle panels, respectively) and 3D glomerular reconstruction (right panels) of *Tg[wt1b:EGFP]* zebrafish glomeruli at 96 hpf; Scale bar = 10 µm. Quantitative graphs of podocytes surface area (B) and the glomerular volume (C) of the glomeruli analyzed for the different pharmacological treatment groups; Ordinary one-way ANOVA with Tukey's multiple comparison test was performed for both graphs; in graph B: DMSO vs 15-keto-PGE$_2$ (*P*=0.0165), 15-keto-PGE$_2$ vs 15-keto-PGE$_2$ + PF-04418948+ ONO-AE3-208 (*P*=0.0021) and DMSO vs 15-keto-PGE$_2$ + PF-04418948 + ONO-AE3-208 (*P*=0.6048). No significant changes were observed in glomerular volume. Values are plotted as mean ± SD; $P < 0.05$ considered significant. In all images, the glomerular podocytes and parietal epithelial cells are shown either in greyscale or in green (EGFP), endothelial cells of glomeruli capillaries are marked in magenta (BSA-AlexaFluor555) and cells nuclei in blue (DAPI). One outlier was identified in the glomerulus surface area analysis for the DMSO and 15-keto-PGE$_2$ condition that were excluded from both the surface area and the glomerular volume analysis. Adapted from reference 64.

The glomerular volume and podocyte surface area were measured in three different conditions: DMSO-treated, 15-keto-PGE$_2$-treated and 15-keto-PGE$_2$+EP2/EP4 blockade (Fig. 18B, C). In contrast to dmPGE$_2$ treatment, the analysis revealed a significant decrease of podocyte surface area in response to 15-keto-PGE$_2$ exposure as compared to DMSO condition (Fig. 18B), while the glomerular volume was only numerically lower in 15-keto-PGE$_2$-treated group. Importantly, both podocyte intercalation and surface

area defects were restored after combined blockade of EP2 and EP4 receptors *in vivo* (Fig. 18A, B).

3.10 MRI analysis did not reveal significant changes of blood oxygenation levels.
[MRI analysis was performed in collaboration with Dr. Thomas Gladytz and Prof. Thoralf Niendorf].

In parallel, a group of MWF rats, whose albuminuria levels were measured (Figure 19A, B) was used for MRI analysis[92] to detect potential differences in renal hemodynamics and oxygenation between MWF control and MWF/EP2+EP4-treated groups.
MRI examination showed that there were no significant changes in the T2* and T2 relaxation times of the blood oxygenation level dependent signal after the EP receptor blockade (Fig. 19C), even though MWF kidneys had shorter relaxation times than historical normal Wistar rats[92]. Only a minor yet significant difference in T2* time in the outer medulla was seen. Additionally, changes in body weight, left ventricular weight (both absolute and relative to body weight), and kidney weight were also assessed. However, no significant changes were observed (Table 12).

Table 12. Rat parameters analyzed.

Parameter	Control	PF-04418948	ONO-AE3-208	PF-04418948 + ONO-AE3-208
BW (g)	328.9 ± 24.1	325.4 ± 15.3	326.5 ± 12.8	309.6 ± 15.5
LVW (g)	0.72 ± 0.07	0.68 ± 0.03	0.72 ± 0.04	0.65 ± 0.05
LVW/BW	2.21 ± 0.09	2.11 ± 0.07	2.21 ± 0.12	2.11 ± 0.13
KW (g)	2.13 ± 0.27	2.07 ± 0.20	2.08 ± 0.14	1.91 ± 0.17
KW/BW (mg/g)	6.47 ± 0.44	6.34 ± 0.39	6.37 ± 0.28	6.16 ± 0.30

BW, body weight; LVW, left ventricular weight; KW, kidney weight. Values presented as means ± SD. Rats per group (*n*=6-8, each); One-way ANOVA with post hoc Bonferroni's multiple comparisons test. Adapted from reference 63.

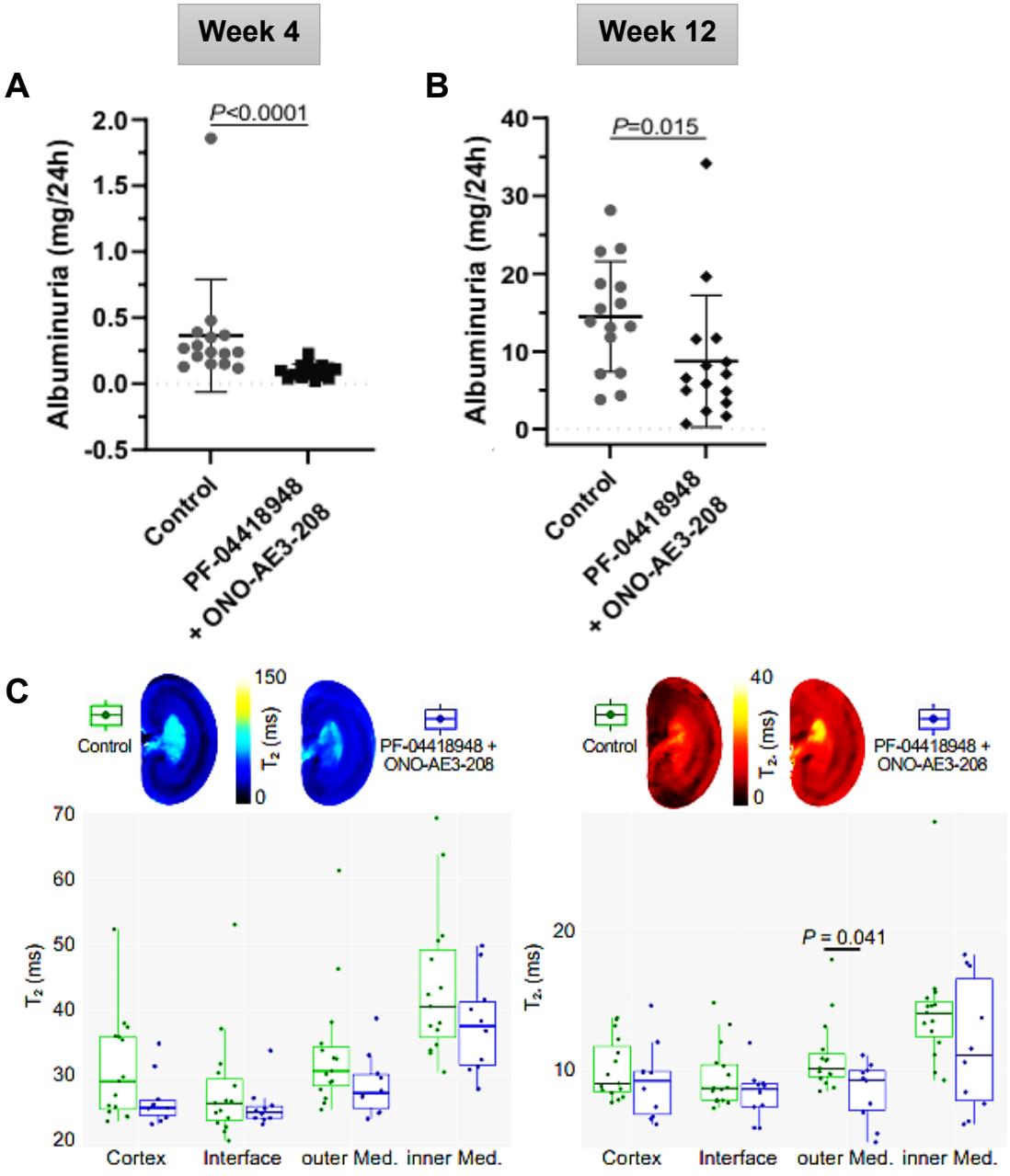

Figure 19. MRI-based assessment of renal oxygenation in the MWF rat after dual blockade of EP2 and EP4 receptors. Urinary albumin excretion of MWF control (*n*=15) vs MWF/EP2+EP4 (*n*=14) rats at week 4 (A) and week 12 (B) of age; one-way ANOVA with post hoc Bonferroni's multiple comparisons test. (C) T_2 and T_2* relaxation times of control MWF and MWF/EP2+EP4 rat kidneys in four kidney layers were compared (Cortex, cortical-medullar Interface, and outer and inner Medulla). On top are examples of T_2 and T_2* maps for both groups; Wilcoxon test was used to compare group differences in the two measured parameters. Adapted from reference 63.

3.11 RNA-seq analysis of MWF rat kidney cortex revealed a potential role of circadian clock genes.

[Preparation of the rat kidney samples, and qPCR analysis were performed by Dr. rer. medic. Angela Schulz (AG Kreutz, SFB-1365), while RNA-seq was conducted in collaboration with Nils Koppers and Prof. Monika Stoll].

To gain deeper insight into how PGE_2 signaling inhibition mediates renoprotective effects, a transcriptome analysis of renal cortex tissue was performed on MWF control rats and MWF rats treated with EP2 and EP4, using bulk RNA-seq.

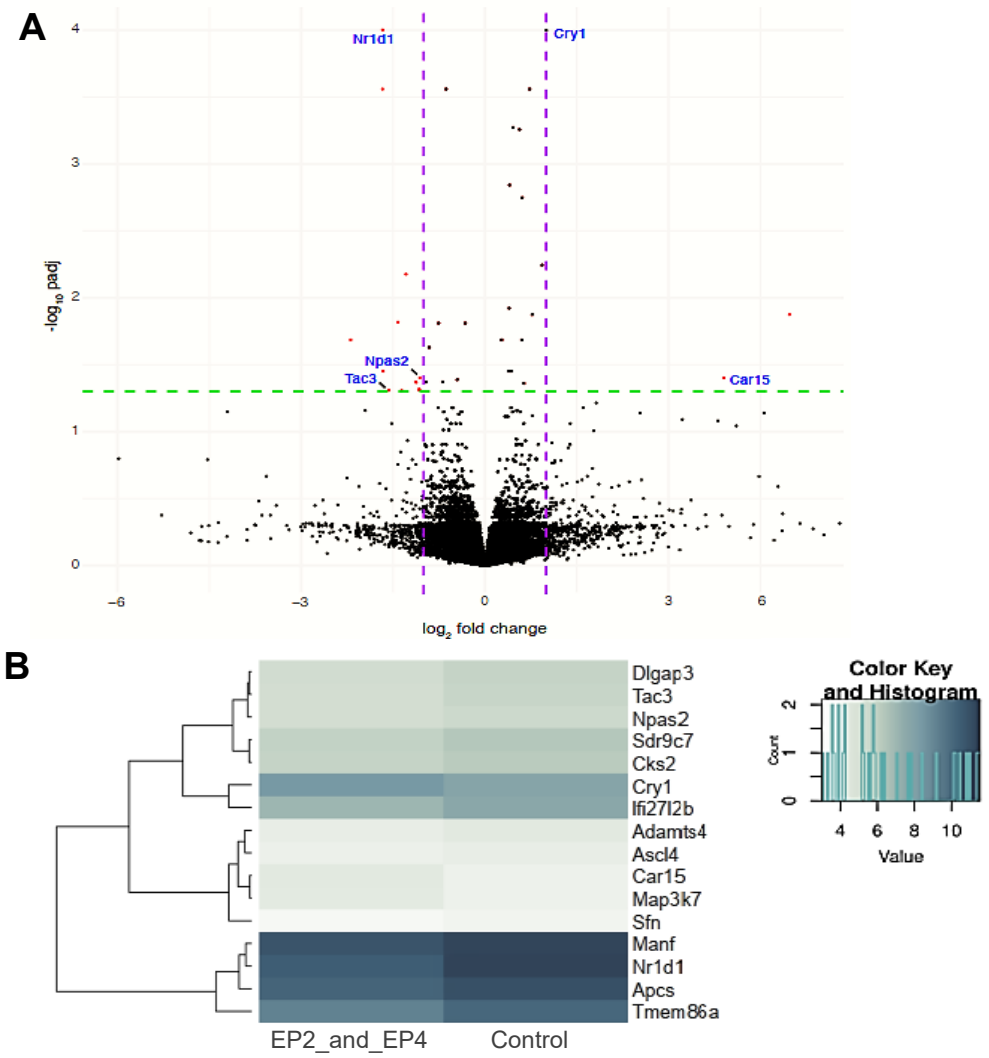

Figure 20. RNA-seq analysis of MWF rat.
(A) Volcano plot showing the comparison of the transcriptome analysis between MWF control and MWF/EP2+EP4-treated rats. The analysis showed 16 genes (in red) with differential expression (including *Cry1* with a log_2 fold change value=0.994). Vertical dotted lines (purple) show the log_2 fold change of < -1 and > +1, while horizontal dotted line (green) demonstrates the $-log_{10}$ of the adjusted *P* value; $P<0.05$ considered significant. (B) Unscaled heatmap demonstrates the expression differences between the significantly differentially expressed genes in the MWF/EP2+EP4-treated group vs the MWF control. Adapted from reference 63.

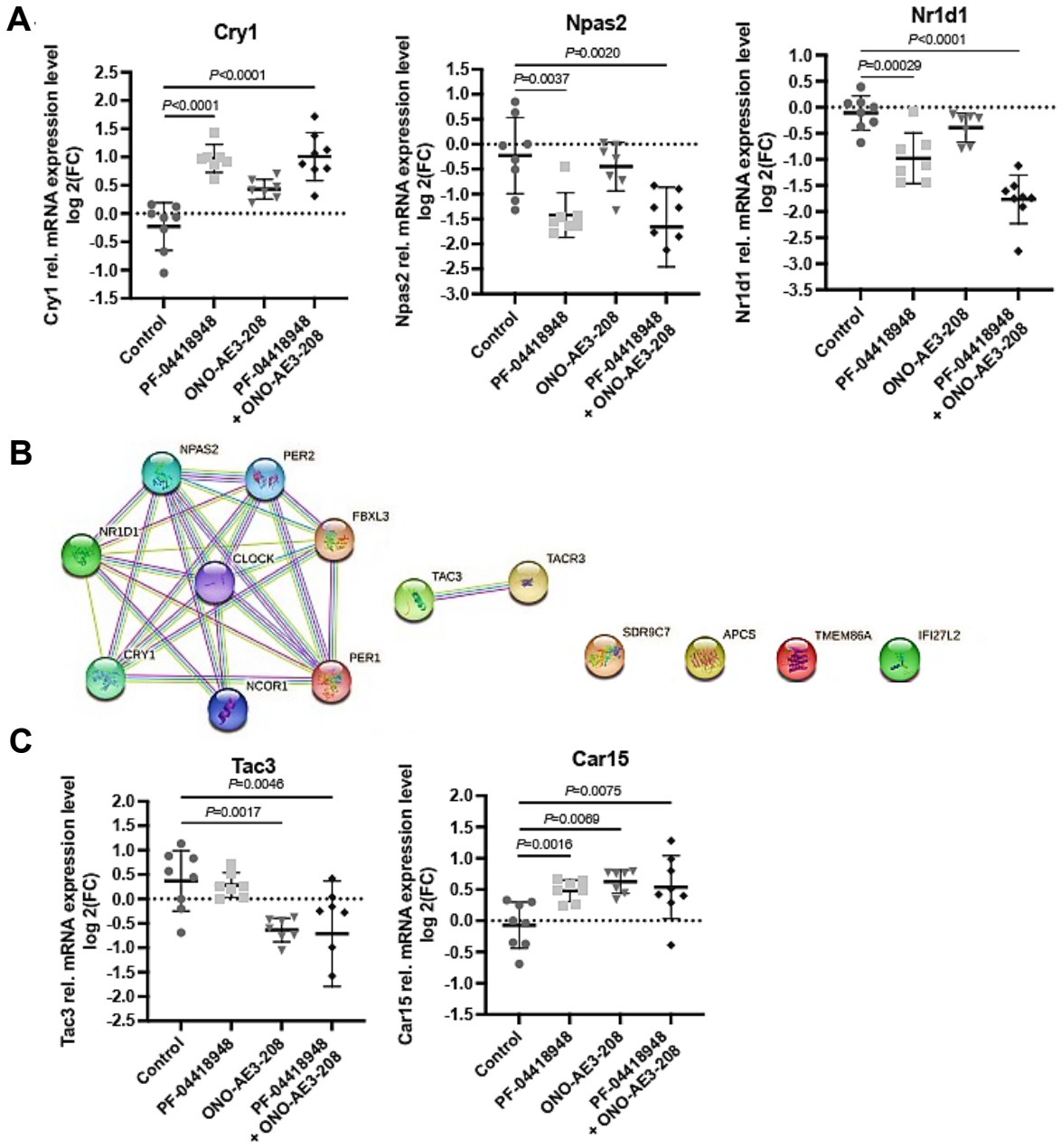

Figure 21. Network and qPCR analysis supporting the involvement of the circadian clock genes.
(A) qPCR analysis showed consistent significant differential expression for three of the main genes responsible of the circadian rhythm regulation, namely *Cry1*, *Npas2* and *Nr1d1*; Gene data were tested for normal distribution using Shapiro-Wilk test (not normally distributed) and were analyzed using Kruskal-Wallis test with Dunn's post-hoc analysis. (B) STRING protein network obtained from the 9 significantly differentially regulated genes (RNA-seq and qPCR confirmation analysis; *Car15* is not included in the network as it was not recognized from the STRING database) derived from the comparison between the MWF control and MWF/EP2+EP4-treated group. *CLOCK*, *PER1/2*, *NCOR1*, *FBXL3* and *TAC3R* appear as STRING predicted functional partners. The network shows known interactions: curated databases (blue), experimentally determined (magenta), text mining (green) and protein homology (purple); high confidence interaction score (0.70). (C) The differential expression of *Car15* and *Tac3* identified by the transcriptome analysis was also confirmed by the qPCR analysis as demonstrated in the present graphs. Data were analyzed by one-way ANOVA with Bonferroni's post hoc test. The genes presented in the graphs are also annotated in the Volcano plot in Figure 18. In all graphs: rats per group (n=6-8, each); data are displayed as mean ± SD; P<0.05 considered significant. Adapted from reference 63.

Only a small number of significantly (adjusted $P<0.05$) differentially regulated genes was identified by the transcriptome analysis in MWF/EP2+EP4-treated animals compared to MWF control (Fig. 20, Table 13).

Table 13. List of the 16 significantly differentially regulated genes identified from the transcriptome analysis of the MWF control vs MWF/EP2+EP4-treated rat kidney.

Symbol	Name	log2foldchange	qPCR analysis
Nr1d1	Nuclear receptor subfamily 1, group D, member 1	-1,659077854	+
Cry1	Cryptochrome circadian regulator 1	0,99431141	+
Tmem86a	Transmembrane protein 86A	-1,669995696	+
Dlgap3	DLG associated protein 3	-1,289196191	-
Map3k7	Mitogen activated protein kinase kinase kinase 7	4,975186668	-
Apcs	Amyloid P component, serum	-1,420401151	+
Sfn	Stratifin	-2,191777326	-
Adamts4	ADAM metallopeptidase with thrombospondin type 1 motif, 4	-1,661107855	-
Npas2	Neuronal PAS domain protein 2	-1,063183984	+
Car15	Carbonic anhydrase 15	3,900118665	+
Manf	Mesencephalic astrocyte-derived neurotrophic factor	-1,132092089	-
Cks2	CDC28 protein kinase regulatory subunit 2	-1,123091492	-
Sdr9c7	Short chain dehydrogenase/reductase family 9C, member 7	-1,070641151	+
Ifi27l2b	Interferon, alpha-inducible protein 27 like 2B	-1,07962446	+
Tac3	Tachykinin precursor 3	-1,569761	+
Ascl4	Achaete-scute family bHLH transcription factor 4	-1,359300585	No amplification

Symbols in the “qPCR analysis” column indicate either confirmed (+) or not confirmed (-) significantly altered gene expression in MWF/EP2+EP4-treated as compared to untreated MWF control rats. Adapted from reference 63.

Among the differentially expressed genes occurred by the RNA-seq analysis, I detected three of the main regulatory genes of the circadian rhythm including *Cry1*, *Npas2*, and *Nr1d1* (Fig. 20, 21A, B) suggesting a potential clock shift as a result of the combined EP2/EP4 receptors blockade (Fig. 22). In addition, qPCR analysis was used as a second step for the validation of the clock genes together with several selected genes identified by their differential expression in RNA-seq analysis (Fig. 21A, C, Fig. 23, Table 13).

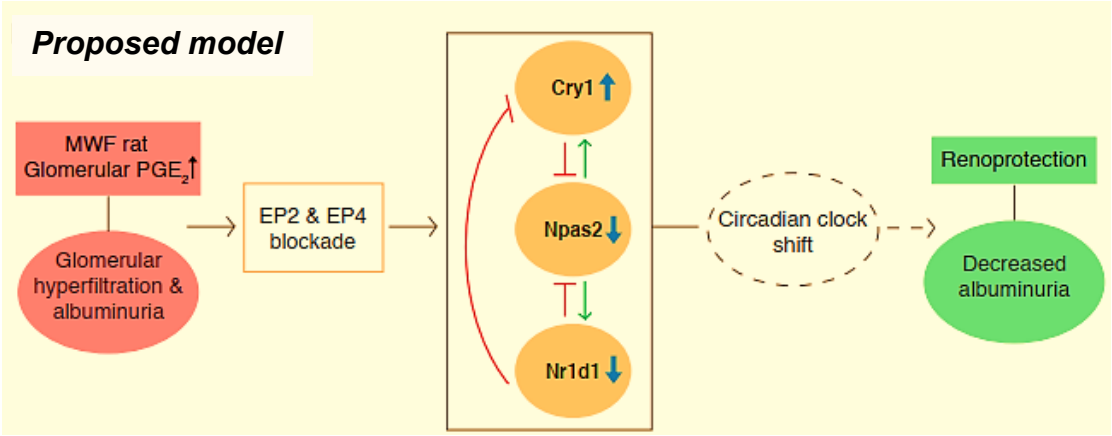

Figure 22. Proposed model arising from the transcriptome analysis. The model suggests a potential circadian clock shift observed in the MWF/EP2+EP4-treated rat compared to the MWF control, supporting the beneficial renoprotective effects of the combined EP2 and EP4 receptors blockade. The dashed ellipse shape and arrow indicate the main speculation suggested here; blue arrows show the up- or down-regulation of the circadian genes that demonstrated significantly differential expression in the transcriptome analysis, while green arrows and red inhibition arcs indicate well-known interactions among the circadian rhythm genes. Adapted from reference 63.

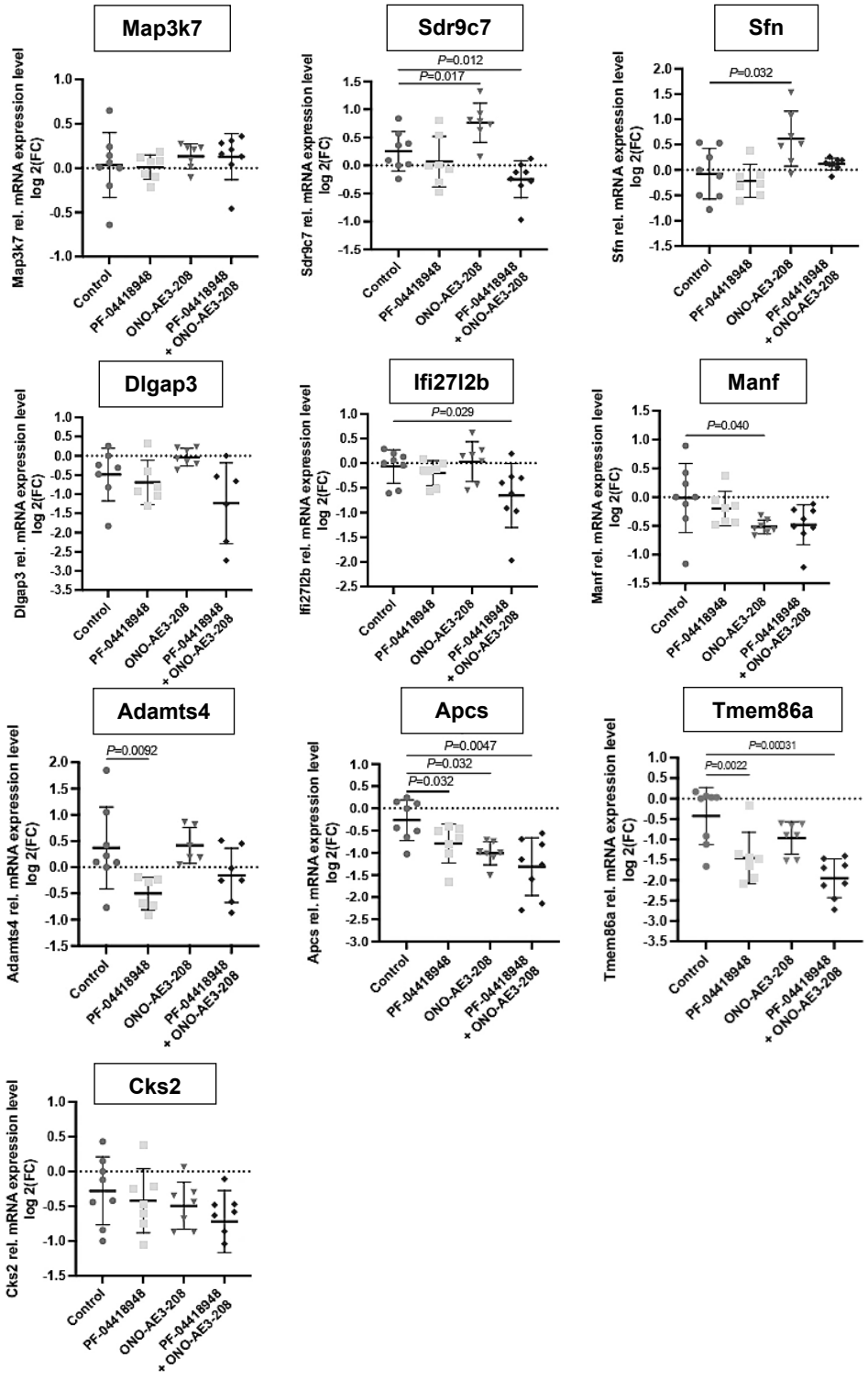

Figure 23. Confirmatory qPCR analysis for the genes identified by RNA-seq analysis in the MWF rat kidney. Relative mRNA expression levels for 10 genes from overall 16 genes identified with significant differential expression in RNA-seq analysis performed in the MWF control MWF/EP2+EP4-treated animals. Adrenoceptor beta 3 (*Adrb3*) showed very low mRNA expression in qPCR analysis, thus excluding a further quantitative analysis. *Ascl4* could not be amplified using the transcript ID ENSRNOT00000044252.3 listed in Ensembl (Ensembl Release 105, Dec 2021). Rats per group (*n*=6-8, each); data are displayed as mean ± SD; the data were tested for normal distribution using Shapiro-Wilk test; Not normally distributed data were analyzed using Kruskal-Wallis test with Dunn's post-hoc analysis (*Adamts4* and *Tmem86a*), while the rest of the data (normally distributed) was analyzed by one-way ANOVA with Bonferroni's post hoc analysis; *P*<0.05 considered significant. Adapted from reference 63.

4. Discussion

4.1 Brief summary of the results

In the present thesis, I investigated the role of prostaglandin E_2 catabolic pathway and specifically of the first metabolite synthesized during PGE_2 inactivation, 15-keto-PGE_2, highlighting the implications of both molecules in renal pathophysiology. In parallel, the potential renoprotective effect of the combined pharmacological blockade of EP2 and EP4 receptors was examined and evaluated *in vivo,* by performing concerted experiments in zebrafish and MWF rat models. In summary, I showed that exogenous exposure of zebrafish embryos to both PGE_2 and 15-keto-PGE_2 exerted significant defects on glomerular cytoarchitecture *in vivo*, mainly affecting podocyte intercalation and surface area and therefore GFB integrity at different stages of renal development, namely at 48 hpf and 96 hpf. Furthermore, I performed for the first time, a detailed 3D high-resolution glomerular morphological analysis of the zebrafish embryonic kidney, revealing that the development of the GFB occurs in distinct stages which are dependent on complex cell-cell interactions between endothelial and podocyte cells.

Importantly, both main hypotheses investigated in the framework of the present thesis were confirmed. First, my experiments revealed for the first time the bioactive role of 15-keto-PGE_2 *in vivo* in the kidney and supported its importance in glomerular and podocyte biology. In addition, the experiments performed in both zebrafish and MWF rats confirmed the second hypothesis, as they revealed a significant suppression of albuminuria phenotype after the dual EP2 and EP4 receptors blockade *in vivo,* thus supporting their renoprotective role. Moreover, bulk transcriptome analysis executed in kidney samples of the MWF rat suggested a potential shift of the renal circadian rhythm in response to the pharmacological blockade of EP2 and EP4 receptors.

4.2 Interpretation of the results

PGE_2 pathway has been extensively studied for its role in kidney physiology and disease, with the majority of the studies focusing on the PGE_2 synthesis, highlighting the renal COX/PGE_2 implications[59,93–96]. However, the importance of PGE_2 degradation and its catabolic products, 15-keto-PGE_2 and 13,14-dihydro-15-keto-PGE_2, in the physiology and/or pathophysiology of the kidney has not been previously investigated. Intriguingly, numerous studies have been conducted to determine the renal implications of 15-hydroprostaglandin dehydrogenase (15-PGDH), the enzyme that catalyzes the

initial step of PGE_2 inactivation and produces 15-keto-PGE_2. 15-PGDH activity has been observed in the kidney of various animal, including the cortex of rabbit kidneys[97,98], maternal rat kidney, fetal rat and lamb kidneys[99]. Inhibiting 15-PGDH protects mice from acute kidney injury (AKI)[100,101], and acute liposaccharide (LPS)-induced renal injury[102]. The present thesis provides evidence for the role of 15-keto-PGE_2 in binding EP2 and EP4 receptor and potentially modulating their signaling. Furthermore, I demonstrated a novel biologically active role of 15-keto-PGE_2 in glomerular morphology and podocyte biology. These results are in agreement with the reported elevated levels of 15-keto-PGE_2 in the isolated glomeruli of the MWF rat[59] and a recently published study supporting 15-keto-PGE_2 bioactive signaling via these receptors *in vitro*[49], further supporting a potential role of this metabolite in kidney pathological states.

Given PGE_2 complex significance in the kidney[93], I first investigated whether this molecule can in fact induce albuminuria *in vivo* in a non-diabetic model. Therefore, I established a zebrafish model that mimics the pathological state of albuminuria *in vivo*. In addition, the combined pharmacological blockade of EP2 and EP4 receptors significantly reverted the PGE_2-induced albuminuria phenotype in both zebrafish and MWF rat, a model which demonstrates increased GH with endogenous elevated levels of glomerular PGE_2[59]. These results are compatible with the reported renoprotective effects of EP4 inhibition in diabetes[103] and in 5/6 nephrectomy renal mass ablation[104,105], as well as with recent *in vitro* data showing a synergistic inhibitory effect on COX2/PGE_2 upregulation by dual EP2 and EP4 blockade in response to fluid flow shear stress in human podocytes[59].

4.3 Embedding the results into the current state of research.

The primary PGE_2 catabolic product, 15-keto-PGE_2 was, until recently, considered to be biologically inactive[45,47]. In recent years, its potential bioactive role has attracted increased research focus[50,52,106–108], while its effects have been reported to be principally mediated through the peroxisome proliferator-activated receptor gamma (PPAR-γ)[50,52,106]. 15-keto-PGE_2 various functions through PPAR-γ activation, have been reported in fungal pathogenesis[50], in Kupffer cells[106], in macrophages in mice with experimental sepsis[107], as well as in different types of cancer, such as in the upregulation of p21 promoter activity in hepatocellular carcinoma[52] and in the suppression of breast cancer[108]. The experiments I performed provide a novel role of

15-keto-PGE_2 in renal physiology and enhance the existing knowledge regarding 15-keto-PGE_2 EP2/EP4-mediated implications in glomerular cytoarchitecture and podocyte biology.

As recently demonstrated by employing dual endothelin receptor blockade hypertension treatment[109], simultaneous blockade of G-protein-coupled receptors offers an intriguing therapeutic alternative. In agreement with the latter, the results presented in my thesis reveal a novel renoprotective effect of the combined blockade of EP2 and EP4 receptors *in vivo*, in the setting of GH and albuminuria under non-diabetic conditions. In partial agreement, a role of EP2 but not EP4 inhibition has been recently supported as a novel opportunity to delay the progression of hyperfiltration-associated CKD[110]. Interestingly and in agreement with the data of the present thesis, a highly specific dual EP2 and EP4 antagonist, namely TPST-1495, has been developed and is currently tested in a phase 1 study in patients with solid tumors[111], demonstrating a more efficient suspension of tumor proliferation and stimulation of anti-cancer immunity, compared to separate EP2/EP4 receptors blockade or even concerted inhibition of all four EP receptors[111].

4.4 Suggestions for practice and/or future research

In the framework of the present thesis, I showed that 15-keto-PGE_2 exerts an important role on physiological glomerular development and impairs podocyte intercalation around glomerular capillaries, a defect that was reverted by combined pharmacological blockade of EP2 and EP4 receptors. However, essential questions arise and warrant further investigation: (a) how exactly 15-keto-PGE_2 modulates EP receptors signalling? (b) Does this process involve full receptor activation or (c) does 15-keto-PGE_2 act in dominant negative manner? In the same context, based on the bioactive effects of 15-keto-PGE_2 in glomerular morphology, more studies are required to explore the potential -secondary to PGE_2 effects- role of 15-keto-PGE_2 in renal hemodynamics and glomerular vascularization, as well as in glomerular hypertension. In addition, the impaired podocyte intercalation occurring after exogenous exposure to 15-keto-PGE_2, raises the issue of the potential contribution of this metabolite in the fine-tuning of the complex interactions between podocytes and endothelial cells and therefore proper GFB maturation, as well as its implication in potential alterations of podocyte-endothelial cell interactions under pathological conditions. Furthermore, the opposite effect that 15-keto-PGE_2 causes to the podocyte surface area, compared to PGE_2, suggests a

potential altered downstream signaling process of the metabolite, however, this needs to be further investigated.

The renoprotective role of the combined EP2 and EP4 receptors blockade was studied here under non-diabetic conditions. Thus, it would be important to investigate, whether the positive effects of dual EP2 and EP4 blocking could be replicated in analogous GH-based experimental settings in diabetes. Moreover, it is yet to be elucidated, how receptor modulation in podocytes and the kidney, as well as downstream signaling and mechanisms, contribute to the positive effects of combined EP2 and EP4 blockade. Lastly, the circadian rhythm shift hypothesis emerged from the transcriptome analysis of the MWF rat kidney underlines the importance of focusing on the circadian clock genes regulation in different cell types of the kidney, including podocytes. The establishment and utilization of transgenic zebrafish or rat lines targeting cell-specific circadian genes in the kidney would improve the current state of knowledge.

5. Conclusions

In the present thesis, I investigated the role of PGE_2/15-keto-PGE_2/EP2/EP4 axis in the glomerular cytoarchitecture, podocyte biology and GFB integrity, as well as in the setting of glomerular hyperfiltration and albuminuria *in vivo*. I showed that both PGE_2 and 15-keto-PGE_2 affect the glomerular development and podocyte intercalation around the glomerular capillaries and therefore the podocyte surface area in the zebrafish embryonic kidney. I have shown here that both PGE_2 and 15-keto-PGE_2 bind EP2 and EP4 receptors *in vitro*, and importantly, the combined pharmacological blockade of these receptors reversed the glomerular morphological defects resulted from the exogenous prostaglandin exposure.

I have established a zebrafish model that mimics *in vivo* the pathological state of albuminuria. Concerted experiments in both zebrafish and MWF rat models demonstrated significant suppression of albuminuria phenotype under non-diabetic conditions by combined EP2 and EP4 receptors blockade, highlighting a novel renoprotective role *in vivo* and supporting the dual blockade of EP receptors as an important therapeutic target. The combined EP receptors blockade caused only marginal changes in the transcriptome analysis of the MWF rat kidney, however, aroused an interesting hypothesis suggesting a shift of the circadian clock after the pharmacological blockade, indicating the potential involvement of the circadian rhythm genes in the albuminuria suppression.

The work presented here, boosts and extends the current state of knowledge, regarding the biologically active role of 15-keto-PGE_2 in renal biology and supports a novel renoprotective effect of combined EP receptors blockade in kidney pathophysiology. In addition, raises new issues paving the way for future research in this area.

Reference list

1. Kriz, W. & Kaissling, B. Chapter 20-Structural Organization of the Mammalian Kidney. *Seldin and Giebisch's The Kidney (Fifth Edition) Academic Press.* 595–691 (2013).
2. McMahon, A. P. Development of the Mammalian Kidney. *Current Topics in Developmental Biology.* **117**, 31-64 (2016).
3. Costantini, F. & Kopan, R. Patterning a complex organ: Branching morphogenesis and nephron segmentation in kidney development. *Dev. Cell* **18**, 698–712 (2010).
4. Krause, M., Rak-Raszewska, A., Pietilä, I., Quaggin, S. & Vainio, S. Signaling during Kidney Development. *Cells* **4**, 112–132 (2015).
5. Pollak, M. R., Quaggin, S. E., Hoenig, M. P. & Dworkin, L. D. The glomerulus: the sphere of influence. *Clin. J. Am. Soc. Nephrol.* **9**, 1461–1469 (2014).
6. Ebefors, K., Lassén, E., Anandakrishnan, N., Azeloglu, E. U. & Daehn, I. S. Modeling the Glomerular Filtration Barrier and Intercellular Crosstalk. *Front. Physiol.* **12**, (2021).
7. Pozzi, A., Jarad, G., Moeckel, G. W., Coffa, S., Zhang, X., Gewin, L., Eremina, V., Hudson, B. G., Borza, D. B., Harris, R. C., Holzman, L. B., Phillips, C. L., Fassler, R., Quaggin, S. E., Miner, J. H. & Zent, R. B1 Integrin Expression By Podocytes Is Required To Maintain Glomerular Structural Integrity. *Dev. Biol.* **316**, 288–301 (2008).
8. Greka, A. & Mundel, P. Cell biology and pathology of podocytes. *Annu. Rev. Physiol.* **74**, 299–323 (2012).
9. Haraldsson, B., Nyström, J. & Deen, W. M. Properties of the glomerular barrier and mechanisms of proteinuria. *Physiol. Rev.* **88**, 451–487 (2008).
10. Butt, L., Unnersjö-Jess, D., Höhne, M., Edwards, A., Binz-Lotter, J., Reilly, D., Hahnfeldt, R., Ziegler, V., Fremter, K., Rinschen, M. M., Helmstädter, M., Ebert, L. K., Castrop, H., Hackl, M. J., Walz, G., Brinkkoetter, P. T., Liebau, M. C., Tory, K., Hoyer, P. F., Beck, B. B., Brismar, H., Blom, H., Schermer, B., Benzing, T. A molecular mechanism explaining albuminuria in kidney disease. *Nat. Metab.* **2**, 461–474 (2020).

11. Wingert, R. A. & Davidson, A. J. The zebrafish pronephros: A model to study nephron segmentation. *Kidney International*. **73**, 1120–1127 (2008).

12. Elmonem, M., Berlingerio, S., van den Heuvel, L., de Witte, P., Lowe, M. & Levtchenko, E. Genetic Renal Diseases: The Emerging Role of Zebrafish Models. *Cells* **7**, 130 (2018).

13. Gerlach, G. F. & Wingert, R. A. Kidney organogenesis in the zebrafish: insights into vertebrate nephrogenesis and regeneration. *Wiley interdisciplinary reviews. Developmental biology*. **2**, 559–585 (2013).

14. Santoriello, C. & Zon, L. I. Hooked! modeling human disease in zebrafish. *Journal of Clinical Investigation*. **122**, 2337–2343 (2012).

15. Outtandy, P., Russell, C., Kleta, R. & Bockenhauer, D. Zebrafish as a model for kidney function and disease. *Pediatric Nephrology*. **34**, 751–762 (2019).

16. Dooley, K. & Zon, L. I. Zebrafish: a model system for the study of human disease. *Curr. Opin. Genet. Dev.* **10**, 252–256 (2000).

17. Lieschke, G. J. & Currie, P. D. Animal models of human disease: zebrafish swim into view. *Nat. Rev. Genet.* **8**, 353–367 (2007).

18. Gehrig, J., Pandey, G. & Westhoff, J. H. Zebrafish as a model for drug screening in genetic kidney diseases. *Frontiers in Pediatrics*. **6**, 183 (2018).

19. MacRae, C. A. & Peterson, R. T. Zebrafish as tools for drug discovery. *Nat. Rev. Drug Discov.* **14**, 721–731 (2015).

20. Rennekamp, A. J. & Peterson, R. T. 15 years of zebrafish chemical screening. *Curr. Opin. Chem. Biol.* **24**, 58–70 (2015).

21. Zhao, S., Huang, J. & Ye, J. A fresh look at zebrafish from the perspective of cancer research. *J. Exp. Clin. Cancer Res.* **34**, 80 (2015).

22. Zang, L., Shimada, Y. & Nishimura, N. Development of a Novel Zebrafish Model for Type 2 Diabetes Mellitus. *Sci. Rep.* **7**, 1461 (2017).

23. Singh, S. P. & Ninov, N. Multicolor Labeling and Tracing of Pancreatic Beta-Cell Proliferation in Zebrafish. *Methods Mol. Biol.* **2128**, 159–179 (2020).

24. Vogel, B., Meder, B., Just, S., Laufer, C., Berger, I., Weber, S., Katus, H. A. & Rottbauer, W. In-vivo characterization of human dilated cardiomyopathy genes in

zebrafish. *Biochem. Biophys. Res. Commun.* **390**, 516–522 (2009).

25. Vazão, H., Rosa, S., Barata, T., Costa, R., Pitrez, P. R., Honório, I., de Vries, M. R., Papatsenko, D., Benedito, R., Saris, D., Khademhosseini, A., Quax, P. H. A., Pereira, C. F., Mercader, N., Fernandes, H. & Ferreira, L. High-throughput identification of small molecules that affect human embryonic vascular development. *Proc. Natl. Acad. Sci. U. S. A.* **114**, E3022–E3031 (2017).

26. Kalueff, A. V, Stewart, A. M. & Gerlai, R. Zebrafish as an emerging model for studying complex brain disorders. *Trends Pharmacol. Sci.* **35**, 63–75 (2014).

27. Hentschel, D. M., Park, K. M., Cilenti, L., Zervos, A. S., Drummond, I. & Bonventre, J. V. Acute renal failure in zebrafish: a novel system to study a complex disease. *Am. J. Physiol. Renal Physiol.* **288**, F923-9 (2005).

28. Mahmood, F., Mozere, M., Zdebik, A. A., Stanescu, H. C., Tobin, J., Beales, P. L., Kleta, R., Bockenhauer, D. & Russell, C. Generation and validation of a zebrafish model of EAST (epilepsy, ataxia, sensorineural deafness and tubulopathy) syndrome. *Dis. Model. Mech.* **6**, 652–660 (2013).

29. Elmonem, M. A., Khalil, R., Khodaparast, L., Khodaparast, L., Arcolino, F. O., Morgan, J., Pastore, A., Tylzanowski, P., Ny, A., Lowe, M., De Witte, P. A., Baelde, H. J., Van Den Heuvel, L. P. & Levtchenko, E. Cystinosis (ctns) zebrafish mutant shows pronephric glomerular and tubular dysfunction. *Sci. Rep.* **7**, 42583 (2017).

30. Drummond, I. A. & Davidson, A. J. Zebrafish Kidney Development. *Methods Cell Biol.* **100**, 233–260 (2010).

31. Hill, A. J., Bello, S. M., Prasch, A. L., Peterson, R. E. & Heideman, W. Water permeability and TCDD-induced edema in zebrafish early-life stages. *Toxicol. Sci.* **78**, 78–87 (2004).

32. Klingbeil, K., Nguyen, T. Q., Fahrner, A., Guthmann, C., Wang, H., Schoels, M., Lilienkamp, M., Franz, H., Eckert, P., Walz, G. & Yakulov, T. A. Corpuscles of Stannius development requires FGF signaling. *Dev. Biol.* **481**, 160–171 (2022).

33. Howe, K., Clark, M. D., Torroja, C. F., Torrance, J., Berthelot, C., Muffato, M., Collins, J. E., Humphray, S., McLaren, K., Matthews, L., McLaren, S., Sealy, I., Caccamo, M., Churcher, C., Scott, C., Barrett, J. C., Koch, R., Rauch, G. J.,

White, S., Chow, W., Kilian, B., Quintais, L. T., Guerra-Assunção, J. A., Zhou, Y., Gu, Y., Yen, J., Vogel, J. H., Eyre, T., Redmond, S., Banerjee, R., Chi, J., Fu, B., Langley, E., Maguire, S. F., Laird, G. K., Lloyd, D., Kenyon, E., Donaldson, S., Sehra, H., Almeida-King, J., Loveland, J., Trevanion, S., Jones, M., Quail, M., Willey, D., Hunt, A., Burton, J., Sims, S., McLay, K., Plumb, B., Davis, J., Clee, C., Oliver, K., Clark, R., Riddle, C., Elliot, D., Threadgold, G., Harden, G., Ware, D., Begum, S., Mortimore, B., Kerry, G., Heath, P., Phillimore, B., Tracey, A., Corby, N., Dunn, M., Johnson, C., Wood, J., Clark, S., Pelan, S., Griffiths, G., Smith, M., Glithero, R., Howden, P., Barker, N., Lloyd, C., Stevens, C., Harley, J., Holt, K., Panagiotidis, G., Lovell, J., Beasley, H., Henderson, C., Gordon, D., Auger, K., Wright, D., Collins, J., Raisen, C., Dyer, L., Leung, K., Robertson, L., Ambridge, K., Leongamornlert, D., McGuire, S., Gilderthorp, R., Griffiths, C., Manthravadi, D., Nichol, S., Barker, G., Whitehead, S., Kay, M., Brown, J., Murnane, C., Gray, E., Humphries, M., Sycamore, N., Barker, D., Saunders, D., Wallis, J., Babbage, A., Hammond, S., Mashreghi-Mohammadi, M., Barr, L., Martin, S., Wray, P., Ellington, A., Matthews, N., Ellwood, M., Woodmansey, R., Clark, G., Cooper, J., Tromans, A., Grafham, D., Skuce, C., Pandian, R., Andrews, R., Harrison, E., Kimberley, A., Garnett, J., Fosker, N., Hall, R., Garner, P., Kelly, D., Bird, C., Palmer, S., Gehring, I., Berger, A., Dooley, C. M., Ersan-Ürün, Z., Eser, C., Geiger, H., Geisler, M., Karotki, L., Kirn, A., Konantz, J., Konantz, M., Oberländer, M., Rudolph-Geiger, S., Teucke, M., Lanz, C., Raddatz, G., Osoegawa, K., Zhu, B., Rapp, A., Widaa, S., Langford, C., Yang, F., Schuster, S. C., Carter, N. P., Harrow, J., Ning, Z., Herrero, J., Searle, S. M., Enright, A., Geisler, R., Plasterk, R. H., Lee, C., Westerfield, M., de Jong, P. J., Zon, L. I., Postlethwait, J. H., Nüsslein-Volhard, C., Hubbard, T. J., Roest Crollius, H., Rogers, J., Stemple, D. L. The zebrafish reference genome sequence and its relationship to the human genome. *Nature* **496**, 498–503 (2013).

34. Park, J. Y., Pillinger, M. H. & Abramson, S. B. Prostaglandin E2 synthesis and secretion: The role of PGE2 synthases. *Clin. Immunol.* **119**, 229–240 (2006).

35. Li, Y., Xia, W., Zhao, F., Wen, Z., Zhang, A., Huang, S., Jia, Z. & Zhang, Y. Prostaglandins in the pathogenesis of kidney diseases. *Oncotarget.* **9**, 26586-26602 (2018).

36. Ugwuagbo, K. C., Maiti, S., Omar, A., Hunter, S., Nault, B., Northam, C. &

Majumder, M. Prostaglandin E2 promotes embryonic vascular development and maturation in zebrafish. *Biol. Open* **8**, bio039768 (2019).

37. North, T. E., Goessling, W., Walkley, C. R., Lengerke, C., Kopani, K. R., Lord, A. M., Weber, G. J., Bowman, T. V., Jang, I. H., Grosser, T., Fitzgerald, G. A., Daley, G. Q., Orkin, S. H. & Zon, L. I. Prostaglandin E2 regulates vertebrate haematopoietic stem cell homeostasis. *Nature* **447**, 1007–1011 (2007).

38. Iwasaki, R., Tsuge, K., Kishimoto, K., Hayashi, Y., Iwaana, T., Hohjoh, H., Inazumi, T., Kawahara, A., Tsuchiya, S. & Sugimoto, Y. Essential role of prostaglandin E2 and the EP3 receptor in lymphatic vessel development during zebrafish embryogenesis. *Sci. Rep.* **9**, 1–11 (2019).

39. Goessling, W., North, T. E., Loewer, S., Lord, A. M., Lee, S., Stoick-Cooper, C. L., Weidinger, G., Puder, M., Daley, G. Q., Moon, R. T. & Zon, L. I. Genetic Interaction of PGE2 and Wnt Signaling Regulates Developmental Specification of Stem Cells and Regeneration. *Cell* **136**, 1136–1147 (2009).

40. Nissim, S., Sherwood, R. I., Wucherpfennig, J., Saunders, D., Harris, J. M., Esain, V., Carroll, K. J., Frechette, G. M., Kim, A. J., Hwang, K. L., Cutting, C. C., Elledge, S., North, T. E. & Goessling, W. Prostaglandin E2 regulates liver versus pancreas cell-fate decisions and endodermal outgrowth. *Dev. Cell* **28**, 423–437 (2014).

41. Hoggatt, J., Singh, P., Sampath, J. & Pelus, L. M. Prostaglandin E2 enhances hematopoietic stem cell homing, survival, and proliferation. *Blood* **113**, 5444–5455 (2009).

42. O'Callaghan, G. & Houston, A. Prostaglandin E2 and the EP receptors in malignancy: Possible therapeutic targets? *British Journal of Pharmacology*. **172**, 5239–5250 (2015).

43. Dunn, M. J. & Hood, V. L. Prostaglandins and the kidney. *Am. J. Physiol. Physiol.* **233**, F169–F184 (1977).

44. Nasrallah, R., Hassouneh, R. & Hébert, R. L. Chronic kidney disease: targeting prostaglandin E 2 receptors. *Am J Physiol Ren. Physiol* **307**, 243–250 (2014).

45. Tai, H.-H., Ensor, C. M., Tong, M., Zhou, H. & Yan, F. Prostaglandin catabolizing enzymes. *Prostaglandins & other Lipid Mediators*. **68-69**, 483-493 (2002).

46. Wu, Y. H., Ko, T. P., Guo, R. T., Hu, S. M., Chuang, L. M. & Wang, A. H. H. J. Structural Basis for Catalytic and Inhibitory Mechanisms of Human Prostaglandin Reductase PTGR2. *Structure.* **16,** 1714-1723 (2008).

47. Chou, W. L., Chuang, L. M., Chou, C. C., Wang, A. H. J., Lawson, J. A., FitzGerald, G. A. & Chang, Z. F. Identification of a novel prostaglandin reductase reveals the involvement of prostaglandin E2 catabolism in regulation of peroxisome proliferator-activated receptor γ activation. *J. Biol. Chem.* **282**, 18162–18172 (2007).

48. Nishigaki, N., Negishi, M. & Ichikawa, A. Two Gs-coupled prostaglandin E receptor subtypes, EP2 and EP4, differ in desensitization and sensitivity to the metabolic inactivation of the agonist. *Mol. Pharmacol.* **50**, 1031 LP – 1037 (1996).

49. Endo, S., Suganami, A., Fukushima, K., Senoo, K., Araki, Y., Regan, J. W., Mashimo, M., Tamura, Y. & Fujino, H. 15-Keto-PGE2 acts as a biased/partial agonist to terminate PGE2-evoked signaling. *J. Biol. Chem.* **295**, 13338–13352 (2020).

50. Evans, R. J., Pline, K., Loynes, C. A., Needs, S., Aldrovandi, M., Tiefenbach, J., Bielska, E., Rubino, R. E., Nicol, C. J., May, R. C., Krause, H. M., O'Donnell, V. B., Renshaw, S. A. & Johnston, S. A. 15-keto-prostaglandin e2 activates host peroxisome proliferator-activated receptor gamma (Ppar-γ) to promote cryptococcus neoformans growth during infection. *PLoS Pathog.* **15**, 1–28 (2019).

51. Yao, L., Chen, W., Song, K., Han, C., Gandhi, C. R., Lim, K. & Wu, T. 15-hydroxyprostaglandin dehydrogenase (15-PGDH) prevents lipopolysaccharide (LPS)-induced acute liver injury. *PLoS One* **12**, e0176106 (2017).

52. Lu, D., Han, C. & Wu, T. 15-PGDH inhibits hepatocellular carcinoma growth through 15-keto-PGE2/PPARγ-mediated activation of p21WAF1/Cip1. *Oncogene* **33**, 1101–1112 (2014).

53. Sugimoto, Y. & Narumiya, S. Prostaglandin E receptors. *Journal of Biological Chemistry.* **282**, 11613–11617 (2007).

54. Li, L., Sluter, M. N., Yu, Y. & Jiang, J. Prostaglandin E receptors as targets for ischemic stroke: Novel evidence and molecular mechanisms of efficacy. *Pharmacol. Res.* **163**, 105238 (2021).

55. Iwasaki, R., Tsuge, K., Morimoto, K., Inazumi, T., Kawahara, O., Kawahara, A., Tsuchiya, S. & Sugimoto, Y. Molecular and pharmacological characterization of zebrafish 'contractile' and 'inhibitory' prostanoid receptors. *Biochem. Biophys. Res. Commun.* **438**(2), 353-358 (2013).

56. Kwok, A. H. Y., Wang, Y. & Leung, F. C. Molecular characterization of prostaglandin F receptor (FP) and E receptor subtype 1 (EP_1) in zebrafish. *Gen. Comp. Endocrinol.* **178**, 216–226 (2012).

57. Poureetezadi, S. J., Cheng, C. N., Chambers, J. M., Drummond, B. E. & Wingert, R. A. Prostaglandin signaling regulates nephron segment patterning of renal progenitors during zebrafish kidney development. *eLife.* **5**, e17551 (2016).

58. Tsuge, K., Iwasaki, R., Morimoto, K., Inazumi, T., Kawahara, O., Kawahara, A., Tsuchiya, S. & Sugimoto, Y. Molecular and pharmacological characterization of zebrafish 'relaxant' prostanoid receptors. *Biochem. Biophys. Res. Commun.* **436**, 685–690 (2013).

59. Mangelsen, E., Rothe, M., Schulz, A., Kourpa, A., Panáková, D., Kreutz, R. & Bolbrinker, J. Concerted EP2 and EP4 Receptor Signaling Stimulates Autocrine Prostaglandin E2 Activation in Human Podocytes. *Cells* **9**, 1256 (2020).

60. Perner, B., Englert, C. & Bollig, F. The Wilms tumor genes wt1a and wt1b control different steps during formation of the zebrafish pronephros. *Dev. Biol.* **309**, 87-96 (2007).

61. Zhou, W. & Hildebrandt, F. Inducible podocyte injury and proteinuria in transgenic zebrafish. *J. Am. Soc. Nephrol.* **23**, 1039–1047 (2012).

62. Dowell, S. J. & Brown, A. J. Yeast assays for G protein-coupled receptors. *Methods Mol. Biol.* **552**, 213–229 (2009).

63. Kourpa, A., Schulz, A., Mangelsen, E., Kaiser-Graf, D., Koppers, N., Stoll, M., Rothe, M., Bader, M., Purfürst, B., Kunz, S., Gladytz, T., Niendorf, T., Bachmann, S., Mutig, K., Bolbrinker, J., Panáková, D. & Reinhold, K. Studies in Zebrafish and Rat Models Support Dual Blockade of EP2 and EP4 (Prostaglandin E2 Receptors Type 2 and 4) for Renoprotection in Glomerular Hyperfiltration and Albuminuria. *Hypertension.* **80**, 771-782 (2023) .

64. Kourpa, A., Kaiser-Graf, D., Sporbert, A., Philippe, A., Catar, R., Rothe, M.,

Mangelsen, E., Schulz, A., Bolbrinker, J., Kreutz, R. & Panáková, D. 15-keto-Prostaglandin E2 exhibits bioactive role by modulating glomerular cytoarchitecture through EP2/EP4 receptors. *Life Sci.* **310**, 121114 (2022).

65. Aleström, P., D'Angelo, L., Midtlyng, P. J., Schorderet, D. F., Schulte-Merker, S., Sohm, F. & Warner, S. Zebrafish: Housing and husbandry recommendations. *Lab. Anim.* **54**, 213–224 (2019).

66. Schulz, A., Müller, N. V*.,* van de Lest, N. A., Eisenreich, A., Schmidbauer, M., Barysenka, A., Purfürst, B., Sporbert, A., Lorenzen, T., Meyer, A. M., Herlan, L., Witten, A., Rühle, F., Zhou, W., de Heer, E., Scharpfenecker, M., Panáková, D., Stoll, M. & Kreutz, R. Analysis of the genomic architecture of a complex trait locus in hypertensive rat models links Tmem63c to kidney damage. *eLife.* **8**, e42068 (2019).

67. Schulz, A. & Kreutz, R. Mapping genetic determinants of kidney damage in rat models. *Hypertens. Res.* **35**, 675–694 (2012).

68. Saleem, M. A., O'Hare, M. J., Reiser, J., Coward, R. J., Inward, C. D., Farren, T., Xing, C. Y., Ni, L., Mathieson, P. W. & Mundel, P. A conditionally immortalized human podocyte cell line demonstrating nephrin and podocin expression. *J. Am. Soc. Nephrol.* **13**, 630–638 (2002).

69. Koop, K., Eikmans, M., Baelde, H. J., Kawachi, H., De Heer, E., Paul, L. C. & Bruijn, J. A. Expression of podocyte-associated molecules in acquired human kidney diseases. *J. Am. Soc. Nephrol.* **14**, 2063–2071 (2003).

70. Kim, D., Paggi, J. M., Park, C., Bennett, C. & Salzberg, S. L. Graph-based genome alignment and genotyping with HISAT2 and HISAT-genotype. *Nat. Biotechnol.* **37**, 907–915 (2019).

71. Miyares, R. L., de Rezende, V. B. & Farber, S. A. Zebrafish yolk lipid processing: a tractable tool for the study of vertebrate lipid transport and metabolism. *Dis. Model. Mech.* **7**, 915–927 (2014).

72. Fraher, D., Sanigorski, A., Mellett, N. A., Meikle, P. J., Sinclair, A. J. & Gibert, Y. Zebrafish Embryonic Lipidomic Analysis Reveals that the Yolk Cell Is Metabolically Active in Processing Lipid. *Cell Rep.* **14**, 1317–1329 (2016).

73. Mitchell, J. A., Akarasereenont, P., Thiemermann, C., Flower, R. J. & Vane, J. R.

Selectivity of nonsteroidal antiinflammatory drugs as inhibitors of constitutive and inducible cyclooxygenase. *Proc. Natl. Acad. Sci. U. S. A.* **90**, 11693–11697 (1993).

74. Niringiyumukiza, J. D., Cai, H. & Xiang, W. Prostaglandin E2 involvement in mammalian female fertility: ovulation, fertilization, embryo development and early implantation. *Reprod. Biol. Endocrinol.* **16**, 43 (2018).

75. Ke, J., Yang, Y., Che, Q., Jiang, F., Wang, H., Chen, Z., Zhu, M., Tong, H., Zhang, H., Yan, X., Wang, X., Wang, F., Liu, Y., Dai, C. & Wan, X. Prostaglandin E2 (PGE2) promotes proliferation and invasion by enhancing SUMO-1 activity via EP4 receptor in endometrial cancer. *Tumor Biol.* **37**, 12203–12211 (2016).

76. Legler, D. F., Bruckner, M., Uetz-von Allmen, E. & Krause, P. Prostaglandin E2 at new glance: Novel insights in functional diversity offer therapeutic chances. *Int. J. Biochem. Cell Biol.* **42**, 198–201 (2010).

77. Kaczynski, P., Bauersachs, S., Goryszewska, E., Baryla, M. & Waclawik, A. Synergistic action of estradiol and PGE2 on endometrial transcriptome in vivo resembles pregnancy effects better than estradiol alone. *Biol. Reprod.* **104**, 818–834 (2021).

78. Cha, Y. I., Kim, S. H., Sepich, D., Gregory Buchanan, F., Solnica-Krezel, L. & DuBois, R. N. Cyclooxygenase-1-derived PGE2 promotes cell motility via the G-protein-coupled EP4 receptor during vertebrate gastrulation. *Genes Dev.* **20**, 77–86 (2006).

79. Dey, I., Lejeune, M. & Chadee, K. Prostaglandin E 2 receptor distribution and function in the gastrointestinal tract. *British Journal of Pharmacology*. **149**, 611–623 (2006).

80. Reinold, H., Ahmadi, S., Depner, U. B., Layh, B., Heindl, C., Hamza, M., Pahl, A., Brune, K., Narumiya, S., Müller, U. & Zeilhofer, H. U. Spinal inflammatory hyperalgesia is mediated by prostaglandin E receptors of the EP2 subtype. *J. Clin. Invest.* **115**, 673–679 (2005).

81. Marra, A. N., Adeeb, B. D., Chambers, B. E., Drummond, B. E., Ulrich, M., Addiego, A., Springer, M., Poureetezadi, S. J., Chambers, J. M., Ronshaugen, M. & Wingert, R. A. Prostaglandin signaling regulates renal multiciliated cell

specification and maturation. *Proc. Natl. Acad. Sci. U. S. A.* **116**, 8409–8418 (2019).

82. Wingert RA, K. P. Molecular Mechanisms of Podocyte Development Revealed by Zebrafish Kidney Research. *Cell Dev. Biol.* **03**, 1000138 (2014).

83. Chen, Z., Luciani, A., Mateos, J. M., Barmettler, G., Giles, R. H., Neuhauss, S. C. F. & Devuyst, O. Transgenic zebrafish modeling low-molecular-weight proteinuria and lysosomal storage diseases. *Kidney Int.* **97**, 1150–1163 (2020).

84. Drummond, I. A. & Davidson, A. J. Zebrafish kidney development. *Methods Cell Biol.* **134**, 391-429 (2016).

85. Majumdar, A. & Drummond, I. A. Podocyte differentiation in the absence of endothelial cells as revealed in the zebrafish avascular mutant, cloche. *Dev. Genet.* **24**, 220–229 (1999).

86. Endlich, N., Simon, O., Göpferich, A., Wegner, H., Moeller, M. J., Rumpel, E., Kotb, A. M. & Endlich, K. Two-photon microscopy reveals stationary podocytes in living zebrafish larvae. *J. Am. Soc. Nephrol.* **25**, 681–686 (2014).

87. Ichimura, K., Fukuyo, Y., Nakamura, T., Powell, R., Sakai, T., Janknecht, R. & Obara, T. Developmental localization of Nephrin in zebrafish and medaka pronephric glomerulus. *J. Histochem. Cytochem.* **61**, 313–324 (2013).

88. Müller, T., Rumpel, E., Hradetzky, S., Bollig, F., Wegner, H., Blumenthal, A., Greinacher, A., Endlich, K. & Endlich, N. Non-muscle myosin IIA is required for the development of the zebrafish glomerulus. *Kidney Int.* **80**, 1055–1063 (2011).

89. Drummond, I. A., Majumdar, A., Hentschel, H., Elger, M., Solnica-Krezel, L., Schier, A. F., Neuhauss, S. C., Stemple, D. L., Zwartkruis, F., Rangini, Z., Driever, W. & Fishman, M. C. Early development of the zebrafish pronephros and analysis of mutations affecting pronephric function. *Development* **125**, 4655–4667 (1998).

90. Cianciolo Cosentino, C., Berto, A., Pelletier, S., Hari, M., Loffing, J., Neuhauss, S. C. F. & Doye, V. Moderate Nucleoporin 133 deficiency leads to glomerular damage in zebrafish. *Sci. Rep.* **9**, 1–14 (2019).

91. Kramer-Zucker, A. G., Wiessner, S., Jensen, A. M. & Drummond, I. A. Organization of the pronephric filtration apparatus in zebrafish requires Nephrin, Podocin and the FERM domain protein Mosaic eyes. *Dev. Biol.* **285**, 316–329

(2005).

92. Pohlmann, A., Zhao, K., Fain, S. B., Prasad, P. V & Niendorf, T. Experimental Protocol for MRI Mapping of the Blood Oxygenation-Sensitive Parameters T(2)* and T(2) in the Kidney. *Methods Mol. Biol.* **2216**, 403–417 (2021).

93. Nasrallah, R., Hassouneh, R. & Hébert, R. L. PGE2, kidney disease, and cardiovascular risk: Beyond hypertension and diabetes. *Journal of the American Society of Nephrology.* **27,** 666–676 (2016).

94. Friedrich, C., Endlich, N., Kriz, W. & Endlich, K. Podocytes are sensitive to fluid shear stress in vitro. *Am. J. Physiol. Physiol.* **291**, F856–F865 (2006).

95. Hao, C.-M. & Breyer, M. D. Physiological regulation of prostaglandins in the kidney. *Annu. Rev. Physiol.* **70**, 357–377 (2008).

96. Wang, L., Wu, Y., Jia, Z., Yu, J. & Huang, S. Roles of EP Receptors in the Regulation of Fluid Balance and Blood Pressure. *Frontiers in Endocrinology.* **13**, 875425 (2022).

97. Sakuma, S., Fujimoto, Y., Nakagawa, H., Hachiki, S., Nishida, H. & Fujita, T. Effect of 13-hydroperoxyoctadecadienoic acid on 15-hydroxy prostaglandin dehydrogenase activity in rabbit kidney cortex. *Prostaglandins* **46**, 157–165 (1993).

98. Sakuma, S., Fujimoto, Y., Hikita, E., Okano, Y., Yamamoto, I. & Fujita, T. Effects of metal ions on 15-hydroxy prostaglandin dehydrogenase activity in rabbit kidney cortex. *Prostaglandins* **40**, 507–514 (1990).

99. Tsai, M. Y. & Einzig, S. Prostaglandin catabolism in fetal and maternal tissues — A study of 15-hydroxyprostaglandin dehydrogenase and Δ13 reductase with specific assay methods. *Prostaglandins, Leukot. Essent. Fat. Acids* **38**, 25–30 (1989).

100. Kim, B. W., Kim, H. J., Kim, S.-H., Baik, H. J., Kang, M. S., Kim, D.-H., Markowitz, S. D., Kang, S. W. & Bae, K. B. 15-Hydroxyprostaglandin dehydrogenase inhibitor prevents contrast-induced acute kidney injury. *Ren. Fail.* **43**, 168–179 (2021).

101. Kim, H. J., Kim, S. H., Kim, M., Baik, H. J., Park, S. J., Kang, M. S., Kim, D. H., Kim, B. W., Markowitz, S. D. & Bae, K. B. Inhibition of 15-PGDH prevents ischemic renal injury by the PGE2/EP4signaling pathway mediating vasodilation,

increased renal blood flow, and increased adenosine/A2Areceptors. *Am. J. Physiol. - Ren. Physiol.* **319**, F1054–F1066 (2020).

102. Miao, S., Lv, C., Liu, Y., Zhao, J., Li, T., Wang, C., Xu, Y., Wang, X., Xiao, X. & Zhang, H. Pharmacologic Blockade of 15-PGDH Protects Against Acute Renal Injury Induced by LPS in Mice. *Frontiers in Physiology.* **11,** 138 (2020).

103. Mohamed, R., Jayakumar, C. & Ramesh, G. Chronic administration of EP4-selective agonist exacerbates albuminuria and fibrosis of the kidney in streptozotocin-induced diabetic mice through IL-6. *Lab. Investig.* **93**, 933–945 (2013).

104. Thieme, K., Majumder, S., Brijmohan, A. S., Batchu, S. N., Bowskill, B. B., Alghamdi, T. A., Advani, S. L., Kabir, M. G., Liu, Y. & Advani, A. EP4 inhibition attenuates the development of diabetic and non-diabetic experimental kidney disease. *Sci. Rep.* **7**, 3442 (2017).

105. Mizukami, K., Yoshida, H., Nozawa, E., Wada, K. & Ugawa, T. Renoprotective effects of the novel prostaglandin EP4 receptor-selective antagonist ASP7657 in 5/6 nephrectomized chronic kidney disease rats. *Naunyn. Schmiedebergs. Arch. Pharmacol.* **392**, 451–459 (2019).

106. Yao, L., Chen, W., Song, K., Han, C., Gandhi, C. R., Lim, K. & Wu, T. 15-hydroxyprostaglandin dehydrogenase (15-PGDH) prevents lipopolysaccharide (LPS)-induced acute liver injury. *PLoS One* **12**, 1–16 (2017).

107. Chen, I. J., Hee, S. W., Liao, C. H., Lin, S. Y., Su, L., Shun, C. T. & Chuang, L. M. Targeting the 15-keto-PGE2-PTGR2 axis modulates systemic inflammation and survival in experimental sepsis. *Free Radic. Biol. Med.* **115**, 113–126 (2018).

108. Lee, E. J., Kim, S.-J., Hahn, Y.-I., Yoon, H.-J., Han, B., Kim, K., Lee, S., Kim, K. P., Suh, Y. G., Na, H.-K. & Surh, Y.-J. 15-Keto prostaglandin E2 suppresses STAT3 signaling and inhibits breast cancer cell growth and progression. *Redox Biol.* **23**, 101175 (2019).

109. Schlaich, M. P., Bellet, M., Weber, M. A., Danaietash, P., Bakris, G. L., Flack, J. M., Dreier, R. F., Sassi-Sayadi, M., Haskell, L. P., Narkiewicz, K., Wang, J.-G. & investigators, =PRECISION. Dual endothelin antagonist aprocitentan for resistant hypertension (PRECISION): a multicentre, blinded, randomised, parallel-group,

phase 3 trial. *Lancet (London, England)* **400**, 1927–1937 (2022).

110. Srivastava, T., Garola, R. E., Zhou, J., Boinpelly, V. C., Priya, L., Ali, M. F., Rezaiekhaligh, M. H., Heruth, D. P., Novak, J., Alon, U. S., Joshi, T., Jiang, Y., McCarthy, E. T., Savin, V. J., Johnson, M. L., Sharma, R. & Sharma, M. Prostanoid receptors in hyperfiltration-mediated glomerular injury: Novel agonists and antagonists reveal opposing roles for EP2 and EP4 receptors. *FASEB J.* **36**, e22559 (2022).

111. Davar, D., Powderly, J. D., Ulahannan, S. V., Johnson, M. L., Sharma, M., Krauss, J. C., Stagg, R., Francica, B., Moon, A., Jenkins, Y., Prasit, P., Dubensky, T. W., Whiting, S. H. & Papadopoulos, K. P. A phase 1 study of TPST-1495 as a single agent and in combination with pembrolizumab in subjects with solid tumors. *J. Clin. Oncol.* **40**, TPS2696–TPS2696 (2022).

Statutory Declaration

"I, Aikaterini Kourpa, by personally signing this document in lieu of an oath, hereby affirm that I prepared the submitted dissertation on the topic **"Investigating the role of PGE_2/15-keto-PGE_2/EP2/EP4 axis in kidney biology and disease" / "Untersuchung der Rolle der PGE_2/15-keto-PGE_2/EP2/EP4-Achse in der Nierenbiologie und bei Nierenerkrankungen"**, independently and without the support of third parties, and that I used no other sources and aids than those stated.

All parts which are based on the publications or presentations of other authors, either in letter or in spirit, are specified as such in accordance with the citing guidelines. The sections on methodology (in particular regarding practical work, laboratory regulations, statistical processing) and results (in particular regarding figures, charts and tables) are exclusively my responsibility.

Furthermore, I declare that I have correctly marked all of the data, the analyses, and the conclusions generated from data obtained in collaboration with other persons, and that I have correctly marked my own contribution and the contributions of other persons (cf. declaration of contribution). I have correctly marked all texts or parts of texts that were generated in collaboration with other persons.

My contributions to any publications to this dissertation correspond to those stated in the below joint declaration made together with the supervisor. All publications created within the scope of the dissertation comply with the guidelines of the ICMJE (International Committee of Medical Journal Editors; http://www.icmje.org) on authorship. In addition, I declare that I shall comply with the regulations of Charité – Universitätsmedizin Berlin on ensuring good scientific practice.

I declare that I have not yet submitted this dissertation in identical or similar form to another Faculty.

The significance of this statutory declaration and the consequences of a false statutory declaration under criminal law (Sections 156, 161 of the German Criminal Code) are known to me."

Date Signature

Declaration of my own contribution to the publications

I, Aikaterini Kourpa, contributed the following to the below listed publications:

Publication 1:

Kourpa, Aikaterini; Kaiser-Graf, Debora; Sporbert, Anje; Philippe, Aurélie; Catar, Rusan; Rothe, Michael; Mangelsen, Eva; Schulz, Angela; Bolbrinker, Juliane; Kreutz, Reinhold; Panáková, Daniela**. **15-keto-Prostaglandin E_2 exhibits bioactive role by modulating glomerular cytoarchitecture through EP2/EP4 receptors**. *Life Sciences* 2022; 310:121114. doi: 10.1016/j.lfs.2022.121114.

**correspondence

Contribution: I performed all the experiments and data analysis in the zebrafish model (transgenic lines *Tg[wt1b:EGFP]* and *Tg[fabp10a:gc-EGFP]*:

- Zebrafish breeding and husbandry.
- Drug treatments (15-keto-PGE_2, EP2 and EP4 antagonist, DMSO) in early (48 hpf) and late developmental (96 hpf) embryonic stages.
- Injection of anesthetized embryos with BSA-AlexaFluor555 conjugate.
- Preparation of samples for lipidomic analysis.
- I established the confocal microscopy imaging parameters of the zebrafish kidney in collaboration with Dr. Anje Sporbert (Max-Delbrück Center for Molecular Medicine, ALM facility) and prepared the samples for final imaging.
- Brightfield, fluorescence and confocal microscopy imaging.
- Phenotypic assessment and quantification.
- I performed the imaging analysis (ImageJ/Fiji, Huygens) and 3D glomerular reconstruction (Imaris). I established the process in collaboration with Dr. Anje Sporbert (Max-Delbrück Center for Molecular Medicine, ALM facility).

I created all the figures included in the publication. I performed the statistical analysis and generated the graphs of Figures 2, 3, 6 and supplemental Figure 1 of the original publication. I wrote the original draft and revised version of the manuscript; and addressed reviewers' questions during the revision process.

Figure 1 panels b, c, d were created by Debora Kaiser-Graf (co-author), who performed the experiments in the yeast model.

Publication 2:

Kourpa, Aikaterini*; Schulz, Angela*; Mangelsen, Eva; Kaiser-Graf, Debora; Koppers, Nils; Stoll, Monika; Rothe, Michael; Bader, Michael; Purfürst, Bettina; Kunz, Severine;

Gladytz, Thomas; Niendorf, Thoralf; Bachmann, Sebastian; Mutig, Kerim; Bolbrinker, Juliane; Panáková, Daniela; Kreutz, Reinhold**. **Studies in Zebrafish and Rat Models Support Dual Blockade of EP2 and EP4 (Prostaglandin E_2 Receptors Type 2 and 4) for Renoprotection in Glomerular Hyperfiltration and Albuminuria.** *Hypertension* 2023;80:771-782. doi:10.1161/HYPERTENSIONAHA.122.20392.

*Authors contributed equally

**correspondence

Contribution: I performed all the experiments and data analysis in the zebrafish model (transgenic lines *Tg[wt1b:EGFP]* and *Tg[fabp10a:gc-EGFP]*:

- Zebrafish breeding and husbandry.
- Drug treatments (dmPGE_2, EP2 and EP4 antagonist, DMSO) at late developmental (96 hpf) embryonic stages.
- Injection of anesthetized embryos with BSA-AlexaFluor555 conjugate.
- Preparation of samples for lipidomic analysis.
- Preparation of samples for confocal microscopy.
- Brightfield, fluorescence and confocal microscopy imaging.
- Phenotypic assessment and quantification.
- Mounting of embryos and cryo-sectioning and performing the immunofluorescence *in situ* hybridization (RNAscope).
- Imaging analysis (ImageJ/Fiji, Huygens) and 3D glomerular reconstruction (Imaris).
- Cutting of semi-thin sections of zebrafish embryos at 96 hpf for electron microscopy. I established the methodology for EM imaging of zebrafish embryonic kidney in collaboration with Dr. Bettina Purfürst and Dr. Severine Kunz (Max-Delbrück Center for Molecular Medicine, EM facility, Berlin Germany)

I performed the quantification of podocyte foot process width and number of slit diaphragms per µm of the GBM in both zebrafish embryos and MWF rats. The electron microscopy imaging of the MWF rats glomeruli was performed in collaboration with Prof. Sebastian Bachmann (Institute of Vegetative Anatomy, Charité–Universitätsmedizin Berlin)

Furthermore, I performed the full STRING protein network analysis of the differentially regulated genes and introduced the circadian clock shift hypothesis presented in Figure 6.

I performed the statistical analysis and generated the graphs of Figures 2 and 4 and supplemental Figure 1 and 7 of the original publication. In addition, I created the final versions of all the figures (main and supplement), the graphical abstract and supplemental Table 2.

I participated in the writing of the original draft of the manuscript, the revised version of the manuscript, and addressed reviewers' questions during the revision process.
Breeding and experimentation on the rats as well as qPCR analysis and rat sample preparation were performed by Dr.rer.medic. Angela Schulz (Institute of Clinical Pharmacology and Toxicology, Charité–Universitätsmedizin Berlin). RNA-sequencing was performed in collaboration with Nils Koppers and Prof. Monika Stoll (Genetic Epidemiology, Institute for Human Genetics, Westfälische Wilhelms University, Münster, Germany). MRI analysis on the MWF rats was performed in collaboration with Dr. Thomas Gladytz and Prof. Thoralf Niendorf (Max-Delbrück Center for Molecular Medicine, Berlin, Germany).

Publication 3:

Mangelsen, Eva.; Rothe, Michael.; Schulz, Angela.; Kourpa, Aikaterini.; Panáková, Daniela.; Kreutz, Reinhold.; Bolbrinker, Juliane**. **Concerted EP2 and EP4 Receptor Signaling Stimulates Autocrine Prostaglandin E2 Activation in Human Podocytes**. *Cells* 2020, 9:1256. doi: 10.3390/cells9051256.

**correspondence

Contribution: My contribution to this publication was the theoretical investigation and the literature review of the effect of COX2/PGE_2 pathway on podocytes injury. I contributed to the experimental design, and the discussion and interpretation of the experimental results.

_____

Signature, date and stamp of first supervising university professor / lecturer

_____

Signature of doctoral candidate

Excerpt from Journal Summary List and Printing copies of the publications

Excerpt from Journal Summary List

Journal Data Filtered By: **Selected JCR Year: 2021** Selected Editions: SCIE,SSCI Selected Categories: **"PHARMACOLOGY and PHARMACY"** Selected Category Scheme: WoS

Gesamtanzahl: 279 Journale

Rank	Full Journal Title	Total Cites	Journal Impact Factor	Eigenfaktor
1	NATURE REVIEWS DRUG DISCOVERY	47,615	112.288	0.04911
2	DRUG RESISTANCE UPDATES	4,905	22.841	0.00358
3	PHARMACOLOGICAL REVIEWS	15,259	18.923	0.00720
4	ADVANCED DRUG DELIVERY REVIEWS	47,828	17.873	0.02501
5	TRENDS IN PHARMACOLOGICAL SCIENCES	16,714	17.638	0.01363
6	Annual Review of Pharmacology and Toxicology	9,807	16.459	0.00557
7	INTERNATIONAL JOURNAL OF ANTIMICROBIAL AGENTS	21,098	15.441	0.02309
8	Acta Pharmaceutica Sinica B	9,420	14.903	0.00922
9	Journal of Pharmaceutical Analysis	3,869	14.026	0.00404
10	PHARMACOLOGY & THERAPEUTICS	23,869	13.400	0.01921
11	MEDICINAL RESEARCH REVIEWS	7,973	12.388	0.00665
12	JOURNAL OF CONTROLLED RELEASE	67,680	11.467	0.03824
13	DRUGS	18,328	11.431	0.01713
14	European Heart Journal-Cardiovascular Pharmacotherapy	1,529	11.177	0.00282
15	PHARMACOLOGICAL RESEARCH	26,468	10.334	0.02692
16	ANTIVIRAL RESEARCH	17,486	10.103	0.01806
17	ALIMENTARY PHARMACOLOGY & THERAPEUTICS	27,559	9.524	0.03078
18	BRITISH JOURNAL OF PHARMACOLOGY	46,366	9.473	0.02492
19	Asian Journal of Pharmaceutical Sciences	3,744	9.273	0.00288
20	DRUG DISCOVERY TODAY	21,224	8.369	0.01633
21	NEUROPSYCHOPHARMACOLOGY	34,562	8.294	0.03279

Rank	Full Journal Title	Total Cites	Journal Impact Factor	Eigenfaktor
22	Expert Opinion on Drug Delivery	10,532	8.129	0.00604
23	BIODRUGS	3,113	7.744	0.00409
24	Current Neuropharmacology	7,580	7.708	0.00713
25	Reviews of Physiology Biochemistry and Pharmacology	920	7.500	0.00043
26	BIOMEDICINE & PHARMACOTHERAPY	52,615	7.419	0.05905
27	Journal of Neuroimmune Pharmacology	4,036	7.285	0.00302
28	ACTA PHARMACOLOGICA SINICA	14,909	7.169	0.01116
29	Expert Opinion on Drug Discovery	5,789	7.050	0.00575
30	CNS Neuroscience & Therapeutics	6,186	7.035	0.00600
31	International Journal of Nanomedicine	39,405	7.033	0.02657
32	DRUG METABOLISM REVIEWS	3,548	6.984	0.00162
33	CLINICAL PHARMACOLOGY & THERAPEUTICS	21,749	6.903	0.01987
34	DRUG DELIVERY	10,117	6.819	0.00867
35	EXPERT OPINION ON THERAPEUTIC TARGETS	6,787	6.797	0.00562
36	LIFE SCIENCES	42,960	6.780	0.03206
37	EXPERT OPINION ON THERAPEUTIC PATENTS	4,626	6.714	0.00389
38	PHYTOMEDICINE	18,290	6.656	0.00959
39	Pharmaceutics	19,762	6.525	0.01881
40	INTERNATIONAL JOURNAL OF PHARMACEUTICS	67,742	6.510	0.03053
41	EXPERT OPINION ON INVESTIGATIONAL DRUGS	6,588	6.498	0.00566
42	CNS DRUGS	6,627	6.497	0.00642
43	PHYTOTHERAPY RESEARCH	22,172	6.388	0.00999
44	PHARMACOTHERAPY	8,339	6.251	0.00772

Selected JCR Year: 2021; Selected Categories: "PHARMACOLOGY and PHARMACY"

Printing copy of the publication

1.Kourpa, Aikaterini; Kaiser-Graf, Debora; Sporbert, Anje; Philippe, Aurélie; Catar, Rusan; Rothe, Michael; Mangelsen, Eva; Schulz, Angela; Bolbrinker, Juliane; Kreutz, Reinhold; Panáková, Daniela. **15-keto-Prostaglandin E_2 exhibits bioactive role by modulating glomerular cytoarchitecture through EP2/EP4 receptors**. *Life Sciences* 2022;310:121114. https://doi.org/10.1016/j.lfs.2022.121114.

Life Sciences 310 (2022) 121114

Contents lists available at ScienceDirect

Life Sciences

journal homepage: www.elsevier.com/locate/lifescie

15-keto-Prostaglandin E_2 exhibits bioactive role by modulating glomerular cytoarchitecture through EP2/EP4 receptors

Aikaterini Kourpa [a,b], Debora Kaiser-Graf [b], Anje Sporbert [c], Aurélie Philippe [d,e], Rusan Catar [d], Michael Rothe [f], Eva Mangelsen [b], Angela Schulz [b], Juliane Bolbrinker [b], Reinhold Kreutz [b], Daniela Panáková [a,*]

[a] Max Delbrück Center for Molecular Medicine in the Helmholtz Association, Buch, Berlin, Germany
[b] Charité-Universitätsmedizin Berlin, Corporate member of Freie Universität Berlin, Humboldt-Universität zu Berlin, and Berlin Institute of Health, Institute of Clinical Pharmacology and Toxicology, Berlin, Germany
[c] Max Delbrück Center for Molecular Medicine in the Helmholtz Association, Advanced Light Microscopy, Buch, Berlin, Germany
[d] Charité-Universitätsmedizin Berlin, Corporate member of Freie Universität Berlin, Humboldt-Universität zu Berlin, and Berlin Institute of Health, Department of Nephrology and Medical Intensive Care, Berlin, Germany
[e] Berlin Institute of Health, Charité-Universitätsmedizin Berlin, BIH Biomedical Innovation Academy, Berlin, Germany
[f] Lipidomix GmbH, Berlin, Germany

ARTICLE INFO

Keywords:
Prostaglandins
15-keto-PGE_2
EP receptors
Zebrafish
Podocytes
Glomerular vascularization

ABSTRACT

Aims: Prostaglandins are important signaling lipids with prostaglandin E_2 (PGE_2) known to be the most abundant prostaglandin across tissues. In kidney, PGE_2 plays an important role in the regulation of kidney homeostasis through its EP receptor signaling. Catabolism of PGE_2 yields the metabolic products that are widely considered biologically inactive. Although recent *in vitro* evidence suggested the ability of 15-keto-PGE_2 (a downstream metabolite of PGE_2) to activate EP receptors, the question whether 15-keto-PGE_2 exhibits physiological roles remains unresolved.
Materials and methods: Pharmacological treatment was performed in transgenic zebrafish embryos using 500 μM 15-keto-PGE_2 and 20 μM EP receptors antagonists' solutions during zebrafish embryonic development. After the exposure period, the embryos were fixed for confocal microscopy imaging and glomerular morphology analysis.
Key findings: Here, we show that 15-keto-PGE_2 can bind and stabilize EP2 and EP4 receptors on the plasma membrane in the yeast model. Using lipidomic analysis, we demonstrate both PGE_2 and 15-keto-PGE_2 are present at considerable levels in zebrafish embryos. Our high-resolution image analysis reveals the exogenous treatment with 15-keto-PGE_2 perturbs glomerular vascularization during zebrafish development. Specifically, we show that the increased levels of 15-keto-PGE_2 cause intercalation defects between podocytes and endothelial cells of glomerular capillaries effectively reducing the surface area of glomerular filtration barrier. Importantly, 15-keto-PGE_2-dependent defects can be fully reversed by combined blockade of the EP2 and EP4 receptors.
Significance: Altogether, our results reveal 15-keto-PGE_2 to be a biologically active metabolite that modulates the EP receptor signaling *in vivo*, thus playing a potential role in kidney biology.

1. Introduction

The human kidney consists of about a million of nephrons that comprise the basic structural and functional unit of the kidney [1–3]. Each nephron contains a glomerulus, the main blood filtration apparatus, a system of proximal and distal tubules, the loop of Henle, as well as the collecting duct, which are responsible for the nutrients, water and ions reabsorption, the maintenance of the normal fluid flow, and the concentration and excretion of the urine [1,3,4]. The glomerulus contains various specialized cells responsible for forming the capillaries network and the glomerular filtration barrier (GFB), the principal blood filtration system. The GFB consists of podocytes, the glomerular basement membrane (GBM) and the fenestrated endothelium [5,6]. In physiological conditions the GFB demonstrates relative impermeability to proteins with molecular weight above 70 kDa and other macromolecules, therefore prevents the excretion of blood cells and large proteins

* Corresponding author.
E-mail address: daniela.panakova@mdc-berlin.de (D. Panáková).

https://doi.org/10.1016/j.lfs.2022.121114
Received 22 August 2022; Received in revised form 6 October 2022; Accepted 17 October 2022
Available online 20 October 2022

into the urine [7]. Upon damage of the GFB, its permeability to the molecules of increasing size is affected resulting in the presence of molecules like albumin or larger in the urine, a pathological condition known as albuminuria [7,8].

Despite the distinct differences between fish and mammals in the formation and/or function of kidney arising most notably from the diverse living environment *i.e.* terrestrial *versus* aquatic, the human nephron shares a similar segmentation pattern with the zebrafish embryonic kidney (pronephros) [9] thus rendering the latter as an important model for studying kidney development and physiology as well as various forms of renal diseases [10–13]. The developing zebrafish pronephros consists of two nephrons with bilateral glomeruli, kidney tubules and a collecting duct [11,14]. In zebrafish, the onset of glomerular filtration takes place at 48 hours post fertilization (hpf), while the glomerular capillarization and the formation of the GFB is completed by 72 hpf [9,14,15].

Prostaglandins (PG) including PGE_2, $PGF_{2\alpha}$ and PGD_2, are important active lipid mediators synthesized from arachidonic acid (AA) with the participation of cyclooxygenases 1 and 2 (COX1, COX2) and specialized prostaglandin synthases [16,17]. They have been found in almost every tissue in humans as well as other vertebrates. Several reports highlight their crucial role in both physiological and pathological conditions including inflammatory response, cancer, homeostasis regulation, hematopoiesis, and kidney physiology [18–25]. Among them, prostaglandin E_2 (PGE_2) is the most abundant prostaglandin in various organs including the kidney, where the role of PGE_2 has been extensively studied in the past years [17,25,26]. PGE_2 contributes to the normal renal physiology as well as pathogenic mechanisms underlying the initiation and progression of chronic kidney disease (CKD) [17,27].

PGE_2 acts through its four G-protein–coupled prostaglandin receptors (EP): EP1, EP2, EP3 and EP4 [28,29]. Recently, we showed that combined EP2 and EP4 signaling is important for autocrine PGE_2 activation in human podocytes [30]. Thus, these receptors could be important targets for the development of therapeutic strategies against multiple renal complications ascribed to prostaglandin signaling [17,25–27,31]. The catabolism of PGE_2 involves two steps [32] (Fig. 1a). The first and also rate-limiting step is catalyzed by 15-prostaglandin dehydrogenase (15-PGDH) and results in the synthesis of 15-keto-PGE_2 [32]. The enzyme that catalyzes the second step of the complete PGE_2 inactivation is prostaglandin reductase (PTGR or Δ^{13}-PG-Reductase) and yields 13,14-dihydro-15-keto-PGE_2 [32,33]. Until recently, these catabolic products, 15-keto-PGE_2 and 13,14-dihydro-15-

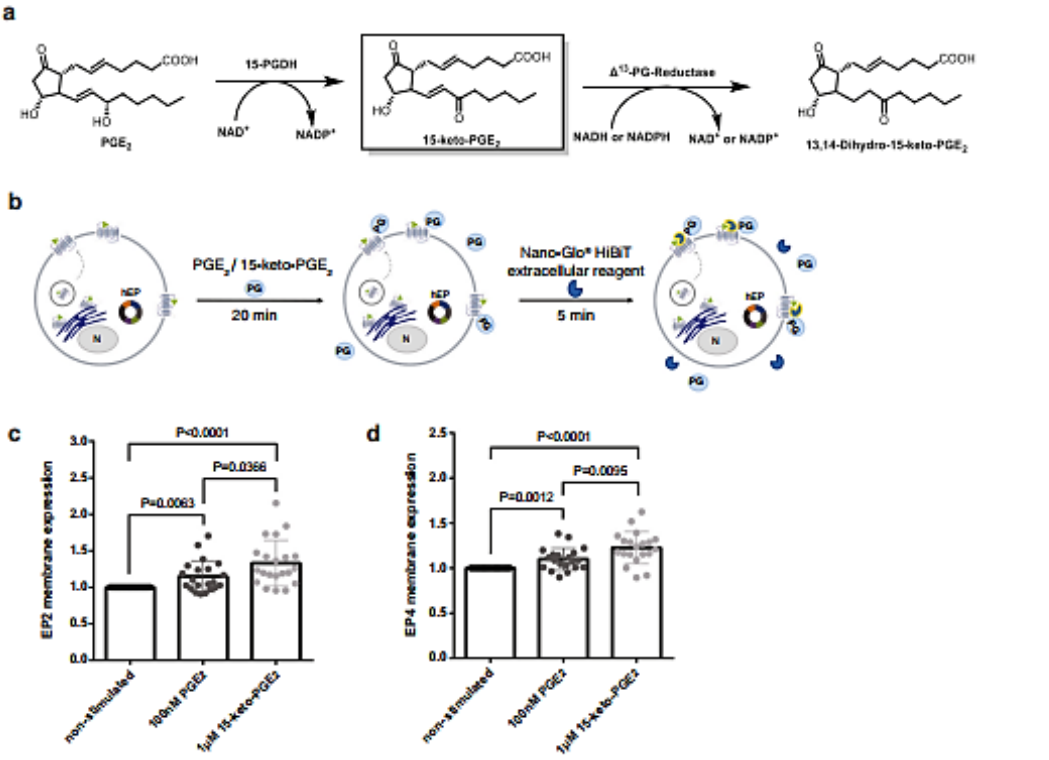

Fig. 1. 15-keto-PGE_2 binds EP receptors *in vitro*. (a) PGE_2 degradation pathway highlighting the first synthesized metabolic product, 15-keto-PGE_2. (b) Schematic of the experimental assay to measure receptor membrane expression using the Nano-Glo® HiBiT Extracellular Detection System. The HiBiT-tagged receptor is synthesized, processed and released from the endoplasmic reticulum (ER) and transported by secretory vesicles to the cell membrane. Yeast expressing HiBiT-tagged hEP2 or HiBiT-tagged hEP4 receptors on the membrane were stimulated with either 100 nM PGE_2, 1 µM 15-keto-PGE_2 or equal volume of medium for non-stimulated controls for 20 min to allow ligand binding. Adding of Nano-Glo® HiBiT Extracellular Reagent (containing Buffer, substrate and LgBiT protein) generated luminescence by structural complementation of LgBiT proteins with extra-cellular displayed HiBiT-tags, and thus allowing quantification of the number of receptors in the membrane; N represents cell nucleus. Quantification graphs of the (c) HiBiT-tagged hEP2 and (d) HiBiT-tagged hEP4 receptors cell membrane expression after 20 min stimulation with PGE_2 (dark grey) and 15-keto-PGE_2 (light grey). Wilcoxon test and Mann-Whitney tests were performed. Values are plotted as mean ± SD; $P < 0.05$ considered significant.

keto-PGE_2, were widely considered as biologically inactive [32,34]. Latest *in vitro* studies have, however, suggested that 15-keto-PGE_2 can activate the production of cAMP *via* EP receptors [35], and may act as a partial agonist of EP2, taking over the signaling roles of PGE_2 [36]. In addition, new evidence indicates 15-keto-PGE_2 is able to stimulate peroxisome proliferator-activated receptor gamma (PPAR-γ) in various models [37–39]. Importantly, the physiological importance of the PGE_2 metabolites, and specifically, 15-keto-PGE_2, in the kidney biology and its potential to activate EP receptors *in vivo* remains unresolved.

Here, we use the yeast model expressing human EP2 (hEP2) and EP4 (hEP4) receptors and the developing zebrafish kidney to examine the signaling potential of 15-keto-PGE_2. We investigate whether 15-keto-PGE_2 is capable of stimulating the EP receptors *in vivo* and further elucidate the potential role of prostaglandin catabolic pathway in kidney biology with the focus on GFB formation and function.

2. Results

2.1. 15-keto-PGE_2 binds EP2 and EP4 receptors in vitro

Although recent *in vitro* studies demonstrated 15-keto-PGE_2, the metabolic product synthesized during the PGE_2 inactivation (Fig. 1a), is able to stimulate G-protein-coupled EP receptors [35,36], its prospective signaling role is not fully resolved. To better understand the interaction between 15-keto-PGE_2 and the EP receptors, we used the Nano-Glo® HiBiT extracellular detection system (see Material and methods for details) applied in the yeast model, in which the single GPCR of the yeast (MMY28 strain) [40] was replaced upon transformation to express individually HiBiT-tagged human EP2 (hEP2) and EP4 (hEP4) receptors (Fig. 1b). This system allowed us to quantify the relative membrane expression of hEP2 and hEP4 receptors before and after prostaglandin

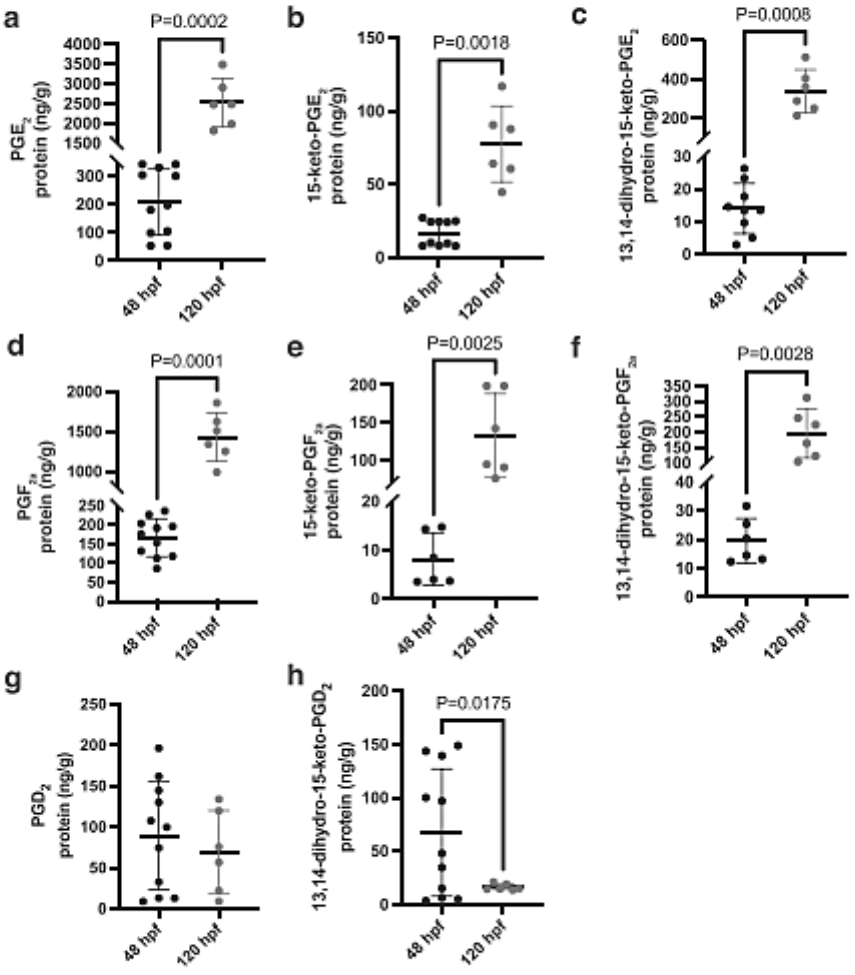

Fig. 2. Prostaglandin lipidomic profiles of developing zebrafish embryos. (a-h) Lipidomic analysis of whole zebrafish embryos at two different developmental stages (48 hpf and 120 hpf) showing the levels of the main prostaglandins and their metabolites: (a) PGE_2 ($P = 0.0002$), (b) 15-keto-PGE_2 ($P = 0.0018$), (c) 13,14-dihydro-15-keto-PGE_2 ($P = 0.0008$), (d) PGF_{2a} ($P = 0.0001$), (e) 15-keto-PGF_{2a} ($P = 0.0025$), (f) 13,14-dihydro-15-keto-PGF_{2a} ($P = 0.0028$), (g) PGD_2 ($P = 0.5006$) and (h) 13,14-dihydro-15-keto-PGD_2 ($P = 0.0175$). For 48 hpf: $N = 11$, $n = 275$ (less points in some of the graphs indicate missing values due to non-detectable levels). For 120 hpf: $N = 6$, $n = 150$. For all graphs, two-tailed unpaired *t*-test with Welch's correction was performed. Values are plotted as mean ± SD; $P < 0.05$ considered significant.

ligand stimulation (Fig. 1b). We incubated the transformed yeast cells with 100 nM PGE_2 or 1 μM 15-keto-PGE_2 for 20 min (Fig. 1c, d). For both hEP2 and hEP4, receptor count on the membrane was significantly increased after the stimulation with PGE_2 as well as with 15-keto-PGE_2 as compared to non-stimulated (absence of ligand) control condition (Fig. 1c, d). These observations suggest that apart from the well-established role of PGE_2 in activation of both EP2 and EP4 receptors [28,30,41–44], 15-keto-PGE_2 has also a potential of binding both EP2 and EP4 receptors and is able to stabilize their membrane localization.

In summary, our *in vitro* experiments indicate 15-keto-PGE_2 is able to bind both EP2 and EP4 receptors in agreement with other data [36]. Although 15-keto-PGE_2 has been shown to activate the production of cAMP *via* EP receptors [35], its downstream steps of receptor activation and signaling require further biochemical investigations. Whether 15-keto-PGE_2 has the bioactive potential to modulate the EP signaling *in vivo* needs to be elucidated.

2.2. PGE_2 is the most abundant prostaglandin during zebrafish embryonic development

To investigate the physiological role of 15-keto-PGE_2 *in vivo*, we used the zebrafish model having several advantageous attributes when it comes to testing the biological effects of small molecules and metabolites. First, we set out to determine what were the levels of 15-keto-PGE_2 in developing zebrafish embryos using the whole embryo lipidomic analysis. It is important to note that throughout the first developmental stages, *i.e.* until around 120 hpf, zebrafish embryo's nutrition depends on the yolk content [45]. Due to this dependency, metabolites and nutrients are not affected by exogenous factors like food intake, rendering the whole embryo lipidomic analysis reliable and fairly accurate [46].

We used the non-targeted metabolomic method based on liquid chromatography electrospray ionization tandem mass spectrometry (LC/ESI-MS/MS) to analyze the total prostaglandin metabolic pathway in the zebrafish embryos at two time points: 48 and 120 hpf, prior to and after the GFB formation, respectively (Fig. 2a-h). We determined the presence of all main prostaglandins, namely PGE_2, PGF_{2a} and PGD_2 as well as their catabolic products in the wild-type zebrafish whole embryo extracts (Fig. 2a-h). PGE_2 appeared to be the most abundant prostaglandin in both developmental stages (Fig. 2a). Markedly, the mean levels of PGE_2 and PGF_{2a} at 120 hpf (2522.13 ng/g and 1427.59 ng/g, respectively) were approximately by one order of magnitude higher compared to 48 hpf (209.36 ng/g and 165.98 ng/g, respectively) (Fig. 2a, d), while the levels of PGD_2 remained constant (Fig. 2g). Compared to PGE_2, its metabolite 15-keto-PGE_2 was also present but at approximately 10-fold lower levels than PGE_2, with the mean levels of 16.82 ng/g and 77.37 ng/g at 48 hpf and 120 hpf, respectively (Fig. 2b). 15-keto-PGE_2 showed higher levels compared to 15-keto-PGF_{2a} metabolite at 48 hpf, while both metabolites were present at similar levels at 120 hpf (Fig. 2b, e). The downstream metabolites of 15-keto-PG, *i.e.* 13,14-dihydro-15-keto-PG followed similar pattern (Fig. 2c, f, h).

Our data provide the quantitative analysis of the prostaglandin pathway during zebrafish development. We showed PGE_2 is the main prostaglandin present in the zebrafish embryos consistent with other animal models and humans [47–50]. Its metabolite, 15-keto-PGE_2 is also relatively highly abundant underscoring its potential role in organismal physiology.

2.3. 15-keto-PGE_2 exposure results in kidney morphological changes

Since PGE_2 has been reported to regulate the kidney development in zebrafish [44,51–53], we opted for investigating the potential biological role of 15-keto-PGE_2 in the kidney formation in this model. We followed a pharmacological approach similar to drug screenings that have previously established prostaglandin effects in the kidney morphogenesis [44]. Embryos were exposed to the DMSO vehicle and 15-keto-PGE_2 (500 μM) prior to the formation of GFB, from 6 hpf to 48 hpf (Fig. 3a).

We used the transgenic line *Tg[wt1b:eGFP]*, in which the parietal epithelium and podocytes of the glomeruli are labeled with GFP fluorescence, to perform phenotypic assessment of the embryo development as well as kidney formation by the combination of brightfield and fluorescence microscopy (Fig. 3b). Apart from the mild fluid accumulation (edema) observed in the yolk area at 48 hpf, no other major phenotypic defects were detected in the embryos after early treatment with 15-keto-PGE_2 (Fig. 3b). Importantly, cardiac development and function including blood circulation did not show any impairment, suggesting no major changes in the overall hemodynamics. However, the pronephros morphology was significantly affected and associated with the impaired glomerular development and defects in the pronephric tubules angle (Fig. 3b, c).

The observed defects in the kidney morphogenesis after 15-keto-PGE_2 exposure suggest, this metabolite may play a potential role in kidney biology. Of note, other organs including liver may be affected as

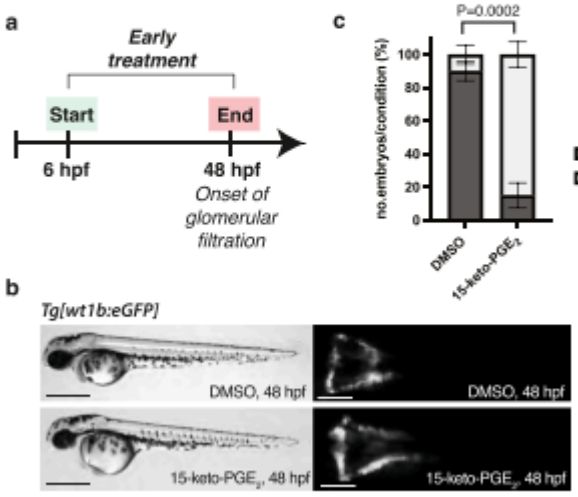

Fig. 3. Zebrafish pronephros is affected after early treatment with 15-keto-PGE_2. (a) Experimental design of the early pharmacological treatment, starting from 6 hpf until 48 hpf. (b) Brightfield and fluorescence microscopy images of *Tg[wt1b:eGFP]* embryos at 48 hpf, following pharmacological treatments with DMSO vehicle 0.88 % (upper panel) and 15-keto-PGE_2 500 μM (lower panel). Scale bar: 500 μm for brightfield images and 200 μm for fluorescent images. (c) Phenotypic quantitative analysis of zebrafish embryos at 48 hpf. Embryos are categorized as "no phenotype" (pronephros morphology remains unaffected after DMSO treatment) or "affected pronephros + yolk edema" (kidney phenotype observed after exposure to 15-keto-PGE_2); $N = 3$, $n = 30$ for both conditions; Percentage values are plotted as mean ± SD; n represents biologically independent samples over N independent experiments; Ordinary two-way ANOVA with Tukey's multiple comparison test ($P = 0.0002$); $P < 0.05$ considered significant.

well, but were not focus of this study.

2.4. Development and vascularization of glomerulus in the zebrafish embryonic kidney

To better understand the morphological changes in the glomerulus after the 15-keto-PGE_2 exposure, we decided to resolve the glomerular cytoarchitecture at the subcellular resolution using 3D confocal laser scanning microscopy. Glomerular morphology alters to a great extent during early kidney development, but its detailed visualization in the developing zebrafish is sparse [14,54–58]. We therefore first analyzed the critical steps in glomerular formation in *Tg[wt1b:EGFP]* in more detail (Fig. 4). In addition to the labeled podocytes and parietal epithelial cells in these transgenics, we performed the angiography using bovine serum albumin (BSA) conjugated with AlexaFluor555 to mark the endothelial cells of glomerular capillaries as previously described [59]. We visualized glomeruli development and its vascularization throughout five different stages; at 30, 48, 52, 72, 120 hpf. At 30 hpf, in nephron primordia stage (the most immature stage of the nephrons) the glomeruli appear as an unvascularized group of cells directly abutting the dorsal aorta in the midline of the embryo (Fig. 4, 30 hpf). At 48 hpf, endothelial cells start invading the space between the bilateral nephron primordia, forcing the invagination of the podocytes resulting in the formation of the glomerular cleft (Fig. 4, 48 hpf). A few hours later, at 52 hpf, the progressive invasion of endothelial cells drives the elaborated intercalation of podocytes around the continuously growing glomerular capillaries (Fig. 4, 52 hpf). At 72 hpf, the podocytes form finger-like projections interwoven with forming capillaries (Fig. 4, 72 hpf), resembling interlaced fingers of clasped hands. At this stage the formation of GFB is complete in zebrafish [14]. Between 72 and 120 hpf, the process of the complex infoldings between the endothelial cells and podocytes continues (Fig. 4, 120 hpf). Ultimately, the progressive infoldings of the GBM driven by cell-cell interactions between endothelial cells and podocytes lead to the complete maturation of the glomeruli along with the functional filtration apparatus.

Our detailed morphological analysis suggests the formation and the maturation of the GFB follow distinct steps that depend on the intricate cell-cell interaction between podocytes and endothelial cells throughout the entire process.

2.5. 15-keto-PGE_2 perturbs the proper GFB formation and maturation in zebrafish

The increased fluid flow shear stress in the glomeruli that arises for instance after unilateral nephrectomy [60], may result in elevated levels of PGE_2 linked to the podocyte damage and potential albuminuria [61,62]. Interestingly, the increased levels of PGE_2 and 15-keto-PGE_2 were also measured in a well-established Münich Wistar Frömter (MWF) rat model of CKD with glomerular hyperfiltration and albuminuria [30], but whether 15-keto-PGE_2 may contributes to the renal pathological phenotype is unresolved. Our results showing that the early treatment with 15-keto-PGE_2 led to possible alterations in glomerular structure (Fig. 3), prompted us to analyze the potential defects in glomerular cytoarchitecture using high-resolution confocal microscopy at the subcellular level (Fig. 5). The early treatment with 15-keto-PGE_2 caused defects in the invasion of endothelial cells as well as podocyte intercalation resulting in the absence of the proper glomerular cleft formation at 48 hpf (Fig. 5a, b). We were then curious whether any changes in glomerular cytoarchitecture could occur after the late treatment with 15-keto-PGE_2 from 72 hpf to 96 hpf, *i.e.* after the formation of GFB (Supplementary Fig. S1a, Fig. 5c, d). First, the late 15-keto-PGE_2 treatment resulted in the defects of the body axis, the absence of the swim bladder formation, and the expansion of the liver in the embryos at 96 hpf (Supplementary Fig. S1a, b). In the glomerulus, the late exposure to the 15-keto-PGE_2 metabolite had a profound impact on its maturation causing similar effects as after the early treatment; the podocyte intercalation around the glomerular capillaries was markedly impaired with the characteristic clustering of podocytes in the embryo midline (Fig. 5c, d).

Could these cellular defects result in the impairment of the GFB function? To that end, we used a GFP-tagged albumin surrogate (gc-EGFP) expressed in the transgenic line *Tg[fabp10a:gc-EGFP]* and circulating in the blood plasma [63]. This model has been widely used to evaluate the GFB integrity and function in zebrafish, since in the case of the GFB damage, the albumin surrogate leaks through the GFB, resulting in the loss of GFP fluorescence in the vasculature [53,63]. We did not observe any significant GFB permeability defects at 96 hpf as the GFP signal was comparable between the control and 15-keto-PGE_2-treated embryos (Supplementary Fig. S1b, c).

Our results demonstrate that 15-keto-PGE_2 can profoundly affect the interaction between podocytes and endothelial cells throughout the glomeruli formation, at the initial stage of glomerular cleft formation as well as during complex infoldings of the GBM, and suggest 15-keto-PGE_2 may have a potential active role in the fine-tuning of the GFB physiology. The fact that late treatment with 15-keto-PGE_2 did not affect GFB permeability may be due to several aspects including relatively short exposure time.

2.6. Glomerular surface area is significantly decreased after exogenous 15-keto-PGE_2 stimulation

To better understand how the impaired podocyte intercalation around the glomerular capillaries after 15-keto-PGE_2 treatment may affect GFB, we proceeded with further morphological analysis of the glomerulus. Using the Imaris software, we obtained the 3D glomerular reconstruction and surface creation by segmentation of the glomeruli labeled with GFP in *Tg[wt1b:eGFP]* transgenics at 96 hpf to quantify the glomerular volume and surface area in the DMSO-treated control and 15-keto-PGE_2-treated embryos (Fig. 6a-c). Glomerular volume showed a numerical decrease in the 15-keto-PGE_2-treated embryos as compared to DMSO controls (Fig. 6b). Importantly, the surface area covered by podocytes was significantly decreased after exposure to the 15-keto-PGE_2 metabolite (Fig. 6c).

The intercalation defects between podocytes and endothelial cells after 15-keto-PGE_2 exposure led to the reduction of GFB surface area that might ultimately affect the GFB function.

2.7. 15-keto-PGE_2-induced defects are mediated through EP2/EP4 receptors

We were wondering whether the 15-keto-PGE_2 treatment induced the observed morphological defects through EP receptor activation. Since our *in vitro* data indicated that 15-keto-PGE_2 binds both EP2 and EP4 receptors, we deployed EP antagonists, PF-04418948 and ONO-AE3-208, blocking EP2 and EP4, respectively. We simultaneously treated zebrafish embryos with 15-keto-PGE_2 and EP2 and EP4 antagonists to test whether blocking the receptors will dampen or block 15-keto-PGE_2-induced effects (Fig. 6a-c). Remarkably, the simultaneous pharmacological blockade of EP2 and EP4 receptors in 15-keto-PGE_2-treated embryos abolished the podocyte clustering and the complexity of the GBM infoldings was restored (Fig. 6a). The quantification of the glomerular volume as well as surface area revealed complete restoration of the 15-keto-PGE_2-induced effects when compared to the vehicle controls (Fig. 6b, c).

In summary, our data provide evidence for 15-keto-PGE_2 modulating EP2 and EP4 receptors signaling *in vivo*.

3. Discussion

The prostaglandin E_2 pathway plays a crucial role in various physiological and pathological conditions and has been extensively reported for its involvement in renal diseases [17,25–27,64,65]. However, the

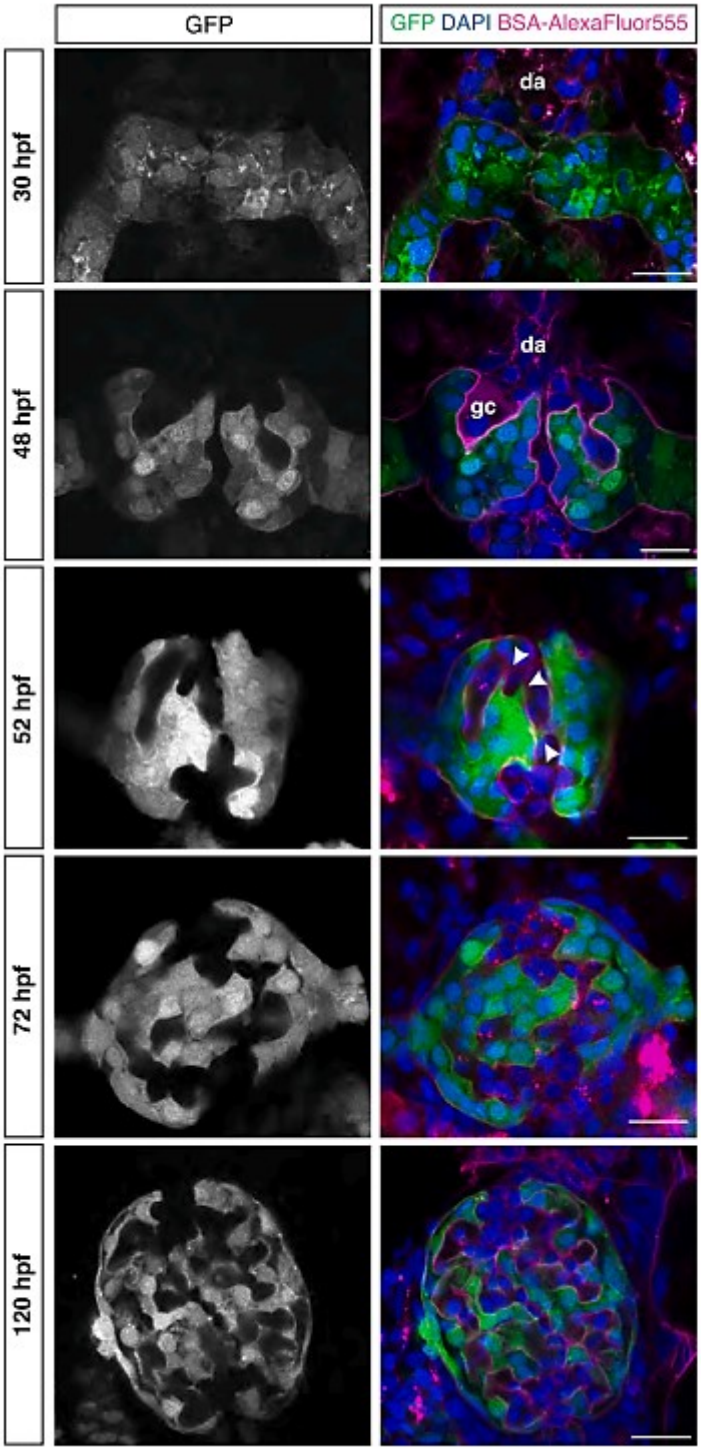

Fig. 4. Glomerular morphogenesis occurs in distinct steps. Zebrafish glomerular developmental stages. Representative high-resolution confocal microscopy images (single confocal section) of the *Tg[wt1b:eGFP]* developing zebrafish embryonic kidney at different developmental stages, 30 hpf (nephron primordia), 48 hpf, 52 hpf, 72 hpf and 120 hpf in an order from top to bottom. The podocytes and parietal epithelial cells in the glomeruli in grey (left), in green (in merge, right), endothelial cells of glomeruli capillaries in magenta (BSA-AlexaFluor555, in merge), cells nuclei in blue (DAPI, in merge). At 52 hpf, podocyte protrusions (arrowheads) start surrounding the capillaries to form the mature GFB. Dorsal aorta (da) and glomerular cleft (gc) are observed at the early developmental stages of the glomerulus. Scale bar = 10 μm. (For interpretation of the references to colour in this figure legend, the reader is referred to the web version of this article.)

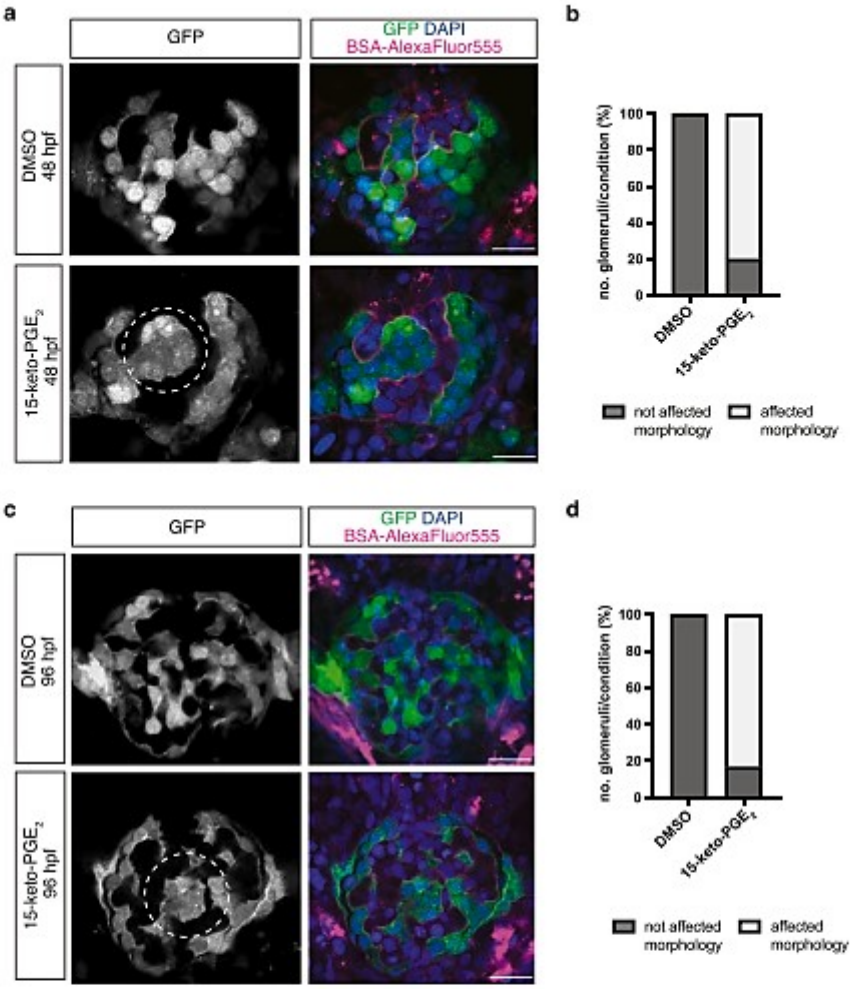

Fig. 5. 15-keto-PGE_2 exposure affects podocyte intercalation process during glomerular vascularization. (a) Representative confocal microscopy images of *Tg[wt1b:eGFP]* zebrafish glomeruli at 48 hpf after DMSO vehicle 0.88 % and 15-keto-PGE_2 500 μM treatment; $N = 2$, $n = 5$ for both conditions; dotted-line circle indicates podocyte consolidation and failure of normal elaboration around the continuously forming glomerular capillaries. (b) Quantification graph showing the percentage of imaged glomeruli with affected morphology at 48 hpf after exposure to DMSO (not affected morphology) and 15-keto-PGE_2 (4 out of 5 imaged glomeruli showed affected morphology). (c) Representative confocal microscopy images of *Tg[wt1b:eGFP]* zebrafish glomeruli at 96 hpf after DMSO vehicle 0.88 % and 15-keto-PGE_2 500 μM treatment; $N = 3$, $n = 7$ for DMSO and $N = 3$, $n = 6$ for 15-keto-PGE_2; dotted-line circle indicates impaired podocyte intercalation around the formed capillaries. (d) Quantification graph showing the percentage of imaged glomeruli with affected morphology at 96 hpf after exposure to DMSO (not affected morphology) and 15-keto-PGE_2 (5 out of 6 imaged glomeruli showed affected morphology). In all images, grey scale images show the podocytes and parietal epithelial cells in the glomeruli; in the merge podocytes and parietal epithelial cells are represented in green (eGFP), endothelial cells of glomeruli capillaries are marked in magenta (BSA-AlexaFluor555) and cells nuclei in blue (DAPI); Scale bar = 10 μm. (For interpretation of the references to colour in this figure legend, the reader is referred to the web version of this article.)

metabolic products of PGE_2 degradation, 15-keto-PGE_2 and 13,14-dihydro-15-keto-PGE_2, have been mainly considered biologically inactive [32,34]. Here, we show that 15-keto-PGE_2 affects the glomerular morphology of the developing zebrafish embryonic kidney through EP2/EP4 receptors. To our best knowledge, our study determines previously unrecognized *in vivo* effects of 15-keto-PGE_2 in kidney biology and outlines its possible modulatory effects on EP2/EP4 signaling.

In recent years, the potential bioactive role of 15-keto-PGE_2 has attracted increased research focus [37–39,66,67]. The 15-keto-PGE_2 effects have been mainly investigated in the context of the peroxisome proliferator-activated receptor gamma (PPAR-γ) signaling [37–39]. Through PPAR-γ activation, 15-keto-PGE_2 inhibits the production of lipopolysaccharide (LPS)-induced inflammatory cytokines in Kupffer cells [38], while in a zebrafish model of cryptococcosis, 15-keto-PGE_2 promotes fungal pathogenesis [37]. Another study demonstrated 15-keto-PGE_2 role in the activation of Nrf2/ARE (nuclear erythroid 2-related factor 2/antioxidant response element) pathway in macrophages in mice with experimental sepsis [66]. In addition, 15-keto-PGE_2

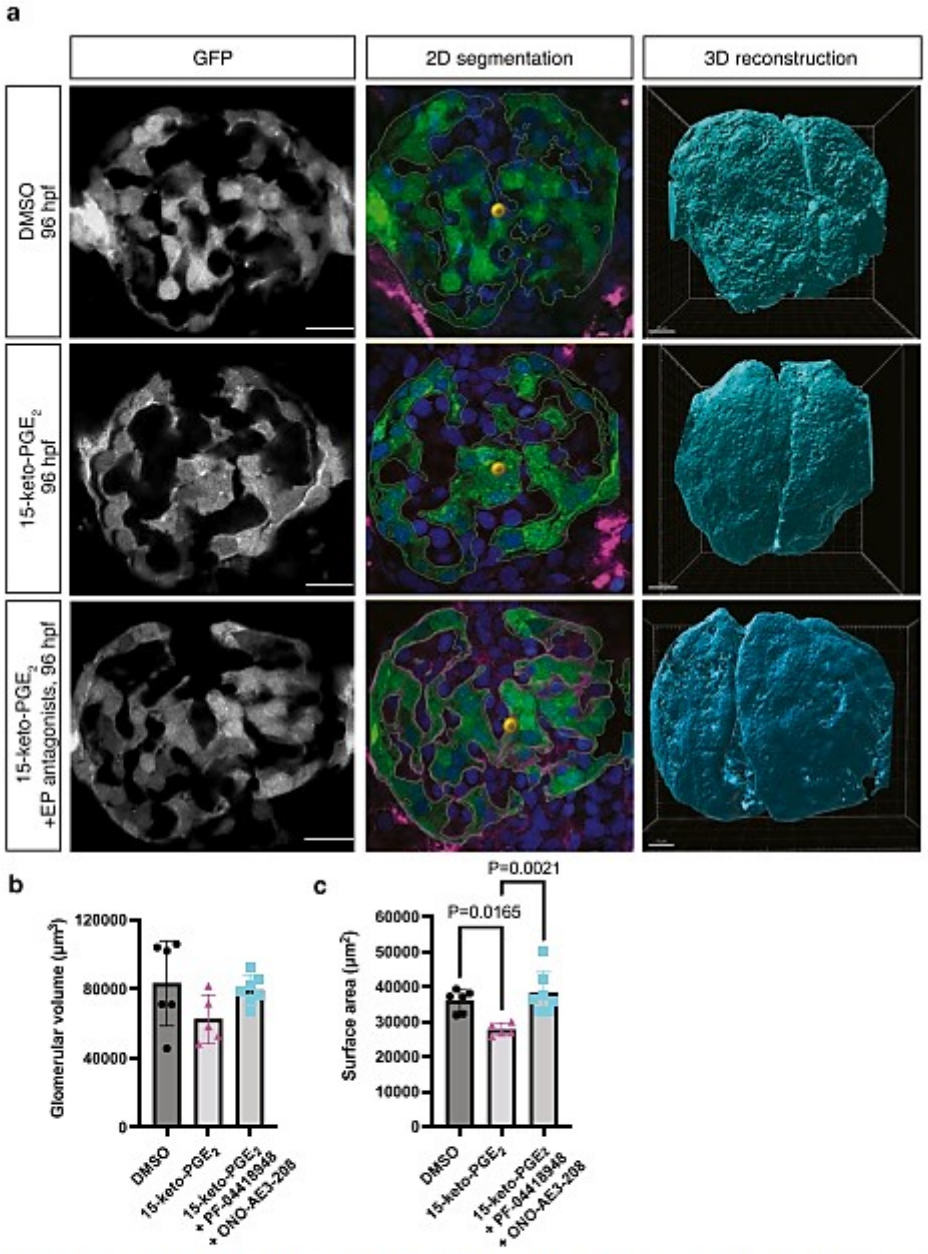

Fig. 6. Combined pharmacological blockade of EP2 and EP4 receptors reverses the effect of 15-keto-PGE_2 exposure. (a) Representative images of 2D surface segmentation and 3D glomerular reconstruction performed with Imaris software using the confocal microscopy images of *Tg(wt1b:eGFP)* zebrafish glomeruli at 96 hpf after pharmacological treatment with DMSO vehicle 0.96 % (top) ($N = 3$, $n = 6$), 15-keto-PGE_2 500 μM (middle) ($N = 3$, $n = 5$), and 15-keto-PGE_2 500 μM + PF-04418948 (EP2 receptor antagonist) 20 μM + ONO-AE3-208 (EP4 receptor antagonist) 20 μM (bottom) ($N = 2$, $n = 7$); *n* represents biologically independent samples over *N* independent experiments; Scale bar = 10 μm. (b-c) Quantitative graphs of the glomerular volume and surface area in the glomeruli analyzed for the different pharmacological treatment groups; Ordinary one-way ANOVA with Tukey's multiple comparison test was performed for both graphs; in graph (b): DMSO *vs* 15-keto-PGE_2 ($P = 0.1362$), 15-keto-PGE_2 *vs* 15-keto-PGE_2 + PF-04418948 + ONO-AE3-208 ($P = 0.2331$), and DMSO *vs* 15-keto-PGE_2 + PF-04418948 + ONO-AE3-208 ($P = 0.9074$); in graph (c): DMSO *vs* 15-keto-PGE_2 ($P = 0.0165$), 15-keto-PGE_2 *vs* 15-keto-PGE_2 + PF-04418948 + ONO-AE3-208 ($P = 0.0021$), and DMSO *vs* 15-keto-PGE_2 + PF-04418948 + ONO-AE3-208 ($P = 0.6048$); Values are plotted as mean ± SD; $P < 0.05$ considered significant.

has been also associated with different types of cancer, as it reportedly increases p21 promoter activity in hepatocellular carcinoma cells through PPAR-γ activation [39] and inhibits STAT3 signaling thus suppressing breast cancer progression in MCF10A-*ras* cells [67].

The importance of 15-keto-PGE_2 in the physiology and/or pathophysiology of the kidney has not been previously investigated. Nevertheless, the role of 15-hydroprostaglandin dehydrogenase (15-PGDH), the enzyme that catalyzes the first step of PGE_2 inactivation and synthesizes 15-keto-PGE_2, has been widely studied for its implication in kidney diseases. 15-PGDH inhibition prevents contrast-induced acute kidney injury [68], ischemic acute kidney injury (AKI) [69] and acute liposaccharide (LPS)-induced renal injury in mice [70]. In addition, 15-PGDH activity has been reported in rabbit kidney cortex [71,72] as well as in maternal rat kidney and fetal rat and lamb kidney [73]. All this evidence suggests that 15-keto-PGE_2 might have a potentially detrimental role in kidney biology.

In the present study, we show that 15-keto-PGE_2 stimulation *in vivo* affects glomerular morphology characterized by the podocyte intercalation defects around the glomerular capillaries in zebrafish embryos. The exogenous treatment with the metabolite does not considerably affect the glomerular volume, but results in the significant decrease of the glomerular surface area highlighting the impaired podocyte intercalation and reduced area of the glomerular filtration barrier. Combined pharmacological blockade of EP2 and EP4 receptors leads to complete reversal of the podocyte intercalation defects caused by 15-keto-PGE_2 exposure. This provides evidence for the role of 15-keto-PGE_2 in modulating EP2 and EP4 receptor signaling and is in agreement with a previous study supporting 15-keto-PGE_2 bioactive signaling *via* these receptors *in vitro* [36].

Our findings suggest a novel physiological role of 15-keto-PGE_2 in the proper GFB and glomerular surface area formation. Moreover, a potential role of this metabolite, in addition to PGE_2, in renal hemodynamics maintenance and blood pressure regulation should be taken into consideration. Given that we have recently shown 15-keto-PGE_2 levels are elevated in the isolated glomeruli of a well-established rat model of CKD with glomerular hyperfiltration and albuminuria [30], the question whether 15-keto-PGE_2 has potential pathophysiological effects in the context of renal biology should be addressed in the future studies. In addition, 15-keto-PGE_2 may affect renal vasculature that could be associated with glomerular hypertension and affect the proper podocyte intercalation, as observed here. Notwithstanding, the latter may outline the possible contribution of 15-keto-PGE_2 in the fine-tuning of the complex interactions between podocytes and endothelial cells that underlie glomerular vascularization and formation of functional and mature GFB.

PGE_2, described as a potent vasodilator in renal vasculature [74], has been widely studied in the regulation of renal hemodynamics, arterial blood pressure and renal blood flow [75–77]. In this context, EP2 and EP3 were highlighted to exert a crucial role in the PGE_2-induced renal hemodynamic responses and vascular functions [78,79]. To the best of our knowledge, implication of 15-keto-PGE_2 in renal hemodynamics is not yet known. Although, we cannot exclude of the potential regulatory effects of 15-keto-PGE_2 on renal hemodynamics, the fact that we do not observe any cardiac defects (the heart formation as well as function are not altered) suggests that overall hemodynamics seems to be unaffected. Second, we observe the defects in podocyte-endothelial interactions already early at the onset of glomerular filtration, *i.e.* before the fully functional glomerular filtration occur, pointing more towards the direct cell-cell interaction deregulation rather than through the hemodynamics alterations. However, to clarify this, further investigation including renal blood flow measurements to assess a potential vasoconstrictor or vasodilator effect of 15-keto-PGE_2, is required.

Altogether, our findings reveal 15-keto-PGE_2 metabolite may modulate EP2 and EP4-dependent signaling during glomerular morphogenesis. Whether this involves full receptor activation or whether 15-keto-PGE_2 acts in dominant negative manner or whether its effects are indirect needs to be further elucidated. Whether in pathological conditions elevated levels of 15-keto-PGE_2 might change podocyte-endothelial cell interactions warrant further studies.

4. Methods

4.1. Zebrafish husbandry

Zebrafish (*Danio rerio*) were bred, raised, and maintained in accordance with the FELASA guidelines [80], the guidelines of the Max-Delbrück Center for Molecular Medicine in the Helmholtz association and the local authority for animal protection (Landesamt für Gesundheit und Soziales, Berlin, Germany). The 'Principles of Laboratory Animal Care' (NIH publication no. 86–23, revised 1985) as well as the current version of German Law on the Protection of Animals and EU directive 2010/63/EU on the protection of animals were followed. Zebrafish transgenic lines used in this study included *Tg(wt1b:eGFP)*^{li1} [81] and *Tg(fabp:gc-EGFP)*^{mi1000} [63]. Embryos were kept in E3 embryo medium (5 mM NaCl, 0.17 mM KCl, 0.33 mM $CaCl_2$, 0.33 mM $MgSO_4$, pH 7.4) under standard laboratory conditions at 28.5 °C in all the experiments.

4.2. Generation of HiBiT-tagged hEP2/hEP4 receptor constructs

To generate hEP2−/hEP4-HiBiT constructs with a HiBiT-taq, the full-length human Prostaglandin E Receptor 2 (hEP2) and human Prostaglandin E Receptor 4 (hEP4) cDNAs were cloned into the pBiT3.1-N [CMV/HiBiT/Blast] vector (Promega) including a short linker attached to the N-terminal receptor sequences. Briefly, template cDNA was prepared from conditionally immortalized human podocytes [82]. Cloning primers were designed spanning either the start codon (forward-primers) or stop codon (reverse-primers) of the hEP2/hEP4 receptor sequences and having 5′ end extensions complementary to the linearized pBiT3.1-N [CMV/HiBiT/Blast] vector containing a restriction site. Primer sequences are listed in Table 1. Full-length hEP2 and hEP4 cDNA sequences were amplified using CloneAmp HiFi PCR Premix (TaKaRa Bio Inc.) and the designed cloning primers.

Restriction digestion of the pBiT3.1-N [CMV/HiBiT/Blast] vector was performed using CutSmart™ Buffer (New England Biolabs) and *EcoR*I and *Xba*I restriction enzymes (New England Biolabs). The PCR products were integrated into the vector using the 5X In-Fusion® HD Enzyme Premix (TaKaRa Bio Inc.) and the resulting plasmid was transformed into One Shot™ TOP10 chemically competent *E.coli* (Thermo Fisher Scientific). The plasmid sequences were verified by Sanger sequencing (LGC genomics).

For transformation into yeast, the hEP2-/hEP4-HiBiT constructs were cloned into the p426GPD yeast plasmid (GlxoSmithKline) [40] using cloning primers listed in Table 1. The forward primer with a 5′ overhang complementary to the yeast plasmid, spanning a *BamH*I restriction site and the HiBiT-tag start codon was designed. The reverse primers with a 5′overhang spanning a restriction site close to the stop codon of the hEP2/hEP4 sequence as well as the respective stop codon were designed. Purified pBiT3.1-N [CMV/HiBiT/Blast] vector (Promega) with integrated hEP2/hEP4 sequence was used as a template for PCR amplification using CloneAmp HiFi PCR Premix (TaKaRa Bio Inc.). Linearized plasmids and PCR products were purified and integrated into the p426GPD, ligation of the plasmid was conducted with the 5X In-Fusion® HD Enzyme Premix (TaKaRa Bio Inc.), the plasmids were transformed into One Shot™ TOP10 chemically competent *E.coli* (Thermo Fisher Scientific). The plasmid sequences were verified by Sanger sequencing (LGC genomics).

4.3. Yeast transformation

P426GPD plasmids carrying either hEP2-HiBiT or hEP4-HiBiT construct were transformed into *S.cerevisiae* (MMY yeast model, GlaxcoSmithKline) using lithium acetate (LiAc)/single-stranded DNA

Table 1
Primer sequences.

Construct name	Forward Primer (5′-3′)	Reverse Primer (5′-3′)
hEP2-HiBiT	CGAGCGGTGGGAATTCGATGGGCAATGCCTCCAATGAC	AAGCTTGACCTCTAGATCAAAGGTCAGCCTGTTTACTGGC
hEP4-HiBiT	CGAGCGGTGGGAATTCCATGTCCACTCCCGGGGTC	AAGCTTGACCTCTAGATTATATACATTTTTCTGATAAGTTCAGTGTTTCACT
hEP2-HiBiT-p426GDP	TAGAACTAGTGGATCCATGGTGAGCGGCTGGCGG	GCTTGATATCGAATTCTCAAAGGTCAGCCTGTTTACTGGC
hEP4-HiBiT-p426GDP	TAGAACTAGTGGATCCATGGTGAGCGGCTGGCGG	GCTTGATATCGAATTCTTATATACATTTTTCTGATAAGTTC

(ssDNA)/polyethylene glycol (PEG) method as previously described [40]. Briefly, 100 mL of yeast extract peptone dextrose (YPD) medium was inoculated with 1.5 mL yeast pre-culture and incubated for 2 h shaking at 30°. Yeast cultures were centrifuged at 600g for 2 min, washed with water, centrifuged at 600g for 1 min and the yeast pellets were suspended in 1 mL LiAcTE. For transformation, 5 μL of ssDNA (10 mg/mL, Sigma-Aldrich), 1 μg plasmids and for mock-transformed controls the corresponding volume of Midiprep Tris buffer solution (Macherey-Nagel), 50 μL yeast solution and 300 μL LiAc PEG TE were mixed by pipetting. After incubation at room temperature for 10 min and heat shock at 42 °C for 20 min, yeast solutions were plated on WHAUL plates supplemented with histidine (WHAUL-His).

4.4. Yeast strain and yeast culture

The used MMY28 yeast strain [40] has the following genotype: *W303-1A fus1::FUS1-HIS3 FUS1-lacZ::LEU2 far1Δ::ura3Δ gpa1Δ::ADE2Δ sst2Δ::ura3Δ MMY9 ste2Δ::G418^R TRP1::Gpa1/G$_{mf(3)}$*. Prior to transformation, yeasts stored on glycerol beads at −80 °C were thawed and plated on YPD plates for 2 days at 30 °C before liquid pre-cultures were incubated in YPD medium shaking overnight at 30 °C. Transformed yeasts grew on WHAUL-His plates for three days. Three clones were picked and transferred on new WHAUL-His plates and incubated overnight at 30 °C. On the next day, prior to the experiments, clones were pre-cultured in WHAUL-His medium overnight shaking at 30 °C in flat 96-well plates (TPP).

4.5. Receptor expression on the yeast cell surface

The expressions of hEP2 receptor and hEP4 receptor on the yeast membrane were investigated with the NanoGlo® Extracellular Detection System (Promega Corporation). The system's principle is based on the expression of a HiBiT-tagged protein/receptor, which upon the incubation with the NanoGlo® Extracellular reagent produces a luminometry signal that reflects the number of receptors on the plasma membrane. If the added ligand of interest is able to bind the HiBiT-tagged receptor, it triggers a modification in the receptor's expression on the plasma membrane, which is manifested by a change in the luminometry signal.

Yeast pre-cultures were diluted 1:5 in WHAUL-medium and 5 μL of yeast dilution were incubated with 100 μL WHAUL-medium supplemented with BU Salts for 20 h. Following 20 h incubation, yeasts were stimulated for 20 min with 100 nM PGE_2, 1 μM 15-keto-PGE_2 or medium only for untreated control. Nine transformed colonies as well as one mock-transformed colony that served as a negative control were investigated at a time. Then, yeasts were treated with the Nano-Glo® Extracellular Detection System according to the manufacturer's instructions. Briefly, yeast solutions after stimulation were transferred to white 96-well plates (Corning Inc.). Thereby, one stimulated yeast solution was split into 2 wells after mixing. Equal volume of the reagent (consisting of NanoGlo® Extracellular Detection Buffer, NanoGlo® HiBiT Extracellular Substrate diluted 1:50 and LgBiT Protein diluted 1:100) was added to the yeast solutions. After 5 min shaking at 300 rpm for 5 min, luminescence was determined with the FLUOstar Omega microplate reader (BMG Labtech) and results were obtained using the Optima software and MARS data analysis software (BMG Labtech). Yeasts with luminescence lower than values of the medium control and the negative (mock-transformed) yeast control were excluded from the analysis, as the transformation was considered unsuccessful.

4.6. Lipidomic analysis of the whole zebrafish embryos

The lipidomic analysis was performed by liquid chromatography electrospray ionization tandem mass spectrometry (LC/ESI-MS/MS) following the protocol we reported recently [30]. The zebrafish embryos at two different developmental stages, 48 hpf and 120 hpf, were frozen using liquid nitrogen and analyzed using an Agilent 1290 HPLC system with binary pump, multisampler and column thermostat with a Zorbax Eclipse plus C-18, 2.1 × 150 mm, 1.8 μm column using a solvent system of aqueous acetic acid (0.05 %) and acetonitrile. A gradient starting with 5 % organic phase was used, which was increased within 0.5 min to 32 %, 16 min to 36.5 %, 20 min to 38 %, 28 min to 98 % and held there for 5 min, was used for the elution. The flow rate was set at 0.3 mL/min and the injection volume was 20 μL. The HPLC was coupled with an Agilent 6495 Triplequad mass spectrometer (Agilent Technologies, Santa Clara, CA, USA) with electrospray ionization source. Source parameters: Drying gas: 115 °C/16 L/min, Sheath gas: 390 °C/12 L/min, Capillary voltage: 4300 V, Nozzle voltage: 1950 V, and Nebulizer pressure: 35 psi.

4.7. Pharmacological treatment, glomerular morphology and functional assessment of the GFB

For the phenotypic assessment of the zebrafish embryonic kidney and the evaluation of GFB integrity the transgenic lines *Tg[wt1b:eGFP]* and *Tg[fabp10a:gc-eGFP]* were used, respectively. For the drug treatment, the E3 medium was completely drawn off the embryos and the solution of DMSO (% adjusted to the solvent ratio in drug solution) (276855, Sigma Aldrich), and 500 μM 15-keto-PGE_2 (Cay14720-1, Cayman) in E3 water were added. For the combined blockade of EP2 and EP4 receptors, a solution of 20 μM EP2 receptor antagonist (PF04418948, Sigma Aldrich) and 20 μM EP4 receptor antagonist (ONO-AE3-208, Sigma Aldrich) in E3 water with 500 μM 15-keto-PGE_2 was used. The drugs were applied to the zebrafish embryos between 6 hpf and 48 hpf for the early treatment and between 72 hpf and 96 hpf for the late treatment. The embryos were placed in a 28.5 °C incubator until phenotypic analysis. For the *in vivo* imaging, 48 hpf and 96 hpf zebrafish embryos were anesthetized with 0.02 % tricaine (*w/v*) in E3 solution and embedded in methyl cellulose. Fluorescent and brightfield images were acquired using Leica M165 stereomicroscope with a Leica DFC450 camera attached.

4.8. Confocal microscopy of zebrafish embryonic kidney and 3D reconstruction of the glomerulus

For the confocal imaging, *Tg[wt1b:eGFP]* zebrafish embryos were used at the time points indicated in the figure legend. Prior to the fixation, the anesthetized embryos (in 0.02 % tricaine (w/v)) were injected in the sinus venosus or the descending cardinal vein with 20 mg/mL BSA Alexa Fluor555 conjugate (A34786, ThermoFisher Scientific) diluted in in 150 mM NaCl. The injected embryos were fixed after 20 min in 4 % PFA (43369, Alfa Aesar) and 0.1 % Triton-X 100 in PBS buffer (D8357, Sigma Aldrich) for 2 h at RT or overnight at 4 °C. Nuclei were stained using 4′,6-Diamidin-2-phenylindol (DAPI, Sigma Aldrich, stock solution 1 mg/mL diluted 1:2000 in PBS) overnight at 4 °C. After removal of the

yolk and mounting in 0,8 % low-melting agarose, the kidneys of whole-mount fixed embryos were imaged using a Confocal Zeiss LSM 980 Airyscan microscope with a LD C-Apochromat 40 x NA1.1 water objective and Zen Blue v.3.2 software. Confocal z-stacks of all channels were sequentially acquired with identical parameters and similar 3D orientation for all samples. Images were analyzed using ImageJ software.

The 3D confocal images were first deconvolved using Huygens Professional 22.04 software. The 2D segmentation for the 3D glomerular surface creation, was performed using Imaris version 9.9 software (Bitplane AG, Zurich, Switzerland). A 3D surface covering the total glomerular volume was created by manually tracing the surface outline of EGFP-positive cells for every second section of the z-stack and in a second step the automated segmentation for the surface creation was used. The fluorescence signal derived by EGFP-positive cells inside the glomeruli was included, while EGFP signal coming from the neck and the early part of proximal convoluted tubule was excluded.

4.9. Statistical analysis

Statistics were performed using GraphPad Prism version 6.07 or 9. Following statistical tests were used: Fig. 1c,d, Wilcoxon test and Mann-Whitney tests were conducted as indicated (*, $P < 0.05$; **, $P < 0.01$; ***, $P < 0.001$; **** $P < 0.0001$); Fig. 2, two-tailed unpaired t-test with Welch's correction; Fig. 3c, two-way ANOVA with Tukey's multiple comparisons; Fig. 6b, c, one-way ANOVA with Tukey's multiple comparisons post-test. Identification of outliers was performed by Grubbs' outliers test ($\alpha = 0.05$). Excluded values: Fig. 1b, c: one outlier was identified among EP2-transfected and two outliers among EP4-transfected yeasts (for all yeast experiments conducted at the same day); Fig. 2: one outlier was identified and removed among the lipidomic PGE_2 values at 48 hpf together with the respective values for the two metabolites; Fig. 6b, c: one outlier was identified in the glomerulus surface area measurements each for the DMSO and 15-keto-PGE_2 condition that were excluded both from the surface area and also the glomerular volume analysis. In all graphs error bars are presented as means ± SD and $P < 0.05$ were considered statistically significant.

Supplementary data to this article can be found online at https://doi.org/10.1016/j.lfs.2022.121114.

CRediT authorship contribution statement

Conceptualization, A.K., J.B., R.K. and D.P.; Methodology and experimentation, A.K., D.K.G., A.P., R.C., A.S, E.M., A.Sch.; Data analysis, A.K., D.K.G, M.R.; Visualization, A.K., D.K.G. and D.P.; Writing – Original Draft, A.K. and D.P. with input from all authors; Revised manuscript, A.K. and D.P.; Funding Acquisition, R.K. and D.P.; Supervision, A.P., R.C., J.B., R.K. and D.P.

Declarations

All methods were carried out in accordance with relevant guidelines and regulations.

The study was carried out in compliance with the ARRIVE guidelines.

Declaration of competing interest

The authors declare that they have no known competing financial interests or personal relationships that could have appeared to influence the work reported in this paper.

Data availability

Data will be made available on request.

Acknowledgements

We thank Christoph Englert (Leibniz Institute on Ageing) and Weibin Zhou (University of Michigan) for sharing the fish *Tg(wt1b:eGFP)* and *Tg (fabp:gc-EGFP)* transgenic lines, respectively. We thank Moin A. Saleem (University of Bristol, UK) for sharing human podocytes line and Simon Dowell (GSK, Stevenage, United Kingdom) for providing the p426GPD yeast plasmid and the yeast strain. We thank Alexander M. Meyer for expert technical support, and the Aquatic Facility and Advanced Light Microscopy Technology Platform at MDC. Work for this project was supported by the Deutsche Forschungsgemeinschaft (DFG, German Research Foundation)—project number 394046635—SFB 1365.

References

[1] F. Costantini, R. Kopan, Patterning a complex organ: branching morphogenesis and nephron segmentation in kidney development, Dev. Cell 18 (2010) 698–712, https://doi.org/10.1016/j.devcel.2010.04.008.
[2] M. Krause, A. Rak-Raszewska, I. Pietilä, S. Quaggin, S. Vainio, Signaling during kidney development, Cells. 4 (2015) 112–132, https://doi.org/10.3390/cells4020112.
[3] W. Kriz, B. Kaissling, Structural organization of the mammalian kidney, in: Seldin and Giebisch's The Kidney, Elsevier, 2008, pp. 479–563, https://doi.org/10.1016/B978-012088488-9.50023-1.
[4] A.P. McMahon, Development of the Mammalian Kidney, 1st ed., Elsevier Inc., 2016 https://doi.org/10.1016/bs.ctdb.2015.10.010.
[5] K. Ebefors, E. Lassén, N. Anandakrishnan, E.U. Azeloglu, I.S. Daehn, Modeling the glomerular filtration barrier and intercellular crosstalk, Front. Physiol. 12 (2021), https://doi.org/10.3389/fphys.2021.689083.
[6] A. Pozzi, G. Jarad, G.W. Moeckel, S. Coffa, X. Zhang, L. Gewin, V. Eremina, B. G. Hudson, D.B. Borza, R.C. Harris, L.B. Holzman, C.L. Phillips, R. Fassler, S. E. Quaggin, J.H. Miner, R. Zent, B1 integrin expression by podocytes is required to maintain glomerular structural integrity, Dev. Biol. 316 (2008) 288–301, https://doi.org/10.1016/j.ydbio.2008.01.022.
[7] B. Haraldsson, J. Nyström, W.M. Deen, Properties of the glomerular barrier and mechanisms of proteinuria, Physiol. Rev. 88 (2008) 451–487, https://doi.org/10.1152/physrev.00055.2006.
[8] L. Butt, D. Unnersjö-Jess, M. Höhne, A. Edwards, J. Binz-Lotter, D. Reilly, R. Hahnfeldt, V. Ziegler, K. Fremter, M.M. Rinschen, M. Helmstädter, L.K. Ebert, H. Castrop, M.J. Hackl, G. Walz, P.T. Brinkkoetter, M.C. Liebau, K. Tory, P. F. Hoyer, B.B. Beck, H. Brismar, H. Blom, B. Schermer, T. Benzing, A molecular mechanism explaining albuminuria in kidney disease, Nat. Metab. 2 (2020) 461–474, https://doi.org/10.1038/s42255-020-0204-y.
[9] R.A. Wingert, A.J. Davidson, The zebrafish pronephros: a model to study nephron segmentation, Kidney Int. 73 (2008) 1120–1127, https://doi.org/10.1038/ki.2008.37.
[10] M. Elmonem, S. Berlingerio, L. van den Heuvel, P. de Witte, M. Lowe, E. Levtchenko, Genetic renal diseases: the emerging role of zebrafish models, Cells. 7 (2018) 130, https://doi.org/10.3390/cells7090130.
[11] G.F. Gerlach, R.A. Wingert, Kidney organogenesis in the zebrafish: insights into vertebrate nephrogenesis and regeneration, Wiley Interdiscip. RevDev. Biol. 2 (2013) 559–585, https://doi.org/10.1002/wdev.92.
[12] C. Santoriello, L.I. Zon, Hooked! Modeling human disease in zebrafish, J. Clin. Invest. 122 (2012) 2337–2343, https://doi.org/10.1172/JCI60434.
[13] P. Outtandy, C. Russell, R. Kleta, D. Bockenhauer, Zebrafish as a model for kidney function and disease, Pediatr. Nephrol. 34 (2019) 751–762, https://doi.org/10.1007/s00467-018-3921-7.
[14] I.A. Drummond, A.J. Davidson, Zebrafish kidney development, Methods Cell Biol. (2016), https://doi.org/10.1016/bs.mcb.2016.03.041.
[15] A.G. Kramer-Zucker, S. Wiessner, A.M. Jensen, I.A. Drummond, Organization of the pronephric filtration apparatus in zebrafish requires nephrin, podocin and the FERM domain protein mosaic eyes, Dev. Biol. 285 (2005) 316–329, https://doi.org/10.1016/j.ydbio.2005.06.038.
[16] J.Y. Park, M.H. Pillinger, S.B. Abramson, Prostaglandin E2 synthesis and secretion: the role of PGE2 synthases, Clin. Immunol. 119 (2006) 229–240, https://doi.org/10.1016/j.clim.2006.01.016.
[17] Y. Li, W. Xia, F. Zhao, Z. Wen, A. Zhang, S. Huang, Z. Jia, Y. Zhang, Prostaglandins in the pathogenesis of kidney diseases. www.oncotarget.com, 2018.
[18] K.C. Ugwuagbo, S. Maiti, A. Omar, S. Hunter, B. Nault, C. Northam, M. Majumder, Prostaglandin E2 promotes embryonic vascular development and maturation in zebrafish, Biol. Open. 8 (2019), https://doi.org/10.1242/bio.039768.
[19] T.E. North, W. Goessling, C.R. Walkley, C. Lengerke, K.R. Kopani, A.M. Lord, G. J. Weber, T.V. Bowman, I.H. Jang, T. Grosser, G.A. Fitzgerald, G.Q. Daley, S. H. Orkin, L.I. Zon, Prostaglandin E2 regulates vertebrate haematopoietic stem cell homeostasis, Nature 447 (2007) 1007–1011, https://doi.org/10.1038/nature05883.
[20] R. Iwasaki, K. Tsuge, K. Kishimoto, Y. Hayashi, T. Iwaana, H. Hohjoh, T. Inazumi, A. Kawahara, S. Tsuchiya, Y. Sugimoto, Essential role of prostaglandin E2 and the EP3 receptor in lymphatic vessel development during zebrafish embryogenesis, Sci. Rep. 9 (2019) 1–11, https://doi.org/10.1038/s41598-019-44095-5.
[21] W. Goessling, T.E. North, S. Loewer, A.M. Lord, S. Lee, C.L. Stoick-Cooper, G. Weidinger, M. Puder, G.Q. Daley, R.T. Moon, L.I. Zon, Genetic interaction of

PGE2 and wnt signaling regulates developmental specification of stem cells and regeneration, Cell 136 (2009) 1136–1147, https://doi.org/10.1016/j.cell.2009.01.015.
[22] S. Nissim, R.I. Sherwood, J. Wucherpfennig, D. Saunders, J.M. Harris, V. Esain, K. J. Carroll, G.M. Frechette, A.J. Kim, K.L. Hwang, C.C. Cutting, S. Elledge, T. E. North, W. Goessling, Prostaglandin E2 regulates liver versus pancreas cell-fate decisions and endodermal outgrowth, Dev. Cell 28 (2014) 423–437, https://doi.org/10.1016/j.devcel.2014.01.006.
[23] J. Hoggatt, P. Singh, J. Sampath, L.M. Pelus, Prostaglandin E2 enhances hematopoietic stem cell homing, survival, and proliferation, Blood 113 (2009) 5444–5455, https://doi.org/10.1182/blood-2009-01-201335.
[24] G. O'Callaghan, A. Houston, Prostaglandin E2 and the EP receptors in malignancy: possible therapeutic targets? Br. J. Pharmacol. 172 (2015) 5239–5250, https://doi.org/10.1111/bph.13331.
[25] V.L. Hood, Prostaglandins and the Kidney, 1977. http://ajprenal.physiology.org/.
[26] R. Nasrallah, R. Hassouneh, R.L. Hébert, PGE2, kidney disease, and cardiovascular risk: beyond hypertension and diabetes, J. Am. Soc. Nephrol. 27 (2016) 666–676, https://doi.org/10.1681/ASN.2015050528.
[27] R. Nasrallah, R. Hassouneh, R.L. Hébert, Chronic kidney disease: targeting prostaglandin E 2 receptors, Am. J. Physiol. Ren. Physiol. 307 (2014) 243–250, https://doi.org/10.1152/ajprenal.00224.2014.-Chronic.
[28] Y. Sugimoto, S. Narumiya, Prostaglandin E receptors, J. Biol. Chem. 282 (2007) 11613–11617, https://doi.org/10.1074/jbc.R600038200.
[29] L. Li, M.N. Sluter, Y. Yu, J. Jiang, Prostaglandin E receptors as targets for ischemic stroke: novel evidence and molecular mechanisms of efficacy, Pharmacol. Res. 163 (2021), 105238, https://doi.org/10.1016/j.phrs.2020.105238.
[30] E. Mangelsen, M. Rothe, A. Schulz, A. Kourpa, D. Paňáková, R. Kreutz, J. Bolbrinker, Concerted EP2 and EP4 receptor signaling stimulates autocrine prostaglandin E2 activation in human podocytes, Cells. 9 (2020), https://doi.org/10.3390/cells9051256.
[31] R.J. Anderson, T. Berl, K.M. McDonald, R.W. Schrier, Prostaglandins: effects on blood pressure, renal blood flow, sodium and water excretion, Kidney Int. 10 (1976) 205–215, https://doi.org/10.1038/ki.1976.99.
[32] H.-H. Tai, C.M. Ensor, M. Tong, H. Zhou, F. Yan, Prostaglandin catabolizing enzymes, 2002.
[33] Y.H. Wu, T.P. Ko, R.T. Guo, S.M. Hu, L.M. Chuang, A.H.H.J. Wang, Structural basis for catalytic and inhibitory mechanisms of human prostaglandin reductase PTGR2, Structure (2008), https://doi.org/10.1016/j.str.2008.09.007.
[34] W.L. Chou, L.M. Chuang, C.C. Chou, A.H.J. Wang, J.A. Lawson, G.A. FitzGerald, Z. F. Chang, Identification of a novel prostaglandin reductase reveals the involvement of prostaglandin E2 catabolism in regulation of peroxisome proliferator-activated receptor γ activation, J. Biol. Chem. 282 (2007) 18162–18172, https://doi.org/10.1074/jbc.M702289200.
[35] N. Nishigaki, M. Negishi, A. Ichikawa, Two gs-coupled prostaglandin E receptor subtypes, EP2 and EP4, differ in desensitization and sensitivity to the metabolic inactivation of the agonist, Mol. Pharmacol. 50 (1996), 1031 LP – 1037, http://molpharm.aspetjournals.org/content/50/4/1031.abstract.
[36] S. Endo, A. Suganami, K. Fukushima, K. Senoo, Y. Araki, J.W. Regan, M. Mashimo, Y. Tamura, H. Fujino, 15-keto-PGE2 acts as a biased/partial agonist to terminate PGE2-evoked signaling, J. Biol. Chem. 295 (2020) 13338–13352, https://doi.org/10.1074/jbc.ra120.013988.
[37] R.J. Evans, K. Pline, C.A. Loynes, S. Needs, M. Aldrovandi, J. Tiefenbach, E. Bielska, R.E. Rubino, C.J. Nicol, R.C. May, H.M. Krause, V.R. O'Donnell, S. A. Renshaw, S.A. Johnston, 15-keto-prostaglandin e2 activates host peroxisome proliferator-activated receptor gamma (Ppar-γ) to promote cryptococcus neoformans growth during infection, PLoS Pathog. 15 (2019) 1–28, https://doi.org/10.1371/journal.ppat.1007597.
[38] L. Yao, W. Chen, K. Song, C. Han, C.R. Gandhi, K. Lim, T. Wu, 15-hydroxyprostaglandin dehydrogenase (15-PGDH) prevents lipopolysaccharide (LPS)-induced acute liver injury, PLoS One. 12 (2017) 1–16, https://doi.org/10.1371/journal.pone.0176106.
[39] D. Lu, C. Han, T. Wu, 15-PGDH inhibits hepatocellular carcinoma growth through 15-keto-PGE2/PPARγ-mediated activation of p21WAF1/Cip1, Oncogene 33 (2014) 1101–1112, https://doi.org/10.1038/onc.2013.69.
[40] S.J. Dowell, A.J. Brown, Yeast assays for G protein-coupled receptors, Methods Mol. Biol. 552 (2009) 213–229, https://doi.org/10.1007/978-1-60327-317-6_15.
[41] Y.I. Cha, S.H. Kim, D. Sepich, F. Gregory Buchanan, L. Solnica-Krezel, R.N. DuBois, Cyclooxygenase-1-derived PGE2 promotes cell motility via the G-protein-coupled EP4 receptor during vertebrate gastrulation, Genes Dev. 20 (2006) 77–86, https://doi.org/10.1101/gad.1374506.
[42] I. Dey, M. Lejeune, K. Chadee, Prostaglandin E 2 receptor distribution and function in the gastrointestinal tract, Br. J. Pharmacol. 149 (2006) 611–623, https://doi.org/10.1038/sj.bjp.0706923.
[43] H. Reinold, S. Ahmadi, U.B. Depner, B. Layh, C. Heindl, M. Hamza, A. Pahl, K. Brune, S. Narumiya, U. Müller, H.U. Zeilhofer, Spinal inflammatory hyperalgesia is mediated by prostaglandin E receptors of the EP2 subtype, J. Clin. Invest. 115 (2005) 673–679, https://doi.org/10.1172/JCI23618.
[44] S.J. Poureetezadi, C.N. Cheng, J.M. Chambers, B.E. Drummond, R.A. Wingert, Prostaglandin signaling regulates nephron segment patterning of renal progenitors during zebrafish kidney development, 2016, https://doi.org/10.7554/eLife.17551.001.
[45] R.L. Miyares, V.B. de Rezende, S.A. Farber, Zebrafish yolk lipid processing: a tractable tool for the study of vertebrate lipid transport and metabolism, Dis. Model. Mech. 7 (2014) 915–927, https://doi.org/10.1242/dmm.015800.
[46] D. Fraher, A. Sanigorski, N.A. Mellett, P.J. Meikle, A.J. Sinclair, Y. Gibert, Zebrafish embryonic lipidomic analysis reveals that the yolk cell is metabolically active in processing lipid, Cell Rep. 14 (2016) 1317–1329, https://doi.org/10.1016/j.celrep.2016.01.016.
[47] J.D. Niringiyumukiza, H. Cai, W. Xiang, Prostaglandin E2 involvement in mammalian female fertility: ovulation, fertilization, embryo development and early implantation, Reprod. Biol. Endocrinol. 16 (2018) 43, https://doi.org/10.1186/s12958-018-0359-5.
[48] J. Ke, Y. Yang, Q. Che, F. Jiang, H. Wang, Z. Chen, M. Zhu, H. Tong, H. Zhang, X. Yan, X. Wang, F. Wang, Y. Liu, C. Dai, X. Wan, Prostaglandin E2 (PGE2) promotes proliferation and invasion by enhancing SUMO-1 activity via EP4 receptor in endometrial cancer, Tumor Biol. 37 (2016) 12203–12211, https://doi.org/10.1007/s13277-016-5087-x.
[49] D.F. Legler, M. Bruckner, E. Uetz-von Allmen, P. Krause, Prostaglandin E2 at new glance: novel insights in functional diversity offer therapeutic chances, Int. J. Biochem. Cell Biol. 42 (2010) 198–201, https://doi.org/10.1016/j.biocel.2009.09.015.
[50] P. Kaczynski, S. Bauersachs, E. Goryszewska, M. Baryla, A. Waclawik, Synergistic action of estradiol and PGE2 on endometrial transcriptome in vivo resembles pregnancy effects better than estradiol alone, Biol. Reprod. 104 (2021) 818–834, https://doi.org/10.1093/biolre/ioaa230.
[51] A.N. Marra, B.D. Adeeb, B.E. Chambers, B.E. Drummond, M. Ulrich, A. Addiego, M. Springer, S.J. Poureetezadi, J.M. Chambers, M. Ronshaugen, R.A. Wingert, Prostaglandin signaling regulates renal multiciliated cell specification and maturation, Proc. Natl. Acad. Sci. U. S. A. 116 (2019) 8409–8418, https://doi.org/10.1073/pnas.1813492116.
[52] K.P. Wingert, RA, Molecular mechanisms of podocyte development revealed by zebrafish kidney research, Cell Dev. Biol. 03 (2014), https://doi.org/10.4172/2168-9296.1000138.
[53] Z. Chen, A. Luciani, J.M. Mateos, G. Barmettler, R.H. Giles, S.C.F. Neuhauss, O. Devuyst, Transgenic zebrafish modeling low-molecular-weight proteinuria and lysosomal storage diseases, Kidney Int. 97 (2020) 1150–1163, https://doi.org/10.1016/j.kint.2019.11.016.
[54] A. Majumdar, I.A. Drummond, Podocyte differentiation in the absence of endothelial cells as revealed in the zebrafish avascular mutant, cloche, Dev. Genet. 24 (1999) 220–229, https://doi.org/10.1002/(SICI)1520-6408(1999)24:3/4<220::AID-DVG5>3.0.CO;2-1.
[55] N. Endlich, O. Simon, A. Göpferich, H. Wegner, M.J. Moeller, E. Rumpel, A. M. Koth, K. Endlich, Two-photon microscopy reveals stationary podocytes in living zebrafish larvae, J. Am. Soc. Nephrol. 25 (2014) 681–686, https://doi.org/10.1681/ASN.2013020178.
[56] K. Ichimura, Y. Fukuyo, T. Nakamura, R. Powell, T. Sakai, R. Janknecht, T. Obara, Developmental localization of nephrin in zebrafish and medaka pronephric glomerulus, J. Histochem. Cytochem. 61 (2013) 313–324, https://doi.org/10.1369/0022155413477115.
[57] T. Müller, E. Rumpel, S. Hradetzky, F. Bollig, H. Wegner, A. Blumenthal, A. Greinacher, K. Endlich, N. Endlich, Non-muscle myosin IIA is required for the development of the zebrafish glomerulus, Kidney Int. 80 (2011) 1055–1063, https://doi.org/10.1038/ki.2011.256.
[58] I.A. Drummond, A. Majumdar, H. Hentschel, M. Elger, L. Solnica-Krezel, A. F. Schier, S.C. Neuhauss, D.L. Stemple, F. Zwartkruis, Z. Rangini, W. Driever, M. C. Fishman, Early development of the zebrafish pronephros and analysis of mutations affecting pronephric function, Development 125 (1998) 4655–4667, https://doi.org/10.1242/dev.125.23.4655.
[59] C. Cianciolo Cosentino, A. Berto, S. Pelletier, M. Hari, J. Loffing, S.C.F. Neuhauss, V. Doye, Moderate nucleoporin 133 deficiency leads to glomerular damage in zebrafish, Sci. Rep. 9 (2019), https://doi.org/10.1038/s41598-019-41202-4.
[60] R. Repetti, N. Majumder, K.C. De Oliveira, J. Meth, T. Yangchen, M. Sharma, T. Srivastava, R. Rohatgi, Unilateral nephrectomy stimulates ERK and is associated with enhanced Na transport, Front. Physiol. 12 (2021) 1–10, https://doi.org/10.3389/fphys.2021.583453.
[61] M. Sharma, R. Sharma, E.T. McCarthy, V.J. Savin, T. Srivastava, Hyperfiltration-associated biomechanical forces in glomerular injury and response: potential role for eicosanoids, Prostaglandins Other Lipid Mediat. 132 (2017) 59–68, https://doi.org/10.1016/j.prostaglandins.2017.01.003.
[62] T. Srivastava, G.E. Celsi, M. Sharma, H. Dai, E.T. McCarthy, M. Ruiz, P.A. Cudmore, U.S. Alon, R. Sharma, V.A. Savin, Fluid flow shear stress over podocytes is increased in the solitary kidney, Nephrol. Dial. Transplant. Off. Publ. Eur. Dial. Transpl. Assoc. - Eur. Ren. Assoc. 29 (2014) 65–72, https://doi.org/10.1093/ndt/gft387.
[63] W. Zhou, F. Hildebrandt, Inducible podocyte injury and proteinuria in transgenic zebrafish, J. Am. Soc. Nephrol. 23 (2012) 1039–1047, https://doi.org/10.1681/ASN.2011080776.
[64] V.L. Hood, Prostaglandins and the Kidney, 1977. www.physiology.org/journal/ajprenal.
[65] M.K. Mansley, C. Niklas, R. Nacken, K. Mandery, H. Glaeser, M.F. Fromm, C. Korbmacher, M. Bertog, Prostaglandin E2 stimulates the epithelial sodium channel (ENaC) in cultured mouse cortical collecting duct cells in an autocrine manner, J. Gen. Physiol. 152 (2020) 1–15, https://doi.org/10.1085/jgp.201912525.
[66] L.J. Chen, S.W. Hee, C.H. Liao, S.Y. Lin, L. Su, C.T. Shun, L.M. Chuang, Targeting the 15-keto-PGE2-PTGR2 axis modulates systemic inflammation and survival in experimental sepsis, Free Radic. Biol. Med. 115 (2018) 113–126, https://doi.org/10.1016/j.freeradbiomed.2017.11.016.
[67] E.J. Lee, S.-J. Kim, Y.-I. Hahn, H.-J. Yoon, B. Han, K. Kim, S. Lee, K.P. Kim, Y. G. Suh, H.-K. Na, Y.-J. Surh, 15-keto prostaglandin E2 suppresses STAT3 signaling and inhibits breast cancer cell growth and progression, Redox Biol. 23 (2019), 101175, https://doi.org/10.1016/j.redox.2019.101175.

[68] B.W. Kim, H.J. Kim, S.-H. Kim, H.J. Baik, M.S. Kang, D.-H. Kim, S.D. Markowitz, S. W. Kang, K.B. Bae, 15-hydroxyprostaglandin dehydrogenase inhibitor prevents contrast-induced acute kidney injury, Ren. Fail. 43 (2021) 168–179, https://doi.org/10.1080/0886022X.2020.1870139.

[69] H.J. Kim, S.H. Kim, M. Kim, H.J. Baik, S.J. Park, M.S. Kang, D.H. Kim, B.W. Kim, S. D. Markowitz, K.B. Bae, Inhibition of 15-PGDH prevents ischemic renal injury by the PGE2/EP4signaling pathway mediating vasodilation, increased renal blood flow, and increased adenosine/A2Areceptors, Am. J. Physiol. - Ren. Physiol. 319 (2020) F1054–F1066, https://doi.org/10.1152/AJPRENAL.00103.2020.

[70] S. Miao, C. Lv, Y. Liu, J. Zhao, T. Li, C. Wang, Y. Xu, X. Wang, X. Xiao, H. Zhang, Pharmacologic blockade of 15-PGDH protects against acute renal injury induced by LPS in mice, Front. Physiol. 11 (2020). https://www.frontiersin.org/articles/10.3389/fphys.2020.00138.

[71] S. Sakuma, Y. Fujimoto, H. Nakagawa, S. Hachiki, H. Nishida, T. Fujita, Effect of 13-hydroperoxyoctadecadienoic acid on 15-hydroxy prostaglandin dehydrogenase activity in rabbit kidney cortex, Prostaglandins 46 (1993) 157–165, https://doi.org/10.1016/0090-6980(93)90041-5.

[72] S. Sakuma, Y. Fujimoto, E. Hikita, Y. Okano, I. Yamamoto, T. Fujita, Effects of metal ions on 15-hydroxy prostaglandin dehydrogenase activity in rabbit kidney cortex, Prostaglandins 40 (1990) 507–514, https://doi.org/10.1016/0090-6980(90)90112-9.

[73] M.Y. Tsai, S. Einzig, Prostaglandin catabolism in fetal and maternal tissues — a study of 15-hydroxyprostaglandin dehydrogenase and Δ13 reductase with specific assay methods, prostaglandins, Leukot. Essent. Fat. Acids. 38 (1989) 25–30, https://doi.org/10.1016/0952-3278(89)90143-9.

[74] W. Ye, H. Zhang, E. Hillas, D.E. Kohan, R.L. Miller, R.D. Nelson, M. Honeggar, T. Yang, Expression and function of COX isoforms in renal medullac evidence for regulation of salt sensitivity and blood pressure, Am. J. Physiol. Renal Physiol. 290 (2006) F542–F549, https://doi.org/10.1152/ajprenal.00232.2005.

[75] J. Wang, M. Liu, X. Zhang, G. Yang, L. Chen, Physiological and pathophysiological implications of PGE2 and the PGE2 synthases in the kidney, Prostaglandins Other Lipid Mediat. 134 (2018) 1–6, https://doi.org/10.1016/j.prostaglandins.2017.10.006.

[76] M. Imanishi, Y. Abe, T. Okahara, T. Yukimura, K. Yamamoto, Effects of prostaglandin I2 and E2 on renal hemodynamics and function and renin release, Jpn. Circ. J. 44 (1980) 875–882, https://doi.org/10.1253/jcj.44.875.

[77] B. Bądzyńska, J. Sadowski, Renal hemodynamic responses to intrarenal infusion of acetylcholine: comparison with effects of PGE2 and NO donor, Kidney Int. 69 (2006) 1774–1779, https://doi.org/10.1038/sj.ki.5000338.

[78] L.P. Audoly, S.L. Tilley, J. Goulet, M. Key, M. Nguyen, J.L. Stock, J.D. McNeish, B. H. Koller, T.M. Coffman, Identification of specific EP receptors responsible for the hemodynamic effects of PGE2, Am. J. Physiol. - Hear. Circ. Physiol. 277 (1999), https://doi.org/10.1152/ajpheart.1999.277.3.h924.

[79] L.P. Audoly, X. Ruan, V.A. Wagner, J.L. Goulet, S.L. Tilley, B.H. Koller, T. M. Coffman, W.J. Arendshorst, P. Laurent, X. Ruan, J.L. Goulet, S.L. Tilley, H. Beverly, T.M. Coffman, W.J. Arendshorst, V.A. Wag, in: Role of EP 2 and EP 3 PGE 2 Receptors in Control of Murine Renal Hemodynamics, 2022, pp. 327–333.

[80] P. Alestrõm, L. D'Angelo, P.J. Midtlyng, D.F. Schorderet, S. Schulte-Merker, F. Sohm, S. Warner, Zebrafish: housing and husbandry recommendations, Lab. Anim. 54 (2019) 213–224, https://doi.org/10.1177/0023677219869037.

[81] B. Perner, C. Englert, F. Bollig, The wilms tumor genes wt1a and wt1b control different steps during formation of the zebrafish pronephros, Dev. Biol. (2007), https://doi.org/10.1016/j.ydbio.2007.06.022.

[82] M.A. Saleem, M.J. O'Hare, J. Reiser, R.J. Coward, C.D. Inward, T. Farren, C. Y. Xing, L. Ni, P.W. Mathieson, P. Mundel, A conditionally immortalized human podocyte cell line demonstrating nephrin and podocin expression, J. Am. Soc. Nephrol. 13 (2002) 630–638, https://doi.org/10.1681/ASN.V133630.

Excerpt from Journal Summary List

Journal Data Filtered By: **Selected JCR Year: 2021** Selected Editions: SCIE,SSCI Selected Categories: **"PERIPHERAL VASCULAR DISEASE"** Selected Category Scheme: WoS
Gesamtanzahl: 67 Journale

Rank	Full Journal Title	Total Cites	Journal Impact Factor	Eigenfaktor
1	CIRCULATION	202,844	39.918	0.20870
2	CIRCULATION RESEARCH	72,814	23.213	0.06601
3	JOURNAL OF THROMBOSIS AND HAEMOSTASIS	30,498	16.036	0.03997
4	ANGIOGENESIS	5,111	10.658	0.00420
5	ARTERIOSCLEROSIS THROMBOSIS AND VASCULAR BIOLOGY	41,650	10.514	0.02858
6	THROMBOSIS RESEARCH	17,586	10.407	0.02314
7	STROKE	86,009	10.170	0.07454
8	HYPERTENSION	47,098	9.897	0.04442
9	Journal of Stroke	2,036	8.632	0.00391
10	International Journal of Stroke	7,698	6.948	0.01415
11	ATHEROSCLEROSIS	29,505	6.847	0.02366
12	THROMBOSIS AND HAEMOSTASIS	19,483	6.681	0.01818
13	EUROPEAN JOURNAL OF VASCULAR AND ENDOVASCULAR SURGERY	12,991	6.427	0.01300
14	SEMINARS IN THROMBOSIS AND HEMOSTASIS	5,619	6.398	0.00559
15	Current Atherosclerosis Reports	3,893	5.967	0.00420
16	Research and Practice in Thrombosis and Haemostasis	2,075	5.953	0.00791
17	European Stroke Journal	1,210	5.894	0.00411
18	HYPERTENSION RESEARCH	7,687	5.528	0.00642
19	Thrombosis Journal	1,305	5.509	0.00195

Printing copy of the publication

2. Kourpa, Aikaterini*; Schulz, Angela*; Mangelsen, Eva; Kaiser-Graf, Debora; Koppers, Nils; Stoll, Monika; Rothe, Michael; Bader, Michael; Purfürst, Bettina; Kunz, Severine; Gladytz, Thomas; Niendorf, Thoralf; Bachmann, Sebastian; Mutig, Kerim; Bolbrinker, Juliane; Panáková, Daniela; Kreutz, Reinhold**. **Studies in Zebrafish and Rat Models Support Dual Blockade of EP2 and EP4 (Prostaglandin E_2 Receptors Type 2 and 4) for Renoprotection in Glomerular Hyperfiltration and Albuminuria.** *Hypertension.* 2023;80:771-782. https://doi.org/10.1161/HYPERTENSIONAHA.122.20392.

Hypertension

ORIGINAL ARTICLE

Studies in Zebrafish and Rat Models Support Dual Blockade of EP2 and EP4 (Prostaglandin E_2 Receptors Type 2 and 4) for Renoprotection in Glomerular Hyperfiltration and Albuminuria

Aikaterini Kourpa, Angela Schulz, Eva Mangelsen, Debora Kaiser-Graf, Nils Koppers, Monika Stoll, Michael Rothe, Michael Bader, Bettina Purfürst, Severine Kunz, Thomas Gladytz, Thoralf Niendorf, Sebastian Bachmann, Kerim Mutig, Juliane Bolbrinker, Daniela Panáková, Reinhold Kreutz

BACKGROUND: Glomerular hyperfiltration (GH) is an important mechanism in the development of albuminuria in hypertension. Upregulation of COX2 (cyclooxygenase 2) and prostaglandin E_2 (PGE_2) was linked to podocyte damage in GH. We explored the potential renoprotective effects of either separate or combined pharmacological blockade of EP2 (PGE_2 receptor type 2) and EP4 (PGE_2 receptor type 4) in GH.

METHODS: We conducted in vivo studies in a transgenic zebrafish model (*Tg[fabp10a:gc-EGFP]*) suitable for analysis of glomerular filtration barrier function and a genetic rat model with GH, albuminuria, and upregulation of PGE_2. Similar pharmacological interventions and primary outcome analysis on albuminuria phenotype development were conducted in both model systems.

RESULTS: Stimulation of zebrafish embryos with PGE_2 induced an albuminuria-like phenotype, thus mimicking the suggested PGE_2 effects on glomerular filtration barrier dysfunction. Both separate and combined blockade of EP2 and EP4 reduced albuminuria phenotypes in zebrafish and rat models. A significant correlation between albuminuria and podocyte damage in electron microscopy imaging was identified in the rat model. Dual blockade of both receptors showed a pronounced synergistic suppression of albuminuria. Importantly, this occurred without changes in arterial blood pressure, glomerular filtration rate, or tissue oxygenation in magnetic resonance imaging, while RNA sequencing analysis implicated a potential role of circadian clock genes.

CONCLUSIONS: Our findings confirm a role of PGE_2 in the development of albuminuria in GH and support the renoprotective potential of combined pharmacological blockade of EP2 and EP4 receptors. These data support further translational research to explore this therapeutic option and a possible role of circadian clock genes. ***(Hypertension.* 2023;80:771–782. DOI: 10.1161/HYPERTENSIONAHA.122.20392.)** • **Supplement Material.**

Key Words: albuminuria ■ hypertension ■ prostaglandin E_2 ■ rats ■ zebrafish

Albuminuria is a hallmark of early kidney damage in diabetes- and hypertension-mediated organ damage.[1–4] Recent observational data in a large health care utilization cohort indicated that changes in albuminuria are strongly associated with the risk of developing end-stage kidney disease and death supporting the prognostic relevance of albuminuria.[5] The factors leading to albuminuria are multifactorial, but

Correspondence to: Reinhold Kreutz, Institute of Clinical Pharmacology and Toxicology, Charité–Universitätsmedizin Berlin, Charitéplatz 1, Berlin 10117, Germany.
Email reinhold.kreutz@charite.de
ORCID iD for Reinhold Kreutz: 0000-0002-4818-211X
*A. Kourpa, A. Schulz, D. Panáková, and R. Kreutz contributed equally.
Supplemental Material is available at https://www.ahajournals.org/doi/suppl/10.1161/HYPERTENSIONAHA.122.20392.
For Sources of Funding and Disclosures, see page 781.

Hypertension is available at www.ahajournals.org/journal/hyp

ORIGINAL ARTICLE

NOVELTY AND RELEVANCE

What Is New?

Complementary in vivo studies were conducted in zebrafish and rat models using the same pharmacological interventions to test their renoprotective potential in glomerular hyperfiltration.

What Is Relevant?

A role of both EP2 (prostaglandin E_2 receptor type 2) and EP4 (prostaglandin E_2 receptor type 4) receptors mediating prostaglandin E_2–induced glomerular injury in glomerular hyperfiltration was identified.

Clinical/Pathophysiological Implications?

The current study supports further translational research to explore the mechanisms and potential of combined EP2 and EP4 blockade in kidney injury with albuminuria due to glomerular hyperfiltration.

Nonstandard Abbreviations and Acronyms

COX2	cyclooxygenase 2
EP2	PGE_2 receptor type 2
EP4	PGE_2 receptor type 4
GFB	glomerular filtration barrier
GH	glomerular hyperfiltration
MWF	Munich Wistar Frömter
MWF-EP2/EP4^{inh}	Munich Wistar Frömter rat treated with combined EP2 and EP4 receptor antagonists
PGE_2	prostaglandin E_2
SGLT-2	sodium-glucose cotransporter-2
SHR	spontaneously hypertensive rat

intrarenal hemodynamic changes resulting in glomerular hyperfiltration (GH) play, among other factors, an important mechanistic role in the development of albuminuria in hypertension and diabetes.[2,3,6] Prostaglandins play important and complex roles in renal physiology and disease processes, while their most abundant form prostaglandin E_2 (PGE_2) has been particularly implicated in renal pathophysiology in hypertension and diabetes.[7] In the setting of GH, podocytes are exposed to increased fluid flow shear stress in Bowman space that contributes to podocyte damage and albuminuria development.[8,9] Previous studies indicated that COX2 (cyclooxygenase 2) and PGE_2 activation are involved in the resulting podocyte damage in response to GH,[10] while PGE_2 is known to increase glomerular permeability for proteins.[7] Our recent in vitro study in human podocytes indicated an activation of the autocrine/paracrine COX2/PGE_2 pathway resulting in podocyte injury in GH by using fluid flow shear stress exposure.[11] This was mediated by concerted signaling via both EP2 (PGE_2 receptor type 2) and EP4 (PGE_2 receptor type 4). We, therefore, set out to study the renoprotective effect of separate and combined pharmacological blockade of EP2 and EP4 receptors in vivo by using complementary animal experiments in zebrafish and rat models.

METHODS

Data supporting the findings of this study are available from the corresponding author upon reasonable request.

Animals

This study involved zebrafish and rat models (Supplemental Methods). A synopsis of the overall study design is presented in Figure 1. Transgenic zebrafish embryos of *Tg[fabp10a:gc-EGFP]*[16] and *Tg[wt1b:EGFP]*[15] were used to evaluate the functional role of glomerular filtration barrier (GFB) integrity and albuminuria phenotype in vivo and the glomerular morphology, respectively (Supplemental Methods). We used males of the MWF (Munich Wistar Frömter) rat with an inherited nephron deficit as a model of GH and albuminuria.[12,13]

Workflow in Zebrafish Models

We assessed the abundance of metabolites in the cyclooxygenase COX-PGE_2-EP2/EP4 pathway in zebrafish embryos at 48 hours post fertilization. Lipidomic analysis was performed by a liquid chromatography tandem mass spectrometry (LC/ESI-MS/MS) method to quantify PGE_2 levels in embryo lysates[11] after COX inhibition by using the COX inhibitor indomethacin.[14] The expression of EP2 and EP4 receptors was evaluated by fluorescent in situ hybridization (Advanced Cell Diagnostics, RNAscope Multiplex Fluorescent V2) of the corresponding *ptger2a* and *ptger4b* genes, respectively, in *Tg[wt1b:EGFP]*.[15] Zebrafish embryos provide a suitable model for the study of GFB development and function.[13,16] To model the increased PGE_2 signaling in zebrafish, embryos were exposed to 16,16-dimethyl PGE_2 after the complete formation of GFB, that is, from 72 to 96 hours post fertilization [13] (Figure 1A). To probe the PGE_2 signaling, embryos were treated with the selective EP2 and EP4 antagonists PF04418948[17,18] and ONO-AE3-208[19,20] or the COX inhibitor indomethacin.[21] High-resolution confocal and electron microscopy imaging was performed as reported recently[13] to analyze glomeruli and GFB (Supplemental Methods).

Workflow in the MWF Rat

Lipidomic analysis using the liquid chromatography tandem mass spectrometry protocol to quantify PGE_2 levels in glomerular

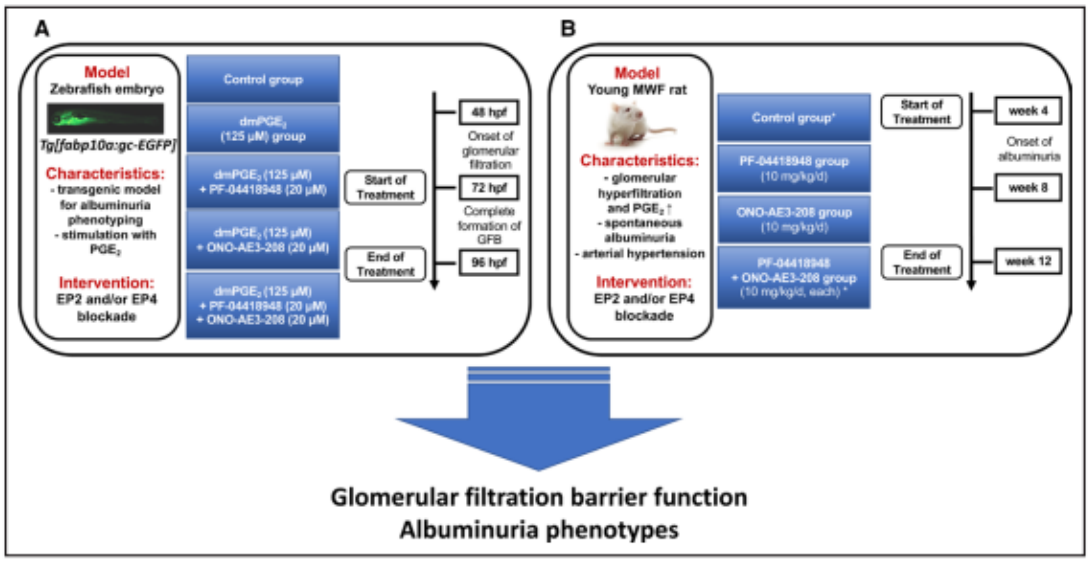

Figure 1. Overall design of in vivo studies in zebrafish and rat models.
To test the potential renoprotective effect on albuminuria phenotypes of either separate or combined pharmacological blockade of EP2 (prostaglandin E_2 [PGE_2] receptor type 2) and EP4 (PGE_2 receptor type 4) in glomerular hyperfiltration (GH), we used 2 complementary animal systems. **A**, Zebrafish embryos of *Tg[fabp10a:gc-EGFP]* were used to evaluate the glomerular filtration barrier (GFB) integrity and albuminuria phenotype in vivo in response to exogenous stimulation with PGE_2 (Supplemental Methods). **B**, MWF (Munich Wistar Frömter) rat model with an inherited nephron deficit, which results in GH, spontaneous development of progressive albuminuria, and mild arterial hypertension,[12] was used. Importantly, MWF animals demonstrate increased endogenous PGE_2 concentrations in isolated glomerular tissue.[11] We performed pharmacological intervention studies in both animal systems of the separate or combined blockade of EP2 and EP4 using PF-04418948 (EP2 antagonist)[17,18] and ONO-AE3-208 (EP4 antagonist)[19,20] vs control (untreated) animals. Zebrafish embryos were treated between 72 and 96 hours post fertilization (hpf) and assessed at 96 hpf (**A**), Young male MWF rats were studied between week 4 and week 12 of age (**B**). In zebrafish experiments, we conducted N=6 experiments with n=120 embryos for all groups except for the separate EP receptor blockade groups, where N=3 and n=60. In rat studies, n=7 to 8 animals were studied in each group. In MWF rats, we performed additional analysis using magnetic resonance imaging (MRI) analysis of tissue oxygenation. In this study, only the groups marked by asterisk (n=14–15), that is, untreated control MWF and MWF rats treated with combined EP2 and EP4 receptor antagonists, were analyzed following the same protocol, while phenotyping focused only on albuminuria and MRI mapping.

tissue[11] demonstrated a significant elevation of PGE_2 levels in isolated glomeruli in young MWF rats at the onset of albuminuria (8 weeks of age) as compared with albuminuria-resistant SHRs (spontaneously hypertensive rats; Figure 1B; Figure S6).[11] We, therefore, tested the effects of either separate or combined pharmacological blockade of EP2 (by PF-04418948) and EP4 receptors (by ONO-AE3-208) in MWF rats (as in zebrafish experiments; Figure 1B). Transcriptome analysis[47] was performed in cortex tissue of kidneys obtained at the end of the study period (Figure 1B). Electron microscopy imaging analysis of GFB in the rat was also performed as reported recently [13] (Supplemental Methods). Magnetic resonance imaging analysis[22] in an additional set of MWF animals was performed to analyze renal hemodynamics and oxygenation. Here, untreated MWF control rats and MWF rats treated with combined EP2 and EP4 receptor blockade (MWF-EP2/EP4^{Inh}) were analyzed. Treatment period was the same as shown in Figure 1B.

Statistical Analysis

Statistical analysis was performed using the GraphPad Prism 9 software (GraphPad Software, CA) or SPSS Statistics 28.0.0.0.2. Data are presented as mean±SD if not otherwise specified, and $P<0.05$ was considered as statistically significant. Data are normally distributed unless otherwise specified. Specific details of the analyses are given in the figures and in Supplemental Methods.

RESULTS

Zebrafish Experiments

COX-PGE2-EP2/EP4 Axis in Zebrafish Embryos

Lipidomic analysis detected PGE_2 levels (59.3±19.1 ng/g) in zebrafish embryos at 48 hours post fertilization, which were profoundly suppressed (7.2±1.6 ng/g, 87.8% suppression) by indomethacin treatment (Figure S1A). Furthermore, EP2 (*ptger2a*) and EP4 (*ptger4b*) receptors are expressed in the glomerulus and tubules of the zebrafish embryonic kidney, however, with a higher abundance in the tubules (Figure S1C through S1E).

Effects of PGE2 Stimulation on Albuminuria Phenotype and GFB

After confirming the presence of the COX-PGE_2-EP2/EP4 axis in zebrafish embryos, we used the zebrafish transgenics

ORIGINAL ARTICLE

Tg[fabp10a:gc-EGFP] to assess the effect of exogenous PGE_2 on GFB. Zebrafish embryos appeared normal after stimulation with PGE_2 and exhibited only lack of swim bladder formation (Figure 2A). However, exposure to PGE_2 resulted in a marked decrease in the fluorescence in the trunk vasculature of *Tg[fabp10a:gc-EGFP]* embryos, thus mimicking an albuminuria-like phenotype (Figure 2A and 2B). The latter could be significantly reversed by either separate or combined blockade of EP2 and EP4 receptors, as well as by indomethacin treatment (Figure 2A and 2B). The effect of combined treatment with both EP2 and EP4 blockers was comparable to either of the separate treatments. In electron microscopy analysis, no apparent changes of the GFB ultrastructure upon short-term 16,16-dimethyl PGE_2 stimulation were observed (Figure 2C and 2D), although the quantification of podocytes' foot processes width[46] was numerically higher as compared with controls in response to 16,16-dimethyl PGE_2 (Figure 2D). To further explore the impact of 16,16-dimethyl PGE_2 stimulation on GFB dysfunction, we analyzed the glomerular cytoarchitecture. This analysis in PGE_2-treated *Tg[wt1b:EGFP]* embryos at 96 hours post fertilization revealed cell intercalation defects between podocytes and endothelial cells of glomerular capillaries. The quantification of these defects showed a significant increase in podocyte surface area. Remarkably, these defects were restored after combined pharmacological blockade of EP2 and EP4 receptors, supporting the importance of the PGE_2-EP2-EP4 signaling axis for GFB integrity (Figure S7).

Rat Experiments

Effect of EP2 and EP4 Receptor Blockade on Albuminuria

Young MWF control rats develop, in agreement with previous studies,[12] a significant increase in albuminuria between weeks 4 and 8 ($P<0.001$; Figure 3A), followed by a further increase until week 12. Accordingly, no group differences were detected at 4 weeks of age. Albuminuria was not significantly lowered by either separate EP2 or EP4 blockade as compared with control. In contrast, combined EP2 and EP4 blockade (MWF-EP2/EP4^{inh}) resulted in a profound and significant suppression of albuminuria at 8 and 12 (−71%) weeks compared with untreated animals (Figure 3A).

Effect of EP2 and EP4 Receptor Blockade on Other In Vivo Phenotypes

Pharmacological treatment with either separate or combined EP2 and EP4 blockade induced no changes in systolic blood pressure (Figure 3B) and creatinine clearance (Figure 3C). Magnetic resonance imaging analysis indicated that the significant reduction in albuminuria by combined EP2 and EP4 receptor blockade (Figure S4A) was not associated with significant differences of the blood oxygenation level–dependent relaxation times T_2^* and T_2 (Figure S4B) as determined by magnetic resonance imaging mapping between the MWF control and MWF-EP2/EP4^{inh} groups. Similarly, no significant group differences for body weight, absolute and relative (in relation to body weight) left ventricular weights, and kidney weights were observed (Table S1).

Analysis of kidney morphology by light microscopy revealed no appreciable tissue injury, particularly in glomeruli, as expected in relatively young MWF animals at 12 weeks of age and no changes in response to the EP2 and EP4 blockade (Figure S2). Accordingly, the targeted expression analysis of selected molecular kidney injury markers in the setting of GH and albuminuria revealed no significant differences between groups, except for *Nphs2* (podocin) showing reduced mRNA expression in response to combined EP2 and EP4 blockade compared with controls (Figure S3).

Electron microscopy imaging of GFB in untreated MWF as compared with MWF-EP2/EP4^{inh} showed no appreciable differences in qualitative analysis (Figure 4A). Quantitative analysis of foot process width of podocytes[46] revealed a numerically lower mean value in response to combined EP2/EP4 blockade in 3 randomly selected animals from each of the MWF control and MWF-EP2/EP4^{inh} groups (Figure 4B); of note, 1 of the 3 treated animals exhibited still elevated albuminuria levels and a foot process width corresponding to untreated animals (Figure 4C). Nevertheless, a significant overall positive correlation between albuminuria and foot process width of podocytes ($r=0.599$; $P=0.0086$) was detected suggesting thus in turn a beneficial effect on podocyte damage by treatment-induced albuminuria reduction (Figure 4C).

RNA Sequencing Analysis of Transcriptome Response to EP2 and EP4 Receptor Blockade

To determine the potential molecular signature through which the inhibition of PGE_2 signaling mediates the nephroprotective effects, we performed transcriptomic analysis in kidney cortex tissue of untreated MWF control and MWF-EP2/EP4^{inh} rats using bulk RNA sequencing. The RNA sequencing analysis identified only a small number of significantly (adjusted $P<0.05$) upregulated and downregulated genes in MWF-EP2/EP4^{inh} animals when compared with MWF control (Figure 5; Table S2). Among the differentially expressed genes, we found key genes regulating circadian rhythm including *Cry1*, *Npas2*, and *Nr1d1* (Figures 5 and 6). Selected genes identified by their differential expression in RNA sequencing analysis were validated in secondary analysis using quantitative real-time polymerase chain reaction[48] (Figure 5C; Figure S5; Tables S2 and S3).

DISCUSSION

A recent study demonstrated increased urinary excretion of podocyte-specific proteins coupled with a decreased

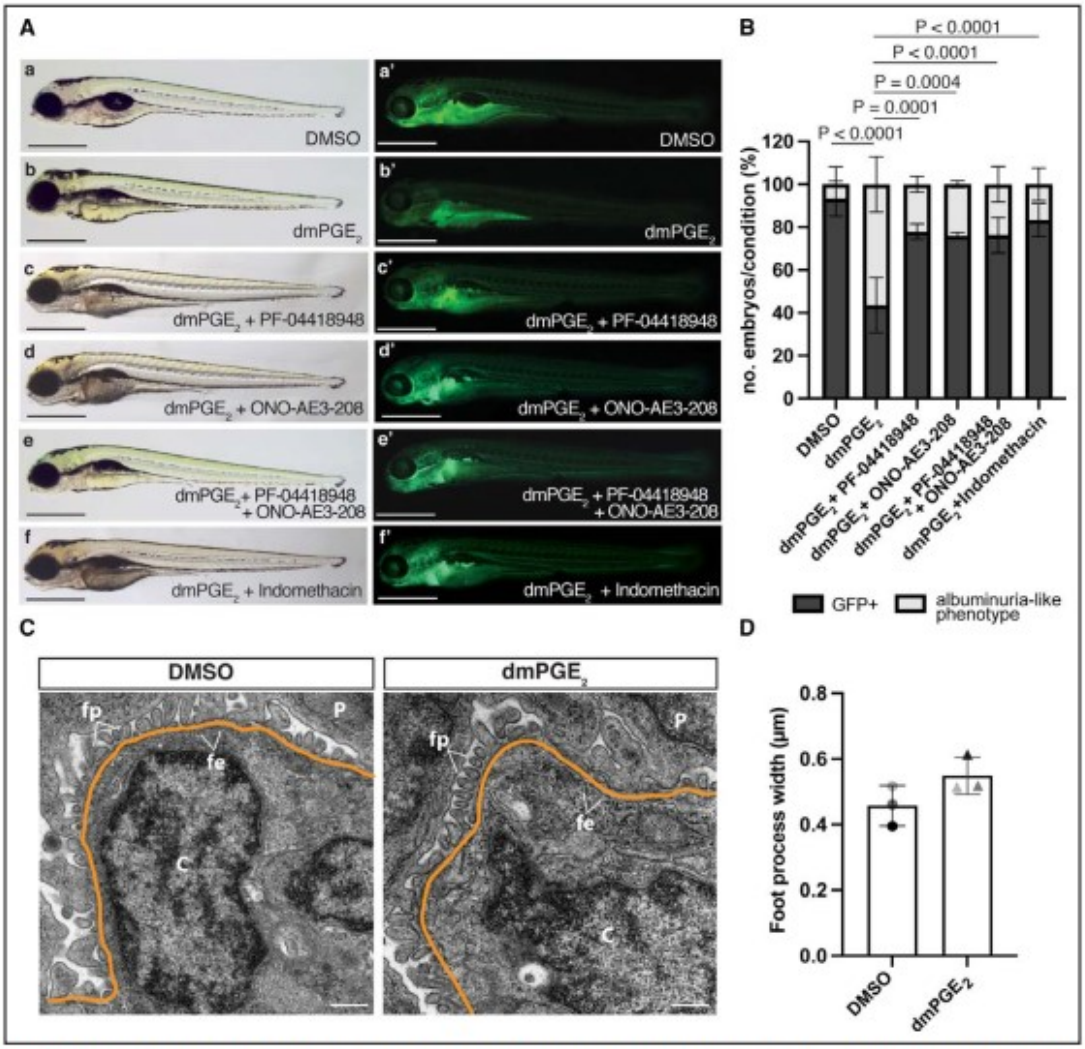

Figure 2. Effects of prostaglandin E2 (PGE_2) stimulation and separate and combined EP2 (PGE_2 receptor type 2) and EP4 (PGE_2 receptor type 4) blockade on albuminuria phenotype and glomerular ultrastructure in zebrafish model.
A, Bright-field and fluorescence microscopy images of *Tg[fabp10a:gc-EGFP]* embryos at 96 hours post fertilization (hpf), following pharmacological treatments: (**Aa** and **Aa'**) dimethyl sulfoxide (DMSO; vehicle) 0.32%, (**Ab** and **Ab'**) 16,16-dimethyl PGE_2 ($dmPGE_2$) 125 µM, (**Ac** and **Ac'**) $dmPGE_2$ 125 µM+PF-04418948 20 µM, (**Ad** and **Ad'**) $dmPGE_2$ 125 µM+ONO-AE3-208 20 µM, (**Ae** and **Ae'**) $dmPGE_2$ 125 µM+PF-04418948 20 µM+ONO-AE3-208 20 µM, (**Af** and **Af'**) $dmPGE_2$ 125 µM+indomethacin 30 µM; N=6, n=120 for all conditions except treatments c and d (N=3; n=60); scale bar, 1 mm. **B**, Phenotypic quantitative analysis of zebrafish embryos at 96 hpf. Embryos are categorized as GFP+ (green fluorescent protein +; visible vitamin D binding protein tagged with enhanced green fluorescent protein fluorescence signal in the trunk vasculature) or albuminuria-like phenotype (partial or complete loss of gc-EGFP fluorescence signal in the trunk vasculature). Percentage values are plotted as mean±SD; n represents biologically independent samples over N independent experiments; ordinary two-way ANOVA with Tukey multiple comparison test. **C**, Representative electron microscopy images of glomerular filtration barrier in the DMSO- (**left**) and $dmPGE_2$-treated (**right**) zebrafish embryos at 96 hpf; scale bar, 1 µm. Glomerular basement membrane is indicated with the colored line. **D**, Quantitative analysis of foot process width (n=3 for each condition); two-tailed unpaired t test with Welch correction (P=0.1303). Values are plotted as mean±SD; P<0.05 considered significant. C indicates capillary; fe, fenestrated endothelium; fp, foot processes; and P, podocyte cell body.

mRNA expression profile of podocyte-specific genes in patients with hypertension.[2] This finding supports a role of podocyte dysfunction leading to detachment of podocytes in patients with hypertension and albuminuria. However, the mechanisms leading to podocyte damage and albuminuria are not well understood. Nevertheless, an increase of fluid flow shear stress upon podocytes represents among other downstream events a functional

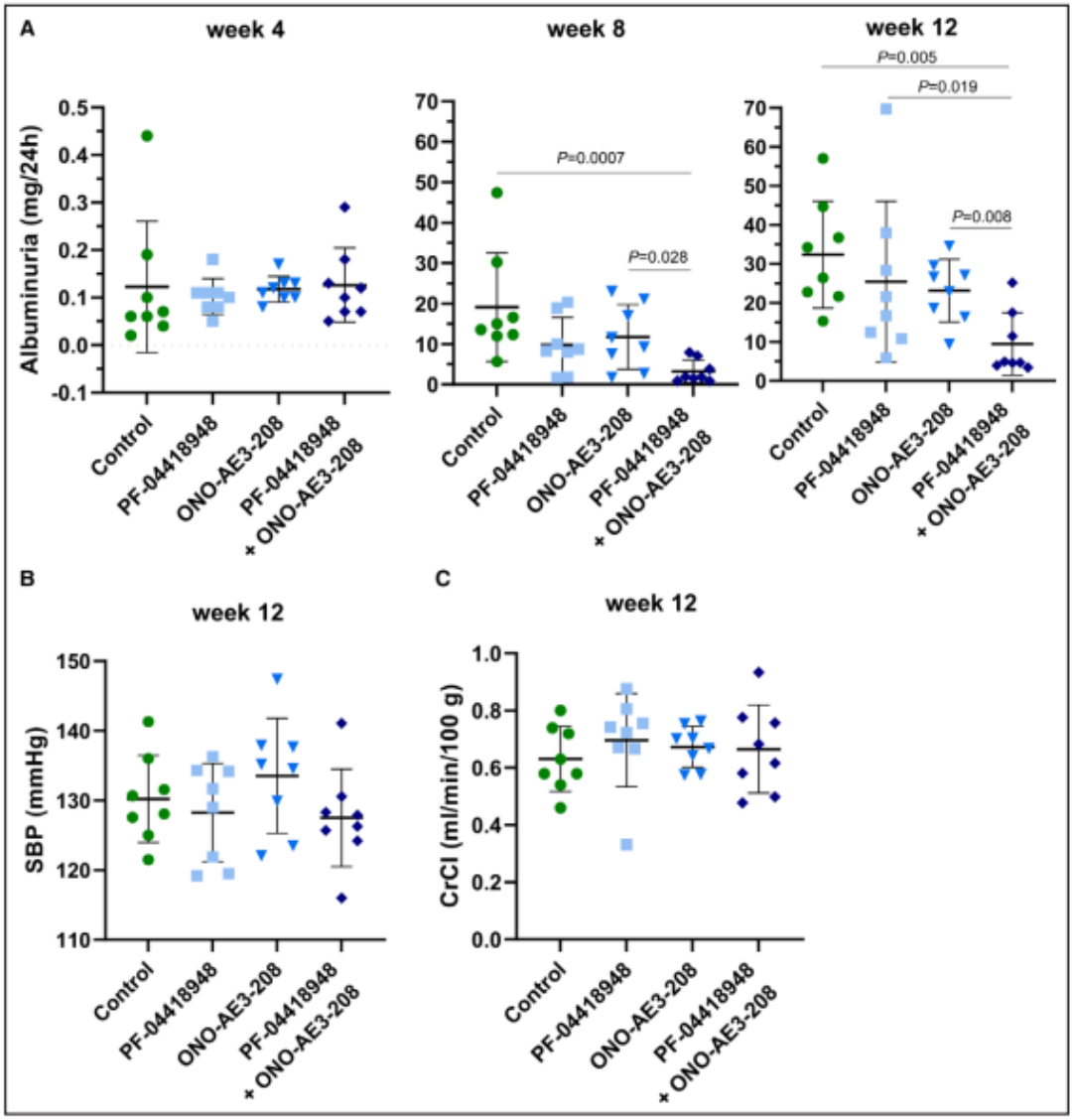

Figure 3. Effects of separate and combined EP2 (prostaglandin E2 [PGE_2] receptor type 2) and EP4 (PGE_2 receptor type 4) blockade on albuminuria development, systolic blood pressure (SBP), and creatinine clearance (CrCl) in the Munich Wistar Frömter (MWF) rat.

A, Time-course analysis of urinary albumin excretion in male MWF rats during the onset of albuminuria between weeks 4 and 12. **B**, SBP. **C**, CrCl. Rats were treated with either separate or combined EP2 (PF-04418948) and EP4 (ONO-AE3-208) antagonists. Rats per group, n=7 to 8, each; values are plotted as mean±SD. Data were analyzed by two-way ANOVA for albuminuria or one-way ANOVA for SBP and CrCl followed by Bonferroni post hoc analysis. In overall two-way ANOVA analysis, a significant interaction between treatment groups and time course (P=0.002) was observed for albuminuria with a significant increase of albuminuria over time and a significant difference between MWF rats treated with combined EP2 and EP4 receptor antagonists (MWF-EP2/EP4^{ab}) compared with all other groups (P<0.01, respectively). At 8 weeks, albuminuria was significantly lower in MWF-EP2/EP4^{ab} compared with control and EP4, whereas at 12 weeks, albuminuria was significantly lower compared with all groups.

consequence regardless of the causes of GH. Our previous findings in human podocytes in cell culture implying both EP2 and EP4 signaling in activation of COX2/PGE_2 in response to fluid flow shear stress[11] prompted us to further investigate the role of EP2 and EP4 in this setting in vivo.

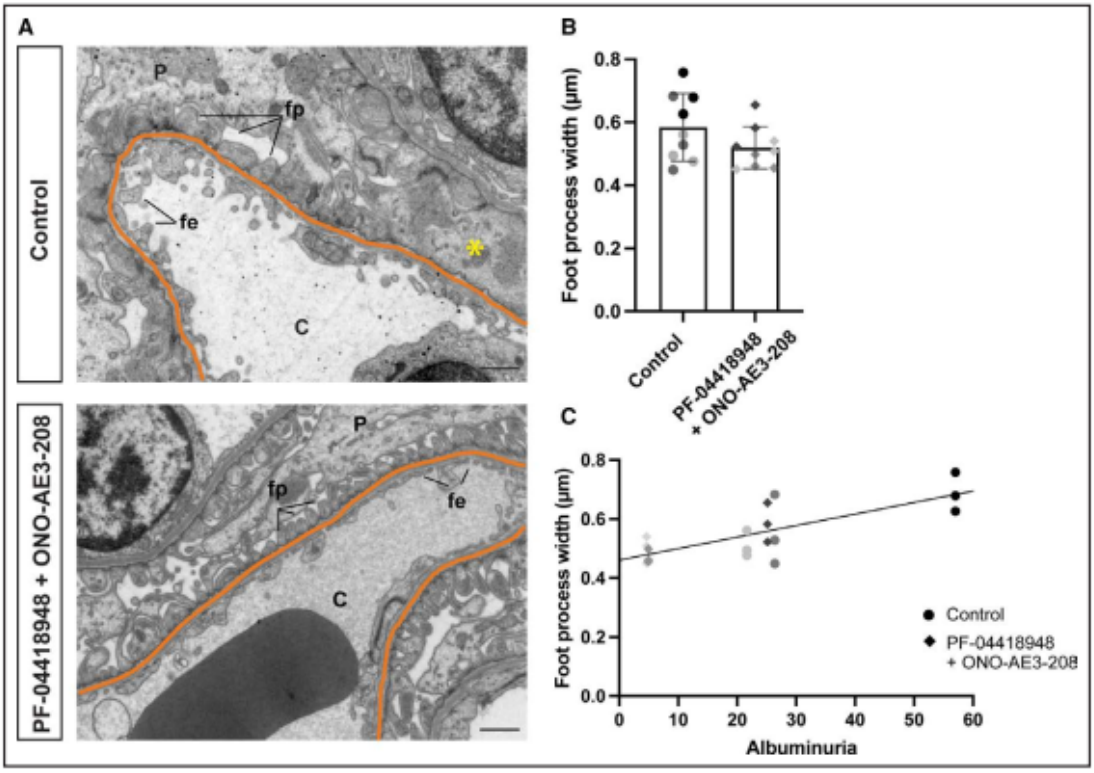

Figure 4. Glomerular ultrastructural analysis after combined inhibition of EP2 (prostaglandin E2 [PGE_2] receptor type 2) and EP4 (PGE_2 receptor type 4) receptors in the Munich Wistar Frömter (MWF) rat.
A, Representative electron microscopy images of glomerular filtration barrier in the MWF rat (control; **top**) and MWF rats treated with combined EP2 and EP4 receptor antagonists at week 12 (**bottom**). Scale bar, 1 µm. Glomerular basement membrane is indicated with the colored line. *Foot process effacement. **B**, Quantitative analysis of foot process width (n=9 glomeruli per group, obtained from 3 animals for each condition). The glomeruli of one animal are represented with different shades of gray in both groups; two-tailed unpaired t test with Welch correction (P=0.1490). **C**, Correlation plots reveal significant correlation between urinary albumin excretion (albuminuria) levels and foot process width; Spearman correlation (r=0.599; P=0.0086). In all graphs, values are plotted as mean±SD. P<0.05 considered significant. C indicates capillary; fe, fenestrated endothelium; fp, foot processes; and P, podocyte cell body.

The activation of COX2/PGE_2 in podocytes is linked to hyperfiltration-associated increases in biomechanical forces, namely tensile stress and fluid flow shear stress in podocytes.[9] PGE_2 signaling via EP2 was previously associated with podocyte responses to fluid flow shear stress and to kidney injury in the solitary kidney.[8] Moreover, in vivo studies in rodent models supported a role of EP4 activation in kidney damage, while renoprotective effects by EP4 inhibition have been shown in diabetes[23] and after profound renal mass ablation by 5/6 nephrectomy.[20,24] A role of EP2 inhibition but not EP4 inhibition has been recently supported in nondiabetic mice after unilateral nephrectomy.[25] However, it should be not dismissed that COX-derived prostaglandins including PGE_2 play an important role in maintaining renal homeostasis and may serve as physiological buffers, protecting kidney function under certain pathophysiological conditions, particularly in states associated with decreased effective arterial blood volume.[7,26,27] Given the multifaceted role of PGE_2 in the kidney,[7] we, therefore, first tested whether PGE_2 can in fact induce albuminuria in vivo in nondiabetic models. The latter was indeed confirmed in zebrafish experiments. We confirmed a renoprotective role by inhibiting EP2 or EP4 in the zebrafish model, while combined blockade of EP2 and EP4 was similarly effective in reducing the PGE_2-induced albuminuria phenotype as either separate blockade.

In addition to other genetic, SHR models[28,29] for the study of renal injury, the MWF rat represents a suitable nondiabetic model because of its inherited nephron deficit and increased GH phenotype with endogenous upregulation of glomerular PGE_2.[11] The nephroprotective effect of EP2 and EP4 blockade was also confirmed in this model; however, combined blockade was clearly superior leading to a profound suppression of albuminuria. Importantly, this occurred in the absence of significant changes in systemic arterial blood pressure and glomerular filtration rate. Moreover, although we cannot

ORIGINAL ARTICLE

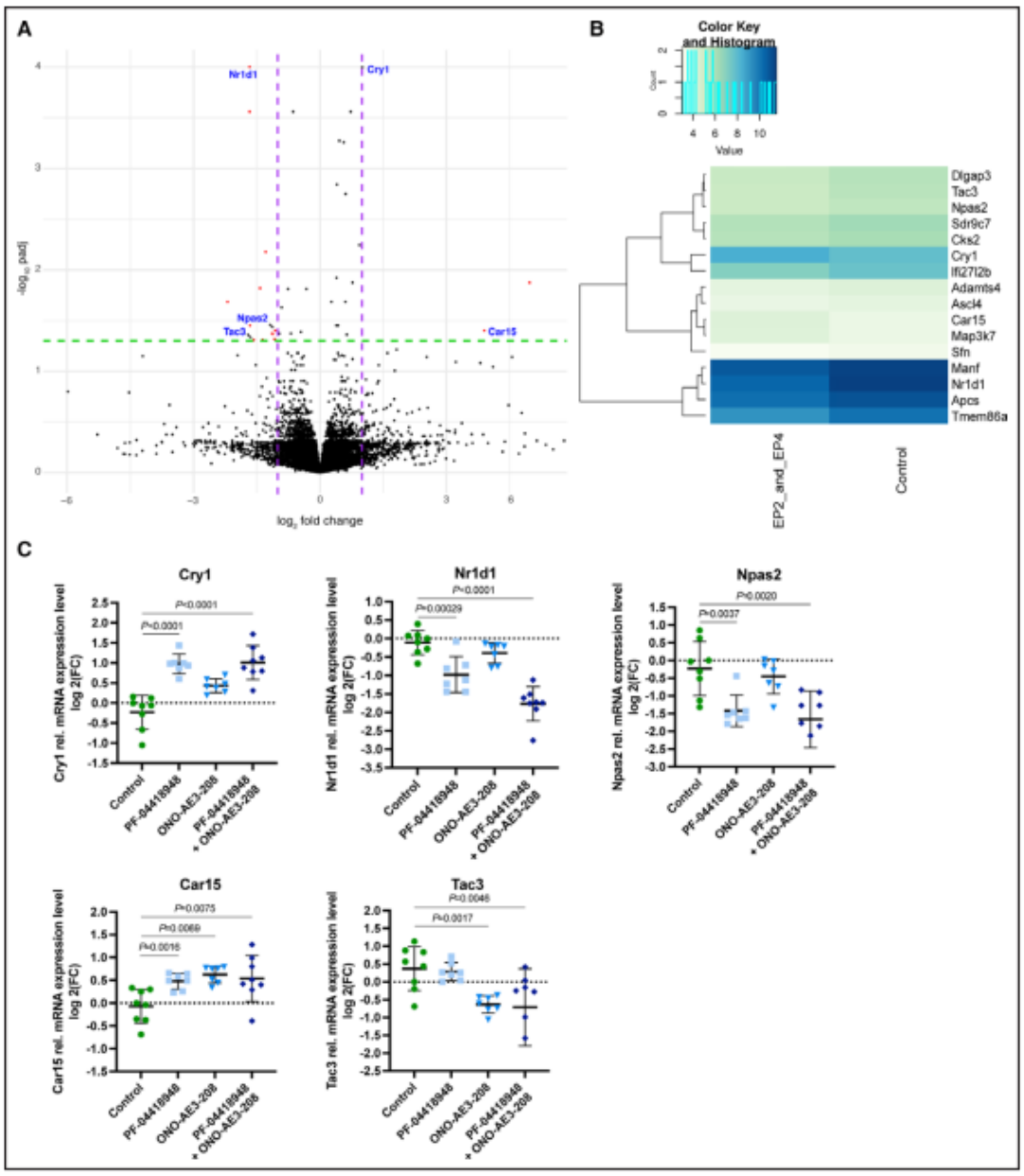

Figure 5. Transcriptome analysis in the Munich Wistar Frömter (MWF) model.

A, Volcano plot showing the comparison of the transcriptome analysis by RNA sequencing (RNA-seq) between untreated MWF control and MWF rats treated with combined EP2 and EP4 receptor antagonists (MWF-EP2/EP4^{inh}). Overall, 16 genes with differential expression (red dots including *Cry1* with a $\log_2$ fold change value=0.994) were identified. Vertical dotted lines (purple) demonstrate the $\log_2$ fold change of <−1 and >+1, while the horizontal dotted line (green) shows the $-\log_{10}$ of the adjusted *P* value ($P<0.05$ considered significant). **B**, Unscaled heat map shows the differences in expression between the significantly differentially regulated genes in the MWF-EP2/EP4^{inh} compared with MWF control. **C**, Separate quantitative real-time polymerase chain reaction (qPCR) analysis showed consistent significant differential expression for 3 main genes associated with circadian rhythm regulation, namely *Cry1*, *Nr1d1*, and *Npas2*. The expression of *Car15* and *Tac3* was also significantly different as identified in the RNA-seq analysis and confirmed by qPCR; respective genes are also annotated in the Volcano plot (**A**). Rats per group (n=6–8, each); data are displayed as mean±SD; gene data were tested for normal distribution using the Shapiro-Wilk test; *Cry1*, *Npas2*, and *Nr1d1* (not normally distributed) were analyzed using the Kruskal-Wallis test with Dunn post hoc analysis, while the rest of the data (normally distributed) were analyzed by one-way ANOVA with Bonferroni post hoc test.

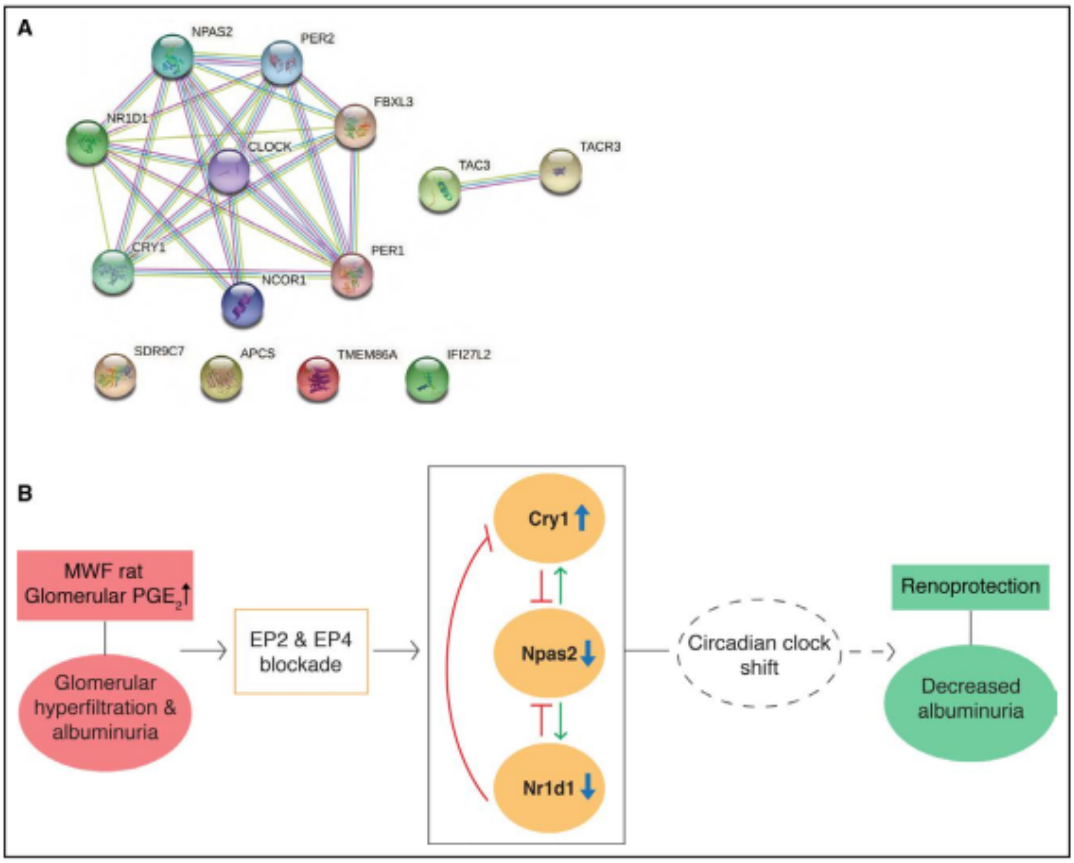

Figure 6. Network analysis supporting the involvement of circadian genes.
A, Full Search Tool for the Retrieval of Interacting Genes/Proteins protein network obtained from the 9 significantly differentially regulated genes derived from the comparison between MWF (Munich Wistar Frömter) control and MWF rats treated with combined EP2 and EP4 receptor antagonists by combining RNA sequencing and quantitative real-time polymerase chain reaction confirmation analysis. *Car15* was not recognized from the STRING database; *CLOCK*, *PER1/2*, *NCOR1*, *FBXL3*, and *TAC3R* appear as predicted functional partners. The network shows known interactions: curated databases (blue), experimentally determined (magenta), text mining (green), and protein homology (purple); high confidence interaction score, 0.70. **B**, Schematic representation of the proposed model arising from the transcriptome analysis. Combined pharmacological blockade of EP2 (prostaglandin E_2 [PGE_2] receptor type 2) and EP4 (PGE_2 receptor type 4) receptors in the MWF rat causes a potential circadian clock shift supporting the renoprotective effects of the dual EP receptor blockade. The dashed ellipse shape and arrow indicate our main speculation; the upregulation or downregulation of significantly differentially regulated genes in our transcriptome analysis is shown by the blue arrows, while the green arrows and red inhibition arcs indicate well-known interactions among the circadian rhythm genes.

rule out subtle differences of intrarenal hemodynamics between untreated animals and animals treated with both EP2 and EP4 antagonists, our magnetic resonance imaging analysis of blood oxygenation did not reveal appreciable group differences ruling out major differences in intrarenal blood flow between groups. The in vivo findings in the rat model are thus in agreement with our in vitro data in human podocytes showing a synergistic (additive) inhibitory effect on COX2/PGE_2 upregulation by combined EP2 and EP4 blockade in response to fluid flow shear stress,[11] as well as our studies in zebrafish. Young adult MWF rats exhibit only mild glomerular damage and develop significant glomerulosclerosis in older age in parallel with progressive albuminuria development.[30] Accordingly, no significant treatment effects by combined EP2 and EP4 blockade on glomerular histology and molecular markers of kidney damage were observed in relatively young animals studied here. In contrast, a significant correlation between podocyte foot process damage and albuminuria in electron microscopy analysis was observed in the overall analysis of treated and untreated animals indicating the potential of podocyte protection by reducing albuminuria with the EP2 and EP4 blockade. The experiments in zebrafish and

the MWF rat model were both conducted in nondiabetic conditions, and it will be, therefore, important to investigate whether the beneficial effect of dual EP2 and EP4 blockade can be replicated in corresponding experimental conditions with GH in diabetes.

In both, our recent in vitro experiments in human podocytes[11] and in the current in vivo study in the rat model, it was shown that dual EP2 and EP4 blockade demonstrated an additive synergistic effect, when compared with a separate blockade. This occurred against the background of reported differential regulation of both receptors[31] including differences regarding agonist-induced internalization that applies to EP4, while EP2 appears resistant to desensitization and internalization.[31,32] Thus, the receptor regulation in podocytes and the kidney and the mechanism contributing to the beneficial effects of combined EP2 and EP4 inhibition remains to be further elucidated. In this regard, RNA sequencing analysis of kidney cortex tissue in the rat experiments indicated that the overall transcriptome is only marginally affected by treatment with EP2 and EP4 antagonists. Thus, only a few genes were differentially expressed in response to treatment including genes related to the transcriptional-translational feedback loops of circadian clocks.[33,34] The expression of *Cry1* (increased expression) and *Nr1d1* (decreased expression), as transcriptional repressors of the main clock regulatory components BMAL-1 (basic helix-loophelix ARNT like 1) and CLOCK (circadian locomotor output cycles kaput), was significantly changed (Figure 5). Furthermore, the expression of the activator *Npas2* of core clock and clock-controlled genes was significantly reduced. Subsequent network analysis supported a potential involvement of circadian clock genes in the response of treatment with EP2 and EP4 antagonists.

The importance of circadian clocks for kidney function has only recently emerged.[33,35] For instance, kidney-associated ciliopathy phenotype was reverted by the circadian clock genes in zebrafish.[36] Importantly, podocyte-specific *Bmal1* deletion led to a 12-hour instead of 24-hour circadian rhythm in mice, supporting the role of an intrinsic circadian clock in podocytes in the control of glomerular filtration.[34] Depending on the experimental setting, previous gene targeting studies in mice suggested both protective[37] and adverse effects[38] of circadian clocks on kidney damage and implicated also a protective effect mediated by controlling COX2 expression.[37] A link between COX2/PGE_2 and the circadian clock system has been demonstrated in experimental studies,[39,40] while its potential relevance in the setting of GH remains unclear. The removal of *Nr1d1* (encoded by *Rev-erb-alpha*) has been linked to the induction of COX2 in endometrial cells,[40] while PGE_2 or its analog, misoprostol, have been shown to upregulate the expression of *Per* genes.[39,41] In agreement, our transcriptomic analysis identified a potential presence of a shift in the circadian clock linked to the COX2-PGE_2-EP2/EP4 pathway in the setting of GH and indicated that PGE_2 signaling is intricately associated with the kidney-intrinsic circadian clock, which warrants further investigation.

Currently, inhibitors of the renin-angiotensin-system, that is, angiotensin-converting enzyme inhibitor and angiotensin receptor blockers, represent the backbone of recommended antihypertensive therapy[42] due to their additional protective properties including renal protection in the setting of GH by reducing intraglomerular capillary pressure. Based on recent evidence from clinical trials, additional treatment with SGLT-2 (sodium-glucose cotransporter-2) inhibitors will provide additional renoprotection in various forms of chronic kidney diseases including patients with albuminuria.[43] The current study supports a novel renoprotective effect by combining the EP2 and EP4 receptors in the setting of GH and albuminuria under nondiabetic conditions. Targeting dual blockade of G-protein–coupled receptors provides an interesting therapeutic option including the treatment of hypertension as recently highlighted by using dual endothelin receptor blockade.[44] In this regard, it is of interest that a highly specific dual EP2 and EP4 antagonist (ie, TPST-1495) has been developed and is currently being tested in a phase 1 study in patients with solid tumors.[45] Hence, the use of dual EP2 and EP4 blockade by TPST-1495 has been shown in preclinical studies to inhibit tumor proliferation and to stimulate anticancer immunity better than inhibiting EP2 or EP4 receptors separately or even all 4 PGE_2 receptors together.[45]

PERSPECTIVES

The COX2/PGE_2 pathway has been implicated in kidney damage in the setting of GH but the role of either both or separate EP2 and EP4 receptors as potential targets for renoprotection in different pathophysiological conditions with GH and hypertension remains unclear. The current study supports further translational research to explore the mechanisms and potential of combined EP2 and EP4 blockade in kidney injury with albuminuria due to GH.

ARTICLE INFORMATION

Received September 30, 2022; accepted January 3, 2023.

Affiliations

Institute of Clinical Pharmacology and Toxicology (A.K., A.S., E.M., D.K.-G., J.B., R.K.), Institute of Vegetative Anatomy (S.B.), and Institute of Translational Physiology (K.M.), Charité–Universitätsmedizin Berlin, Germany. Max-Delbrück Center for Molecular Medicine in the Helmholtz Association, Berlin, Germany (A.K., M.B., B.P., S.K., T.G., T.N., D.P.). Genetic Epidemiology, Institute for Human Genetics, Westfälische Wilhelms University, Münster, Germany (N.K., M.S.). Lipidomix GmbH, Berlin, Germany (M.R.). German Center for Cardiovascular Research, Partner Site Berlin, Germany (M.B.). Charité–Universitätsmedizin Berlin, Germany (M.B.). Institute for Biology, University of Lübeck, Germany (M.B.).

Acknowledgments

We acknowledge the contributions of Karen Böhme, Bettina Bublath, Petra Karsten, Claudia Plum, Christina Schiel, and Katja Dörfel for excellent laboratory

assistance. *Tg(fabp10a:gc-EGFP)* and *Tg(wt1b:GFP)* zebrafish lines were kindly provided by Weibin Zhou and Christoph Englert, respectively.

Sources of Funding

This research was funded by the Deutsche Forschungsgemeinschaft (project number: 394046635—SFB 1365).

Disclosures

None.

REFERENCES

1. Schmieder RE, Messerli FH, Garavaglia G, Nunez B. Glomerular hyperfiltration indicates early target organ damage in essential hypertension. *JAMA*. 1990;264:2775–2780.
2. Perez-Hernandez J, Olivares MD, Solaz E, Martinez F, Martínez-Hervas S, Pichler G, Chaves FJ, Redon J, Cortes R. Urinary podocyte-associated molecules and albuminuria in hypertension. *J Hypertens*. 2018;36:1712–1718. doi: 10.1097/hjh.0000000000001747
3. Benzing T, Salant D. Insights into glomerular filtration and albuminuria. *N Engl J Med*. 2021;384:1437–1446. doi: 10.1056/nejmra1808786
4. Cortinovis M, Perico N, Ruggenenti P, Remuzzi A, Remuzzi G. Glomerular hyperfiltration. *Nat Rev Nephrol*. 2022;18:435–451. doi: 10.1038/s41581-022-00559-y
5. Carrero JJ, Grams ME, Sang Y, Arnlov J, Gasparini A, Matsushita K, Qureshi AR, Evans M, Barany P, Lindholm B, et al. Albuminuria changes are associated with subsequent risk of end-stage renal disease and mortality. *Kidney Int*. 2017;91:244–251. doi: 10.1016/j.kint.2016.09.037
6. Martinez F, Mansego ML, Chaves FJ, Redon J. Genetic bases of urinary albumin excretion and related traits in hypertension. *J Hypertens*. 2010;28:213–225. doi: 10.1097/hjh.0b013e328333afb3
7. Nasrallah R, Hassouneh R, Hebert RL. PGE2, kidney disease, and cardiovascular risk: beyond hypertension and diabetes. *J Am Soc Nephrol: JASN*. 2016;27:666–676. doi: 10.1681/ASN.2015050528
8. Srivastava T, Celsi GE, Sharma M, Dai H, McCarthy ET, Ruiz M, Cudmore PA, Alon US, Sharma R, Savin VA. Fluid flow shear stress over podocytes is increased in the solitary kidney. *Nephrol, Dial, Transpl*. 2014;29:65–72. doi: 10.1093/ndt/gft387
9. Friedrich C, Endlich N, Kriz W, Endlich K. Podocytes are sensitive to fluid shear stress in vitro. *Am J Physiol Renal Physiol*. 2006;291:F856–F865. doi: 10.1152/ajprenal.00196.2005
10. Srivastava T, Alon US, Cudmore PA, Tarakji B, Kats A, Garola RE, Duncan RS, McCarthy ET, Sharma R, Johnson ML, et al. Cyclooxygenase-2, prostaglandin E2, and prostanoid receptor EP2 in fluid flow shear stress-mediated injury in the solitary kidney. *Am J Physiol Renal Physiol*. 2014;307:F1323–F1333. doi: 10.1152/ajprenal.00335.2014
11. Mangelsen E, Rothe M, Schulz A, Kourpa A, Panakova D, Kreutz R, Bolbrinker J. Concerted EP2 and EP4 receptor signaling stimulates autocrine prostaglandin E2 activation in human podocytes. *Cells*. 2020;9:1256. doi: 10.3390/cells9051256
12. Schulz A, Kreutz R. Mapping genetic determinants of kidney damage in rat models. *Hyperten Res*. 2012;35:675–694. doi: 10.1038/hr.2012.77
13. Schulz A, Muller NV, van de Lest NA, Eisenreich A, Schmidbauer M, Barysenka A, Purfurst B, Sporbert A, Lorenzen T, Meyer AM, et al. Analysis of the genomic architecture of a complex trait locus in hypertensive rat models links Tmem63c to kidney damage. *eLife*. 2019;8e42068. doi: 10.7554/eLife.42068
14. Warner TD, Giuliano F, Vojnovic I, Bukasa A, Mitchell JA, Vane JR. Nonsteroid drug selectivities for cyclo-oxygenase-1 rather than cyclo-oxygenase-2 are associated with human gastrointestinal toxicity: a full in vitro analysis. *Proc Natl Acad Sci USA*. 1999;96:7563–7568. doi: 10.1073/pnas.96.13.7563
15. Perner B, Englert C, Bollig F. The Wilms tumor genes wt1a and wt1b control different steps during formation of the zebrafish pronephros. *Dev Biol*. 2007;309:87–96. doi: 10.1016/j.ydbio.2007.06.022
16. Zhou W, Hildebrandt F. Inducible podocyte injury and proteinuria in transgenic zebrafish. *J Am Soc Nephrol*. 2012;23:1039–1047. doi: 10.1681/asn.2011080776
17. Ma X, Aoki T, Tsuruyama T, Narumiya S. Definition of prostaglandin E2-EP2 signals in the colon tumor microenvironment that amplify inflammation and tumor growth. *Cancer Res*. 2015;75:2822–2832. doi: 10.1158/0008-5472.can-15-0125
18. af Forselles KJ, Root J, Clarke T, Davey D, Aughton K, Dack K, Pullen N. In vitro and in vivo characterization of PF-04418948, a novel, potent and selective prostaglandin EP(2) receptor antagonist. *Br J Pharmacol*. 2011;164:1847–1856. doi: 10.1111/j.1476-5381.2011.01495.x
19. Kabashima K, Saji T, Murata T, Nagamachi M, Matsuoka T, Segi E, Tsuboi K, Sugimoto Y, Kobayashi T, Miyachi Y, et al. The prostaglandin receptor EP4 suppresses colitis, mucosal damage and CD4 cell activation in the gut. *J Clin Invest*. 2002;109:883–893. doi: 10.1172/jci0214459
20. Thieme K, Majumder S, Brijmohan AS, Batchu SN, Bowskill BB, Alghamdi TA, Advani SL, Kabir MG, Liu Y, Advani A. EP4 inhibition attenuates the development of diabetic and non-diabetic experimental kidney disease. *Sci Rep*. 2017;7:3442. doi: 10.1038/s41598-017-03237-3
21. Mitchell JA, Akarasereenont P, Thiemermann C, Flower RJ, Vane JR. Selectivity of nonsteroidal antiinflammatory drugs as inhibitors of constitutive and inducible cyclooxygenase. *Proc Natl Acad Sci USA*. 1993;90:11693–11697. doi: 10.1073/pnas.90.24.11693
22. Pohlmann A, Zhao K, Fain SB, Prasad PV, Niendorf T. Experimental protocol for MRI mapping of the blood oxygenation-sensitive parameters T(2)* and T(2) in the kidney. *Methods Mol Biol (Clifton, NJ)*. 2021;2216:403–417. doi: 10.1007/978-1-0716-0978-1_23
23. Mohamed R, Jayakumar C, Ramesh G. Chronic administration of EP4-selective agonist exacerbates albuminuria and fibrosis of the kidney in streptozotocin-induced diabetic mice through IL-6. *Lab Invest*. 2013;93:933–945. doi: 10.1038/labinvest.2013.85
24. Mizukami K, Yoshida H, Nozawa E, Wada K, Ugawa T. Renoprotective effects of the novel prostaglandin EP4 receptor-selective antagonist ASP7657 in 5/6 nephrectomized chronic kidney disease rats. *Naunyn-Schmiedeberg's Arch Pharmacol*. 2019;392:451–459. doi: 10.1007/s00210-018-01600-3
25. Srivastava T, Garola RE, Zhou J, Boinpelly VC, Priya L, Ali MF, Rezaiekhaligh MH, Heruth DP, Novak J, Alon US, et al. Prostanoid receptors in hyperfiltration-mediated glomerular injury: novel agonists and antagonists reveal opposing roles for EP2 and EP4 receptors. *FASEB J*. 2022;36:e22559. doi: 10.1096/fj.202200875R
26. Hao CM, Breyer MD. Physiological regulation of prostaglandins in the kidney. *Annu Rev Physiol*. 2008;70:357–377. doi: 10.1146/annurev.physiol.70.113006.100614
27. Wang L, Wu Y, Jia Z, Yu J, Huang S. Roles of EP receptors in the regulation of fluid balance and blood pressure. *Front Endocrinol*. 2022;13:875425. doi: 10.3389/fendo.2022.875425
28. Dhande IS, Cranford SM, Zhu Y, Kneedler SC, Hicks MJ, Wenderfer SE, Braun MC, Doris PA. Susceptibility to hypertensive renal disease in the spontaneously hypertensive rat is influenced by 2 loci affecting blood pressure and immunoglobulin repertoire. *Hypertension (Dallas, Tex: 1979)*. 2018;71:700–708. doi: 10.1161/HYPERTENSIONAHA.117.10593
29. Takeuchi F, Liang YQ, Isono M, Ang MY, Mori K, Kato N. Transcriptomic response in the heart and kidney to different types of antihypertensive drug administration. *Hypertension (Dallas, Tex: 1979)*. 2022;79:413–423. doi: 10.1161/HYPERTENSIONAHA.121.18026
30. van Es N, Schulz A, Ijpelaar D, van der Wal A, Kuhn K, Schutten S, Kossmehl P, Nyengaard JR, de Heer E, Kreutz R. Elimination of severe albuminuria in aging hypertensive rats by exchange of 2 chromosomes in double-consomic rats. *Hypertension (Dallas, Tex: 1979)*. 2011;58:219–224. doi: 10.1161/HYPERTENSIONAHA.111.170621
31. Biringer RG. A review of prostanoid receptors: expression, characterization, regulation, and mechanism of action. *J Cell Commun Signal*. 2021;15:155–184. doi: 10.1007/s12079-020-00585-0
32. Sluter MN, Hou R, Li L, Yasmen N, Yu Y, Liu J, Jiang J. EP2 antagonists (2011-2021): a decade's journey from discovery to therapeutics. *J Med Chem*. 2021;64:11816–11836. doi: 10.1021/acs.jmedchem.1c00816
33. Costello HM, Johnston JG, Juffre A, Crislip GR, Gumz ML. Circadian clocks of the kidney: function, mechanism, and regulation. *Physiol Rev*. 2022;102:1669–1701. doi: 10.1152/physrev.00045.2021
34. Ansermet C, Centeno G, Nikolaeva S, Maillard MP, Pradervand S, Firsov D. The intrinsic circadian clock in podocytes controls glomerular filtration rate. *Sci Rep*. 2019;9:16089. doi: 10.1038/s41598-019-52682-9
35. Firsov D, Bonny O. Circadian rhythms and the kidney. *Nat Rev Nephrol*. 2018;14:626–635. doi: 10.1038/s41581-018-0048-9
36. Kayser N, Zaiser F, Veenstra AC, Wang H, Göcmen B, Eckert P, Franz H, Köttgen A, Walz G, Yakulov TA. Clock genes rescue nphp mutations in zebrafish. *Hum Mol Genet*. 2022;31:4143–4158. doi: 10.1093/hmg/ddac160
37. Chen WD, Yeh JK, Peng MT, Shie SS, Lin SL, Yang CH, Chen TH, Hung KC, Wang CC, Hsieh IC, et al. Circadian CLOCK mediates activation of transforming growth factor-β signaling and renal fibrosis through cyclooxygenase 2. *Am J Pathol*. 2015;185:3152–3163. doi: 10.1016/j.ajpath.2015.08.003
38. Fletcher EK, Morgan J, Kennaway DR, Bienvenu LA, Rickard AJ, Delbridge LMD, Fuller PJ, Clyne CD, Young MJ. Deoxycorticosterone/

ORIGINAL ARTICLE

salt-mediated cardiac inflammation and fibrosis are dependent on functional CLOCK signaling in male mice. *Endocrinology*. 2017;158:2906–2917. doi: 10.1210/en.2016-1911

39. Tsuchiya Y, Minami I, Kadotani H, Nishida E. Resetting of peripheral circadian clock by prostaglandin E2. *EMBO Rep*. 2005;6:256–261. doi: 10.1038/sj.embor.7400356
40. Isayama K, Zhao L, Chen H, Yamauchi N, Shigeyoshi Y, Hashimoto S, Hattori MA. Removal of Rev-erbα inhibition contributes to the prostaglandin G/H synthase 2 expression in rat endometrial stromal cells. *Am J Physiol Endocrinol Metab*. 2015;308:E650–E661. doi: 10.1152/ajpendo.00533.2014
41. Wu X, Bos IST, Conlon TM, Ansari M, Verschut V, van der Koog L, Verkleij LA, D'Ambrosi A, Matveyenko A, Schiller HB,et al. A transcriptomics-guided drug target discovery strategy identifies receptor ligands for lung regeneration. *Sci Adv*. 2022;8:eabj9949. doi: 10.1126/sciadv.abj9949
42. Whelton PK, Carey RM, Mancia G, Kreutz R, Bundy JD, Williams B. Harmonization of the American College of Cardiology/American Heart Association and European Society of Cardiology/European Society of Hypertension blood pressure/hypertension guidelines: comparisons, reflections, and recommendations. *Circulation*. 2022;101161:868. doi: 10.1161/CIRCULATIONAHA.121.054602
43. Sarafidis P, Ortiz A, Ferro CJ, Halimi JM, Kreutz R, Mallamaci F, Mancia G, Wanner C. Sodium--glucose co-transporter-2 inhibitors for patients with diabetic and nondiabetic chronic kidney disease: a new era has already begun. *J Hypertens*. 2021;39:1090–1097. doi: 10.1097/hjh.0000000000002776
44. Schlaich MP, Bellet M, Weber MA, Danaietash P, Bakris GL, Flack JM, Dreier RF, Sassi-Sayadi M, Haskell LP, Narkiewicz K, et al. Dual endothelin antagonist aprocitentan for resistant hypertension (PRECISION): a multicentre, blinded, randomised, parallel-group, phase 3 trial. *Lancet (London, England)*. 2022;400:1927–1937. doi: 10.1016/S0140-6736(22)02034-7
45. Davar D, Powderly JD, Ullahannan SV, Johnson ML, Sharma M, Krauss JC, Stagg R, Francica B, Moon A, Jenkins Y,et al. A phase 1 study of TPST-1495 as a single agent and in combination with pembrolizumab in subjects with solid tumors. *J Clin Oncol*. 2022;40:TPS2696–TPS2696. 10.1200/jco.2022.40.16_suppl.tps2696

Excerpt from Journal Summary List

Journal Data Filtered By: **Selected JCR Year: 2018** Selected Editions: SCIE,SSCI
Selected Categories: **"CELL BIOLOGY"** Selected Category Scheme: WoS
Gesamtanzahl: 193 Journale

Rank	Full Journal Title	Total Cites	Journal Impact Factor	Eigenfactor Score
1	NATURE REVIEWS MOLECULAR CELL BIOLOGY	45,869	43.351	0.091360
2	CELL	242,829	36.216	0.571850
3	NATURE MEDICINE	79,243	30.641	0.162840
4	CANCER CELL	36,056	23.916	0.091050
5	Cell Metabolism	34,829	22.415	0.099550
6	Cell Stem Cell	24,628	21.464	0.087030
7	CELL RESEARCH	15,131	17.848	0.038680
8	NATURE CELL BIOLOGY	40,615	17.728	0.082430
9	Science Translational Medicine	30,485	17.161	0.121980
10	TRENDS IN CELL BIOLOGY	14,380	16.588	0.034120
11	MOLECULAR CELL	62,812	14.548	0.170680
12	NATURE STRUCTURAL & MOLECULAR BIOLOGY	27,166	12.109	0.069440
13	EMBO JOURNAL	65,212	11.227	0.067930
14	Autophagy	16,161	11.059	0.032630
15	TRENDS IN MOLECULAR MEDICINE	9,946	11.028	0.018900
16	Journal of Extracellular Vesicles	3,675	11.000	0.012110
17	Annual Review of Cell and Developmental Biology	9,734	10.833	0.016750
18	AGEING RESEARCH REVIEWS	6,539	10.390	0.015890
19	CURRENT BIOLOGY	60,772	9.193	0.135820
20	DEVELOPMENTAL CELL	28,572	9.190	0.068550

Rank	Full Journal Title	Total Cites	Journal Impact Factor	Eigenfactor Score
21	Cold Spring Harbor Perspectives in Biology	15,375	9.110	0.041830
22	GENES & DEVELOPMENT	54,563	8.990	0.072340
23	JOURNAL OF CELL BIOLOGY	67,347	8.891	0.075660
24	Cell Systems	2,275	8.640	0.016280
25	PLANT CELL	52,034	8.631	0.057800
26	EMBO REPORTS	13,786	8.383	0.029850
27	CURRENT OPINION IN CELL BIOLOGY	13,417	8.233	0.025790
28	CELL DEATH AND DIFFERENTIATION	19,729	8.086	0.030290
29	Cell Reports	39,510	7.815	0.235540
30	Protein & Cell	3,243	7.575	0.009080
31	AGING CELL	8,993	7.346	0.018810
32	CURRENT OPINION IN STRUCTURAL BIOLOGY	11,066	7.052	0.024160
33	CELLULAR AND MOLECULAR LIFE SCIENCES	24,422	7.014	0.038970
34	MATRIX BIOLOGY	5,699	6.986	0.009540
35	ONCOGENE	63,249	6.634	0.074600
36	Tissue Engineering Part B-Reviews	3,550	6.512	0.004970
37	Science Signaling	11,403	6.481	0.033700
38	Cell Death & Disease	19,001	5.959	0.051780
39	Signal Transduction and Targeted Therapy	371	5.873	0.000990
40	Cells	1,412	5.656	0.003990
41	STEM CELLS	21,467	5.614	0.030220
42	Aging-US	5,185	5.515	0.012440

Selected JCR Year: 2018; Selected Categories: "CELL BIOLOGY"

Printing copy of the publication

3. Mangelsen, Eva.; Rothe, Michael.; Schulz, Angela.; Kourpa, Aikaterini.; Panáková, Daniela.; Kreutz, Reinhold.; Bolbrinker, Juliane**. **Concerted EP2 and EP4 Receptor Signaling Stimulates Autocrine Prostaglandin E2 Activation in Human Podocytes**. *Cells* 2020, 9, 1256. https://doi.org/10.3390/cells9051256.

cells

MDPI

Article

Concerted EP2 and EP4 Receptor Signaling Stimulates Autocrine Prostaglandin E_2 Activation in Human Podocytes

Eva Mangelsen [1], Michael Rothe [2], Angela Schulz [1], Aikaterini Kourpa [3], Daniela Panáková [3,4], Reinhold Kreutz [1,4] and Juliane Bolbrinker [1,*]

1 Charité – Universitätsmedizin Berlin, Corporate Member of Freie Universität Berlin, Humboldt-Universität zu Berlin, and Berlin Institute of Health, Institute of Clinical Pharmacology and Toxicology, Charitéplatz 1, 10117 Berlin, Germany; eva.mangelsen@charite.de (E.M.); angela-martina.schulz@charite.de (A.S.); reinhold.kreutz@charite.de (R.K.)

2 Lipidomix GmbH, Robert-Rössle-Str. 10, B55, 13125 Berlin, Germany; michael.rothe@lipidomix.de

3 Max Delbrück Center for Molecular Medicine in the Helmholtz Association, Electrochemical Signaling in Development and Disease, Robert-Rössle-Str. 10, 13125 Berlin, Germany; Aikaterini.Kourpa@mdc-berlin.de (A.K.); Daniela.Panakova@mdc-berlin.de (D.P.)

4 DZHK (German Centre for Cardiovascular Research), Partner Site Berlin, Potsdamer Straße 58, 10785 Berlin, Germany

* Correspondence: juliane.bolbrinker@charite.de; Tel.: +49-30-450-525-225

Received: 31 March 2020; Accepted: 14 May 2020; Published: 19 May 2020

check for updates

Abstract: Glomerular hyperfiltration is an important mechanism in the development of albuminuria. During hyperfiltration, podocytes are exposed to increased fluid flow shear stress (FFSS) in Bowman's space. Elevated Prostaglandin E2 (PGE_2) synthesis and upregulated cyclooxygenase 2 (Cox2) are associated with podocyte injury by FFSS. We aimed to elucidate a PGE_2 autocrine/paracrine pathway in human podocytes (hPC). We developed a modified liquid chromatography tandem mass spectrometry (LC/ESI-MS/MS) protocol to quantify cellular PGE_2, 15-keto-PGE_2, and 13,14-dihydro-15-keto-PGE_2 levels. hPC were treated with PGE_2 with or without separate or combined blockade of prostaglandin E receptors (EP), EP2, and EP4. Furthermore, the effect of FFSS on *COX2*, *PTGER2*, and *PTGER4* expression in hPC was quantified. In hPC, stimulation with PGE_2 led to an EP2- and EP4-dependent increase in cyclic adenosine monophosphate (cAMP) and *COX2*, and induced cellular PGE_2. *PTGER4* was downregulated after PGE_2 stimulation in hPC. In the corresponding LC/ESI-MS/MS in vivo analysis at the tissue level, increased PGE_2 and 15-keto-PGE_2 levels were observed in isolated glomeruli obtained from a well-established rat model with glomerular hyperfiltration, the Munich Wistar Frömter rat. *COX2* and *PTGER2* were upregulated by FFSS. Our data thus support an autocrine/paracrine COX2/PGE_2 pathway in hPC linked to concerted EP2 and EP4 signaling.

Keywords: podocyte; hyperfiltration; chronic kidney disease; prostaglandin E2; COX2; EP2; EP4; G protein-coupled receptor (GPCR) signaling; LC/ESI-MS/MS; MWF; SHR

1. Introduction

Podocytes are terminally differentiated epithelial cells that form the third layer of the glomerular filter with their interdigitating foot processes [1]. Their high degree of differentiation permits podocytes to accomplish their highly specialized functions. However, it limits their regenerative capacity, making them particularly vulnerable to pathological conditions such as glomerular hyperfiltration. When nephron number is reduced, compensatory changes of the remaining functional nephrons lead to adaptation of glomerular hemodynamics, resulting in increased glomerular filtration rate (GFR) in

the single nephron and concomitantly in higher ultrafiltrate flow in Bowman's space [2–4] (reviewed in [5]). This causes increased fluid flow shear stress (FFSS) and contributes to podocyte damage [3, 6]. Perturbation of the glomerular filtration barrier contributes to proteinuria, glomerulosclerosis, and alteration in GFR, and thus promotes the gradual decline in renal function as observed in chronic kidney disease (CKD) (reviewed in [7–9]).

Understanding the pathomechanisms underlying podocyte damage due to glomerular hyperfiltration might help to identify therapeutical targets to protect against maladaptive responses of podocytes, which otherwise contribute to renal damage. Previous studies support a pathophysiological role of Cox2 (Ptgs2, cyclooxygenase 2) and prostaglandin E2 (PGE_2) activation for development of albuminuria by increasing the permeability of the glomerular filtration barrier (reviewed in [5]). Furthermore, upregulation of Cox2 and Ptger2 (prostaglandin E receptor 2, EP2) was shown in uninephrectomized mice and murine podocytes exposed to FFSS, i.e., in two different experimental settings to study hyperfiltration [10]. These data suggest that PGE_2 synthesis and signaling may play a role in podocyte responses to hyperfiltration.

Cox2 is long known to mediate increased synthesis of PGE_2 upon diverse stimuli (reviewed in [11,12]). Extracellularly, PGE_2 exerts its effects via four different G-protein coupled prostaglandin E receptors (EP1–4) in human and rodents (reviewed in [13]). EP1, -2 and -4 mRNA expression was reported in mouse podocytes, EP2 and -4 were also detected on protein level [14]. However, the expression of EP in human podocytes (hPC) is unclear. Both EP2 and EP4 stimulate adenylate cyclase activity leading to elevated cyclic adenosine monophosphate (cAMP) levels while EP1 increases intracellular Ca^{2+} (reviewed in [15–17]).

An autocrine/paracrine pathway between PGE_2 and Cox2 was described previously, indicating that PGE_2 leads to upregulation of Cox2 in osteocyte-like cells (murine long bone osteocyte Y4, MLO-Y4) [18]. This, in turn, increases synthesis of intracellular PGE_2, which again induces Cox2. It remains a matter of debate which EP mediates this mutual amplification: In mouse podocytes, EP4 and the p38 mitogen-activated protein kinase (MAPK) signaling pathway were described to be involved in PGE_2-mediated Cox2 upregulation and cAMP increase [19]. In other cell types, activation of EP2 with or without EP4-coupled cAMP/proteinkinase A (PKA) pathway was shown to upregulate Cox2 following PGE_2-treatment [20–22]. EP2 signaling was shown to be the relevant mechanism in response to FFSS in mouse podocytes [14]. Indeed, the PGE_2-Cox2-EP2 axis is suggested to be the relevant target for podocyte damage induced by FFSS [10,23]. So far, the mechanisms involved have not been investigated in hPC in detail. In this study, we therefore aimed to elucidate an autocrine/paracrine PGE_2/COX2 pathway in hPC and to identify which EP contributes to this crosstalk. We determined *COX2*, *PTGER2*, and *PTGER4* expression in hPC after PGE_2 stimulation and FFSS. Our results corroborate recent findings in murine models of hyperfiltration on autocrine/paracrine Cox2 and PGE_2 activation in hPC. Moreover, we find this pathway in hPC to be linked to concerted EP2 and EP4 signaling.

Importantly, distinct analysis of cellular PGE_2 and its metabolites is crucial to elucidate their pathophysiological role in podocyte damage [10,23]. However, precise measurement of intracellular prostaglandins remains challenging. Enzyme-linked immunosorbent assays (ELISA) are widely used but have their limitations, e.g., the lack of standardization across different kits and low specificity, selectivity, and throughput compared to liquid chromatography tandem mass spectrometry (LC-MS/MS) methods [24,25]. As a limitation, LC-MS/MS oftentimes requires large quantities of samples which are difficult to obtain in cell culture experiments [26–32]. We were able to overcome these obstacles and provide an approach to analyze prostaglandins in hPC by liquid chromatography electrospray ionization tandem mass spectrometry (LC/ESI-MS/MS). With our modified LC/ESI-MS/MS protocol, we were able to precisely quantify cellular PGE_2, 15-keto-PGE_2, and 13,14-dihydro-15-keto-PGE_2 levels. After stimulation with PGE_2, the cellular PGE_2-content was elevated, which was completely blocked by pharmacological inhibition EP2 and EP4. In addition, we performed corresponding in vivo analysis at the tissue level by using the LC/ESI-MS/MS methodology and demonstrated increased PGE_2 and

15-keto-PGE_2 levels in isolated glomeruli obtained from a well-established rat model with glomerular hyperfiltration, i.e., the Munich Wistar Frömter rat (MWF).

Our findings on elevated glomerular PGE_2 and 15-keto-PGE_2 levels strengthen the hypothesis that glomerular PGE_2-induction associates with albuminuria due to podocyte damage.

2. Materials and Methods

2.1. Cell Culture

Conditionally immortalized hPC (kindly provided by Moin A. Saleem, University of Bristol, UK) were cultured according to the original protocol [33,34] with slight modifications. The cells proliferate at 33 °C and transform to differentiated hPC when kept at ≥37 °C exhibiting podocyte-specific markers [34]. Briefly, podocytes were grown at 33 °C and 5% CO_2 in Roswell Park Memorial Institute (RPMI)-1640 medium (cat. no. BS.F1215, Bio&SELL, Feucht/Nürnberg, Germany) supplemented with 1% Insulin-Transferrin-Selenium 100X (cat. no. 41400-045, Gibco, Grand Island, NY, USA), 10% fetal bovine serum (FBS, cat. no. F7524, Sigma, Steinheim, Germany) and 1% ZellShield® to prevent contamination (cat. no. 13-0150, Minerva Biolabs, Berlin, Germany). Medium was changed 2–3 times per week. At confluency of 70–80%, podocytes were transferred to 37–38 °C until full confluence and proliferation arrest. Subsequently, cells were kept for a minimum of 14 days at 37–38 °C to obtain full differentiation. Differentiated phenotype was confirmed by analysis of the marker synaptopodin by immunofluorescence (see Supplement Figure S1a,b). Characterization also included overall comparison of the cellular shape ("cobblestone-like" in undifferentiated state and "arborized" in differentiated hPC [33]) by light microscopy, synaptopodin mRNA expression, as well as nephrin and podocin protein detection by immunofluorescence and western blot (see Supplement Figures S1c–e and S2). Prior to experiments, cells were detached with Trypsin 0.25%/EDTA 0.02% solution (cat. no. L-2163, Biochrom, Berlin, Germany), seeded in 12-well plates at 1×10^5 cells per well and kept in RPMI-1640 medium with supplements for adherence overnight. All experimental treatments were carried out in supplement-free RPMI-1640 medium at 37–38 °C with cell passages between 5 and 22.

2.2. PGE_2 Treatment and Inhibition of EP Receptors

PF-04418948 (cat. no. PZ0213, Sigma, Steinheim, Germany) served as EP2 antagonist [35,36] and ONO-AE3-208 (cat. no. 14522, Cayman Chemical, Ann Arbor, MI, USA) was chosen as EP4 antagonist [37,38]. Stock solutions of PGE_2 (cat. no. 14010, Cayman Chemical, Ann Arbor, MI, USA), PF-04418948, and ONO-AE3-208 with 10 mM were prepared in DMSO (cat. no. D2650, Sigma, Steinheim, Germany) and stored at −20 °C until further use.

Podocytes were treated with PGE_2 at 10 nM–1 µM concentrations as PGE_2-concentrations up to 1 µM are commonly used for in vitro experiments in murine podocytes [39,40]. For inhibition experiments, 1 µM or even higher concentrations of the selective EP2 and/or EP4 antagonist were used in previous studies [36,37,41–43]. In a pilot study, treatment with PGE_2 and EP2 antagonist (1 µM each) did not show inhibitory effects (Supplement Figure S4). Thus, antagonists were added concomitantly to PGE_2 100 nM for the indicated time-points.

2.3. Determination of Intracellular cAMP Levels

Intracellular cAMP levels were measured using an ELISA kit (cat. no. ADI-901-163, Enzo Life Sciences, Farmingdale, NY, USA). Cells were lysed in 300–400 µL 0.1 M HCl containing 0.1% Triton X-100 and samples were processed according to the manufacturer's instructions for the non-acetylated format. PGE_2 stimulated samples were diluted 1:5, and samples of PGE_2 stimulation plus co-incubation with either the EP2 or the EP4 antagonist were diluted 1:2–3 in lysis buffer. Optical density was measured at 415 nm and cAMP concentrations were normalized for protein content for each sample. Protein amount was quantified by a colorimetric kit (cat. no. 23227, Pierce™ BCA Protein Assay Kit,

Thermo Fisher Scientific, Rockford, IL, USA). Experiments for cAMP consisted of n = 3–6 samples per experimental group and were performed once or in duplicate as indicated.

2.4. Reverse Transcription and Quantitative Real-Time PCR

Total RNA of hPC was isolated using the RNeasy® Micro Kit (cat. no. 74004, Qiagen, Hilden, Germany) following the manufacturer's protocol. RNA quality was controlled by a 260/280 nm absorption ratio. For cDNA synthesis, total RNA was reverse-transcribed using the First Strand cDNA Synthesis Kit (cat. no. K1612, Thermo Fisher Scientific, Vilnius, Lithuania).

Quantitative Real-Time PCR (qPCR) was conducted in a CFX96 Touch PCR system (Bio-Rad, München, Germany; software version 3.1.1517.0823) or in a 7500 Fast Real-Time PCR System (Applied Biosystems, Darmstadt, Germany; software version 2.0.6) using the comparative quantitative cycle method with SYBR-green (cat. no. 4,385,612 and 100029284, Thermo Fisher Scientific, Vilnius, Lithuania) as reported previously [44,45] Expression analysis of each sample was done in three technical replicates and only samples with an intra-triplicate standard deviation (SD) < 0.2 were used for further calculation. Normalization of expression was done by the reference gene glyceraldehyde 3-phosphate dehydrogenase *(GAPDH)*. ΔΔCt was normalized to the untreated controls in hPC. All results were plotted as log2 of fold change (FC) (2^-ΔΔCt). Primer sequences are listed in Table 1. Primers were purchased from Eurofins Genomics, Ebersberg, Germany or Tib Molbiol, Berlin, Germany and specificity of detected reverse transcriptase (RT)-PCR products was confirmed by sequencing at Eurofins Genomics, Ebersberg, Germany. *COX2*-qPCR for hPC consisted of n = 3–8 samples per experimental group and were performed in duplicate or triplicate as indicated.

Table 1. Primer sequences for human (h) genes of interest.

Gene	Forward Primer (5′-3′)	Reverse Primer (5′-3′)
hGAPDH	gagtcaacggatttggtcgt	gatctcgctcctggaagatg
hCOX2	tgatgattgcccgactcccttg	tgaaagctggccctcgcttatg
hPTGER1	ttcggcctccaccttctttg	cgcagtaggatgtacacccaag
hPTGER2	gacggaccacctcattctcc	tccgacaacagaggactgaac
hPTGER3	tctccgctcctgataatgatg	atctttccaaatggtcgctc
hPTGER4	ttactcattgccacctccct	agtcaaaggacatcttctgcca

2.5. LC/ESI-MS/MS for Analysis of Prostaglandins

2.5.1. Sample Preparation

After stimulation or inhibition experiments, supernatants were removed and stored at −80 °C. Cells were washed twice with cold phosphate buffered saline (PBS), PBS was completely aspirated from wells, and the 12-well plates were immediately stored at −80 °C until further processing. Before analysis, cells were scraped from plate and suspended in 500 µL water. A 50 µL aliquot was taken for total protein measurement following the Lowry protocol.

The cell suspensions were spiked with an internal standard consisting of 14,15-Epoxyeicosatrienoic acid-d8, 14,15-Dihydroxyeicosatrienoic acid-d11, 15-Hydroxyeicosatetraenoic acid-d8, 20-Hydroxyeicosatetraenoic acid-d6, Leukotriene B_4-d4, PGE_2-d4 1 ng each (Cayman Chemical, Ann Arbor, MI, USA). In addition, 500 µL methanol and 5 µL 2,6-di-tert-butyl-4-methylphenol (BHT, 10 mg/mL) were added and shaken vigorously.

The total prostaglandins were released using phospholipase A2 from honey bee Apis Mellifera (Sigma-Aldrich, Taufkirchen, Germany) as described previously [46]. After pH adjustment to 6, acetic acid samples were extracted by solid phase extraction (SPE) using Bond Elute Certify II columns (Agilent Technologies, Santa Clara, CA, USA), which were preconditioned with 3 mL methanol, followed by 3 mL of 0.1 mol/L phosphate buffer containing 5% methanol (pH 6). SPE-columns were then washed with 3 mL methanol/H_2O (40/50, *v/v*). For elution, 2 mL of n-hexane:ethyl acetate 25:75

with 1% acetic acid was used. The extraction was performed with an SPE Vacuum Manifold. The eluate was evaporated on a heating block at 40 °C under a stream of nitrogen to obtain a solid residue which was dissolved in 100 µL methanol/water 60:40 and transferred in an HPLC autosampler vial (HPLC, high performance liquid chromatography).

Experiments for analysis of prostaglandins in hPC consisted of $n = 3–6$ replicates per experimental group and. Experiments were performed once or in triplicate (on different cell passages and on different days) as indicated.

Rat glomeruli obtained by differential sieving of one kidney as described below were divided into 3 parts and stored at −80 °C until further analysis. One aliquot with approximately 1/3 total kidney was prepared as described for cells, but without application of phospholipase A2.

For rat plasma, 200 µL plasma were spiked with internal standard and BHT. In addition, 20 µL glycerol and 500 µL acetonitrile was added and shaken vigorously. pH was adjusted at 6 with 2 mL phosphate buffer (0.1 mol/L). The samples were centrifuged and the clear supernatant was extracted using SPE as described above.

Experiments for analysis of prostaglandins in rat glomeruli or plasma consisted of $n = 8–10$ glomerular isolated or plasma samples of $n = 8–10$ different animals per rat strain.

2.5.2. LC/ESI-MS/MS

The residues were analyzed using an Agilent 1290 HPLC system with binary pump, multisampler and column thermostat with a Zorbax Eclipse plus C-18, 2.1 × 150 mm, 1.8 µm column using a solvent system of aqueous acetic acid (0.05%) and acetonitrile. The elution gradient was started with 5% organic phase, which was increased within 0.5 min to 32%, 16 min to 36.5%, 20 min to 38%, 28 min to 98% and held there for 5 min. The flow rate was set at 0.3 mL/min, the injection volume was 20 µL. The HPLC was coupled with an Agilent 6495 Triplequad mass spectrometer (Agilent Technologies, Santa Clara, CA, USA) with electrospray ionisation source. The source parameters were Drying gas: 115 °C/16 L/min, Sheath gas: 390 °C/12 L/min, Capillary voltage: 4300 V, Nozzle voltage: 1950 V, and Nebulizer pressure: 35 psi.

Analysis was performed with Multiple Reaction Monitoring in negative mode. For details, see Table S1. Unless stated otherwise, all solvents and chemicals were purchased from VWR International GmbH, Darmstadt, Germany.

2.6. FFSS

For FFSS, 1×10^5–6×10^5 cells where seeded on collagen IV coated Culture Slips® (cat. no. CS-C/IV, Dunn Labortechnik GmbH, Asbach, Germany), which are glass slides coated with collagen type IV and rimmed with a 1.0 mm wide polytetrafluoroethylene border to limit cell culture growth to the portion of the slip exposed to fluid flow. FFSS experiments were performed as previously described with slight modifications [23]. The Streamer® Shear Stress Device (cat. no. STR-400, Dunn Labortechnik GmbH, Asbach, Germany) was installed in a 38 °C incubator with 5% CO_2 and prepared as follows: 400 mL of PBS followed by RPMI-1640 medium were pumped through the device for approximately 10 min each. Prior to each change of content, flow direction was reversed to empty the tubes from the previous liquid. After washing, medium was replaced by 400 mL of new medium. The system was checked for leaks and air bubbles were eliminated. After preparation of the streamer, flow direction was again reversed until the streamer was half-filled by medium. Tubes were released from the pump, the system was taken out of the incubator, Culture Slips® with hPC were inserted in the Streamer®, and the system was placed back into the incubator. All 6 slots of the Streamer® were filled to allow consistent flow. Based on previous research, we applied FFSS at 2 dynes/cm^2 for 2 h [23]. At the end of each experiment, flow rate was reversed and cells were released from the device. Control cells were put in the same incubator with the same medium but were not exposed to FFSS.

2.7. Animals

The MWF rat served as a model for CKD with albuminuria, while the spontaneously hypertensive rat (SHR) served as a control strain. SHR rats develop hypertension early in life but are resistant to albuminuria development as reviewed in [47].

Male rats at 8 weeks of age were deployed from our MWF/Rkb (RRID:RGD_724569, laboratory code Rkb https://www.nationalacademies.org/ilar/lab-code-database) and SHR/Rkb (RRID:RGD_631696, laboratory code Rkb https://www.nationalacademies.org/ilar/lab-code-database) colonies at Charité—Universitätsmedizin Berlin, Germany. Rats were kept under standard conditions as described previously [44]. All experimental work in rat models was performed in accordance with the guidelines of the Charité—Universitätsmedizin Berlin and the local authority for animal protection (Landesamt für Gesundheit und Soziales, Berlin, Germany) for the use of laboratory animals. The registration numbers for the rat experiments are G 130/16 (approved 2 August 2016) and T 0189/02 (approved 31 August 2018). Anesthesia was achieved by ketamine-xylazine (87 and 13 mg/kg body weight, respectively). Kidneys were obtained, decapsulated, and sieved using a 125 µm steel sieve (Retsch GmbH, Haan, Germany) rinsed by PBS. The filtrate was then placed on a 71 µm steel sieve (Retsch GmbH, Haan, Germany) and washed with PBS. Glomeruli were kept on the sieve and were separated from the flow-through. Glomeruli were rinsed off the sieve with PBS, centrifuged, snap-frozen, and stored at −80 °C until further processing. Plasma was obtained by retrobulbary punction or punction of vena cava and collected in ethylenediaminetetraacetic acid (EDTA)-containing vials, centrifuged at 2 min at 4 °C, and stored subsequently at −80 °C.

2.8. Statistics

Statistical analysis was conducted using GraphPad Prism 8.4.0 (GraphPad Software, San Diego, CA, USA). Normal distribution was tested with the Shapiro–Wilk test. Normally distributed data were compared either by unpaired, two-tailed Student's *t*-test or one-way ANOVA with Tukey's or Dunnett's multiple comparisons test as indicated. Multiple comparisons tests after one-way ANOVA were used to compare every mean to every other mean (Tukey' follow up test) or to a control mean (Dunnett's follow up test). Results not normally distributed were analyzed by Mann–Whitney test or Kruskal–Wallis test with Dunn's multiple comparisons test as indicated. Significance level was set at $p < 0.05$. Statistical details for specific experiment can be found within figures and figure legends.

3. Results

3.1. PGE_2 Leads to EP2- and EP4- Dependent Increased cAMP Levels in Differentiated hPC

Stimulation of hPC with 100 nM PGE_2 led to an immediate time-dependent increase in intracellular cAMP levels detected after 1 min onward and retained at least until 40 min of PGE_2 stimulation (Figure 1). As intracellular cAMP levels remained comparably high until 20 min of PGE_2 stimulation, this incubation time was chosen for subsequent cAMP measurements.

Analysis of EP expression on hPC revealed the presence of *PTGER1*, *PTGER2*, and *PTGER4* mRNA in differentiated hPC (Figure S3), which encode for EP1, EP2, and EP4, respectively. As only EP2 and EP4 are reported to mediate an increase in intracellular cAMP (reviewed in [15–17]), we next investigated the effect of pharmacological inhibition of EP2 and EP4 signaling on PGE_2-stimulated intracellular cAMP levels in hPC. Therefore, either the selective antagonist of EP2 (PF-04418948, 1 µM) or EP4 (ONO-AE3-208, 1 µM) were co-incubated with 100 nM PGE_2 individually and in combination (Figure 2). Upon PGE_2 stimulation, antagonism of either EP2 (−92.5%) or EP4 (−63.7%) alone resulted in a marked albeit only partial decrease of intracellular cAMP levels compared to stimulated hPC without antagonists. In contrast, the PGE_2 stimulated intracellular cAMP increase was completely abrogated by combined EP2 and EP4 antagonism (Figure 2), suggesting that, in hPC, both EP2 and EP4 may mediate PGE_2-dependent signaling.

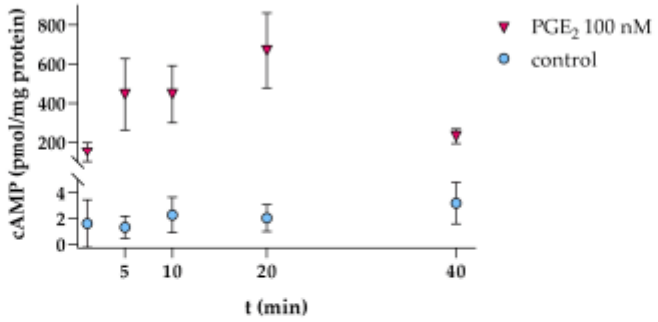

Figure 1. Intracellular cAMP levels in hPC are increased by PGE_2 stimulation (100 nM, pink triangles) in a time-dependent manner. For several controls (blue circles), cAMP levels fell below the lowest concentration of the recommended standard curve (0.78 pmol/mL) and were therefore set to zero. Each data point represents the mean ± SD of one experiment with n = 3–4 samples per time-point.

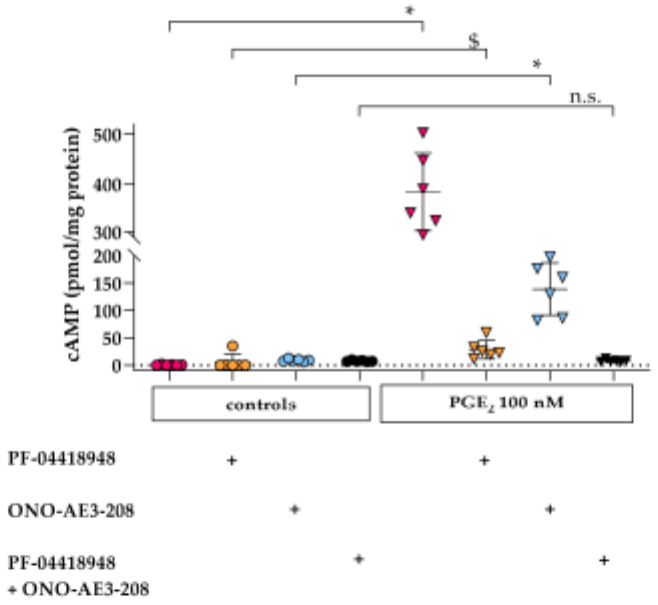

Figure 2. Intracellular cAMP is increased by PGE_2 stimulation via EP2 and EP4 in hPC. Representative cAMP levels following PGE_2 stimulation for 20 min without concomitant EP2 or EP4 antagonist (100 nM, pink triangles) compared to controls without PGE_2 (pink circles), after co-incubation with either EP2 antagonist (PF-04418948, 1 µM, orange triangles) or EP4 antagonist (ONO-AE3-208, 1 µM, blue triangles) compared to controls without PGE_2 (orange circles for EP2 antagonist, blue circles for EP4 antagonist), and co-incubation of PGE_2 with both antagonists simultaneously (1 µM each, black triangles) compared to controls without PGE_2 (black circles). Each data point represents a single sample and plotted as mean ± SD (horizontal lines) per treatment group consisting of n = 6 samples. For several controls, cAMP levels fell below the lowest concentration of the recommended standard curve (0.78 pmol/mL) and were therefore set to zero. Experiments were done in duplicate on different cell passages and on different dates, each consisting of n = 3–6 replicates per treatment, except for the separate EP4 inhibition, which was only performed once. Statistics: *, $p < 0.01$; $, $p < 0.05$; *n.s.*, not significant, assessed by a Mann–Whitney test. + denotes addition of the respective EP antagonists.

3.2. PGE_2 Induces *COX2* Gene Expression via EP2 and EP4 Signaling in Differentiated hPC

Stimulation of hPC with PGE_2 for 2 h revealed a dose-dependent upregulation of *COX2* mRNA expression (Figure 3a). In order to elucidate the role of EP2 and EP4 in PGE_2-mediated *COX2* upregulation, either the selective EP2 antagonist PF-04418948 (1 µM) or the selective EP4 antagonist ONO-AE3-208 (1 µM) were co-incubated with 100 nM PGE_2 individually or in combination (Figure 3b). Upon PGE_2 stimulation, antagonism of either EP2 or EP4 alone resulted in an increase in *COX2* mRNA although lower compared to PGE_2-stimulated hPC without antagonists (Figure 3b). Combined EP2 and EP4 antagonism completely inhibited PGE_2-mediated *COX2* upregulation (Figure 3b), suggesting that PGE_2 signals via both EP2 and EP4 to regulate *COX2* levels in a positive feedback loop.

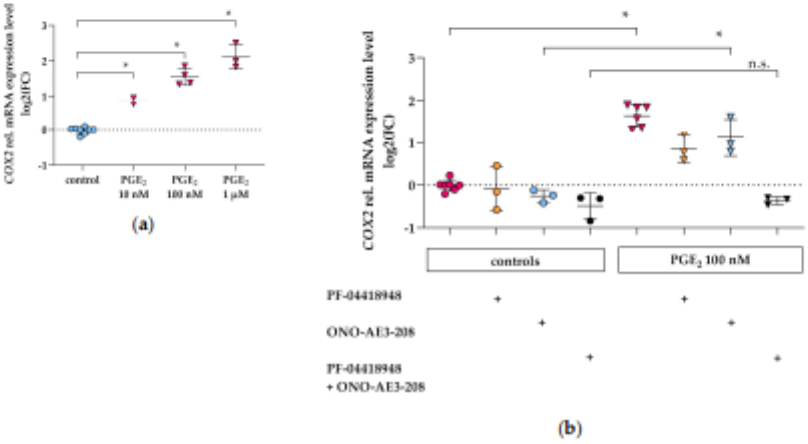

Figure 3. *COX2* gene expression is increased by PGE_2 via EP2 and EP4 in hPC. qPCR results are presented as relative mRNA expression level normalized to *GAPDH* and referred to control group. (**a**) *COX2* levels following PGE_2 stimulation (pink triangles) for 2 h were upregulated in a dose-dependent manner compared to untreated control (blue circles). Each data point represents the mean of an independent experiment (performed at least in duplicate on different cell passages and on different dates, each consisting of n = 3–8 replicates per treatment) and plotted as combined mean ± SD (horizontal lines). SD was not plotted when only two independent experiments were performed. Statistics: *, $p < 0.01$, assessed by one-way ANOVA with Dunnett's follow-up test; (**b**) *COX2* levels following PGE_2 stimulation for 2 h without concomitant EP2 or EP4 antagonist (100 nM, pink triangles) compared to controls without PGE_2 (pink circles), after co-incubation with either EP2 antagonist (PF-04418948, 1 µM, orange triangles) or EP4 antagonist (ONO-AE3-208, 1 µM, blue triangles) compared to controls without PGE_2 (orange circles for EP2 antagonist, blue circles for EP4 antagonist), and co-incubation of PGE_2 with both antagonists simultaneously (1 µM each, black triangles) compared to controls without PGE_2 (black circles) obtained in three independent experiments. Each data point represents the mean of an independent experiment (performed at least in triplicate on different cell passages and on different dates, each consisting of n = 3–6 replicates per treatment) and plotted as combined mean ± SD (horizontal lines). + indicates addition of the respective EP antagonists. Statistics: *, $p < 0.01$; n.s., not significant, assessed by two-tailed Student's t-test.

3.3. PGE_2 Reduces *PTGER2* and *PTGER4* Gene Expression Which Is Not Modified by EP2 or EP4 Antagonists in Differentiated hPC

Stimulation of hPC with rising concentrations of PGE_2 for 2 h revealed inconsistent changes of *PTGER2* mRNA expression: 10 nM and 1 µM did not significantly change *PTGER2* expression, whereas PGE_2 100 nM slightly reduced *PTGER2* expression (Figure 4a). The weak downregulation by *PTGER2* of 100 nM PGE_2 was not abrogated by co-incubation with the selective EP4 antagonist ONO-AE3-208 (1 µM) (Figure 4b).

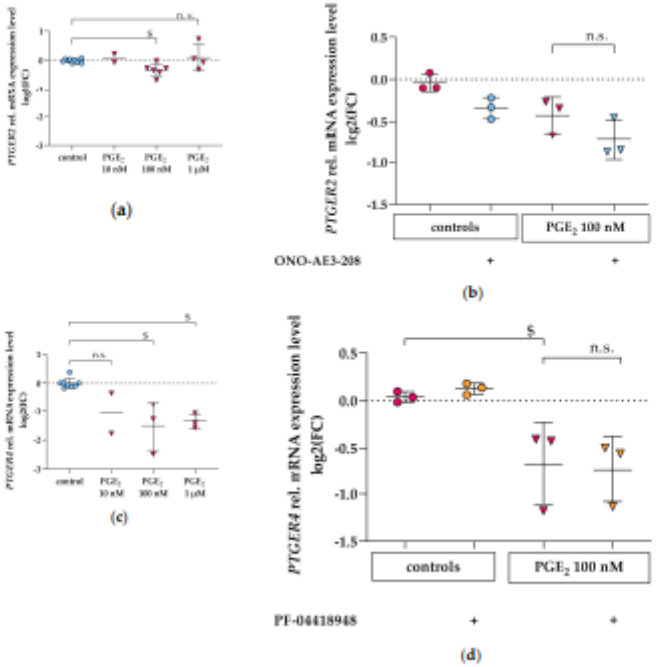

Figure 4. *PTGER2 and PTGER4* gene expression in hPC after PGE_2 stimulation and following co-incubation with EP antagonists. qPCR results are presented as relative mRNA expression level normalized to *GAPDH* and referred to control group. (**a**) *PTGER2* levels following PGE_2 stimulation with 10 nM, 100 nM, and 1 µM (pink triangles) for 2 h compared to untreated control (blue circles). Each data point represents the mean of an independent experiment (performed at least in duplicate on different cell passages and on different dates, each consisting of n = 3–8 replicates per treatment) and plotted as combined mean ± SD (horizontal lines). SD was not plotted when only two independent experiments were performed. Statistics: $, $p < 0.05$, assessed by one-way ANOVA with Dunnett's follow-up test; (**b**) *PTGER2* levels following PGE_2 stimulation for 2 h without concomitant EP4 antagonist (100 nM, pink triangles) compared to controls without PGE_2 (pink circles), and after co-incubation with EP4 antagonist (ONO-AE3-208, 1 µM, blue triangles) compared to controls without PGE_2 (blue circles) obtained in three independent experiments. Each data point represents the mean of an independent experiment (performed in triplicate on different cell passages and on different dates, each consisting of n = 3–6 replicates per treatment) and plotted as combined mean ± SD (horizontal lines). + denotes addition of ONO-AE3-208. Statistics: *n*.s., not significant, assessed by a Mann–Whitney test; (**c**) *PTGER4* levels following PGE_2 stimulation with 10 nM, 100 nM, and 1 µM (pink triangles) for 2 h compared to untreated control (blue circles). Each data point represents the mean of an independent experiment (performed at least in duplicate on different cell passages and on different dates, each consisting of n = 3–8 replicates per treatment) and plotted as combined mean ± SD (horizontal lines). SD was not plotted when only two independent experiments were performed. Statistics: $, $p < 0.05$, assessed by a Kruskal–Wallis test with Dunn's multiple comparisons test; (**d**) *PTGER4* levels following PGE_2 stimulation for 2 h without concomitant EP2 antagonist (100 nM, pink triangles) compared to controls without PGE_2 (pink circles), after co-incubation with EP2 antagonist (PF-04418948, 1 µM, orange triangles) compared to controls without PGE_2 (orange circles) obtained in three independent experiments. Each data point represents the mean of an independent experiment (performed in triplicate on different cell passages and on different dates, each consisting of n = 5–6 replicates per treatment) and plotted as combined mean ± SD (horizontal lines). + denotes addition of PF-04418948. Statistics: $, $p < 0.05$; *n*.s., not significant, assessed by a two-tailed Student's *t*-test.

Stimulation of hPC with PGE_2 for 2 h revealed a dose-dependent reduction of *PTGER4* mRNA expression (Figure 4c). In order to elucidate the role of EP2 in PGE_2-mediated *PTGER4* downregulation, the selective EP2 antagonist PF-04418948 (1 µM) was co-incubated with 100 nM PGE_2 (Figure 4d). The PGE_2-induced decrease in *PTGER4* mRNA was not abolished by co-incubation with the EP2 antagonist (Figure 4d).

3.4. Cellular PGE_2 and Metabolite Profile in hPC after PGE_2 Stimulation: Effects of EP2 and EP4 Blockade

To investigate whether PGE_2 stimulation and subsequent *COX2* induction lead to changes in cellular levels of PGE_2 and its downstream metabolites 15-keto-PGE_2 and 13,14-dihydro-15-keto-PGE_2 (Figure 5a), hPC were analyzed by LC/ESI-MS/MS. After stimulation with PGE_2, the cellular PGE_2-content was elevated (Figure 5b), while 15-keto-PGE_2 and 13,14-dihydro-15-keto-PGE_2 remained at control levels. Pharmacological inhibition of EP2 and EP4 reduced cellular PGE_2 significantly (Figure 5c). Our findings point towards an autocrine PGE_2-EP2/EP4-COX2 signaling axis in hPC.

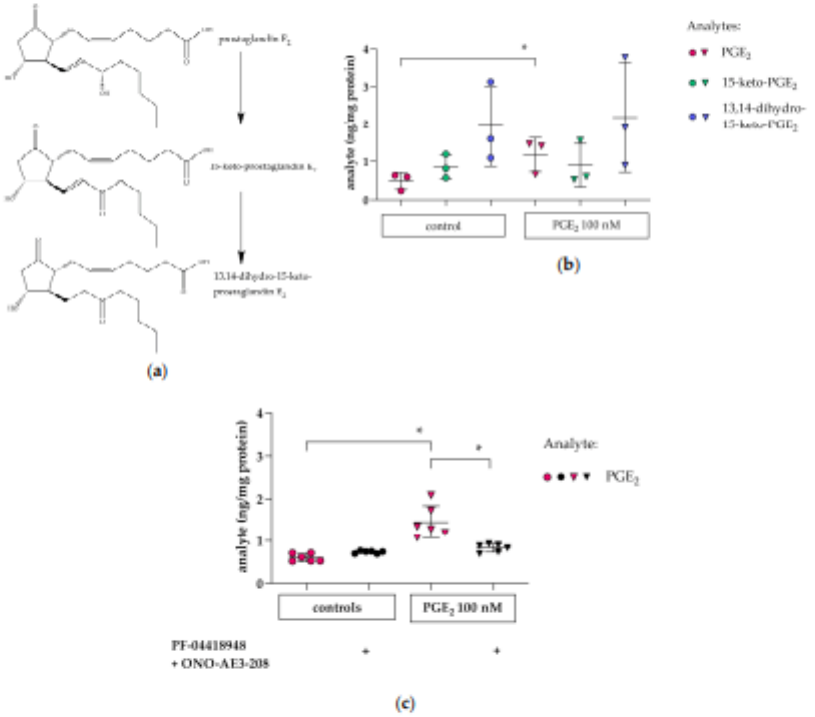

Figure 5. PGE_2 and its metabolites were measured by LC/ESI-MS/MS in hPC. (**a**) structure of PGE_2 and its metabolites; (**b**) levels of cellular PGE_2 (pink), 15-keto-PGE_2 (green), and 13,14-dihydro-15-keto-PGE_2 (blue) were measured after PGE_2 stimulation for 2 h (100 nM, triangles) and in untreated controls (circles). PGE_2 levels were increased in PGE_2-stimulated cells (pink triangles) vs. controls (pink circles). Each datapoint represents the mean of an independent experiment (performed in triplicate on different cell passages and on different dates, each consisting of n = 3–6 replicates per treatment) and plotted as combined mean ± SD (horizontal lines). Statistics: *, $p < 0.01$, assessed by a two-tailed Student's t-test in each experiment; (**c**) elevated cellular PGE_2 levels caused by PGE_2 stimulation (pink triangles) were abrogated by simultaneous co-incubation with combined EP2 and EP4 antagonism (PF-04418948 and ONO-AE3-208, respectively, 1 µM each). + indicates addition of combined EP antagonists. Each datapoint represents a single sample and plotted as mean ± SD (horizontal lines) per treatment group consisting of n = 6 replicates obtained in a single experiment. Statistics: *, $p < 0.01$, assessed by a two-tailed Student's t-test.

3.5. Glomerular PGE_2 and Metabolite Profile in Glomeruli and Plasma in the CKD MWF Model

Analysis of PGE_2 and its subsequent metabolites 15-keto-PGE_2 and 13,14-dihydro-15-keto-PGE_2 in glomeruli and plasma of MWF and SHR at eight weeks of age revealed an increase of glomerular PGE_2 and 15-keto-PGE_2 levels in MWF compared to SHR. No difference was observed for 13,14-dihydro-15-keto-PGE_2 (Figure 6a). In plasma, levels of PGE_2 and 13,14-dihydro-15-keto-PGE_2 did not differ between MWF and SHR (Figure 6b). The metabolite 15-keto-PGE_2 in plasma was below level of detection (data not shown).

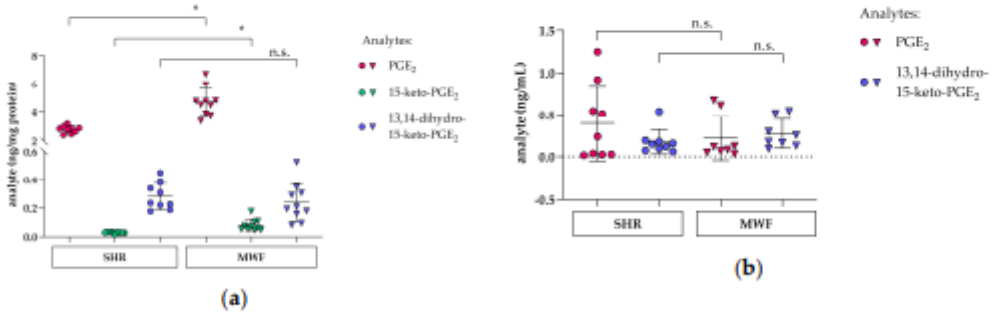

Figure 6. Levels of PGE_2 (pink), 15-keto-PGE_2 (green) and 13,14-dihydro-15-keto-PGE_2 (blue) were measured in glomeruli of MWF (triangles) and SHR (circles) at 8 weeks of age. (**a**) glomerular PGE_2 and 15-keto-PGE_2 levels were increased in MWF (pink and green triangles, respectively) compared to SHR (pink and green circles, respectively), whereas glomerular 13,14-dihydro-15-keto-PGE_2 (blue circles and triangles) did not differ between both strains. Each data point represents a single animal and plotted as mean ± SD (horizontal lines) per rat strain consisting of n = 9–10 animals each. Statistics: *, $p < 0.01$; n.s., not significant assessed by a two-tailed Student's t-test; (**b**) levels of PGE_2 (pink) and 13,14-dihydro-15-keto-PGE_2 (blue) in plasma did not differ between MWF (triangles) and SHR (circles). Each data point represents a single animal and plotted as mean ± SD (horizontal lines) per rat strain consisting of n = 8–9 animals, each. Statistics: n.s., not significant assessed by the Mann–Whitney test.

3.6. FFSS Increases *COX2* and *PTGER2* Gene Expression in hPC

FFSS was previously shown to elevate intracellular PGE_2 levels and Cox2 in murine podocytes [10,23]. We therefore investigated *COX2* mRNA expression after FFSS in hPC. FFSS led to increased *COX2* mRNA expression in hPC as shown in Figure 7.

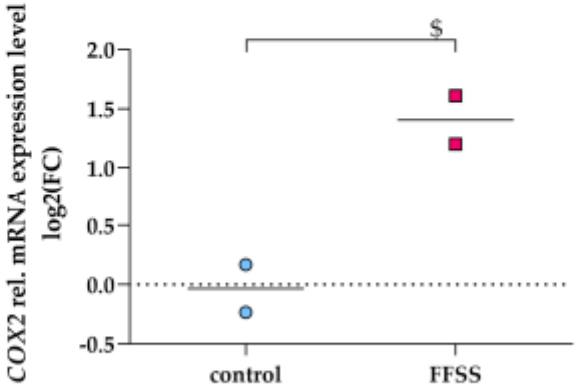

Figure 7. FFSS upregulated *COX2* gene expression in hPC (pink squares). qPCR results are presented as relative mRNA expression level normalized to *GAPDH* and referred to control group (blue circles). *COX2* upregulation was quantified after 2 h of FFSS with 2 dynes/cm^2. Statistics: $, $p < 0.05$, assessed

by a two-tailed Student's *t*-test. Each datapoint represents the mean of an independent experiment (performed in duplicate on different cell passages and on different dates, each consisting of $n = 5–6$ replicates per treatment) and plotted as combined mean (horizontal lines).

Furthermore, EP2 protein was reported to be upregulated upon FFSS in murine podocytes [10]. In hPC, FFSS slightly upregulated *PTGER2* (Figure 8a), whereas *PTGER4* expression did not change compared to control (Figure 8b).

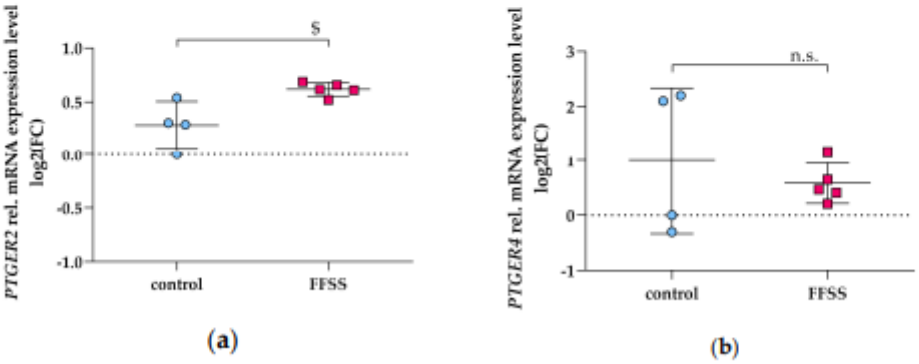

Figure 8. *PTGER2* and *PTGER4* gene expression in hPC subjected to FFSS (pink squares). qPCR results are presented as relative mRNA expression level normalized to *GAPDH* and referred to control group (blue circles). mRNA expression of *PTGER2* (**a**) and *PTGER4* (**b**) was quantified after 2 h of FFSS with 2 dynes/cm^2. Statistics: $, $p < 0.05$, assessed by a two-tailed Student's *t*-test. Each datapoint represents a single sample and plotted as mean ± SD (horizontal lines) per treatment group consisting of $n = 4–5$ replicates obtained in a single experiment.

4. Discussion

Recent studies in murine models of hyperfiltration support a pathophysiological role of autocrine/paracrine COX2/PGE_2 activation on podocyte damage, thus contributing to disturbances of the glomerular filtration barrier including the development of albuminuria [10,14,23] (reviewed in [2,5]). These findings suggest that induction of COX2 associates with podocyte damage, while selective or non-selective inhibition of COX2 reduces proteinuria in animal models as well as in patients (reviewed in [48]). So far, the mechanisms involved have not been investigated in detail.

In mouse podocytes, EP1, -2 and -4 expression was reported and EP2 and -4 were also detected on protein level [14]. In this study, we corroborate these findings in hPC, which also express EP1, -2 and -4. EP4 is known as a constitutively expressed protein reflected by abundant protein levels in untreated murine podocytes compared to EP2 [10]. Our results on apparently lower *PTGER4* mRNA expression compared to *PTGER2* in hPC should be interpreted with caution as they need to be confirmed on the protein level in future investigations. Stimulation of hPC with PGE_2 led to an immediate intracellular cAMP increase starting at 1 min after PGE_2 stimulation until at least 40 min of stimulation (Figure 1). Of note, the detected intracellular cAMP levels are net levels resulting from cAMP generation by adenylate cyclase and its concomitant degradation by phosphodiesterases. Phosphodiesterase activity was only blocked at the end of the stimulation experiments by adding HCl. Previous studies in immortalized murine podocytes revealed a similar time-course of cAMP increase occurring within the first 30 min after EP2 and/or EP4 stimulation [39,49,50]. In our experimental setting in hPC, this PGE_2-stimulated intracellular cAMP increase was only completely abrogated by combined EP2 and EP4 antagonism pointing towards a comparable role of both receptors for cAMP induction in hPC (Figure 2). Multiple intracellular signaling pathways have been described for either

EP2 and EP4 (reviewed in [51]). PGE_2 stimulation of EP2 and EP4 activated the transcription factors T-cell factor (Tcf) and lymphocyte enhancer factor (Lef) signaling via PKA- and phosphatidylinositol 3-kinase/proteinkinase B (PI3K/Akt)-dependent phosphorylation of glycogen synthase kinase 3 (GSK3), thus promoting translocation of the transcription cofactor β-catenin into the nucleus where interaction with Tcf and Lef modulated gene expression, e.g., of COX2 [52,53]. However, participation of EP2 in PI3K/Akt signaling remains a matter of debate, as some investigators suggest that only EP4 but not EP2 are linked with PI3K/Akt [54]. Mechanotransduction in murine podocytes was previously suggested to be mediated by Akt-GSK3β-β-catenin, extracellular-signal regulated kinases (ERK)1/2, and p38MAPK, but not cAMP-PKA signaling upon FFSS [40]. The lack of cAMP elevation upon FFSS in that study might be explained, though by the experimental design as intracellular cAMP was measured at the earliest 2 h after applying FFSS. In contrast, the cAMP-PKA pathway was shown to be involved upon PGE_2 stimulation of murine podocytes [40], which better matches our setting of PGE_2 stimulation of hPC. Moreover, the cAMP-PKA pathway has been shown in intracellular signaling upon FFSS in osteocytes [55,56].

We detected upregulation of *COX2* by PGE_2 in a dose-dependent fashion with both EP2 and EP4 being involved in hPC (Figure 3). PGE_2 stimulation of EP2 and EP4 was reported to increase cAMP response element-binding protein (CREB), which was demonstrated to be PKA-dependent for EP2, whereas EP4-coupled PI3K signaling was suggested to counteract CREB formation [57–60]. Of note, transcription of *COX2* can be modulated by CREB, as CRE is part of the COX2 promotor [61,62]. Therefore, subsequent PKA/CREB activation could play a role for the observed increase in *COX2* expression following intracellular cAMP level elevation in hPC. To further investigate this aspect, experiments with PKA-inhibitors, e.g., H-89, will be performed as well as analysis of CREB phosphorylation status, and activation of the transcription factors Tcf and Lef. Functional analysis of COX2 protein activity might also be helpful. However, previous data in various cell types including murine podocytes already revealed that COX2 protein is indeed increased after 2 h stimulation with PGE_2 [19,58]. Taken together, our results on concerted EP2 and EP4 signaling being involved in upregulation of intracellular cAMP and *COX2* levels represent a novel finding. To validate our results on the role of EP2 and EP4 on the intracellular cAMP increase and upregulation of *COX2*, effects of hPC stimulation with an EP2 and/or EP4 agonist without PGE_2 should be investigated in future experiments.

Accompanied by these findings, PGE_2 stimulation also increased cellular PGE_2, i.e., PGE_2, which is released from membranes and appears intracellularly (Figure 5b). This effect is abrogated by combined EP2- and EP4-antagonism (Figure 5c). Intracellularly generated PGE_2 is degraded by 15-prostaglandin dehydrogenase (HPGD) to 15-keto-PGE_2, which is then terminally inactivated, albeit with different efficiency, by prostaglandin reductase (PTGR) 1, -2 and -3 to 13,14-dihydro-15-keto-PGE_2 [63,64] (reviewed in [65]). Intracellular PGE_2 was reported to exit the cell by simple diffusion or by an efflux transport mediated by prostaglandin transporter (PGT), i.e., solute carrier organic anion transporter family, member 2A1 (OATP2A1), or ATP-binding cassette, subfamily C, member 4 (MRP4) [66–68].

Elevated PGE_2 levels were previously associated with podocyte damage, suggesting that it might be a biomarker of progressive CKD [10,69]. LC-MS/MS based methods are beneficial to precisely study cellular prostaglandin metabolism with a maximum of selectivity and specificity. However, cell culture experiments are mainly restricted to small sample amounts that might hamper analysis by LC-MS/MS [26–32]. Here, we present a refined protocol for prostaglandin analysis in cells by LC/ESI/MS-MS. This might help to further elucidate cellular prostaglandin metabolism under pathophysiological conditions particularly in vitro but also in vivo. The observed increases in cellular PGE_2 content upon PGE_2 stimulation in hPC might be due to several mechanisms. One possibility is that extracellular PGE_2 enters the podocyte by simple diffusion or by uptake transport mediated by OATP2A1, which was previously reported to facilitate bidirectional transport of PGE_2 over membranes [66–68]. A second reason could be autocrine/paracrine mechanisms, i.e., extracellular PGE_2 activates EP2 and EP4 signaling, thus increasing COX2 transcription and translation. As COX2 delineates the rate-limiting step of PGE_2 synthesis (reviewed in [70]), its induction leads to higher

cellular PGE_2 levels. Our results support the latter option, as combined inhibition of EP2 and EP4 signaling diminished the increase in cellular PGE_2 levels.

In our corresponding in vivo study, we employed the MWF model, which represents a suitable model with glomerular hyperfiltration and thus FFSS [47]. The MWF model was previously extensively characterized (reviewed [47]). Thus, the MWF model is a non-diabetic inbred, genetic model with an inherited nephron deficit of 30–50% depending on the comparator rat strain [71,72]. Consequently, male MWF rats are characterized by increased single nephron glomerular filtration rate but with normal mean glomerular capillary pressure [72,73]. In addition, MWF rats develop mild arterial hypertension and spontaneous progressive albuminuria [47]. Thus, male MWF rats develop spontaneous albuminuria at an early age between weeks 4 and 8 after birth and subsequently progressive proteinuria and glomerulosclerosis [74]. The latter was also demonstrated in the MWF strain from our own colony and thus in the animals used in the current study [47]. Early onset albuminuria in young MWF animals occurs at six weeks of age and is preceded by glomerular hypertrophy, accompanied by focal and segmental loss of podoplanin and followed by podocyte foot process effacement at 8 weeks of age, i.e., at onset of albuminuria [75]. For these reasons, we selected animals at this age for our analysis in the current study. As a comparator strain, we use the previously characterized spontaneously hypertensive rats (SHR) that are resistant to albuminuria development [71,76]. Taken together, we showed the feasibility of the LC/ESI-MS/MS methodology to characterize the PGE_2 pathway at the glomerular tissue level by using the MWF strain. The observed increases in both PGE_2 and 15-keto-PGE_2 in isolated glomeruli of MWF support the activation of this pathway in glomerular hyperfiltration. However, these results should be viewed against the background that the cellular origin of this finding was not determined, and thus the contribution of other cell types, e.g., glomerular endothelial cells or mesangial cells remains unclear. Up to now, direct isolation of podocytes from glomeruli was reported for transgenic mice [77–80]. In the rat, there seem to be more technical difficulties as transgenic implementation of fluorescent dyes was not yet accomplished. Antibody staining for podocyte markers and subsequent analysis by FACS is possible [81], but whether isolated primary rat podocytes can be subjected to transcriptomic, proteomic, or lipidomic analysis remains to be investigated. Urinary PGE_2 was suggested as a biomarker for adaptive hyperfiltration in human solitary kidney [69]. The analysis of the urinary PGE_2 and metabolite profile in our CKD MWF model is currently not established due to experimental challenges to establish robust LS/ESI-MS/MS analysis in rat urine. In contrast, the profile in plasma did not differ significantly between MWF and SHR (Figure 6b). In plasma, dilution of prostaglandins might be a major problem as 15-keto-PGE_2 levels were below the limit of detection. Therefore, plasma levels provide rather a rough estimate, while analysis of glomeruli offers a closer insight into podocyte prostaglandin metabolism.

Besides mimicking hyperfiltration by exogenous supplementation with PGE_2, we also applied FFSS on hPC. This model aimed to imitate intensified flow of the ultrafiltrate in Bowman's space, thus causing podocyte injury. Similar to PGE_2 treatment, FFSS leads to upregulation of *COX2* (Figure 7). Our data corroborate the work by Srivastava and coworkers, who suggested Akt/GSK3β-βcatenin and the MAPK pathway to be involved in mechanotransduction on mouse podocytes [10,40]. We thus aim to investigate these signaling pathways in hPC upon FFSS in our future work. We corroborate recent findings that EP2 is upregulated by FFSS while EP4 expression is not changed [10] (Figure 8).

5. Conclusions

An autocrine/paracrine pathway between COX2 and PGE_2 exists also in hPC and is mediated by both EP2 and EP4. Distinct analysis of cellular PGE_2 and its metabolites was enabled by a modified protocol using LS/ESI-MS/MS. Elevated PGE_2 and 15-keto-PGE_2 levels were detected in glomeruli of MWF, a model for CKD, thereby strengthening the hypothesis that glomerular PGE_2 accumulation is associated with albuminuria due to podocyte damage. Understanding prostaglandin signaling in hPC may contribute to identifying novel target pathways to protect against maladaptive responses to hyperfiltration in podocytes.

Supplementary Materials: The following are available online at http://www.mdpi.com/2073-4409/9/5/1256/s1, Figure S1: Differentiation of hPC was confirmed by immunofluorescence of synaptopodin, podocin, and nephrin, Figure S2: Characterization of differentiated and undifferentiated hPC. Figure S3: Expression of EP receptors in hPC, Figure S4: EP2 antagonist does not inhibit PGE_2 mediated *COX2* upregulation when applied with the same concentration as PGE_2. Table 1: Multiple Reaction Monitoring in negative mode for LC/ESI-MS/MS

Author Contributions: Conceptualization, J.B., D.P., and R.K.; methodology, A.S., E.M., and M.R.; validation, J.B. and E.M.; formal analysis, J.B. and E.M.; investigation, E.M., A.K., and M.R.; resources, R.K.; data curation, J.B.; writing—original draft preparation, E.M.; writing—review and editing, J.B. and R.K.; visualization, E.M.; supervision, J.B., D.P., and R.K.; project administration, J.B. and R.K.; funding acquisition, D.P. and R.K. All authors have read and agreed to the published version of the manuscript.

Funding: This research was funded by the Deutsche Forschungsgemeinschaft (DFG, German Research Foundation)—project number 394046635—SFB 1365. The FFSS device was funded by the Sonnenfeld-Stiftung, Berlin, Germany.

Acknowledgments: We thankfully acknowledge the contributions of Karen Böhme, Bettina Bublath, Petra Karsten, and Claudia Plum for excellent laboratory or animal assistance. We furthermore thank Jörg Rösner and the Charité Neuroscience Research Center for support with confocal microscopy and Moin A. Saleem, University of Bristol, UK for providing hPC.

Conflicts of Interest: The authors declare no conflict of interest.

References

1. Pavenstadt, H.; Kriz, W.; Kretzler, M. Cell biology of the glomerular podocyte. *Physiol. Rev.* **2003**, *83*, 253–307. [CrossRef] [PubMed]
2. Srivastava, T.; Hariharan, S.; Alon, U.S.; McCarthy, E.T.; Sharma, R.; El-Meanawy, A.; Savin, V.J.; Sharma, M. Hyperfiltration-mediated Injury in the Remaining Kidney of a Transplant Donor. *Transplantation* **2018**, *102*, 1624–1635. [CrossRef] [PubMed]
3. Srivastava, T.; Celsi, G.E.; Sharma, M.; Dai, H.; McCarthy, E.T.; Ruiz, M.; Cudmore, P.A.; Alon, U.S.; Sharma, R.; Savin, V.A. Fluid flow shear stress over podocytes is increased in the solitary kidney. *Nephrol Dial. Transpl.* **2014**, *29*, 65–72. [CrossRef] [PubMed]
4. Brenner, B.M. Nephron adaptation to renal injury or ablation. *Am. J. Physiol.* **1985**, *249*, F324–F337. [CrossRef]
5. Sharma, M.; Sharma, R.; McCarthy, E.T.; Savin, V.J.; Srivastava, T. Hyperfiltration-associated biomechanical forces in glomerular injury and response: Potential role for eicosanoids. *Prostaglandins Lipid Mediat.* **2017**, *132*, 59–68. [CrossRef]
6. Friedrich, C.; Endlich, N.; Kriz, W.; Endlich, K. Podocytes are sensitive to fluid shear stress in vitro. *Am. J. Physiol. Ren. Physiol.* **2006**, *291*, F856–865. [CrossRef]
7. Endlich, N.; Endlich, K. The challenge and response of podocytes to glomerular hypertension. *Semin. Nephrol* **2012**, *32*, 327–341. [CrossRef]
8. Brenner, B.M.; Lawler, E.V.; Mackenzie, H.S. The hyperfiltration theory: A paradigm shift in nephrology. *Kidney Int.* **1996**, *49*, 1774–1777. [CrossRef]
9. Futrakul, N.; Sridama, V.; Futrakul, P. Microalbuminuria–A biomarker of renal microvascular disease. *Ren Fail.* **2009**, *31*, 140–143. [CrossRef]
10. Srivastava, T.; Alon, U.S.; Cudmore, P.A.; Tarakji, B.; Kats, A.; Garola, R.E.; Duncan, R.S.; McCarthy, E.T.; Sharma, R.; Johnson, M.L.; et al. Cyclooxygenase-2, prostaglandin E2, and prostanoid receptor EP2 in fluid flow shear stress-mediated injury in the solitary kidney. *Am. J. Physiol. Ren. Physiol.* **2014**, *307*, F1323–1333. [CrossRef]
11. Smith, W.L. The eicosanoids and their biochemical mechanisms of action. *Biochem. J.* **1989**, *259*, 315–324. [CrossRef] [PubMed]
12. Samuelsson, B.; Granstrom, E.; Green, K.; Hamberg, M.; Hammarstrom, S. Prostaglandins. *Annu. Rev. Biochem.* **1975**, *44*, 669–695. [CrossRef] [PubMed]
13. Narumiya, S.; Sugimoto, Y.; Ushikubi, F. Prostanoid receptors: structures, properties, and functions. *Physiol. Rev.* **1999**, *79*, 1193–1226. [CrossRef] [PubMed]
14. Srivastava, T.; McCarthy, E.T.; Sharma, R.; Kats, A.; Carlton, C.G.; Alon, U.S.; Cudmore, P.A.; El-Meanawy, A.; Sharma, M. Fluid flow shear stress upregulates prostanoid receptor EP2 but not EP4 in murine podocytes. *Prostaglandins Lipid Mediat.* **2013**, *104–105*, 49–57. [CrossRef]

15. Funk, C.D. Prostaglandins and leukotrienes: advances in eicosanoid biology. *Science (N. Y.)* **2001**, *294*, 1871–1875. [CrossRef]
16. Sugimoto, Y.; Narumiya, S.; Ichikawa, A. Distribution and function of prostanoid receptors: studies from knockout mice. *Prog Lipid Res.* **2000**, *39*, 289–314. [CrossRef]
17. Negishi, M.; Sugimoto, Y.; Ichikawa, A. Molecular mechanisms of diverse actions of prostanoid receptors. *Biochim. Biophys Acta* **1995**, *1259*, 109–119. [CrossRef]
18. Cheng, B.; Kato, Y.; Zhao, S.; Luo, J.; Sprague, E.; Bonewald, L.F.; Jiang, J.X. PGE(2) is essential for gap junction-mediated intercellular communication between osteocyte-like MLO-Y4 cells in response to mechanical strain. *Endocrinology* **2001**, *142*, 3464–3473. [CrossRef]
19. Faour, W.H.; Gomi, K.; Kennedy, C.R. PGE(2) induces COX-2 expression in podocytes via the EP(4) receptor through a PKA-independent mechanism. *Cell. Signal.* **2008**, *20*, 2156–2164. [CrossRef]
20. Pino, M.S.; Nawrocki, S.T.; Cognetti, F.; Abruzzese, J.L.; Xiong, H.Q.; McConkey, D.J. Prostaglandin E2 drives cyclooxygenase-2 expression via cyclic AMP response element activation in human pancreatic cancer cells. *Cancer Biol. Ther.* **2005**, *4*, 1263–1269. [CrossRef]
21. Ansari, K.M.; Sung, Y.M.; He, G.; Fischer, S.M. Prostaglandin receptor EP2 is responsible for cyclooxygenase-2 induction by prostaglandin E2 in mouse skin. *Carcinogenesis* **2007**, *28*, 2063–2068. [CrossRef] [PubMed]
22. Díaz-Muñoz, M.D.; Osma-García, I.C.; Fresno, M.; Iñiguez, M.A. Involvement of PGE2and the cAMP signalling pathway in the up-regulation of COX-2 and mPGES-1 expression in LPS-activated macrophages. *Biochem. J.* **2012**, *443*, 451–461. [CrossRef] [PubMed]
23. Srivastava, T.; McCarthy, E.T.; Sharma, R.; Cudmore, P.A.; Sharma, M.; Johnson, M.L.; Bonewald, L.F. Prostaglandin E(2) is crucial in the response of podocytes to fluid flow shear stress. *J. Cell Commun. Signal.* **2010**, *4*, 79–90. [CrossRef] [PubMed]
24. Faupel-Badger, J.M.; Fuhrman, B.J.; Xu, X.; Falk, R.T.; Keefer, L.K.; Veenstra, T.D.; Hoover, R.N.; Ziegler, R.G. Comparison of liquid chromatography-tandem mass spectrometry, RIA, and ELISA methods for measurement of urinary estrogens. *Cancer Epidemiol. Biomark. Prev.* **2010**, *19*, 292–300. [CrossRef] [PubMed]
25. Gandhi, A.S.; Budac, D.; Khayrullina, T.; Staal, R.; Chandrasena, G. Quantitative analysis of lipids: a higher-throughput LC-MS/MS-based method and its comparison to ELISA. *Future Sci. OA* **2017**, *3*, Fso157. [CrossRef] [PubMed]
26. Mesaros, C.; Lee, S.H.; Blair, I.A. Analysis of epoxyeicosatrienoic acids by chiral liquid chromatography/electron capture atmospheric pressure chemical ionization mass spectrometry using [13C]-analog internal standards. *Rapid Commun. Mass Spectrom.* **2010**, *24*, 3237–3247. [CrossRef]
27. Nithipatikom, K.; Laabs, N.D.; Isbell, M.A.; Campbell, W.B. Liquid chromatographic-mass spectrometric determination of cyclooxygenase metabolites of arachidonic acid in cultured cells. *J. Chromatogr. B Anal. Technol. Biomed. Life Sci.* **2003**, *785*, 135–145. [CrossRef]
28. Kempen, E.C.; Yang, P.; Felix, E.; Madden, T.; Newman, R.A. Simultaneous quantification of arachidonic acid metabolites in cultured tumor cells using high-performance liquid chromatography/electrospray ionization tandem mass spectrometry. *Anal. Biochem.* **2001**, *297*, 183–190. [CrossRef]
29. Rund, K.M.; Ostermann, A.I.; Kutzner, L.; Galano, J.M.; Oger, C.; Vigor, C.; Wecklein, S.; Seiwert, N.; Durand, T.; Schebb, N.H. Development of an LC-ESI(-)-MS/MS method for the simultaneous quantification of 35 isoprostanes and isofurans derived from the major n3- and n6-PUFAs. *Anal. Chim. Acta* **2018**, *1037*, 63–74. [CrossRef]
30. Deems, R.; Buczynski, M.W.; Bowers-Gentry, R.; Harkewicz, R.; Dennis, E.A. Detection and quantitation of eicosanoids via high performance liquid chromatography-electrospray ionization-mass spectrometry. *Methods Enzym.* **2007**, *432*, 59–82. [CrossRef]
31. Bollinger, J.G.; Thompson, W.; Lai, Y.; Oslund, R.C.; Hallstrand, T.S.; Sadilek, M.; Turecek, F.; Gelb, M.H. Improved sensitivity mass spectrometric detection of eicosanoids by charge reversal derivatization. *Anal. Chem.* **2010**, *82*, 6790–6796. [CrossRef] [PubMed]
32. Le Faouder, P.; Baillif, V.; Spreadbury, I.; Motta, J.P.; Rousset, P.; Chene, G.; Guigne, C.; Terce, F.; Vanner, S.; Vergnolle, N.; et al. LC-MS/MS method for rapid and concomitant quantification of pro-inflammatory and pro-resolving polyunsaturated fatty acid metabolites. *J. Chromatogr. B Anal. Technol. Biomed. Life Sci.* **2013**, *932*, 123–133. [CrossRef]

33. Saleem, M.A.; O'Hare, M.J.; Reiser, J.; Coward, R.J.; Inward, C.D.; Farren, T.; Xing, C.Y.; Ni, L.; Mathieson, P.W.; Mundel, P. A conditionally immortalized human podocyte cell line demonstrating nephrin and podocin expression. *J. Am. Soc. Nephrol.* **2002**, *13*, 630–638. [PubMed]
34. Ni, L.; Saleem, M.; Mathieson, P.W. Podocyte culture: Tricks of the trade. *Nephrology (Carlton Vic.)* **2012**, *12*, 525–531. [CrossRef] [PubMed]
35. Ma, X.; Aoki, T.; Tsuruyama, T.; Narumiya, S. Definition of Prostaglandin E2-EP2 Signals in the Colon Tumor Microenvironment That Amplify Inflammation and Tumor Growth. *Cancer Res.* **2015**, *75*, 2822–2832. [CrossRef] [PubMed]
36. af Forselles, K.J.; Root, J.; Clarke, T.; Davey, D.; Aughton, K.; Dack, K.; Pullen, N. In vitro and in vivo characterization of PF-04418948, a novel, potent and selective prostaglandin EP(2) receptor antagonist. *Br. J. Pharmacol.* **2011**, *164*, 1847–1856. [CrossRef]
37. Thieme, K.; Majumder, S.; Brijmohan, A.S.; Batchu, S.N.; Bowskill, B.B.; Alghamdi, T.A.; Advani, S.L.; Kabir, M.G.; Liu, Y.; Advani, A. EP4 inhibition attenuates the development of diabetic and non-diabetic experimental kidney disease. *Sci. Rep.* **2017**, *7*, 3442. [CrossRef]
38. Kabashima, K.; Saji, T.; Murata, T.; Nagamachi, M.; Matsuoka, T.; Segi, E.; Tsuboi, K.; Sugimoto, Y.; Kobayashi, T.; Miyachi, Y.; et al. The prostaglandin receptor EP4 suppresses colitis, mucosal damage and CD4 cell activation in the gut. *J. Clin. Investig.* **2002**, *109*, 883–893. [CrossRef]
39. Bek, M.; Nusing, R.; Kowark, P.; Henger, A.; Mundel, P.; Pavenstadt, H. Characterization of prostanoid receptors in podocytes. *J. Am. Soc. Nephrol.* **1999**, *10*, 2084–2093.
40. Srivastava, T.; Dai, H.; Heruth, D.P.; Alon, U.S.; Garola, R.E.; Zhou, J.; Duncan, R.S.; El-Meanawy, A.; McCarthy, E.T.; Sharma, R.; et al. Mechanotransduction signaling in podocytes from fluid flow shear stress. *Am. J. Physiol. Ren. Physiol.* **2018**, *314*, F22–F34. [CrossRef]
41. Dey, I.; Giembycz, M.A.; Chadee, K. Prostaglandin E(2) couples through EP(4) prostanoid receptors to induce IL-8 production in human colonic epithelial cell lines. *Br. J. Pharmacol.* **2009**, *156*, 475–485. [CrossRef] [PubMed]
42. Lee, J.; Aoki, T.; Thumkeo, D.; Siriwach, R.; Yao, C.; Narumiya, S. T cell-intrinsic prostaglandin E2-EP2/EP4 signaling is critical in pathogenic TH17 cell-driven inflammation. *J. Allergy Clin. Immunol.* **2019**, *143*, 631–643. [CrossRef] [PubMed]
43. Liu, C.; Zhu, P.; Wang, W.; Li, W.; Shu, Q.; Chen, Z.J.; Myatt, L.; Sun, K. Inhibition of lysyl oxidase by prostaglandin E2 via EP2/EP4 receptors in human amnion fibroblasts: Implications for parturition. *Mol. Cell. Endocrinol.* **2016**, *424*, 118–127. [CrossRef] [PubMed]
44. Schulz, A.; Muller, N.V.; van de Lest, N.A.; Eisenreich, A.; Schmidbauer, M.; Barysenka, A.; Purfurst, B.; Sporbert, A.; Lorenzen, T.; Meyer, A.M.; et al. Analysis of the genomic architecture of a complex trait locus in hypertensive rat models links Tmem63c to kidney damage. *eLife* **2019**, *8*. [CrossRef]
45. Livak, K.J.; Schmittgen, T.D. Analysis of relative gene expression data using real-time quantitative PCR and the 2(-Delta Delta C(T)) Method. *Methods* **2001**, *25*, 402–408. [CrossRef] [PubMed]
46. Jiang, H.; McGiff, J.C.; Quilley, J.; Sacerdoti, D.; Reddy, L.M.; Falck, J.R.; Zhang, F.; Lerea, K.M.; Wong, P.Y. Identification of 5,6-trans-epoxyeicosatrienoic acid in the phospholipids of red blood cells. *J. Biol. Chem.* **2004**, *279*, 36412–36418. [CrossRef]
47. Schulz, A.; Kreutz, R. Mapping genetic determinants of kidney damage in rat models. *Hypertens. Res.* **2012**, *35*, 675–694. [CrossRef]
48. Vogt, L.; Laverman, G.D.; Navis, G. Time for a comeback of NSAIDs in proteinuric chronic kidney disease? *Neth. J. Med.* **2010**, *68*, 400–407.
49. Liu, J.; Zhang, Y.D.; Chen, X.L.; Zhu, X.L.; Chen, X.; Wu, J.H.; Guo, N.F. The protective effect of the EP2 receptor on TGF-beta1 induced podocyte injury via the PI3K/Akt signaling pathway. *PLoS ONE* **2018**, *13*, e0197158. [CrossRef]
50. Lemieux, L.I.; Rahal, S.S.; Kennedy, C.R. PGE2 reduces arachidonic acid release in murine podocytes: evidence for an autocrine feedback loop. *Am. J. Physiol. Cell Physiol.* **2003**, *284*, C302–309. [CrossRef]
51. Regan, J.W. EP2 and EP4 prostanoid receptor signaling. *Life Sci.* **2003**, *74*, 143–153. [CrossRef] [PubMed]
52. Fujino, H.; West, K.A.; Regan, J.W. Phosphorylation of glycogen synthase kinase-3 and stimulation of T-cell factor signaling following activation of EP2 and EP4 prostanoid receptors by prostaglandin E2. *J. Biol. Chem.* **2002**, *277*, 2614–2619. [CrossRef] [PubMed]

53. Hsu, H.H.; Lin, Y.M.; Shen, C.Y.; Shibu, M.A.; Li, S.Y.; Chang, S.H.; Lin, C.C.; Chen, R.J.; Viswanadha, V.P.; Shih, H.N.; et al. Prostaglandin E2-Induced COX-2 Expressions via EP2 and EP4 Signaling Pathways in Human LoVo Colon Cancer Cells. *Int. J. Mol. Sci.* **2017**, *18*, 1132. [CrossRef] [PubMed]
54. Fujino, H.; Xu, W.; Regan, J.W. Prostaglandin E2 induced functional expression of early growth response factor-1 by EP4, but not EP2, prostanoid receptors via the phosphatidylinositol 3-kinase and extracellular signal-regulated kinases. *J. Biol. Chem.* **2003**, *278*, 12151–12156. [CrossRef]
55. Kitase, Y.; Barragan, L.; Qing, H.; Kondoh, S.; Jiang, J.X.; Johnson, M.L.; Bonewald, L.F. Mechanical induction of PGE2 in osteocytes blocks glucocorticoid-induced apoptosis through both the beta-catenin and PKA pathways. *J. Bone Min. Res.* **2010**, *25*, 2657–2668. [CrossRef]
56. Cherian, P.P.; Cheng, B.; Gu, S.; Sprague, E.; Bonewald, L.F.; Jiang, J.X. Effects of mechanical strain on the function of Gap junctions in osteocytes are mediated through the prostaglandin EP2 receptor. *J. Biol. Chem.* **2003**, *278*, 43146–43156. [CrossRef]
57. Fujino, H.; Salvi, S.; Regan, J.W. Differential regulation of phosphorylation of the cAMP response element-binding protein after activation of EP2 and EP4 prostanoid receptors by prostaglandin E2. *Mol. Pharmacol.* **2005**, *68*, 251–259. [CrossRef]
58. Lu, J.W.; Wang, W.S.; Zhou, Q.; Gan, X.W.; Myatt, L.; Sun, K. Activation of prostaglandin EP4 receptor attenuates the induction of cyclooxygenase-2 expression by EP2 receptor activation in human amnion fibroblasts: implications for parturition. *Faseb J. Off. Publ. Fed. Am. Soc. Exp. Biol.* **2019**, *33*, 8148–8160. [CrossRef]
59. Majumder, M.; Xin, X.; Liu, L.; Tutunea-Fatan, E.; Rodriguez-Torres, M.; Vincent, K.; Postovit, L.M.; Hess, D.; Lala, P.K. COX-2 Induces Breast Cancer Stem Cells via EP4/PI3K/AKT/NOTCH/WNT Axis. *Stem Cells* **2016**, *34*, 2290–2305. [CrossRef]
60. Vo, B.T.; Morton, D., Jr.; Komaragiri, S.; Millena, A.C.; Leath, C.; Khan, S.A. TGF-beta effects on prostate cancer cell migration and invasion are mediated by PGE2 through activation of PI3K/AKT/mTOR pathway. *Endocrinology* **2013**, *154*, 1768–1779. [CrossRef]
61. Gao, F.; Zafar, M.I.; Juttner, S.; Hocker, M.; Wiedenmann, B. Expression and Molecular Regulation of the Cox2 Gene in Gastroenteropancreatic Neuroendocrine Tumors and Antiproliferation of Nonsteroidal Anti-Inflammatory Drugs (NSAIDs). *Med. Sci. Monit.* **2018**, *24*, 8125–8140. [CrossRef] [PubMed]
62. Mesa, J.; Alsina, C.; Oppermann, U.; Pares, X.; Farres, J.; Porte, S. Human prostaglandin reductase 1 (PGR1): Substrate specificity, inhibitor analysis and site-directed mutagenesis. *Chem. Biol. Interact.* **2015**, *234*, 105–113. [CrossRef] [PubMed]
63. Yu, Y.H.; Chang, Y.C.; Su, T.H.; Nong, J.Y.; Li, C.C.; Chuang, L.M. Prostaglandin reductase-3 negatively modulates adipogenesis through regulation of PPARgamma activity. *J. Lipid Res.* **2013**, *54*, 2391–2399. [CrossRef] [PubMed]
64. Tai, H.H.; Ensor, C.M.; Tong, M.; Zhou, H.; Yan, F. Prostaglandin catabolizing enzymes. *Prostaglandins Lipid Mediat.* **2002**, *68–69*, 483–493. [CrossRef]
65. Reid, G.; Wielinga, P.; Zelcer, N.; van der Heijden, I.; Kuil, A.; de Haas, M.; Wijnholds, J.; Borst, P. The human multidrug resistance protein MRP4 functions as a prostaglandin efflux transporter and is inhibited by nonsteroidal antiinflammatory drugs. *Proc. Natl. Acad. Sci. USA* **2003**, *100*, 9244–9249. [CrossRef]
66. Chan, B.S.; Satriano, J.A.; Pucci, M.; Schuster, V.L. Mechanism of prostaglandin E2 transport across the plasma membrane of HeLa cells and Xenopus oocytes expressing the prostaglandin transporter ''PGT''. *J. Biol. Chem.* **1998**, *273*, 6689–6697. [CrossRef]
67. Shirasaka, Y.; Shichiri, M.; Kasai, T.; Ohno, Y.; Nakanishi, T.; Hayashi, K.; Nishiura, A.; Tamai, I. A role of prostaglandin transporter in regulating PGE(2) release from human bronchial epithelial BEAS-2B cells in response to LPS. *J. Endocrinol.* **2013**, *217*, 265–274. [CrossRef]
68. Kosaka, T.; Miyata, A.; Ihara, H.; Hara, S.; Sugimoto, T.; Takeda, O.; Takahashi, E.; Tanabe, T. Characterization of the human gene (PTGS2) encoding prostaglandin-endoperoxide synthase 2. *Eur. J. Biochem.* **1994**, *221*, 889–897. [CrossRef]
69. Srivastava, T.; Ju, W.; Milne, G.L.; Rezaiekhaligh, M.H.; Staggs, V.S.; Alon, U.S.; Sharma, R.; Zhou, J.; El-Meanawy, A.; McCarthy, E.T.; et al. Urinary prostaglandin E2 is a biomarker of early adaptive hyperfiltration in solitary functioning kidney. *Prostaglandins Lipid Mediat.* **2020**, *146*, 106403. [CrossRef]
70. Needleman, P.; Turk, J.; Jakschik, B.A.; Morrison, A.R.; Lefkowith, J.B. Arachidonic acid metabolism. *Annu. Rev. Biochem.* **1986**, *55*, 69–102. [CrossRef]

71. Schulz, A.; Weiss, J.; Schlesener, M.; Hansch, J.; Wehland, M.; Wendt, N.; Kossmehl, P.; Sietmann, A.; Grimm, D.; Stoll, M.; et al. Development of overt proteinuria in the Munich Wistar Fromter rat is suppressed by replacement of chromosome 6 in a consomic rat strain. *J. Am. Soc. Nephrol.* **2007**, *18*, 113–121. [CrossRef] [PubMed]
72. Fassi, A.; Sangalli, F.; Maffi, R.; Colombi, F.; Mohamed, E.I.; Brenner, B.M.; Remuzzi, G.; Remuzzi, A. Progressive glomerular injury in the MWF rat is predicted by inborn nephron deficit. *J. Am. Soc. Nephrol.* **1998**, *9*, 1399–1406. [PubMed]
73. Remuzzi, A.; Puntorieri, S.; Mazzoleni, A.; Remuzzi, G. Sex related differences in glomerular ultrafiltration and proteinuria in Munich-Wistar rats. *Kidney Int.* **1988**, *34*, 481–486. [CrossRef] [PubMed]
74. Macconi, D.; Bonomelli, M.; Benigni, A.; Plati, T.; Sangalli, F.; Longaretti, L.; Conti, S.; Kawachi, H.; Hill, P.; Remuzzi, G.; et al. Pathophysiologic implications of reduced podocyte number in a rat model of progressive glomerular injury. *Am. J. Pathol.* **2006**, *168*, 42–54. [CrossRef] [PubMed]
75. Ijpelaar, D.H.; Schulz, A.; Koop, K.; Schlesener, M.; Bruijn, J.A.; Kerjaschki, D.; Kreutz, R.; de Heer, E. Glomerular hypertrophy precedes albuminuria and segmental loss of podoplanin in podocytes in Munich-Wistar-Frömter rats. *Am. J. Physiol. Ren. Physiol.* **2008**, *294*, F758–F767. [CrossRef]
76. van Es, N.; Schulz, A.; Ijpelaar, D.; van der Wal, A.; Kuhn, K.; Schutten, S.; Kossmehl, P.; Nyengaard, J.R.; de Heer, E.; Kreutz, R. Elimination of severe albuminuria in aging hypertensive rats by exchange of 2 chromosomes in double-consomic rats. *Hypertension* **2011**, *58*, 219–224. [CrossRef]
77. Boerries, M.; Grahammer, F.; Eiselein, S.; Buck, M.; Meyer, C.; Goedel, M.; Bechtel, W.; Zschiedrich, S.; Pfeifer, D.; Laloe, D.; et al. Molecular fingerprinting of the podocyte reveals novel gene and protein regulatory networks. *Kidney Int.* **2013**, *83*, 1052–1064. [CrossRef]
78. Schell, C.; Baumhakl, L.; Salou, S.; Conzelmann, A.C.; Meyer, C.; Helmstadter, M.; Wrede, C.; Grahammer, F.; Eimer, S.; Kerjaschki, D.; et al. N-wasp is required for stabilization of podocyte foot processes. *J. Am. Soc. Nephrol.* **2013**, *24*, 713–721. [CrossRef]
79. Staffel, J.; Valletta, D.; Federlein, A.; Ehm, K.; Volkmann, R.; Fuchsl, A.M.; Witzgall, R.; Kuhn, M.; Schweda, F. Natriuretic Peptide Receptor Guanylyl Cyclase-A in Podocytes is Renoprotective but Dispensable for Physiologic Renal Function. *J. Am. Soc. Nephrol.* **2017**, *28*, 260–277. [CrossRef]
80. Koehler, S.; Kuczkowski, A.; Kuehne, L.; Jungst, C.; Hoehne, M.; Grahammer, F.; Eddy, S.; Kretzler, M.; Beck, B.B.; Hohfeld, J.; et al. Proteome Analysis of Isolated Podocytes Reveals Stress Responses in Glomerular Sclerosis. *J. Am. Soc. Nephrol.* **2020**, *31*, 544–559. [CrossRef]
81. Sharma, R.; Waller, A.P.; Agrawal, S.; Wolfgang, K.J.; Luu, H.; Shahzad, K.; Isermann, B.; Smoyer, W.E.; Nieman, M.T.; Kerlin, B.A. Thrombin-Induced Podocyte Injury Is Protease-Activated Receptor Dependent. *J. Am. Soc. Nephrol.* **2017**, *28*, 2618–2630. [CrossRef] [PubMed]

Curriculum Vitae

For data protection reasons, my CV will not be published in the electronic version of my work.

Publication list

Kourpa, Aikaterini*; Schulz, Angela*; Mangelsen, Eva; Kaiser-Graf, Debora; Koppers, Nils; Stoll, Monika; Rothe, Michael; Bader, Michael; Purfürst, Bettina; Kunz, Severine; Gladytz, Thomas; Niendorf, Thoralf; Bachmann, Sebastian; Mutig, Kerim; Bolbrinker, Juliane; Panáková, Daniela; Kreutz, Reinhold**. **Studies in Zebrafish and Rat Models Support Dual Blockade of EP2 and EP4 (Prostaglandin E_2 Receptors Type 2 and 4) for Renoprotection in Glomerular Hyperfiltration and Albuminuria.** *Hypertension.* 2023;80:771-782. https://doi.org/10.1161/HYPERTENSIONAHA.122.20392 Impact Factor: 9,897

Kourpa, Aikaterini; Kaiser-Graf, Debora; Sporbert, Anje; Philippe, Aurélie; Catar, Rusan; Rothe, Michael; Mangelsen, Eva; Schulz, Angela; Bolbrinker, Juliane; Kreutz, Reinhold; Panáková, Daniela**. **15-keto-Prostaglandin E_2 exhibits bioactive role by modulating glomerular cytoarchitecture through EP2/EP4 receptors**. *Life Sciences* 2022;310. https://doi.org/10.1016/j.lfs.2022.121114 Impact Factor: 6,78

Mangelsen, Eva.; Rothe, Michael.; Schulz, Angela.; Kourpa, Aikaterini.; Panáková, Daniela.; Kreutz, Reinhold.; Bolbrinker, Juliane**. **Concerted EP2 and EP4 Receptor Signaling Stimulates Autocrine Prostaglandin E2 Activation in Human Podocytes**. *Cells* 2020, 9, 1256. https://doi.org/10.3390/cells9051256 Impact Factor: 6,60

Kourpa, K.; Strataki, V.; Manarolaki, E.; Rupprecht, F.; Langer, J.D.; Tsiotis, G**. **Label-free quantitative analysis of enriched heterocysts from two hydrogenase mutants from *Anabaena* sp. PCC 7120.** *Proteomics* 2019, 19 (19). https://doi.org/10.1002/pmic.201800332 Impact Factor: 3,254

(*Authors contributed equally, ** correspondence)

Acknowledgments

Foremost, I would like to thank my supervisors, Prof. Reinhold Kreutz and Dr. Daniela Panáková, for giving me the opportunity to be part of the SFB-1365 Renoprotection program, as well as for their guidance and continuous support on this thesis. Thank you for all the knowledge and expertise you shared with me and helped me become a better and more confident scientist.

I would like to thank PD Dr. med Juliane Bolbrinker for agreeing to be the third supervisor during my PhD studies and for her valuable feedback and support.

I would also like to thank all the reviewers that agreed to participate in the doctoral examination procedure and evaluated my thesis.

My sincere thanks go to Dr. Anje Sporbert (MDC Advanced Light Microscopy Facility), Dr. Bettina Purfürst and Dr. Severine Kunz (MDC Electron Microscopy Facility) for the excellent collaboration we had through the last years. I am particularly grateful to Christina Schiel not only for her excellent technical support with the electron microscopy experiments, but also for her friendship and continuous help. I would also like to acknowledge the MDC Fish Facility for their expert support.

Many thanks to all the current and previous members of the Panáková lab, Laura Bartolini, Nicola V. Müller, Anne Merks, Mai Phan and Babette Furchtbar for the nice atmosphere they create in the lab. Special thanks go to Sara Lelek and Kevin Manuel Mendez Acevedo for the insightful and beneficial discussions we had, as well as for their friendship and great support all these years.

I would also like to thank the members of the Kreutz lab for the excellent collaboration we had, especially Eva Mangelsen, Angela Schulz and Debora Kaiser-Graf, who also supported me with the german version of the thesis abstract.

My deep gratitude goes to my parents, Vasilis and Yianna, and to my sister, Marina, for their support and love, and for their constant presence in my life.

Above all, I would like to thank my husband Theodore for his love, patience, and constant support, and for being by my side every day, no matter if tears or smiles. I could not imagine doing this without you.